Light-Controlled Energy Transfer

DISSERTATION

zur Erlangung des akademischen Grades
doctor rerum naturalium
(Dr. rer. nat.)
im Fach Chemie
eingereicht an der

Mathematisch-Naturwissenschaftlichen Fakultät
der Humboldt-Universität zu Berlin
von

Lic. Javier Moreno Ortego

Präsident der Humboldt-Universität zu Berlin
Prof. Dr. Jan-Hendrik Olbertz

Dekan der Mathematisch-Naturwissenschaftlichen Fakultät
Prof. Dr. Elmar Kulke

Gutachter:	1. Prof. Stefan Hecht, Ph.D. 2. Prof. Dr. Josef Wachtveitl 3. Prof. Dr. Hans Börner
Tag der mündlichen Prüfung:	14.07.2015

Die vorliegende Arbeit wurde in der Zeit von Oktober 2011 bis Mai 2015 am Institut für Chemie der Humboldt-Universität zu Berlin unter der Anleitung von Prof. Stefan Hecht, Ph.D. angefertigt.

Danksagung

Prof. Stefan Hecht, Ph.D. danke ich neben den wertvollen fachlichen Gesprächen, für die Möglichkeit meiner Kreativität freien Lauf zu geben und das Vertrauen, anspruchsvolle und reizende Themen unter hervorragenden Arbeitsbedingungen zu bearbeiten.

Der gesamten Arbeitsgruppe möchte ich für die freundliche Atmosphäre danken. Ein besonderer Dank geht an alle meine Laborkollegen, gesondert zu erwähnen sind Mirko Lohse und Johannes Gurke, die langjährig den Laboralltag bereichert haben. Mein weiterer Dank geht an Dr. David Bleger, für die stetige Hilfsbereitschaft und fachliche Kompetenz. Herrn Dr. Lutz Grubert danke ich für die Beihilfe in der Elektrochemischen Charakterisierung und den zahlreichen fachlichen Diskussionen. An Dr. Joachim Leistner geht mein Dank für die Hilfe und Einarbeitung in den analytischen Trennmethoden. Bei der Synthetischen Unterstützung möchte ich Jutta Schwarz sowie meinen studentischen Hilfskräften Sarah Volkmann und Malte Brie dankbar sein.

Bei Dr. Erik Ø. Johnsen möchte ich mich herzlichst bedanken für die enthusiastische, lehrreiche Betreuung in meiner Studienzeit und die daraus entstandene Freundschaft. Allen Service-Mitarbeitern der analytischen Abteilungen des Instituts möchte ich für die Durchführung zahlreicher Analysen danken.

Ein großer Dank geht an die Arbeitsgruppe von Prof. Dr. Niko P. Ernsting für die offene Hilfsbereitschaft und den zahlreichen Einladungen zum Kaffee, mit gesondertem Dank an Dr. Sergey Kovalenko - Thank you for everything, for your support, advice and guidance. Ich möchte mich auch bei Prof. Dr. Josef Wachtveitl und Felix Schweighöfer für die äußerst engagierte und zielstrebige Zusammenarbeit bedanken. Dr. Salvo Chiantia und Dr. Sara Bobone möchte ich für die sehr hilfreiche und freundliche Zusammenarbeit danken - grazie mille.

Alejandra de Miguel verdient mein größter liebenswürdiger Dank, da ohne ihre tägliche und gefühlvolle Unterstützung diese Dissertation nicht vollendet werden könnte. Mi agradecimiento especial a mi madre Gloria Ortego y a mi padre Luis Moreno así como a mis abuelos Gloria Esteban y Arturo Ortego, que siempre han creído en mí, me han apoyado incondicionalmente y me han motivado a perseverar ante las adversidades. Os quiero.

Abstract

Reversibility is one of the most striking features of novel responsive materials, as it enables the repeated and dynamic alteration of properties on demand. Light as a stimulus offers very high spatial, temporal, as well as energetic resolution. Additionally, it is possible to exploit extraordinary penetration depth into materials and tissues due to its non-invasive character. Unfortunately, a fundamental resolution limitation is encountered once the nanoscopic scale is reached. Abbe's law of diffraction limits the maximum spatial resolution to half of the wavelength of the light used. However, fluorescence microscopy and nonlinear optics have recently proven to effectively overcome this limitation.

With the purpose of designing stable and photomodulable fluorophores for their direct application in subdiffraction microscopy techniques, the synthesis and characterization of new far-red emitting photoswitchable fluorophores has been accomplished. The electronic coupling between components was profoundly studied, and the structure-property relation established. Fluorescence emission was efficiently modulated or switched *On* and *Off* by the interaction of the photochromic-unit with the fluorescent-unit. Thus, a general concept for the design of these molecular constructs was developed. Additionally, encapsulation experiments in micelles were performed to investigate the water solubility of the synthesized compounds. Additionally, the comprehensive characterization of the excited state dynamics is achieved. Finally, potential applications were examined with fluorescence microscopy, encapsulating the dyads in giant uni-lamellar vesicles under biological conditions to explore the feasibility to obtain highly resolved subdiffraction images.

Exploiting the advantages of nonlinear processes, the synthesis and characterization of photoswitches, which are able to be switched indirectly through an initial sensitized event was studied. With this determination a two-photon absorbing triarylamine chromophore was covalently linked to an electron poor azobenzene. In-depth characterization of the excited state dynamics was performed and two-photon induced isomerization of the dyad was confirmed. Similarly a triplet-emitting $Ir(ppy)_2$-L dye was covalently linked to an azobenzene. In this construct PET should promote the switching of the photoswitch after an initial reduction caused by a photoinduced charge-separation. A detailed study of the electrochemical properties was set and guidelines towards the improvement of the system were succinctly mentioned.

Zusammenfassung

Reversibilität ist eine der auffälligsten Merkmale von neuartigen Materialien, da sie die wiederholte und dynamische Änderung von Eigenschaften auf Bedarf ermöglicht. Licht als Stimulus bietet eine sehr hohe räumliche, zeitliche, aber auch energetische Auflösung. Zusätzlich ist es möglich, eine außerordentliche Eindringtiefe in Materialien und Gewebe aufgrund seines nicht-invasiven Charakters auszunutzen. Leider unterliegt Licht sobald die nanoskopische Skala erreicht ist, einer grundlegenden Auflösungs limitiation. Abbe's Beugungsgesetz begrenzt die maximale räumliche Auflösung auf die Hälfte der Wellenlänge des verwendeten Lichts. Allerdings war es möglich mittels Fluoreszenzmikroskopie oder der nichtlinearen Optik diese Einschränkung effektiv zu überwinden.

Mit dem Ziel stabile und photomodulierbare Fluorophore für ihre direkte Anwendung in der hochaufgelösten Mikroskopie, wurde die Synthese und Charakterisierung von neuen fern-Rot emittierender photoschaltbarer Fluorophore erreicht. Hierbei wurde die elektronische Kopplung zwischen den Komponenten tiefgreifend untersucht, und die Struktur-Eigenschafts-Beziehung etabliert. Durch die Wechselwirkung der photochromen Einheit mit dem Fluorophor, konnte die Fluoreszenzemission ein- und ausgeschaltet werden. Somit wurde ein allgemeines Konzept für die Gestaltung dieser molekularen Konstrukte entwickelt. Zusätzlich wurden Einkapselungs Experimente in Micellen durchgeführt, um die Wasserlöslichkeit der synthetisierten Verbindungen zu untersuchen. Die umfassende Charakterisierung der Dynamik im angeregten Zustand wurde durchgeführt. Schließlich wurden mögliche Anwendungen mittels Fluoreszenzmikroskopie geprüft. Um hochaufgelöste Bilder unter biologischen Bedingungen zu erhalten, wurde die Verkapselung der Dyaden in riesige unilamellare Vesikel erprobt.

Unter Ausnutzung der Vorteile nichtlinearer Prozesse wurde die Synthese und Charakterisierung von photochromen Verbindungen untersucht, die in der Lage indirekt durch einen anfänglichen sensibilisierten Prozess geschaltet werden. Zu diesem Zweck wurde ein Triarylamin Chromophor als Zwei-Photonenabsorber kovalent an einen Azobenzol verbunden. Die Charakterisierung der angeregten Zustandsdynamik wurde ausgeführt und die zwei Photonen induzierte Isomerisierung der Dyade bestätigt. Ebenso wurde ein Triplett emittierender Ir(ppy)$_2$-L Farbstoff kovalent an einen Azobenzol verbunden. Eine detaillierte Untersuchung der elektrochemischen Eigenschaften wurde durchgeführt und Richtlinien zur Verbesserung des Systems wurden kurz und bündig genannt.

Table of Contents

Acknowledgements .... **v**

Abstract .... **vii**

Zusammenfassung .... **ix**

Table of Contents .... **xi**

1. Introduction **1**

1.1 Aim of this work 3

2. General part **4**

2.1 Photochromism 4

2.1.1 Photoisomerization Efficiency 7

2.2 Diarylethene Photoswitches 10

2.2.1 Molecular Structure 10

2.2.2 Synthesis of Diarylethenes 12

2.2.3 Photochemical Properties 13

2.3 Azobenzene Photoswitches 17

2.3.1 Molecular Structure 17

2.3.2 Synthesis of Azobenzenes 17

2.3.3 Photochemical Properties 19

2.3.3.1 Normal Azobenzenes 20

2.3.3.2 Aminoazobenzenes 23

2.3.3.3 Pseudostilbenes 23

2.3.3.4 Visible Light Addressable Azobenzenes 23

2.3.4 Electrochemical Properties 25

2.4 Elemental Photophysical Processes 29

2.4.1 Excitation Energy Transfer 29

2.4.1.1 Energy Transfer Mechanisms 30

2.4.1.1 Applications 34

2.4.2 Photoinduced Electron Transfer 35

2.4.2.1 Electron Transfer Processes 36

2.4.2.2 Applications 37

2.4.3 Fundamentals of Two-photon Absorption 38

2.4.3.1 Two-Photon Absorption Cross-Section 39

2.4.3.2 Design of Two-Photon Chromophores 41

2.4.3.3 Applications 44

2.5 BODIPY Fluorophores 45

2.5.1 Molecular Structure 46

2.5.2 Synthesis of BODIPYs 48

2.5.3 Applications 50

2.6 Sensitization 52

2.6.1 Triarylamine Fluorophores 53

2.6.1.1 Synthesis of Triarylamines 53

2.6.1.2 Photophysical Properties 54

2.6.1.3 Applications 55

2.6.2 Ir(III) Complexes as Triplett Emitters 56

2.6.2.1 Synthesis of Ir(C^N)$_2$LX Complexes 57

2.6.2.2 Photophysical Properties 58

2.8.2.3 Applications 60

2.7 Photoswitches as Energy Acceptors 61

2.7.1 Fluorescence Modulation with Diarylethenes 62

2.7.2 Sensitization and Amplification 69

3. Results and Discussion 75

3.1 Reversibly Photomodulating the Emission of Fluorophore-Photoswitch Dyads 75

3.1.1 Target Definition 75

3.1.2 Synthesis and Characterization 77

3.1.3 Transient Absorption Spectroscopy 103

3.1.4 Solubilization in Aqueous Media 112

3.2 Sensitized Two-Photon *cis→trans* Isomerization of Azobenzenes 117

3.2.1 Target Definition 117

3.2.2 Synthesis and Characterization 118

3.2.3 Transient Absorption Spectroscopy 136

3.3 PET Mediated *cis→trans* Isomerization of Azobenzenes 149

3.3.1 Target Definition 149

3.3.2 Synthesis and Characterization 150

4. Conclusions and Outlook 161

4.1 Reversibly Photomodulating the Emission of Fluorophore-Photoswitch Dyads 161

4.2 Sensitized Two-Photon *cis→trans* Isomerization of Azobenzenes 164

4.3 PET Mediated *cis→trans* Isomerization of Azobenzenes 166

5. Experimental Section 169

5.1 Materials and Methods 169

5.1.1 Analytical Instrumentation 169

5.1.2 Chemicals and Solvents 169

5.2 Synthesis and Characterization Data 170

5.3 Procedures 200

References 205

List of Abbreviations 223

1. Introduction

Natural sciences comprise several disciplines, which study and investigate the natural behavior of the fundamental processes involved in the existence of the Universe. Chemistry is the discipline, which studies the composition, structure, properties and change of matter. In the field of organic chemistry, research is focused in the structure-properties relation of organic substances which by means of chemical reactions are modified and improved to meet modern society's demands for ever improving materials. Organic compounds are efficiently modified by the synthetic chemist, whose applications range from drugs, dyes and electronics up to tailor-made polymers. The design of functional materials in the nanometric scale, which are able to respond to external stimuli, is a heavily researched field of great interest. Stimuli-responsive materials are intended to address the chemist's ambition to gain control over inherent features of a given system. This features include electron- and energy transfer processes,[1] aggregation behavior,[2] as well as catalytic activity.[3] The most popular external stimuli to enable the reversible control of properties in molecules include variations of pH,[4] light,[5] or the tip of a scanning tunneling microscope (STM).[6] Of the stimuli mentioned, light has the striking features of being non-invasive besides enabling a superior spatial and temporal resolution. It has however to be pointed out that the maximum resolution of light is traditionally limited by Abbe's law of diffraction which is directly proportional to the wavelength of the light used. In fact the maximum resolution conventionally attainable is half of the wavelength employed.

Overcoming Abbe's diffraction limit has been recently accomplished by the advent of modern optics and powerful lasers, developing two main fields of research. Firstly by means of super-resolution fluorescence microscopy it was possible to attain images with a resolution as high as 20 nm, employing very fast pulses of light to selectively stimulate the blinking of fluorophores.[7] Applying this approach, an ensemble of fluorophores was recorded in different frames, where in each individual frame only a subset of fluorophores was allowed to emit light while the rest were selectively deactivated. Subsequent merging of all the accumulated frames to a single superimposed image enhanced vastly the resolution of a given area, resulting in subdiffraction resolution. This technique was primarily developed by Stefan W. Hell since the late 1990s and for his tremendous accomplishment in the field he was awarded in 2014 with the Nobel Prize in Chemistry. Superresolution microscopy has matured from an exclusive and highly specialized method for imaging a limited set of suitable sample types, to a widespread, general purpose mode of fluorescence microscopy, whose applications can be found not only in Biology but also in the study of engineered nanostructured materials.[8] The vast development of this technique is stimulated by the fact that the resolution is limited up to a single emissive molecule. Being the only drawback of the method, the need to use laser sources whose power and focusing depend on the lifetime of the Off-state of the fluorescent molecule employed. Secondly the innovations in nonlinear optics and the research of multi-photon chromophores which interact with at least two simultaneous light-stimuli, enabled to increase even further the spatial resolution of light-responsive materials. In contrast to conventional linear absorption, the rate for an electronic transition to take place in two-photon absorption is dependent from the square of the light intensity. This difference causes that the required photon density for a given electronic transition is only reached at the focal-point of the laser-beam. Because the window of excitation can be extended to the infrared region, two-photon materials have been also very popular in photodynamic therapy of cancer. Employing sources of light with longer wavelengths, an increased tissue penetration depth was achieved and simultaneously less cellular damage was caused. Similarly optical data storage exploits the ability of two-photon excitation to address molecules deep within a sample without affecting other areas. The field of optical computing, which replaces semiconducting transistors with nonlinear materials as optical transistor is focusing great interest. These nonlinear materials are employed to create optical logic gates which should vastly improve the miniaturization down to the molecular level. Storage and retrieval of information in the volume of a substance is hence made possible, rather than only on a surface as is done on the DVD. Therefore, 3D optical data storage has the possibility to provide media that contain extremely dense data capacities on a single disc. It is worth mentioning that although particularly requested by subdiffraction microscopoy and nonlinear optics, there are few examples known in the literature for materials capable of reversibly respond to specific light-stimuli with subdiffraction resolution.

1.1 Aim of This Work

The aim of this work is divided into two main branches. One branch includes the synthesis and characterization of new far-red emitting photoswitchable fluorophores whose fluorescence emission can be modulated or switched *On* and *Off* by the interaction of the photochromic-unit with the fluorescent-unit. Thus, a general concept for the design of this molecular materials is developed. The influence of the electronic communication between the components is studied in detail and encapsulation experiments in micelles are performed to investigate the water solubility of the depicted system. Furthermore, a comprehensive characterization of the excited state dynamics is performed to discern the accurate deactivation channels of the molecules in their different open and closed states. Potential applications are investigated with fluorescence microscopy, encapsulating the dyads in giant uni-lamellar vesicles (GUVs) under biological conditions to explore the feasibility to obtain highly resolved subdiffraction images.

The second branch of this work is focused on the synthesis and characterization of photoswitches which are able to be switched indirectly through an initial sensitized process, which is either obtained by two-photon irradiation or promotes the subsequent amplification of the first switching event. With this purpose a two-photon responsive triarylamine chromophore is covalently linked to an electron poor azobenzene (AB). Comprehensive characterization of the excited state dynamics is performed to discern the accurate deactivation channels of the excited molecule and two-photon induced isomerization of the dyad is studied. Similarly a triplet-emitting Ir(ppy)$_2$-L dye is covalently linked to an AB. In this construct PET should promote the switching of the AB-moiety after an initial reduction caused by the photoinduced charge-separation. A detailed study of the electrochemical properties is set and guidelines towards the improvement of the system are succinctly mentioned.

2. General Part

2.1 Photochromism

Photochromism is defined as “reversible transformation of a chemical species induced in one or both directions by absorption of electromagnetic radiation between two forms, A and B having different absorption spectra".[9] Molecules which undergo reversible changes between two species, having distinct absorption spectra or physical properties upon irradiation with light, are called photochromic molecules or photoswitches (**Scheme 2-1**).[10]

$$\mathrm{A} \underset{h\nu_2 \text{ or } \Delta}{\overset{h\nu_1}{\rightleftharpoons}} \mathrm{B}$$

Scheme 2-1: Photochromism as a reversible transformation between two isomers of a molecule.

Several kinds of photochromic molecules are known, the most popular derivatives of which are illustrated in **Scheme 2-2**. The AB class has been known for decades and is one of the best studied photoswitches due to its simplicity and ease of modification, However,it is widely used and new emerging applications are continuiously developed (**Scheme 2-2a**). UV-light induced isomerization promotes a large geometrical change from the thermodynamically more stable *trans*-AB to the *cis*-AB which originates additionally a large variation in the dipole moment. ABs are specifically useful for the modification of molecular geometries,[11] directed alteration of shapes in preorganized ensembles on materials and surfaces,[12,13] or conformational changes in biomacromolecules.[14] AB is a T-type photoswitch, denoting that it converts back to its thermodynamically more stable *trans*-isomer thermally over time. However, the *cis*→trans isomerization is also possible through the photochemical pathway.

The spiropyrans, similarly to the ABs, exhibit the UV-light induced formation of the merocyanine form as reversible by both visible light as well as thermally (**Scheme 2-2b**). The switching to the merocyanine form involves a charge separation, which causes an even larger alteration of the dipole moment as compared to the AB class.[15]

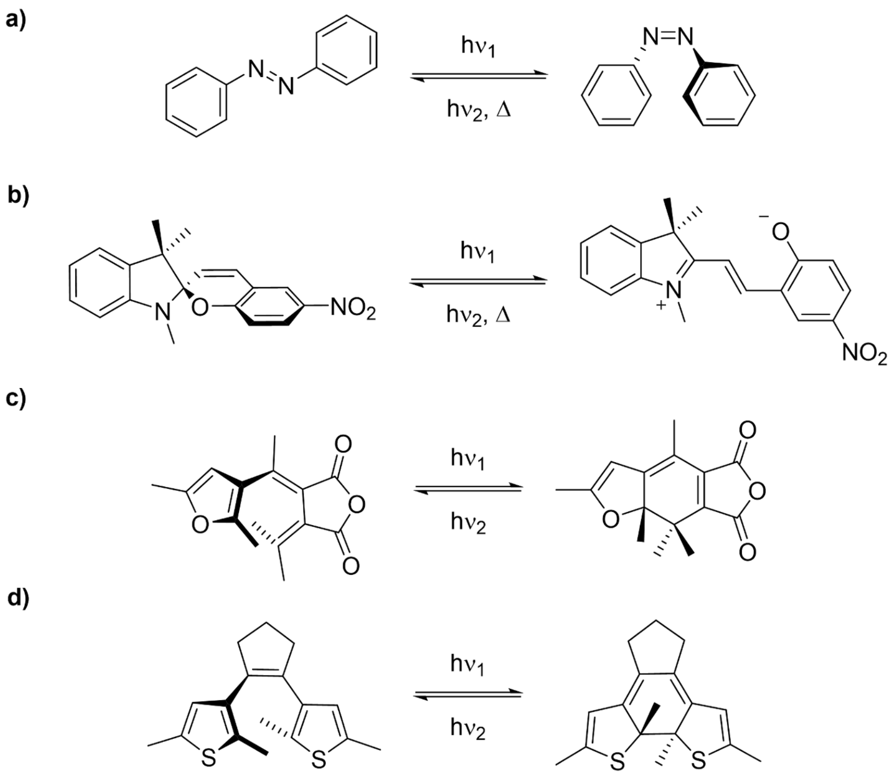

Scheme 2-2: Examples of photochromic compounds a) azobenzenes, b) spiropyrans, c) furilfulgides and d) diarylethenes.

Unfortunately, spiropyran is susceptible to a number of irreversible side-reactions in solution. Most research results incorporating spiropyrans as switches rely on the molecule being attached to a bulk surface or nanoparticles limiting its translational freedom and thus inhibiting unwanted intermolecular fatigue-reactions.[16] This immobilization can also be realized through the incorporation of the switch into polymer blends.

Fulgides are photochromic compounds suitable for use in optical data storage media.[17] Irradiation with UV or visible light induces electrocyclic ring-closure/ ring-opening reactions, leading to the production of closed or open isomers according to **Scheme 2-2c**. Generation of the so-called Z isomer by UV irradiation of the open isomer can be minimized by proper substitution.[18] Thermal stability of both isomers at room temperature, full reversibility of the photoreactions without photochemical fatigue, high conversion efficiencies due to both clearly separated absorption bands with high extinction coefficients and high reaction quantum yields with minor environmental effects in liquid solution and rigid polymer matrix are their main properties. However, fulgides are synthetically challenging and do not tolerate variations in the substitution pattern.

Diarylethenes (DAEs) are the most promising candidates for future applications, due to their synthetic availability and possibility of introducing many different substituents, which allow an accurate design of their properties. DAEs can be rendered as P-type photoswitches and thus both the ring-open as well as the ring-closed isomers are thermally stable constituting a system that is solely addressable with light. Irradiation with UV or visible light induces electrocyclic ring-closure/ ring-opening reactions, leading to the production of closed or open isomers according to **Scheme 2-2d**. The isomerization process is accompanied by a small change in the molecular geometry and can thus be achieved in densely packed ensembles within a confined space.[19] The most important feature of DAEs is the great change in conjugation exhibited upon irradiation with light (**Scheme 2-3**), enabling electronic communication between their different substituents. Ongoing research is also focused to improve the switching behavior[20] as well as their thermal stability and their fatigue resistance upon long cycles of irradiation.[21]

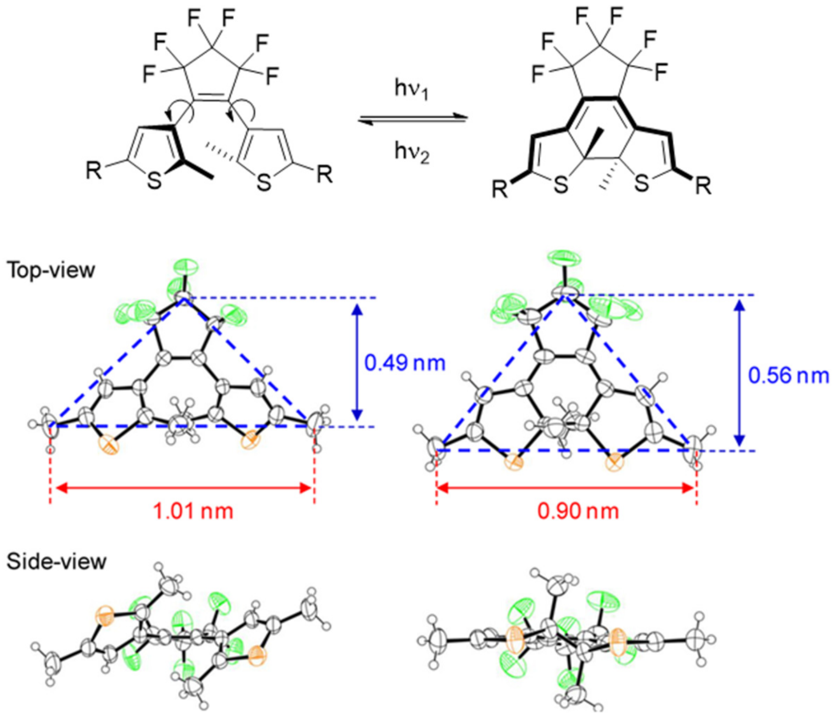

Scheme 2-3: Conjugation change in DAEs. After UV-light irradiation, conrotatory electrocyclic ring-closure (top). Crystallographic structures of DAE, almost no structural change upon cyclization (middle, bottom).[200]

2.1.1 Photoisomerization Efficiency

The photoisomerization efficiency of a photochromic system is characterized by the isomerization quantum yield for the photochemical reaction and the composition of the two isomers at the photostationary state (PSS). Under irradiation with light of a certain wavelength λ_{irr} the isomer A converts into the isomer B with the quantum yield ϕ_{irr} (**Scheme 2-1**). To describe this process an integral photoisomerization quantum yield γ_{AB} can be postulated as

$$\gamma_{AB} = \frac{N_{reac}}{N_{absA}} \tag{2.1.1}$$

where N_{absA} is the number of photons absorbed by the molecule A and N_{reac} is the number of photons that have induced the photoreaction from A to B.[22] For practical reasons a differential quantum yield ϕ_{AB} defined as

$$\phi_{AB} = -\frac{dc_A}{dt} \cdot \frac{1}{I_{absA}} = -\dot{c_A} \cdot \frac{1}{I_{absA}} \tag{2.1.2}$$

is usually favored as it assumes an infinitesimally small change in concentration over a given time interval. [13e] Here, $\dot{c_A}$ is the differential change of the concentration of species A over time and I_{absA} the amount of light absorbed by species A as a function of c_A. According to Lambert-Beer's law I_{absA} can be defined as

$$I_{absA} = 1000 \cdot I_0 \cdot \varepsilon_A \cdot c_A \cdot \frac{1 - 10^{-A'}}{A'} \tag{2.1.3}$$

with a correction factor of 1000 cm^{3}L^{-1}, the incident photon irradiance I_0 $[E \cdot cm^{-2} \cdot s^{-1}]$,[23] the molar absorptivity of species A ε_A , and the overall absorbance at the irradiation wavelength A' .[13e,24] Equations (2.1.2) and (2.1.3) are combined to give the differential expression of a uniform photochemical reaction where the product B is photoinactive

$$\frac{dc_A}{dt} = -1000 \cdot I_0 \cdot \varepsilon_A \cdot \phi_{AB} \cdot c_A \cdot \frac{1 - 10^{-A'}}{A'} \tag{2.1.4}$$

If both species A and B absorb at the irradiation wavelength, *i.e.* their molar absorptivities ε are different from 0, and the reaction is photoreversible, forward and backward reactions have to be taken into account with

$$\frac{dc_A}{dt} = -1000 \cdot I_0 \cdot (\varepsilon_A \cdot \phi_{AB} \cdot c_A - \varepsilon_B \cdot \phi_{BA} \cdot c_B) \cdot \frac{1 - 10^{-A'}}{A'} \tag{2.1.5}$$

This equation cannot be solved to give a closed-form expression and consequently it is practical to make an approximation. The initial slope method (or 'method of initial rates') is a method to measure ϕ_{AB} in an approach where the contribution of species B to the overall absorbance is assumed to be negligible and thus the rate of the back reaction can be neglected. Additionally, within the 5% conversion limit the photokinetic factor $\frac{1-10^{-A'}}{A'}$ is assumed to remain constant. Applying these restraints to Equation (2.1.5) while considering that $\dot{c_A} = -\dot{c_B}$ gives the term

$$\frac{dc_B}{dt} = 1000 \cdot I_0 \cdot \varepsilon_A \cdot \phi_{AB} \cdot c_A \cdot \frac{1 - 10^{-A'}}{A'} \tag{2.1.6}$$

A' can be expressed as the sum of the overall absorbances of the species existing in solution:

$$A' = \varepsilon_A \cdot c_A + \varepsilon_B \cdot c_B \tag{2.1.7}$$

and $c_B \approx 0$ as, Equation (2.1.6) can be altered accordingly to

$$\frac{dc_B}{dt} = 1000 \cdot I_0 \cdot \phi_{AB} \cdot \left(1 - 10^{-A'}\right) \tag{2.1.8}$$

If the reaction is monitored by absorption spectroscopy at a wavelength where $\varepsilon_A = 0$, the concentration of species B can be directly expressed through its absorbance A_B at that wavelength and subsequently results in the equation

$$\frac{dA_B}{dt} = 1000 \cdot I_0 \cdot \phi_{AB} \cdot \varepsilon_B \cdot \left(1 - 10^{-A'}\right) \tag{2.1.9}$$

where the quantum yield ϕ_{AB} can be extracted as the slope of a pseudo-linear relation.

A direct consequence of the overlapping absorption bands of species A and B in the UV-range is that the conversion to the photoproduct converges non-quantitatively during the photocyclization reaction and a PSS is reached. This can be explained by consulting Equation (2.1.5) and the fact that $\dot{c}_A = 0$ at $t = \infty$ and results in the expression

$$\frac{C_A^\infty}{C_B^\infty} = \frac{\phi_{BA} \cdot \varepsilon_B}{\phi_{AB} \cdot \varepsilon_A} \tag{2.1.10}$$

that determines the composition at the PSS through the ratio of $\phi_{BA} \cdot \varepsilon_B$ and $\phi_{AB} \cdot \varepsilon_A$. When the absorptivities are known the quantum yields can also be determined with equation (2.1.10) where C_A^∞ and C_B^∞ are the concentrations of the two components in the PSS. These concentrations can be calculated via the absorbance A_∞ in the PSS and the total concentration C_0 according to

$$C_A^\infty = \frac{A_\infty - \varepsilon_B \cdot C_0}{d(\varepsilon_A - \varepsilon_B)} \tag{2.1.11}$$

and

$$C_B^\infty = C_0 - C_A^\infty \tag{2.1.12}$$

Expressions (2.1.11) and (2.1.12) can be also employed to determine the concentration of any species at a given time, which is necessary for the determination of photoisomerization yields in the case of photoswitches, such as ABs, with overlapping absorption bands over the whole spectrum.[24]

To enrich the PSS with one of the isomers, photoswitches are engineered with well separated absorption regions of their switching states and a specific (narrow) irradiation wavelength is used to selectively address only one isomer. The ideal case hence would be if the absorption regions of species A and B would not overlap at all, thereby the photochemical back reaction could be almost eliminated. Other approaches to by-pass this limitation include the indirect excitation of one of the species by means of an orthogonally generated stimulus.

2.2 Diarylethene Photoswitches

2.2.1 Molecular Structure

DAEs are related to their parent compound stilbene. Stilbene is well known to undergo *trans*→cis photoisomerization under irradiation of UV light, but *cis*-stilbene can additionally undergo a subsequent 6 π-electrocyclization. The second photoisomerization yields dihydrophenanthrene upon irradiation with UV-light (**Scheme 2-4**). This process is poorly reversible under aerated conditions, as the ring-closed dihydrophenanthrene readily oxidizes to the more stable phenanthrene. Photocyclization followed by oxidative dehydrogenation is a very popular route for the synthesis of condensed ring systems, however, reversible photochromism is thereby suppressed. The straightforward approach to replace the oxidatively labile protons in the dihydrophenanthrene with small non-reactive functionalities like methyl- or methoxygroups, has proven to successfully inhibit the oxidation to the aromatically stabilized phenanthrene.

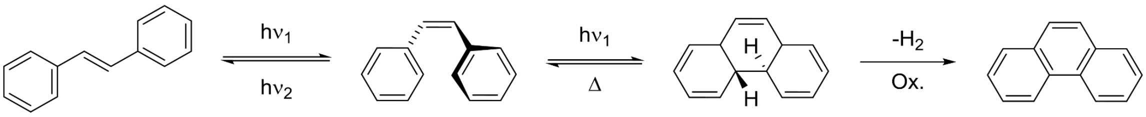

Scheme 2-4: E/ Z photoisomerization, photocyclization reaction of stilbene to dihydrophenanthrene and irreversible oxidation to phenanthrene in presence of air.

Unfortunately the thermal half-life of the ring-closed dimethylphenanthrene was rather short ($\tau_{1/2}$ = 1.5 min, 20 °C)[25] making this compound useless for practical applications as a switch. Thermal reversibility is originated by the higher aromatic stabilization energy of the ring-open form. If the aromatic stabilization is larger as compared to the ring-closed dihydrophenanthrene derivative, the former is destabilized considerably. Thermodynamics force the system back to the energetically more favorable state in the ring-open form. Under this assumption it was observed that the incorporation of aromatically less stabilized moieties, such as thienyl-residues, diminished the energy difference between the ring-open and the ring-closed forms. Thermal half-life of the ring-closed form could be thus extended extensively (**Scheme 2-5**).[26]

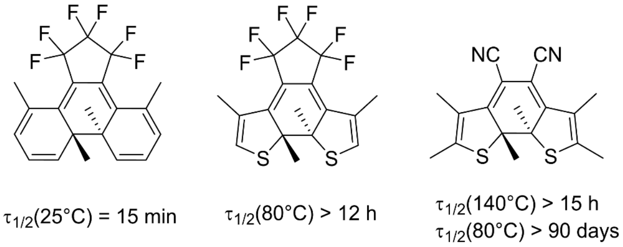

Scheme 2-5: Thermal half-life values ($\tau_{½}$) of the ring-closed forms of different DAEs.

As research on DAEs intensified over the past few decades, many different aryl groups have been included and most of them show thermally irreversible and fatigue-resistant photochromic reactions. Amongst them are benzo[b]thiophene,[27] furane,[28] benzofurane,[29] indole,[30] thiazole,[31] pyridine,[32] and various polycyclic aromatic hydrocarbons.[33]

The switching performance is further enhanced by constraining the photochemically active C-C double bond on the two aryl moieties in the *cis*-geometry. The locked double-bond efficiently suppresses the otherwise competing *trans→cis* isomerization of the molecule, causing a remarkable increase in the photochemical quantum yield for the ring-closing reaction. This is achieved by a covalent substitution of the double bond via incorporation into a suitable cyclic structure. The most commonly found structures are perfluorocyclopentenes,[34] perhydrocyclopentenes,[35] maleimides,[36] and five-membered heteroaromatic rings[37] (**Scheme 2-6**). Even though four- and six-membered rings have been incorporated into DAEs, five-membered rings, are seen as the compromise between the extended planarity of the four-membered ring bridges, with low photoisomerization quantum yield, and the overemphasized aryl-bridge torsion angle of the six-membered bridges with poor electronic communication of the substituents.[38]

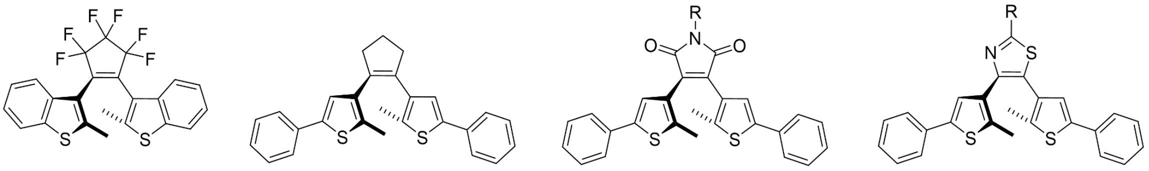

Scheme 2-6: Common bridge motifs for the design of DAEs. From left to right, hexafluorocyclopentene, cyclopentene, maleimide and five-membered heteroaromatic rings.

2.2.2 Synthesis of Diarylethenes

The synthesis of DAEs differs strongly depending on the bridging unit. Many successful routes for the synthesis of differently substituted DAEs have been published in the literature, the most important and general of which are depicted in **Scheme 2-7**.[39]

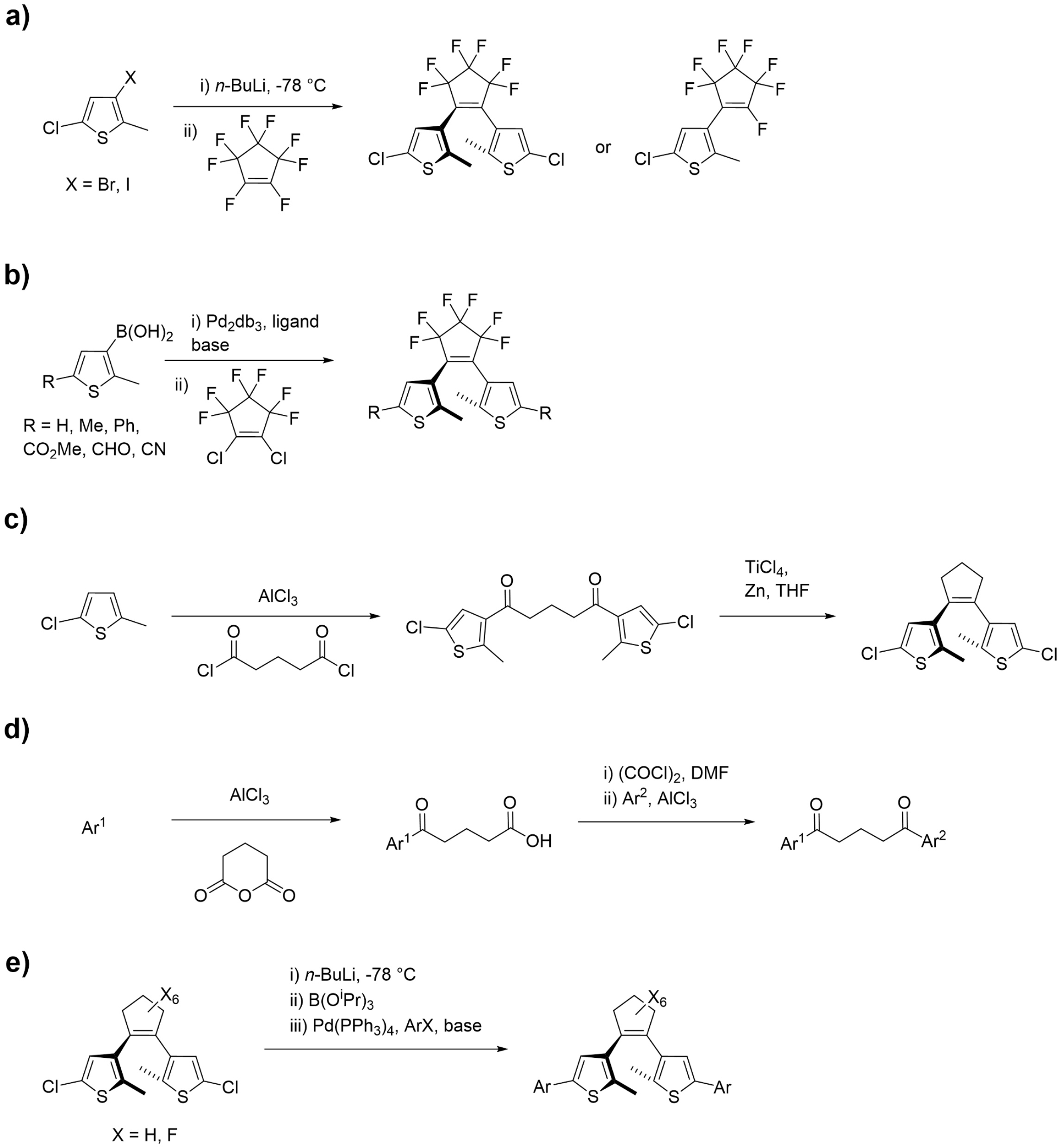
a)
X
Cl
S
X = Br, I
i) n-BuLi, -78 °C
ii)
F F F F F F F F
or
b)
B(OH)2
R
R = H, Me, Ph,
CO2Me, CHO, CN
i) Pd2db3, ligand
base
ii)
Cl Cl
c)
AlCl3
O O
TiCl4,
Zn, THF
d)
Ar1
AlCl3
OH
i) (COCl)2, DMF
ii) Ar2, AlCl3
Ar2
e)
X6
X = H, F
i) n-BuLi, -78 °C
ii) B(OiPr)3
iii) Pd(PPh3)4, ArX, base
Ar

Scheme 2-7: Different synthetic approaches towards DAEs.

Perfluorocyclopentene derived DAEs are amongst the most popular because they exhibit the highest reversible durability and photo-responsibility. Generally they are being synthesized by an organolithium reagent induced halogen-metal exchange on an aryl moiety followed by a nucleophilic addition/ elimination sequence employing octafluorocyclopentene, under moisture free conditions and low temperatures (**Scheme 2-7a**).[2] This route has proven also suitable for the synthesis of non-symmetrical DAEs and typically provides moderately reproducible yields. During the course of this work this approach was further improved and modified until reaching quantitative yields, the reader is referred to Chapter 3.1.2 for a detailed description of this optimized approach. However, the volatility of octafluorocyclopentene under ambient conditions as well as its high cost have promoted the development of palladium-catalyzed cross coupling of aryl boronic acids to dichlorohexafluorocyclopentene, being easier to handle and less expensive (**Scheme 2-7b**).[23a]

Perhydrocyclopentene derivatives can be synthesized under slightly milder conditions via Friedel-Crafts-acylation to the aryl moiety with glutaryl dichloride and subsequent McMurry Coupling (**Scheme 2-7d**).[27] The synthesis of non-symmetric cyclopentene DAEs is synthetically more challenging and was approached by a consecutive Friedel-Crafts ring-opening reaction of an aryl moiety to glutaric acid anhydride followed by generation of the acid chloride and a Friedel-Crafts acylation with the second aryl moiety (**Scheme 2-7d**).[40] Once the aryl moieties are connected to the central double bond, subsequent post-functionalization offers the possibility to readily introduce different substituents (**Scheme 2-7e**).[31] This is generally carried out by halogen-metal exchange of the remaining aryl-chloride with an organolithium reagent. This lithiated compounds are subsequently functionalized with an electrophile to introduce a convenient functional group for further conversion, such as palladium-catalyzed cross-coupling reactions.

2.2.3 Photochemical Properties

The photochemical properties of DAEs have been concisely studied with the main purpose of enabling the control of several chemical and physical properties.[41] Photoisomerization proceeds by means of an electrocyclic rearrangement of the included 1,3,5-hexatriene system to 1,3-cyclohexadiene. Accordant to Woodward Hoffmann's rules of maintaining orbital symmetry,[42] the cyclisation proceeds conrotatory through a photochemically excited state, which is only possible starting from the anti-parallel (a-p) conformer of the ring-open isomer (**Scheme 2-8**).

A thermal ring-closure would proceed disrotatory which does not occur due to the endergonic nature of the reaction. As mentioned earlier, depending on the substituents the cycloreversion can be photochemically or thermally induced. The photoactive a-p form and the photoinactive parallel (p) form are constantly equilibrating at ambient conditions due to a small rotational energy barrier. Cyclisation quantum yields between 0.1 to 0.5 are usually obtained, whereas 0.5 represents the highest reachable value if p and a-p conformers are present in a ratio of (1:1).[10] DAEs can further be effectively forced into the a-p conformation by including hydrogen bond formation in between the aryl unit and the bridge.[43] In the noteworthy examples shown in **Scheme 2-9** the cyclization quantum yield is raised to 0.83[43] and 0.98[44] by intramolecular conformational locking. However, due to the nature of hydrogen bonds, intramolecular interactions are weakened in polar and in protic solvents. Recently our group reported on a system that addressed this topic by employing steric repulsion of substituents incorporated in the bridge. Under this assumption, the cyclisation quantum yield of dithienylethenes could be raised up to 0.83.[45]

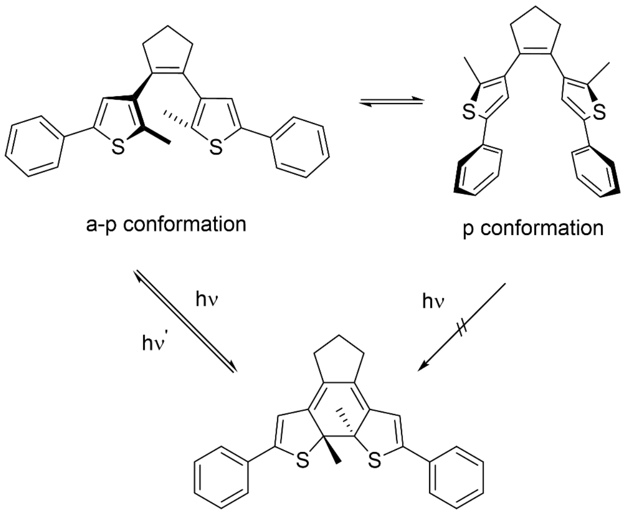

Scheme 2-8: Dynamic equilibrium between the p and a-p form with subsequent photocyclization from the a-p conformer only.

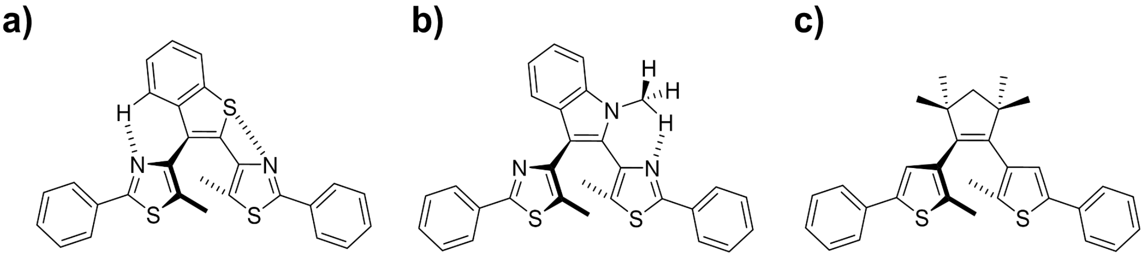

ϕ_{oc} = 0.98 (hexane)
ϕ_{oc} = 0.54 (methanol)

ϕ_{oc} = 0.83 (hexane)

ϕ_{oc} = 0.83 (acetonitrile)

Scheme 2-9: Populating the a-p- conformation of the ring-open isomer to increase photoisomerization quantum yield via a) combination of hydrogen bonding and S-N heteroatom interactions, b) hydrogen bonding, c) sterical overcrowding.

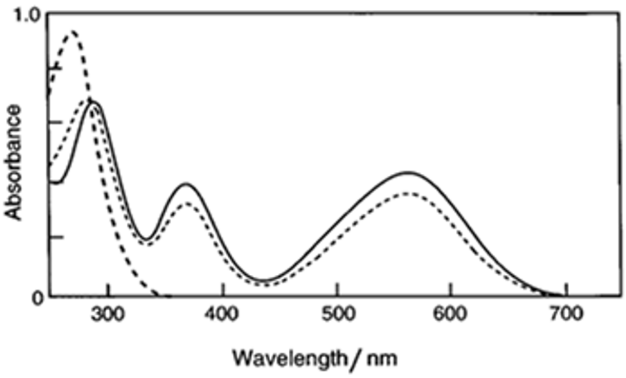

Figure 2-1: Absorption spectra of open-ring (broken line) and closed-ring (solid line) isomers and at the PSS (dotted line) by irradiation with 313 nm.

The absorption spectra of DAEs are characterized by short-wavelength absorptions of the colorless ring-opened isomers around 300 nm. Upon UV-light irradiation the cyclisation is initiated, shifting the $S_0 \rightarrow S_1$ to longer wavelengths originating a broadened and bathochromically shifted absorption band. The strongly colored closed isomer has a characteristic coloration dependent on the extent of conjugation in the system. By cyclisation, the π-conjugation is substantially increased along the whole molecular backbone. This change is rationalized by taking into account that in the open form DAEs are constituted by isolated heteroaromatic rings. Upon photoisomerization they change to an extended conjugated π-system resulting in an increase of the HOMO- and a decrease of the LUMO-energy level. Consequently, the energy gap becomes smaller and the absorptions shifts to larger wavelengths. Typical absorption spectra of both isomers of a DAE derivative are shown in **Figure 2-1**. Since both isomers absorb UV light, a PSS is established, with its composition being dependent on the cyclisation and cycloreversion isomerization quantum yields.

Applications of photoswitches rely on the possibility to reversibly influence properties of a given system. The property which quantifies the number of cycles a photoswitch can reversibly perform without losing substantial performance is called fatigue resistance. DAEs feature in general almost no side reactions during the photoisomerization process. Some derivatives can be switched more than 10^4 times in solution while preserving an absorption of 80% of their initial value. But it is important to mention that this excellent fatigue resistance does not apply for all switches of the DAE class. In some switches, a very specific side reaction can be observed (**Scheme 2-10**).[46]

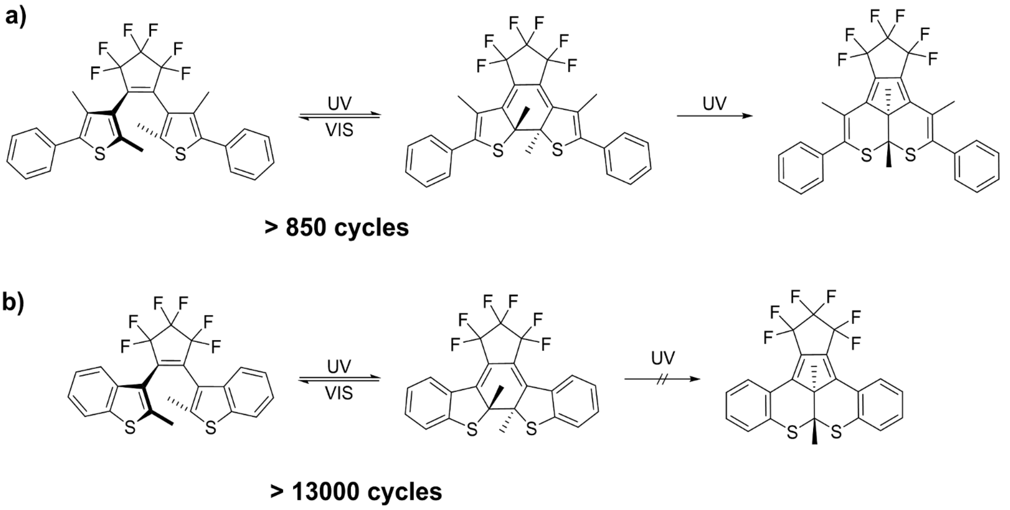

Scheme 2-10: Thiophene substituted DAEs undergo irreversible by-product formation, after a small amount of irradiation cycles, while b) benzo[b]thiophene derived DAEs do not show such degradation.[34]

The by-product shows an absorption band at similar wavelengths as the ring-closed isomer due to the almost identical conjugational system, but the optical density is reduced due to a smaller extinction coefficient.[47] Unfortunately, the by-product's mechanism of formation is still only scarcely investigated and is strongly dependent on the combination of aryl units, bridge moiety and substituents. This current lack of study makes it hardly predictable to design fatigue resistant DAEs bearing more sophisticated substitution patterns for novel applications.

2.3 Azobenzene Photoswitches

2.3.1 Molecular Structure

ABs are due to the presence of a N-N double-bond in their molecular structure classified as azocompounds. Aromatic azocompounds are intensively colored substances which are substantially more stable than their aliphatic analogues, which tend to decompose by elimination of N_2 gas at elevated Temperatures. The particular properties which ABs possess arise from being able to exist in two stable isomeric forms (Scheme 2-2a).[48] The Isomerization of the N-N double-bond can be achieved by means of electrochemical stimulation,[49] mechanical strain[50] or irradiation with light.[51] Photoisomerization is several orders of magnitude faster than the thermal *cis→trans* back isomerization, therefore both processes can be approximated as independent from each other. Because the thermal *cis→trans* back isomerization can never be completely suppressed, ABs are classified as T-type photoswitches. The geometry of the thermodynamically more stable *trans*-isomer is elongated and planar, whereas the *cis*-isomer has a distorted configuration to minimize steric repulsions, causing also a less delocalized electron density along the molecular backbone. The distance between C4 and C4' is diminished from 9 Å in *trans*-AB to 6 Å in *cis*-AB (**Scheme 2-11**).

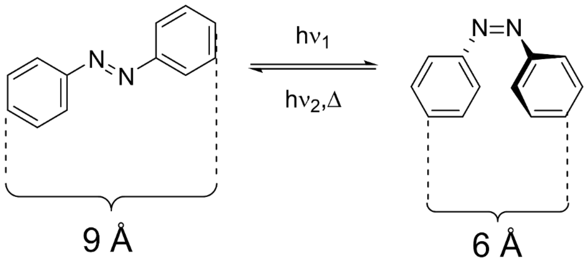

Scheme 2-11: Geometrical change of AB upon photoisomerization.

2.3.2 Synthesis of Azobenzenes

There are several efficient synthetic protocols available to synthesize ABs.[52] A distinction has been made between reductive and oxidative procedures. Meanwhile there are also Buchwald-Hartwig type Pd-catalyzed cross-coupling reactions which enable, after deprotection and oxidation of the coupling-products, the synthesis of ABs (**Scheme 2-12**).

One of the first and most widespread methods for the synthesis of ABs is the classical Azo-coupling. In this procedure, an aniline-derivative is diazotized and subsequently reacted in an electrophilic aromatic substitution (S_EAr) with an electron-rich phenole. Since diazonium-salts are weak electrophiles their reactivity has often to be increased by using acceptor-substituted electron-poor anilines for their synthesis. ABs obtained by this procedure bear therefore donor-acceptor substituents in their molecular structure.

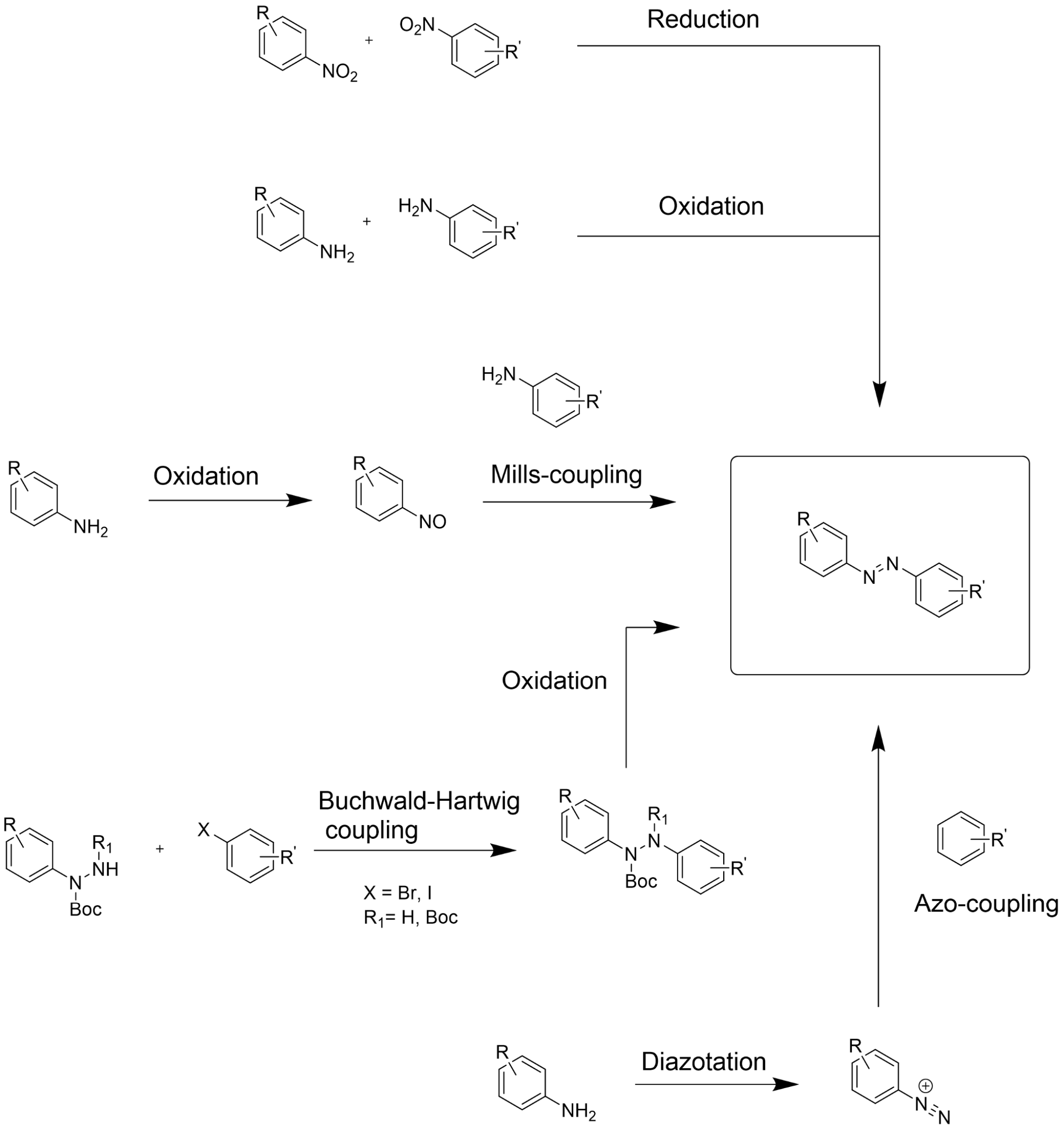
R
NO2
+
O2N
R'
Reduction
NH2
H2N
Oxidation
Oxidation
NO
Mills-coupling
N=N
Oxidation
Buchwald-Hartwig coupling
X = Br, I
R1= H, Boc
R1
NH
N
Boc
X
Azo-coupling
Diazotation
N≡N

Scheme 2-12: Synthetic routes towards the obtention of ABs.

Another very important synthetic route towards the obtention of ABs is the so called Mills-coupling. In this procedure an aniline is oxidized under very mild conditions, selectively, to the nitroso-compound. With this purpose the oxidant of choice was Oxone™ in a biphasic medium of DCM/ H_2O.[53] This mixture ensures the efficient separation of the water soluble aniline and hydroxylamine derivatives from water insoluble nitroso-compound. By this means condensation reactions of this species are prevented and the nitroso-compound is separated from the aqueous reaction medium, pushing the reaction equilibrium to the product-side. The reaction proceeds through nucleophilic addition of the NH_2-group of the aniline to the NO-group of the nitroso-compound. Subsequent H_2O-elimination yields the desired AB. During the course of this work, the conditions for this reaction have been optimized to afford quantitative yields in the synthesis of unreactive electron-poor non-symmetrical ABs. The optimized protocol will be discussed in detail in Chapter 3.2.2.

This synthetic procedure is also convenient for the obtention of *meta (m)*-substituted ABs and unlike other conventional procedures, it is also compatible with hydroxy and amino functionalities. Among other synthetic procedures for the obtention of symmetric ABs are the reductive or the oxidative azo-coupling, for the latter Ag_2CO_3, MnO_2 or hypervalent iodine-compounds are employed as oxidants. Unfortunately the yields are rather low with very long reaction times and harsh reaction conditions. Similarly for the reductive-coupling, nitro-aromatics are employed in combination with a reducing agent such as $LiAlH_4$, $NaBH_4$ or Zn/ NaOH. The strongly basic conditions of this procedure impose a reduced functional group tolerance. The Buchwald-Hartwig-type cross-coupling reaction enables the synthesis of hydrazine derivatives, which are readily oxidized to the corresponding AB. Hereby a Boc-protected hydrazine is reacted with an aryl-halogenide in the presence of a Pd-catalyst, a base and a ligand. Subsequent deprotection of the Boc-group yields the diphenylhydrazine which is then oxidized in presence of NBS/ pyridine or CuI/ Cs_2CO_3 to the AB.

2.3.3 Photochemical Properties

The two isomers of ABs can be switched with particular wavelengths of light: ultraviolet light, which corresponds to the energy gap of the π-π^* (S_2 state) transition, for *trans→cis* conversion, and blue light, which is equivalent to that of the n-π^* (S_1 state) transition, for *cis→trans* isomerization. Substituents on the AB have a dramatic influence on the thermal half-life, spectral shape and isomerization mechanism. Taking the relative energies involved in the n- π^* and π-π^* transitions, a classification into normal AB (nAB), amino AB (aAB) and pseduostilbenes (ppAB) can be performed (**Scheme 2-13**). ABs enjoy an outstanding photostability, which even after prolonged irradiation times, photodegradation can be neglected.

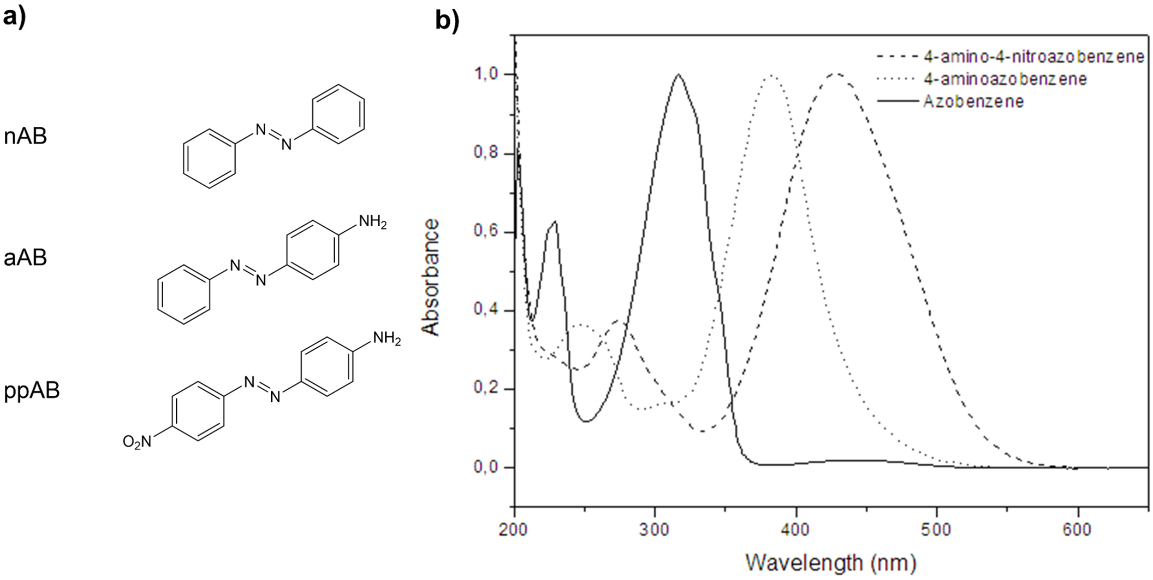

Scheme 2-13: a) Examples of the different AB-types and b) their corresponding absorption spectra.

2.3.3.1 Normal Azobenzenes

Normal azobenzenes (nAB) possess in their *trans*-form two well separated bands. The symmetry forbidden n- π^* transition (S_1 state) is localized in the visible region of the spectrum (ε_{450} = 400 L mol^{-1} cm^{-1}). This transition is allowed due to the distortions in the planar molecular geometry and the coupling of the ^{1}(π-π^*)-state (S_2 state) with the ^{1}(n- π^*)-state.[54] The much more intense band in the UV-region, which is symmetry allowed (ε_{310} = 22000 L mol^{-1} cm^{-1}) is ascribed to the π-π^* transition. Photoisomerization can be achieved either by addressing the S_1- or the S_2-state. However, photoisomerization from the S_1 state is more efficient and has a higher photoisomerization yield. This observation is a contradiction to Kashas rules.[55]

By contrast, the *cis*-form has a hypsochromically shifted and significantly lower intensity π-π^* transition (ε_{270} = 5000 L mol^{-1} cm^{-1}, ε_{250} = 11000 L mol^{-1} cm^{-1}). The n- π^* transition (ε_{450} = 1500 L mol^{-1} cm^{-1}) is much more intense in this form which is caused by the deformation of the bent structure, which can be even further enhanced by 2- and 2'-substituents in the AB.[56] Photoisomerization in this form can be also achieved either by addressing the S_1- or the S_2-state.

The mechanism involved in the *trans→cis* photoisomerization is yet unclear and many studies have been performed to achieve its elucidation. The two major isomerization pathways involve either the rotation or the inversion of the N-N double-bond (**Scheme 2-14**).[57]

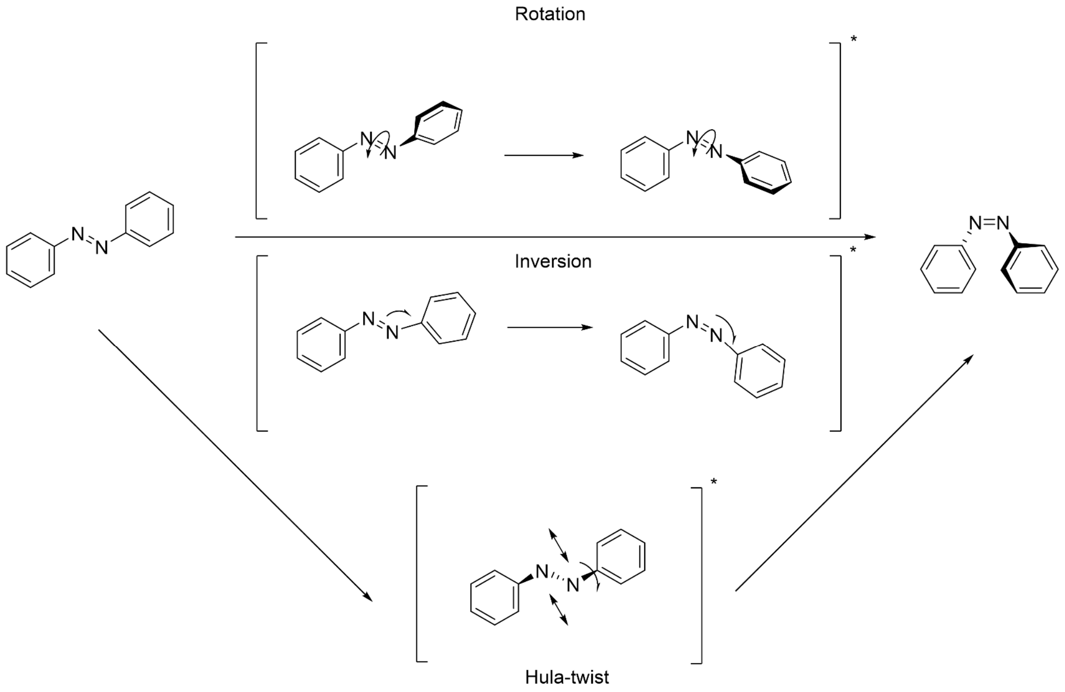

Scheme 2-14: Rotation and inversion mechanisms involved in the *trans→cis* isomerization of AB.

The rotation mechanism comprises the cleavage of the π-bond of the N-N double-bond, the so formed N-N single-bond can now freely rotate. During the rotation, the dihedral angle of the C-N-N-C chain is changed, while the N-N-C angle is fixed at 120°.[58] For the example of the inversion mechanism the N-N-C angle is increased to 180° and the C-N-N-C dihedral is fixed at 0°. As a result of this configuration, a sp-hybridized Nitrogen is formed.[59] Besides this two mechanisms, in literature there is also found the concerted inversion and the inversion assisted rotation mechanism.[57,60]

To explain the wavelength dependent quantum yields, it was stipulated that two from the excited-state dependent inversion mechanisms are responsible during the photoisomerization. Employing transient spectroscopy and quantum mechanical calculations it was proven that the $S_2 \rightarrow S_1$ process has a quantum yield close to 1.0.[55,61] A closer examination of the transition energies in relation to the dihedral and bond angles pictures that no conical intersection is formed for the pure inversion mechanism.[57,62] A rotation dominated mechanism is therefore involved. After excitation of the AB into the S_2-state, the transition into the S_1-state proceeds along different geometries depending on the substituents. If large C-N-N-C dihedral angles are present, then the $S_1 \rightarrow S_0$ transition leads to the *trans*-form.[55] For small dihedral angles, the $S_1 \rightarrow S_0$ transition leads to the *cis*-form. If the photoisomerization is addressed by direct excitation to the S_1-state, less excess energy is available for the formation of small dihedral angles. Due to a preferential formation of large C-N-N-C dihedrals, a substantial increase of the *trans*-form is observed and hence the overall quantum yield is lower for the formation of the *cis*-form. Through this discussion it is possible to explain the deviation of Kashas rule. However, this mechanism is unable to explain how rotation-hindered ABs, with sterically demanding substituents in 2- and 2'-position do not suffer a substantial reduction of the quantum yield. Similarly ABs embedded in a solid-matrix or with covalently-bridged phenyl-rings are also able to efficiently switch. Because of this divergences, a concerted inversion mechanism is currently being discussed by different research groups.[63] In this mechanism a pedal-like movement is involved, which requires little volume to proceed and would be able to explain the isomerization of rotation-hindered ABs. A significative breakthrough demonstrating the validity of the hula-twist isomerization pathway was recently achieved by transient spectroscopy measurements, where the excitation dynamics were proven to be independent of the solvent viscosity.[64]

The discussion for the *cis*→*trans* isomerization is more straightforward, as theoretical and experimental results point towards a purely rotation governed mechanism.[65] In the case of the thermal *cis*→*trans* isomerization an inversion mechanism is involved. The isomerization was independent of the polarity, viscosity and the influence of sterically hindered substituents.[66]

2.3.3.2 Aminoazobenzenes

Aminoazobenzenes (aAB) are those ABs which have in *ortho* (*o*)- or *para* (*p*)-position an amino-, hydroxy- or alcoxy-substituent. The most significant difference is observed in the ~70 nm bathochromically shifted π-π* transition which overlaps the unchanged n-π* transition. This class of ABs exhibit a large solvatochromic effect upon varying solvent polarity.[67] It was also observed that the substitution pattern of the aAB influences the mechanism of *trans→cis* photoisomerization. In the case of 4-aminoazobenzene the rotation mechanism is responsible for the process whereas for 4-(*N,N*-dimethylamino)azobenzene the inversion mechanism is preferred.[68] The *cis→trans* thermal isomerization is much faster in this class of ABs and displays a large solvent dependence. 4-(*N,N*-dimethylamino)azobenzene has a thermal half-life ranging from minutes up to hours, depending on the type of solvent employed.[68]

2.3.3.3 Pseudostilbenes

ABs with electron donating and electron accepting substituents are classified as pseudostilbene azobenzenes (ppAB). Caused by the donor-acceptor substitution pattern a strong CT-band is originated which is bathochromically shifted and completely overlaps the n-π* transition. According to theoretical studies ppAB photoisomerize *trans→cis* by a rotation mechanism. However, experimental confirmation is still pending.[68] The thermal *cis→trans* isomerization is remarkably fast in this class of ABs, observing a large solvent influence. The determined thermal half-lifes for this compounds range the ms timescale. Protonated or complexated ppABs with a lewis acid, exhibit a similar behavior, where the n-π* band disappears and the π-π* transition is bathochromically shifted.[69]

2.3.3.4 Visible Light Addressable Azobenzenes

In the previous examples at least one of the forms in the AB required the irradiation of UV light for the photoisomerization, or the thermal back-reaction was so fast that without irradiation the system could not be isolated. The development of visible light fully addressable bistable ABs which avoid the poorly penetrating and cell-damaging UV light has been a topic of much interest in recent years. One possibility is to combine ABs with photosensitizers, for a thorough description the reader is referred to Chapter 2.7.2. Another strategy follows the approach of splitting the n-π* absorption bands of the *trans*- and *cis*-isomers, which overlap in the 400-500 nm region. The separation of the two n-π* bands unlocks the possibility to address selectively in both forms the S_1 state with visible light.[70] This was accomplished by the introduction of o-substituents in the AB structure. The first examples include an ethylene-bridged AB[71] and a tetra-*o*-methoxy AB (**Scheme 2-15**).[70] It was extraordinary that for the tetra-*o*-methoxy AB, the absorptions maximum of the n-π* band in the *trans*-form was shifted to 480 nm while improving significantly the thermal half-life (14 days in DMSO). Furthermore the *cis*-form had a 36 nm blue-shifted n-π* band which enabled the *trans→cis* photoisomerization with 530 nm light (PSS = 80%, *cis*-form) and the *cis→trans* isomerization with 430 nm light (PSS = 85% *trans*-form).[70a] The red-shifted n-π* band in the *trans*-form is originated by the repulsion of the nonbonding electron pairs of the azo double-bond with the methoxy-groups which raises the relative energy of the HOMO. Photoisomerization to the *cis*-form reduces the repulsion and the n-π* band is consequently in the expected wavelength-region for *cis*-ABs.

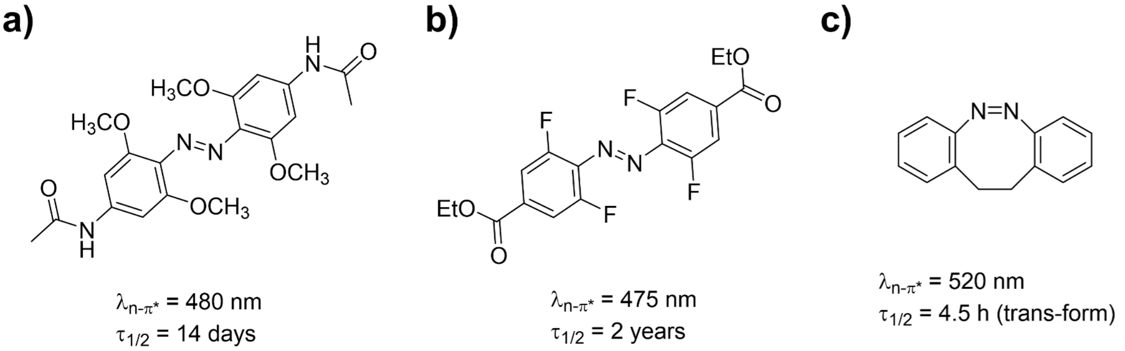
a)
H
N
O
H3CO
H3CO
N=N
OCH3
O
N
H
OCH3
$\lambda_{n-\pi^*}$ = 480 nm
$\tau_{1/2}$ = 14 days
b)
EtO
F
O
F
N=N
F
EtO
F
O
$\lambda_{n-\pi^*}$ = 475 nm
$\tau_{1/2}$ = 2 years
c)
N=N
$\lambda_{n-\pi^*}$ = 520 nm
$\tau_{1/2}$ = 4.5 h (trans-form)

Scheme 2-15: Bistable with visible light fully addressable ABs. a) tetra-*o*-methoxy AB,[70] b) tetra-*o*-fluoro AB[72] and c) ethylene-bridged AB.[71]

An improved system was attained by Bléger et al. by the introduction of four *o*-fluorine substituents in the AB (**Scheme 2-15b**).[72] It was anticipated that electron-withdrawing groups (EWGs) such as *o*-fluorine would stabilize the nonbonding orbital of the *cis*-form and thereby increase the energy of the n-π* band. In fact, the *cis*-form had a 42 nm blue-shifted n-π* band (**Figure 2-2**). This additional effect was rationalized due to the diminished electron density of the nonbinding orbitals caused by the strong –I effect of the fluorine-atoms. Irradiation of the *trans*-form with visible light (λ > 500nm) generated 91% of the *cis*-form, whose thermal half-life was extraordinary long (~2 years).

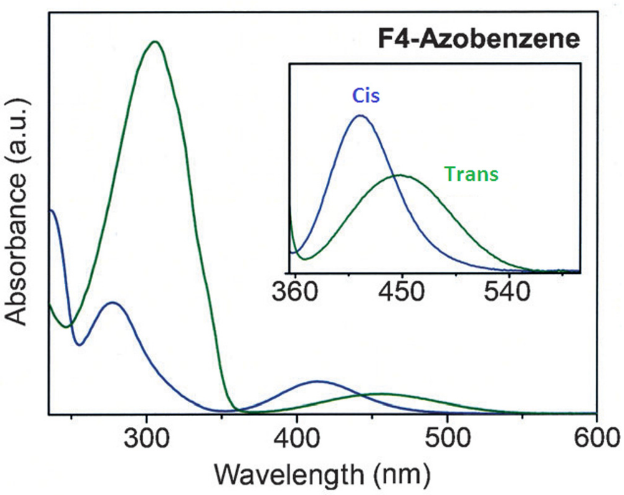

Figure 2-2: Absorption spectra of *trans*- and *cis*-tetra-*o*-fluoro AB.[72]

The ethylene-bridged AB is also fully addressable by visible light, interestingly in this case the stability of the *cis*-form is greatly enhanced. The ethylene-bridge constrains the molecule and achieves that the *cis*-form is thermodynamically more stable.[71]

2.3.4 Electrochemical Properties

The electrochemical behavior of ABs has been by far less studied than the photochemical properties. Mullier published in 1978 that *cis*-AB in aprotic solvents could be reduced to the radical anion by a one-electron process in an electrochemical cell.[73] He successfully reduced *cis*-AB forming the radical-anion and made the observation that this radical-anion rapidly isomerized to the *trans*-form of the AB. Furthermore he observed that the so formed radical-anion of the *trans*-form reacted with other neutral *cis*-form ABs, initiating a cascade of events where rapidly the whole mixture was converted to the *trans*-form (**Scheme 2-16**).

1) $$\text{cis} + e^{-} \longrightarrow \text{cis}^{\cdot -}$$

2) $$\text{cis}^{\cdot -} \longrightarrow \text{trans}^{\cdot -}$$

3) $$\text{trans}^{\cdot -} + \text{cis} \longrightarrow \text{trans} + \text{cis}^{\cdot -}$$

Scheme 2-16: 1) Electrochemical behavior of *cis*-AB upon reduction and 2) subsequent electrochemical isomerization to the radical-anion *trans*-form. 3) Generation of neutral *trans*-form by transfer of one electron to non-reduced *cis*-form.

He made this assumption supported by the fact that even if the reduction potential of the *cis*-form is different than that of the *trans*-form, only the peak corresponding to the reduction potential of the *trans*-form was observable. Performing afterwards a more concise study upon varying temperature (-22 °C) and very fast scan-rates he was able to observe the reduction potential corresponding to the *cis*-form, which interestingly was more cathodic than for the *trans*-form. It was noteworthy that the reduction potential of the *trans*-form was independent of the temperature. He estimated that the life-time of *cis*-AB radical anions is in the order of 0.1 ms at room temperature, which is much more rapid than for other radical anions derived from C-C double-bonds, usually in the order of seconds at room temperature. The oxidation of the *cis*- and *trans*-forms was unchanged upon varying temperature and scan-rates and the difference between them is very small. This actually means that the difference between reduction and oxidation becomes larger for *cis*-AB than for *trans*-AB. He concluded that the rate for heterogeneous electron transfer (ET) is smaller for *cis*-AB than for *trans*-AB (**Scheme 2-17**).

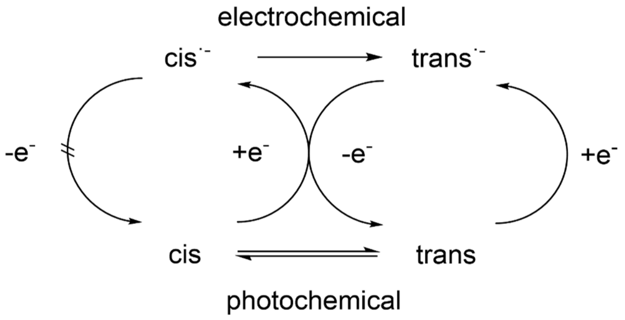

Scheme 2-17: Electrochemical pathway for *cis→trans* isomerization of ABs. Radical-anion of *cis*-form is unable to revert back to neutral *cis*-form.

Based on these findings a very detailed study on the *cis→trans* electrochemical isomerization of arylazosulfides was published by Hapiot in 1997.[74] He was able to show by means of spectroelectrochemistry the clear conversion of the *cis*- into the *trans*-isomer and identified this process as electrocatalytic. Scanning the potential towards negative values, the spectrum of the *cis*-isomer is observed from -0.50 V vs. Fc/ Fc$^+$ to about -1.0 V vs. Fc/ Fc$^+$; at this potential located well in front of the azosulfide reduction wave, a sudden increase of the intensity is observed and the spectrum of *trans*-isomer is built-up. At more negative potentials, the spectrum of the radical anion is observed and on the reverse scan *trans*-isomer is essentially restored (**Figure 2-3**). The reader is referred to Chapter 3.2.2 for examples of this process in the current work.

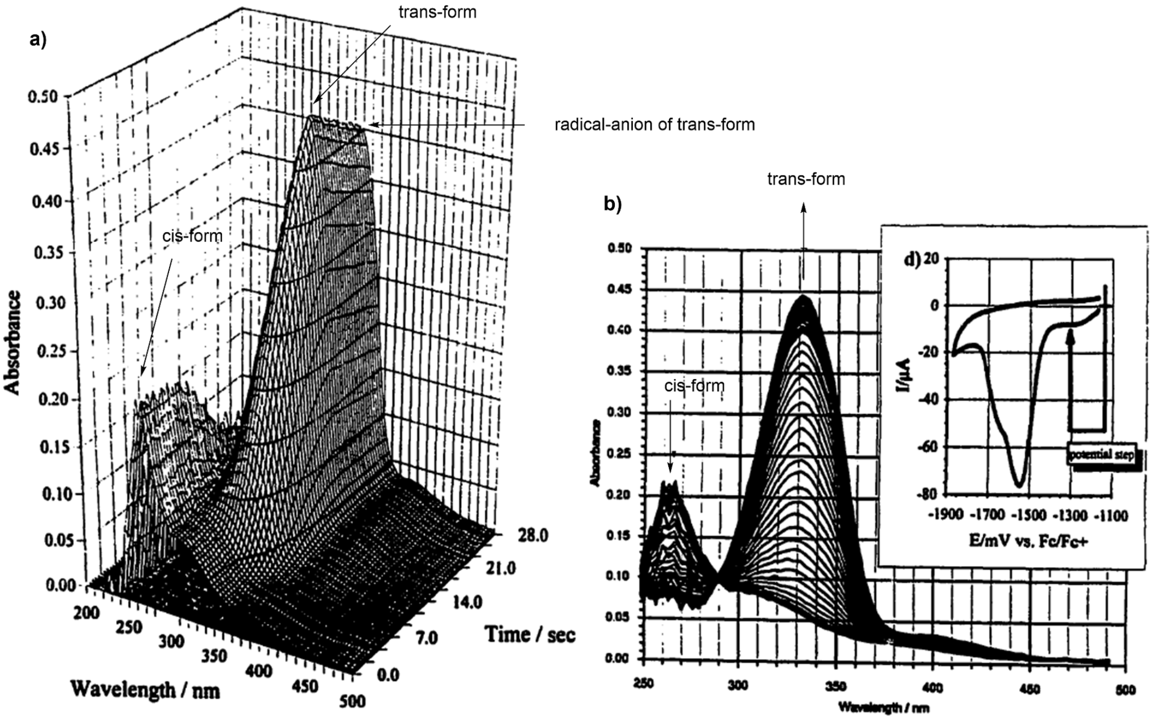

Figure 2-3: Spectroelectrochemical reduction of *cis*-azoarylsulfide. a) Starting form a pure *cis*-mixture upon reaching its reduction potential, rapidly all *cis*-form is converted to the *trans*-form. Subsequently the reduction of the *trans*-form proceeds. b) Spectral-change upon reaching the reduction potential required for the *cis*-form reduction, inset is the cyclic voltammogram corresponding to the applied potential.[74]

Since then further examples of this mechanism have been made with other types of ABs and it was even possible to switch *cis*-AB in liquid crystals under a low applied electrical-field without supporting electrolyte.[75] The resulting variation of transmittance reveals the effect of the electric-field-induced *cis→trans* isomerization. With each pulse. When the electric field is on, the transmittance of the mixture drops to the dark state due to the homeotropic orientation of liquid crystal molecules, whereas when the field is off, the transmittance increases due to orientational relaxation of liquid crystal molecules. Interestingly, after six electric pulses, the transmittance does not recover to the level corresponding to the two-phase morphology formed after UV irradiation inducing *trans→cis* photoisomerization; instead it reaches the initial transmittance of the homogeneous mixture before UV irradiation, which indicates complete conversion of the *cis*-AB back to the *trans*-isomer (**Figure 2-4**).

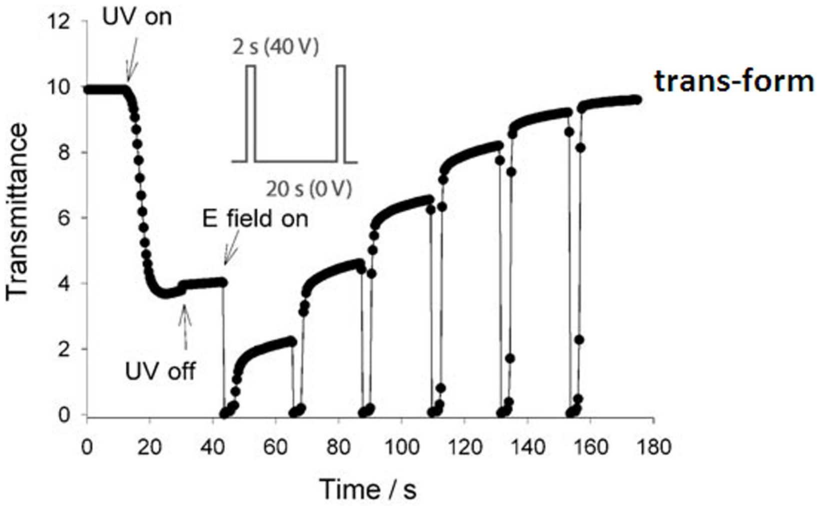

Figure 2-4: AB derivative in nematic liquid crystal BL006. Changes in transmittance (633 nm probe light) in response to UV irradiation and subsequent electric pulses (8 V μm^{-1}, 2 s duration).[75]

Illustrative examples for the catalytic electrochemical *cis→trans* isomerization under an applied external electrical field can be found for ABs in amphiphiles[76] and azobenzene doped liquid crystals dispersed in polymers.[77]

2.4 Elemental Photophysical Processes

2.4.1 Excitation Energy Transfer

An essential process that occurs in the excited state is the transfer of excitation energy. Whenever the emission spectrum of a donor fluorophore overlaps with the absorption spectrum of another molecule, termed as an acceptor (**Scheme 2-18**) excitation energy transfer takes place. The acceptor of the excitation energy does not need to be fluorescent. However, if the acceptor is fluorescent, it will result in the emission of light by the acceptor. A distinction should be made between heterotransfer and homotransfer, and between radiative and non-radiative transfer. Non-radiative energy transfer does not involve emission of light by the donor. Therefore it is not the result of donor emission being absorbed by the acceptor. There is no intermediate photon in non-radiative energy transfer. The donor and acceptor are coupled by a dipole-dipole interaction and the rate of energy transfer depends upon the extent of spectral overlap of the emission spectrum of the donor with the absorption spectrum of the acceptor, the quantum yield of the donor, the relative orientation of the donor and acceptor transition dipoles, as well as the distance between the donor and acceptor molecules. The distance dependence of non-radiative energy transfer has resulted in its widespread use to measure distances between donors and acceptors.[78] The efficiency of this energy transfer is inversely proportional to the sixth power of the distance between donor and acceptor, making it extremely sensitive to small changes in distance.

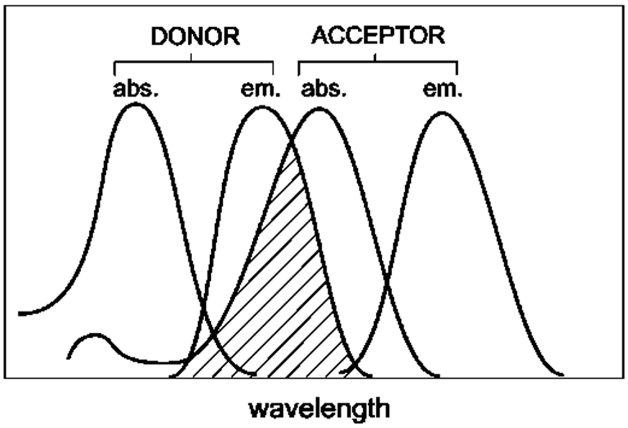

Scheme 2-18: Overlap integral between the emission spectrum of the donor and the absorption spectrum of the acceptor.

2.4.1.1 Energy Transfer Mechanisms

Heterotransfer involves the energy transfer from an excited molecule D* (donor) to another that is chemically different, which is defined as A (acceptor). Conversely homotransfer takes place when the transfer of energy occurs from an excited molecule D* to a chemically identical molecule D (**Scheme 2-19**).

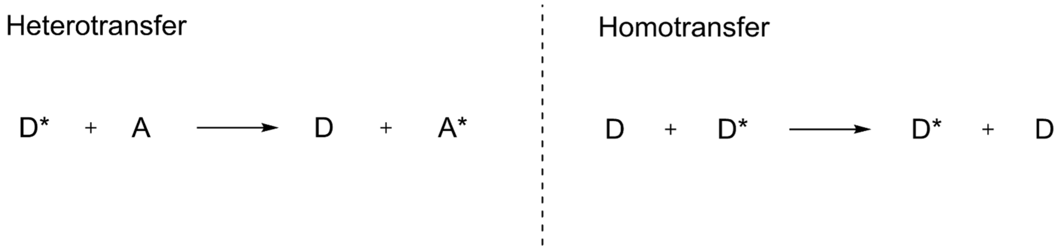
Heterotransfer
$D^* + A \longrightarrow D + A^*$
Homotransfer
$D + D^* \longrightarrow D^* + D$

Scheme 2-19: Possible scenarios for excitation energy transfer between molecules.

Radiative transfer is a two-step process (**Scheme 2-20**), a photon is emitted by a molecule D and is subsequently absorbed by a molecule A. It does not require any interaction between the molecules and it depends on the spectral overlap and the concentration of the sample.

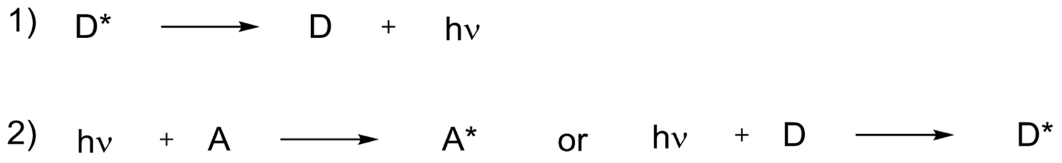
1) $D^* \longrightarrow D + h\nu$
2) $h\nu + A \longrightarrow A^*$ or $h\nu + D \longrightarrow D^*$

Scheme 2-20: Description of the radiative trivial energy transfer mechanism.

As result of this transfer a decrease of the donor fluorescence intensity in the region of spectral overlap is observed. Such a distortion of the fluorescence spectrum is called the inner filter effect and is strongly dependent on the concentration. In the case of radiative transfer between identical molecules, the fluorescence decays more slowly as a result of successive re-absorptions and re-emissions hereby the fluorescence anisotropy is also affected.

Depending on the specific system and range between donor and acceptors two main energy transfer mechanisms can occur (**Scheme 2-21**).

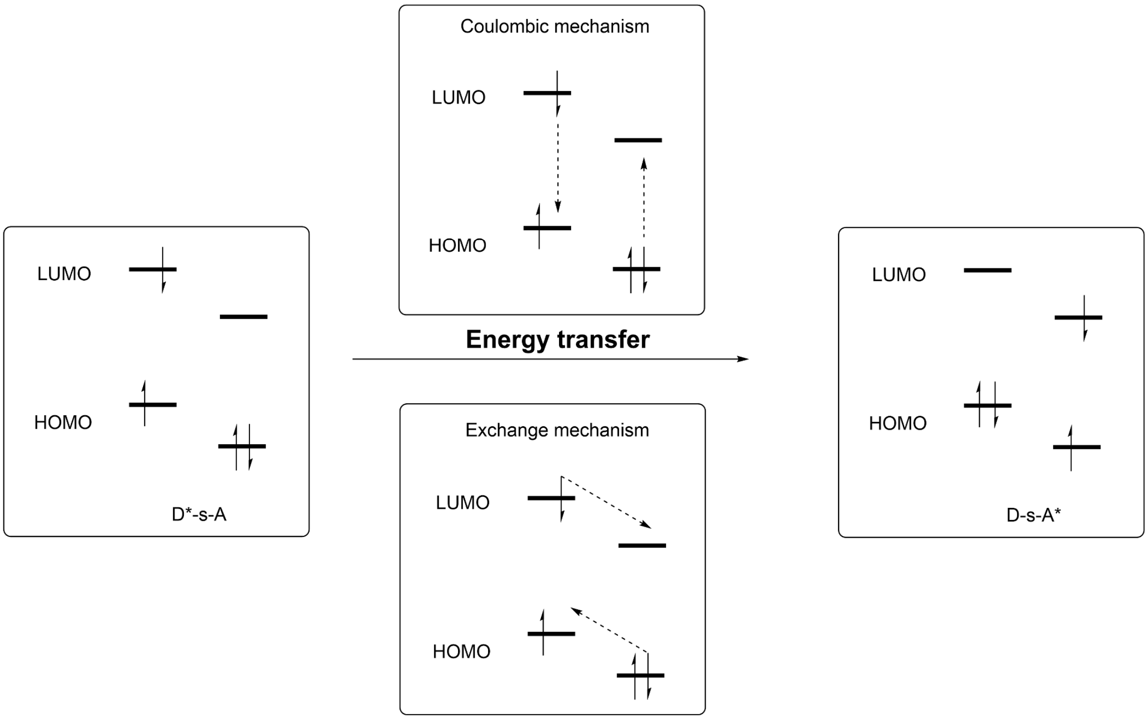

Scheme 2-21: Representation of the coulombic and exchange energy transfer mechanisms.

The quantitative foundations of molecular electronic energy transfer were laid by Theodor Förster from 1946, and as homage to his contributions non-radiative energy transfer is generally called FRET (Förster Resonance Energy Transfer) which is explained by the coulombic mechanism. FRET is based on the concept of a fluorophore as an oscillating dipole, which can exchange energy with another dipole with a similar resonance frequency. The Förster theory treats the limit in which there are only Coulombic interactions, meaning that the molecules are far enough from each other to have no orbital overlap (electrons are unambiguously on one molecule or the other).This process takes place at distances less than the wavelength and results from short- or long-range interactions between molecules. FRET is possible at distances up to nearly 20 nm. The transfer of excitation energy requires some interaction between a donor molecule and an acceptor molecule, and it can occur if the emission spectrum of the donor overlaps the absorption spectrum of the acceptor, so that several vibronic transitions in the donor have the same energy as the corresponding transitions in the acceptor and are coupled (**Scheme 2-22**). A high intrinsic probability is achieved if the spectral overlap between donor and acceptor is maximized.[79]

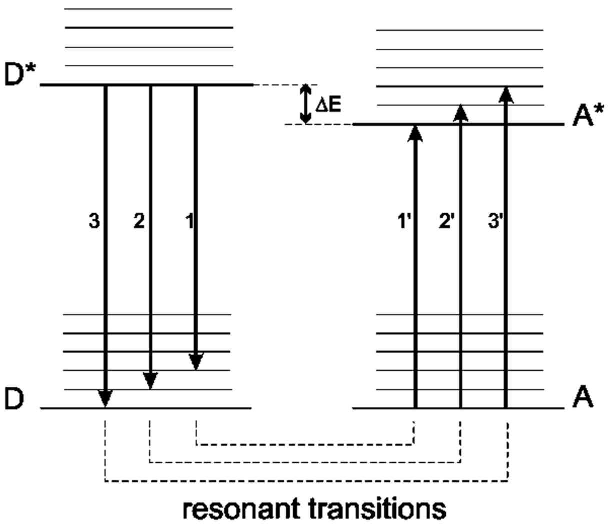

Scheme 2-22: Energy level scheme of donor and acceptor molecules showing the coupled transitions in the case where vibrational relaxation is faster than energy transfer.

FRET is best understood by considering a single donor and acceptor separated by a distance *r*. The rate of coulombic energy transfer for a donor and acceptor separated by a distance *r* is given by

$$k_T^C(r) = \frac{\phi_D \kappa^2}{\tau_D r^6}\left(\frac{9000\,\ln(10)}{128\,\pi^6 N_{Av} n^4}\right)\int_0^\infty F_D(\lambda)\varepsilon_A(\lambda)\lambda^4\,d\lambda \qquad (2.4.1.1)$$

where ϕ_D is the quantum yield of the donor in the absence of acceptor, *n* is the refractive index of the medium, N_{Av} is Avogadro‘s number, τ_D is the fluorescence lifetime of the donor, $F_D(\lambda)$ is the corrected fluorescence intensity of the donor in the wavelength range λ to λ + $\Delta\lambda$, with the total intensity (area under the curve) normalized to unity; $\varepsilon_A(\lambda)$ is the extinction coefficient of the acceptor at λ, which is typically in units of M^{-1} cm^{-1}; κ^2 is a factor describing the relative orientation in space of the transition dipoles of the donor and acceptor and is usually assumed to be $\frac{2}{3}$, which is appropriate for dynamic random averaging of the donor and acceptor.[78] The overlap integral $J(\lambda)$ expresses the degree of spectral overlap between the donor emission and the acceplor absorption.

$$J(\lambda) = \int_0^\infty F_D(\lambda)\varepsilon_A(\lambda)\lambda^4\,d\lambda = \frac{\int_0^\infty F_D(\lambda)\varepsilon_A(\lambda)\lambda^4\,d\lambda}{\int_0^\infty F_D(\lambda)\,d\lambda} \qquad (2.4.1.2)$$

In calculating $J(\lambda)$, the corrected emission spectrum with its area normalized to unity should be used. For convenience (2.4.1.1) is written in terms of the Förster distance Ro. at which the transfer rate $k_T^C(r)$ is equal to the decay rate of the donor in the absence of acceptor $(\tau_D)^{-1}$, at this distance one-half of the donor molecules decay by energy transfer and one-half decay by the usual radiative and non-radiative rates.

$$R_0^6 = \left(\frac{9000\ \ln(10)\phi_D\kappa^2}{128\ \pi^5 N_{Av} n^4}\right) J(\lambda) \tag{2.4.1.3}$$

For convenience equation (2.4.1.3) is simplified by substitution of the physical constants employed and if the wavelength is expressed in nm then R_0 is expressed in Å with

$$R_0 = 0.211\ \left(\phi_D \kappa^2 n^{-4} J(\lambda)\right)^{1/6} \tag{2.4.1.4}$$

For fixed distances between donor-acceptor pairs, such as labeled proteins, the energy transfer efficiency E can be determined by measuring the relative fluorescence intensity of the donor in the absence F_D and presence of the acceptor F_{DA}.

$$E = 1 - \frac{F_{DA}}{F_D} \tag{2.4.1.5}$$

Short-range energy transfer or with very weak coupling is called Dexter-type and is explained with the exchange mechanism. This process requires a wavefunction overlap between donor and acceptor, which means it only occurs in short distances. The exchange interaction can be viewed as a double ET process, where one-electron moves from the LUMO of the excited donor to the LUMO of the acceptor, and the other from the acceptor HOMO to the donor HOMO (Scheme 2-21).Which is given by

$$k_T^{Ex} = \frac{4\pi^2}{h}(H^{En})^2 J_{Ex}(\lambda) \tag{2.4.1.6}$$

where H^{En} is obtained from the electronic coupling between donor and acceptor, which is exponentially dependent on distance

$$H^{En} = H^{En}\ (0) e^{\left[-\frac{\beta_{En}}{2}(r-r_0)\right]} \tag{2.4.1.7}$$

and $J_{Ex}(\lambda)$ is the Dexter spectral overlap, where the emission spectrum of donor and absorption spectrum of acceptor, are both normalized to unity, so that the rate constant for Dexter-type energy transfer is independent of the oscillator strength of both transitions

$$J_{Ex}(\lambda) = \int_0^{\infty} F_D(\lambda)\varepsilon_A(\lambda)\, d\lambda \qquad (2.4.1.8)$$

The spin selection rules for this type of mechanism arise from the need to obey spin conservation in the reacting pair as a whole. As the transition dipole moments are not involved, the Dexter mechanism is operative even for spin-forbidden situations involving triplet states. (**Scheme 2-23**).[80]

$$\mathrm{D(T_1)^*\ -\ s\ -\ A(S_0)} \xrightarrow[\text{Exchange mechanism}]{\text{triplet-triplet energy tarsfer}} \mathrm{D(S_0)\ -\ s\ -\ A(T_1)^*}$$

Scheme 2-23: Spin forbidden triplet-triplet energy transfer, enabled by Dexter-type energy transfer.

2.4.1.2 Applications

Because FRET can be reliably assumed to depend on the sixth power of distance, the transfer efficiency is used for structural determinations in measuring distances between sites in proteins,[81] the protein folding,[82] the relative orientation,[83] macromolecular associations[84] and enhanced acceptor emission studies.[85] By this means, it is also possible to determine the energy transfer for donor-acceptor pairs in random solutions. In this regime the term A_0 is employed, which denotes the critical concentration and represents the acceptor concentration that results in 76% energy transfer. This concentration, in moles per liter can be calculated from

$$A_0 = \frac{3000}{2\pi^{3/2} N_{Av} R_0^3} \qquad (2.4.1.8)$$

this expression evidences that the acceptor concentrations need to be very high for energy transfer between unlinked donors and acceptors. For measuring intermolecular FRET effects, the inner filter effect has to be considered due to the high acceptor concentrations and resulting high optical densities.

2.4.2 Photoinduced Electron Transfer

Photoinduced electron transfer (PET) is a key step in photosynthesis, which allows converting solar light into chemical energy. It can be considered as one of the simplest chemical reactions, as it does not involve the breaking and forming of any chemical bonds. Instead, it is the transfer of an electron from a donor to an acceptor. Furthermore, it is a fundamental mechanism responsible for the fluorescence quenching or enhancement of fluorophores when photoactive materials interact with light. The Marcus theory gives a quantitative description of the rate constant of ET in solution if the interaction between the donor and acceptor if the encounter pair is weak.[86] PET causes charge separation and is followed by spontaneous back-ET reactions that regenerate the initial ground-state. To describe the ET process from a donor to an acceptor, Libby[87] and later Marcus[88] developed a model (**Scheme 2-24**).

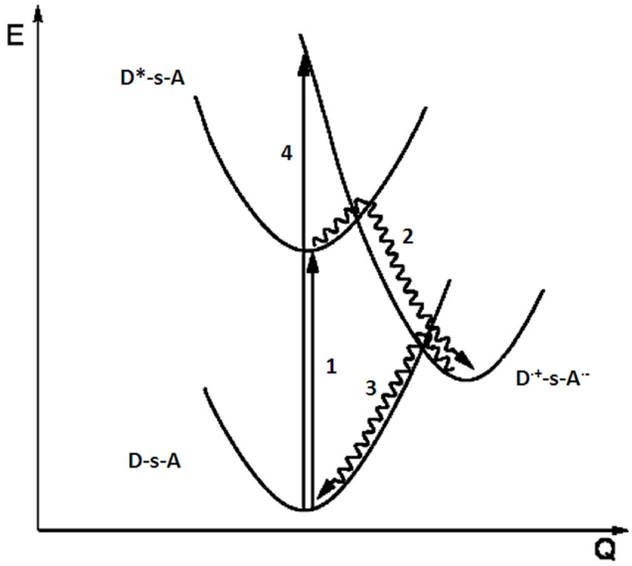

Scheme 2-24: Marcus model for ET processes. 1) photoexcitation; 2) photoinduced ET; 3) thermal back-ET; 4) Libby model.

The main difference between the Libby and Marcus theory is originated by the assumption that in the Libby model a first steep vertical energetic jump has to be paid to reach directly the product curve. Without any consideration of the thermal energy required. Whereas the Marcus' theory makes this consideration, requiring much lower energy to achieve the transition state for ET. Therefore thermal energy is used to reorganize the molecular structure and the solvent structure along the reaction coordinate to overcome the crossing energy barrier at the crossing point of the product and reactant curves. More details on optical ET and related topics can be found in the literature.[89]

2.4.2.1 Electron Transfer Mechanisms

In a given donor-spacer-acceptor molecule, ET is an intrinsically adiabatic process,[90] in which the rate of ET is governed by its distance dependence. If there is strong dependence the mechanism proceeds via tunneling, whereas if the distance dependence is weak, the process can be ascribed to a hopping mechanism.

The tunnel effect mechanism is often referred to as of super-exchange, where the transfer of electrons from the donor is promoted along an energetically isolated spacer or bridge. During the ET the orbitals of the bridge are solely employed as a coupling medium without any nuclear motion or rearrangement.[91] The incoherent, sequential or hopping ET involves intermediate states with a defined nuclear rearrangement of the bridge and the medium. These states have to be energetically accessible and promote structural changes in the molecule.

The superexchange mechanism (**Scheme 2-25**) was first defined by Kramers and afterwards by Anderson.[87] Herein, the charge will never be localized on the spacer, therefore, the states formed during the ET along the bridge to reach the acceptor are virtual states.

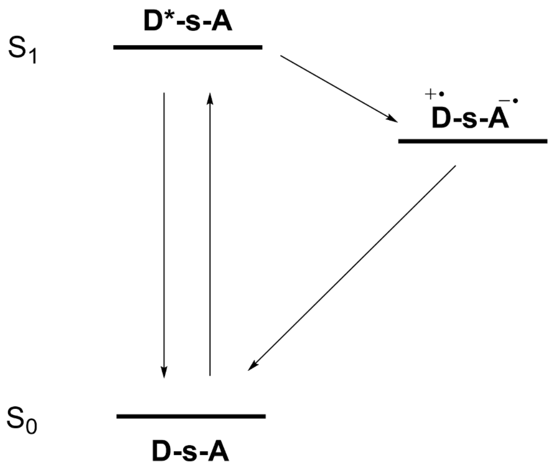

Scheme 2-25: ET according to the superexchange mechanism.

The larger the spacer, the higher is the probability that a hopping mechanism is involved in the ET. According to Jortner,[92] the ET takes place when i) there is an almost resonant charge injection, ii) there is a significant vibrational overlap between the states of the ionic pairs where the charge is localized in each sequential step along the spacer, iii) a vibrational overlap exists between the last states of the ionic pair when the charge is localized on the spacer and the acceptor. Therefore this mechanism is sensitive to the charge diffusion from the donor to the acceptor. When the molecule is excited, a first ET from the donor to the spacer takes place. Thereby the radical-anion of the spacer and the radical-cation of the donor are formed. Afterwards, a second ET proceeds from the spacer radical-anion to the acceptor, forming the final charge-separated state (**Scheme 2-26**).

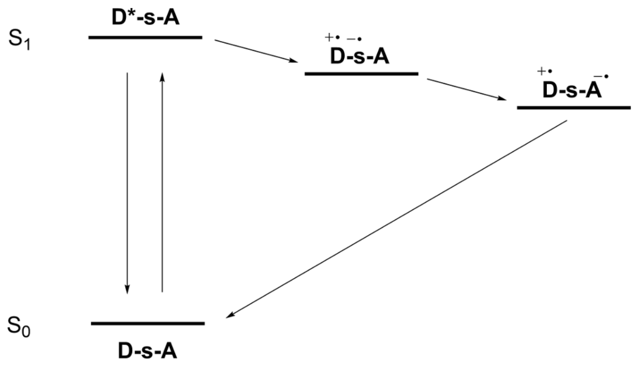

Scheme 2-26: Sequential ET mechanism.

Consequently, if the energy barrier involved between the spacer and the acceptor is very large, the super-exchange mechanism would be more favorable. Additionally, if the molecular reorganization energy is comparable to the energy involved in each step of the hopping mechanism, both the superexchange and hopping mechanism would be competing, causing little distance dependence in the rate. When there is complete mixing among the donor-bridge-acceptor orbitals (large coupling limit) the bridge essentially acts as an incoherent molecular wire, as happens for conjugated conducting polymers, and the system is expected to behave according to an ohmic regime where the distance dependence of the rate varies inversely with bridge length.[93]

2.4.2.2 Applications

The most important application of PET is the conversion of solar energy into either chemical energy (stored in fuels) or electricity (photovoltaics). Artificial photosynthesis is the process to efficiently harvest and convert light into energy by means of photovoltaic cells.[94] Furthermore, PET is a redox reaction which is of essential interest in biology, as it is involved in many metabolic processes such as ATP synthesis and enzymatic activity.[95] It also plays an important role in industrial proceedings such as polymerization, photography or electrochemistry.[96] It also finds widespread use in the design of fluorescent indicators and sensors.[97] The reverse process to PET is displayed by light emitting diodes (LED)[98]. In this devices potential gradients are used to create excited states that decay by light emission.

2.4.3 Fundamentals of Two-Photon Absorption

Shortly after the foundation of the quantum theory of light was set, Maria Göpert-Mayer postulated in 1931 the possibility that two photons whose frequency addition equaled the excitation frequency required for a given nuclear transition, where able to achieve the excitation in the same way as only one photon could.[99] However, it was several decades later when the Laser was developed and a high intensity monochromatic light source was available, when her theory could be proven (**Scheme 2-27**).[100]

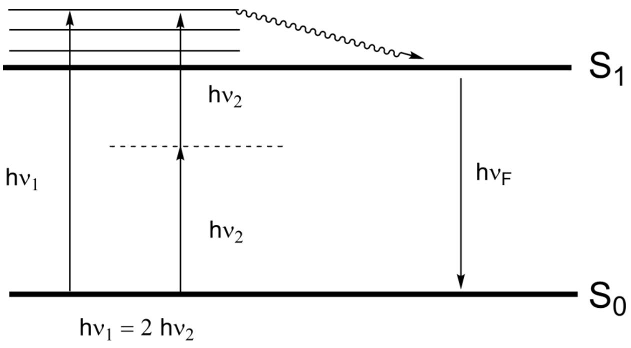

Scheme 2-27: Jablonski diagram for two-photon excitation.

Light can be viewed as an oscillating electric field. As light passes through matter, that oscillating field induces polarization in the medium. For weak light intensities, the electromagnetic radiation induces a macroscopic polarization P in the material, which is proportional to the electric field E of the light and related to it through the electric susceptibility χ. For an intense field, the relation is no longer linear, but is expressed as a Taylor expansion of P as a function of E (Eq. 2.4.3.1). The first order electric susceptibility is responsible for the linear polarization, while the higher order susceptibilities (χ^2, χ^3...) account for the nonlinear effects.

$$P = P_0 + \chi E + \chi^2 E^2 + \chi^3 E^3 + \cdots \qquad (2.4.3.1)$$

On a molecular scale, the molecular polarization μ is used to describe this properties (Eq. 2.4.3.2). In the first term, μ_0 is the intrinsic dipole of the molecule. The coefficient α determines the response of the molecule to an external electric field. The coefficient β and γ are, respectively, the hyperpolarizability and the second hyperpolarizability of the molecule.

$$\mu = \mu_0 + \alpha E + \beta E^2 + \gamma E^3 + \cdots \qquad (2.4.3.2)$$

The molecular term β determines the efficiency of the two-photon absorption (2PA), and therefore chemists focus their efforts in maximizing this value. It has to be noted that β will be zero for molecules with a center of symmetry.[101]

2.4.3.1 Two-photon Absorption Cross-Section

The amount of light absorbed in any plane at a distance z is proportional to the incident intensity at this plane. Focusing the beam of light changes the size of the beam but does not change the amount of light passing through a plane, being the emission intensity constant at all positions across the cuvette. This process can be described as follows

$$\frac{dI(z)}{dz} = -\alpha I(z) - \beta I^2(z) - \gamma I^3(z) - \cdots \qquad (2.4.3.3)$$

where z is the direction of the light beam with intensity *I*, and α, β, γ are the absorption coefficients for the one-, two- or three-photon absorption of the medium. For the case where no linear absorption is possible (α = 0) and only 2PA is taking place, we can describe as follows

$$\frac{dI(z)}{dz} = -\beta I^2(z) \qquad (2.4.3.4)$$

which states that the amount of light absorbed by the medium is proportional to the square of the intensity of the incident light. As a result, focusing the beam of light decreases its size but also increases its intensity. Resulting in a not constant amount of light absorbed across the cuvette, which has a maximum of incident light intensity at the focal point of the laser beam (**Scheme 2-28**). This effect generates a strongly localized excitation.

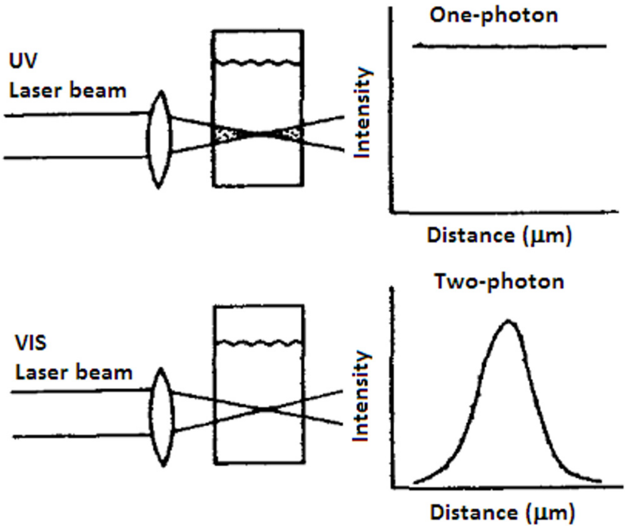

Scheme 2-28: Schematic comparison of one- and two-photon excitation.

β is a wavelength dependent coefficient, which depends on the concentration of absorbing molecules. The 2PA cross-section $\sigma^{(2)}$ of a molecule is independent of the concentration and is defined as

$$\beta(\lambda) = \sigma^{(2)'}(\lambda) N_{Av} c \cdot 10^{-3} \qquad (2.4.3.5)$$

where N_{Av} ist Avogadro's constant and c is the molar concentration of the sample. In most cases $\sigma^{(2)'}$ is multiplied with the photon energy as follows:

$$\sigma^{(2)}(\lambda) = \sigma^{(2)'}(\lambda) \cdot h\upsilon \qquad (2.4.3.6)$$

The units for the 2PA cross-section are cm^{4}s and are usually in the range of 10^{-51} to 10^{-46} cm^{4}s. The corresponding SI-unit is the GM or Göppert-Mayer, where 1 GM = 10^{-50} cm^{4}s.

The determination of $\sigma^{(2)}$ can be performed either by the measurement of the nonlinear transmission by means of the "open" or "closed" Z-scan technique[102] or by the two-photon excited fluorescence method.[103] As outcome of a collaboration from this work, a new methodology was developed, where by means of transient spectroscopy it was possible to relate the bleach signal with $\sigma^{(2)}$ enabling the determination of absolute 2PA cross-sections.

2.4.3.2 Design of Two-Photon Chromophores

As previously mentioned the 2PA cross section $\sigma^{(2)}$ is a molecular property and hence it is controlled by the molecular structure. The permanent ground-state dipole moment and the transition dipole connected to the ground state or the excited state are theoretically considered to be key factors in the 2PA of a molecule.[104] Under this consideration, push-pull chromophores have the largest dipole moment change during a transition, and therefore are commonly introduced in the backbone of 2PA-chromophores. Extension of the π-bridge to increase the separation of the donor-acceptor units is beneficial as it leads to states with extended charge separation. However, to avoid a detrimental effect the molecule has to remain coplanar.[105] Hence, the most frequently employed structural motifs for two-photon materials are donor–bridge–acceptor (D–π–A) dipoles, donor–bridge–donor (D–π–D) and donor–acceptor–donor (D–A–D) quadrupoles as well as two- or three-dimensionally branched octupoles (**Scheme 2-29**).

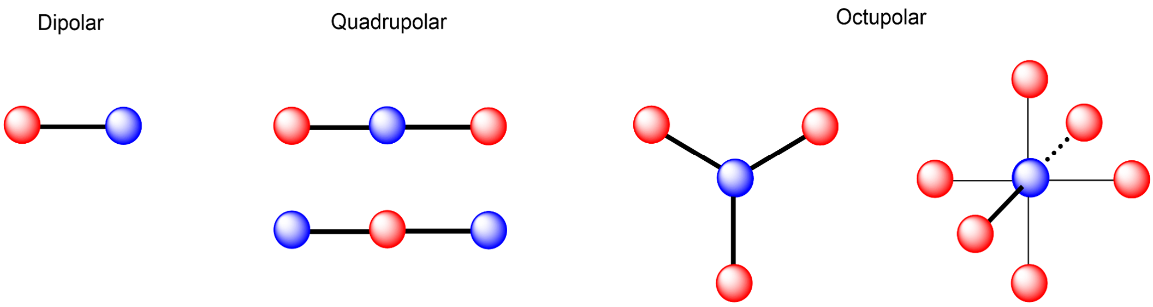

Scheme 2-29: Schematic representation of the most common design architectures in organic 2PA-chromophores. Red circles are electron-rich moieties and blue circles are electron-poor moieties. The black lines represent π-bridges.

Due to their chemical stability and high electron density the most commonly used donor-units in 2PA-chromophores are fully-substituted amines (alkyl or aryl). Acceptor-groups such as cyano-, nitro- or malononitrile-groups are commonly incorporated to the backbone. These functional groups resemble highly efficient electron-accepting properties and readily form in conjunction with electron-donors intramolecular charge transfer bands. Polarizable π-bridges such as biphenyl, fluorenyl, dihydrophenanthrenyl or thienyl linked by double- or triple-bonds have been employed to increase the conjugation length.

Dipolar 2PA-chromophores are those linear and planar molecules who resemble a strong charge transfer band. This property is inherent to conjugated molecules which have at each side of the molecule a strong electron-donor and a strong electron-acceptor (**Scheme 2-30**).[103]

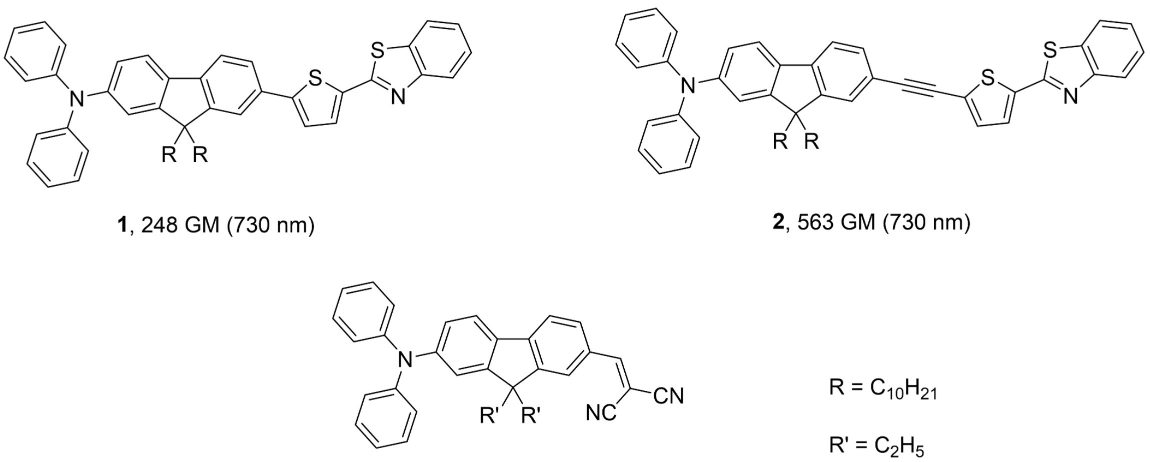

1, 248 GM (730 nm)

2, 563 GM (730 nm)

3, 615 GM (800 nm)

R = $C_{10}H_{21}$

R' = C_2H_5

Scheme 2-30: Representative dipolar 2PA-chromophores. Absorption maxima at which the $\sigma^{(2)}$ was determined are in brackets.[103]

On hand of these molecules it can be seen how an increase of the conjugation length from **1** to **2**, with an additional triple-bond, or an increase of the acceptor-strength like in **3**, introducing a malononitrile moiety, increases the $\sigma^{(2)}$.

Brédas, Marder, Perry and co-workers simultaneously described high $\sigma^{(2)}$ for symmetrical structures based on the direct correlation between large changes in quadrupole moment during photoexcitation and the 2PA cross section.[106] Accordingly, such quadrupolar molecules with alternating vinyl and 1,4-arylene groups as the π-bridges between two identical electron-pulling or electron-pushing terminal groups are favored as more two-photon responsive chromophores (**Scheme 2-31**). In addition, quadrupolar compounds have higher fluorescence quantum yields relative to corresponding dipolar compounds, most likely due to cancellation of D–A dipoles which otherwise would tend to induce charge transfer quenching of fluorescence.[107]

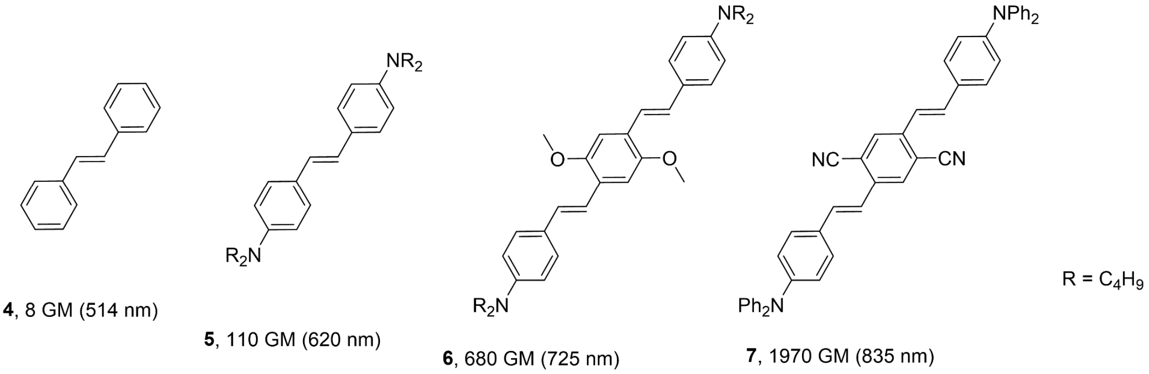

4, 8 GM (514 nm)

5, 110 GM (620 nm)

6, 680 GM (725 nm)

7, 1970 GM (835 nm)

Scheme 2-31: Representative quadrupolar 2PA-chromophores. Absorption maxima at which the $\sigma^{(2)}$ was determined are in brackets.[106]

Increase of the quadrupolar moment by substituting **4** with two electron-rich dialkylamine-units dramatically enhanced the $\sigma^{(2)}$ of **5** and led to an additional red-shift of the 2PA-maximum. Furthermore, an improved $\sigma^{(2)}$ was observed if the quadrupolar charge distribution was enhanced. This was achieved by introducing an electron-rich in **6** or an electron-poor core in **7**. For compound **7** the effect was even more pronounced due to the alternating D-A-D substitution pattern which promotes a high quadrupolar moment.

Multidimensional conjugation and the use of molecular branching to further enhance the cross section values of 2PA molecules were first demonstrated in the three-branched structures (**Scheme 2-32**).[108] Octupolar 2PA-chromophores comprise the unification of the dipolar and quadrupolar design principles with the added dimensionality. Thus, two or more dipolar molecules are joined together with extended conjugation. The flow of intramolecular charge transfer can be either from the ends to the center of the molecule or vice versa ("outside in" or "inside out"). These types of 2PA chromophores are octupolar when their overall molecular geometry belongs to the following symmetry classification: (octahedral) O_h, (tetrahedral) T_d, trigonal planar D_{nh} (n: 3, 4, ...), and trigonal bipyramid (C_{3h}).[109]

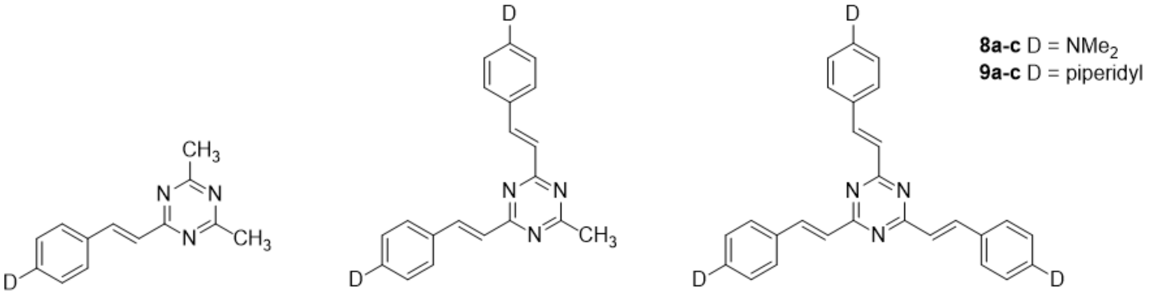

8a, 343 GM
9a, 363 GM

8b, 1140 GM
9b, 1345 GM

8c, 2405 GM
9c, 2523 GM

Scheme 2-32: Three-branched octupolar 2PA-chromophores. Cooperative effects where observed along the series, with a larger increase of the overall $\sigma^{(2)}$ than the sum of the individual branches.[108]

In strongly coupled octupolar chromophores a cooperative effect was observed. The nonlinear increase of the $\sigma^{(2)}$ can be evidenced in the series of compounds **8** and **9**. The synergistic interactions between the 2PA units via conjugation or perhaps through-space electronic interactions have been exploited using dendritic structures and also has been investigated and validated with novel dendrimers and hyperbranched polymers.[110]

2.4.3.3 Applications

There are multiple application fields for two-photon materials and depending on the application further properties have to be considered in their design (absorbance, fluorescence, photostability, solubility and biocompatibility). These compounds are largely employed in the second-harmonic generation or frequency doubling of lasers,[111] optical limiting in microfabrication procedures[112] as well as in the 3D data-storage[113] or even photodynamic therapy.[114] One of the main driving-forces for the expansion of 2PA-materials was the advances achieved in microscopy.[115]

Excitation with the double of wavelength than for the one-photon process, reduces irradiation damage, increases penetration depth and diminishes scattering because biological samples are transparent in the NIR-range. Furthermore the required light-intensity for the 2PA is only achieved in the focal point of the laser, which allows an extraordinary high 3D-resolution.

2.5 BODIPY Fluorophores

Among the numerous classes of highly fluorescent dyes, the family based on 4,4-difluoro-4-bora-3a,4a-diaza-s-indacene,[116] better known as boron-dipyrromethene (BODIPY) (**Scheme 2-33**),[117] has outstanding properties as a candidate in a DAE-fluorophore dyad. The robustness against light and chemicals, the relatively high molar extinction coefficients and fluorescence quantum yields, negligible triplet-state formation, narrow emission bandwidths with high peak intensities, small stoke-shift, good solubility, resistance towards self-aggregation in solution, excitation/ emission wavelengths in the visible spectral region (above 500 nm), fluorescence lifetimes in the nanosecond range as well as solvent independent fluorescence emission and well-studied photophysical behavior, define the BODIPY unit as an excellent fluorophore for gated fluorescence readout.[118]

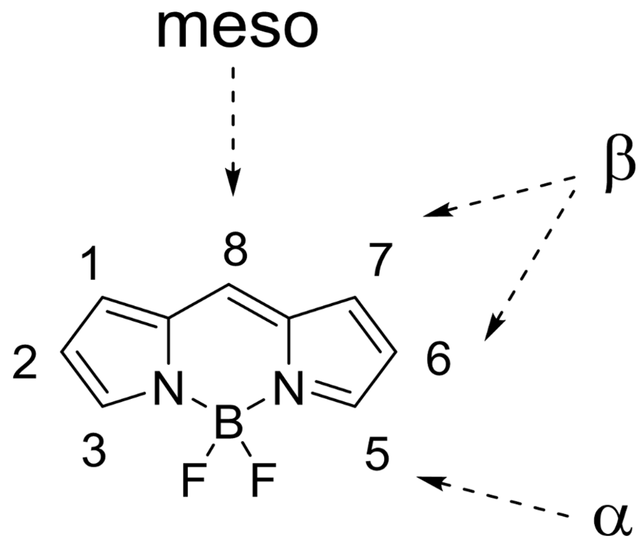

Scheme 2-33: Representation of the BODIPY framework with IUPAC numbering. The 8-position is often specified as *meso*. The 3,5-positions are sometimes referred to as α, while β is used to denote the 2,6-positions. All the positions of the BODIPY core are possible sites for functionalization.

BODIPY dye fluorescence has been extensively studied and there are many examples of gated fluorescence control by means of intramolecular fluorescence quenching mechanisms including ET and energy transfer. [119] These processes can be exploited in conjunction with a photoswitch and will be discussed later in Chapter 2.7.1.

2.5.1 Molecular Structure

In 1968, Treibs and Kreuzer noticed that the acylation of 2,4- dimethylpyrrole **10**, with acetic anhydride and boron trifluoride as Lewis acid catalyst, resulted in the formation of a highly fluorescent compound **13**, rather than the desired acylated pyrroles **11**.[120] The compound arose from an acid catalyzed condensation of pyrroles **10** and **11** to dipyrrin **12**, followed by complexation with a boron difluoride unit to give the dye **13** (**Scheme 2-34**).

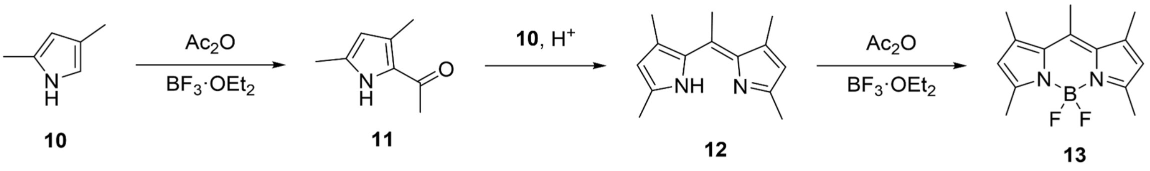

Scheme 2-34: First described one-pot synthesis of a BODIPY.

BODIPYs are uncharged (**Scheme 2-35**), and their characteristics are mostly independent of solvent polarity. The complexes are stable in physiological *p*H-range, only decomposing in strong acidic and basic conditions.[121] Furthermore, biological studies have shown that these compounds have a low toxicity, and are compatible with in vivo studies. [122]

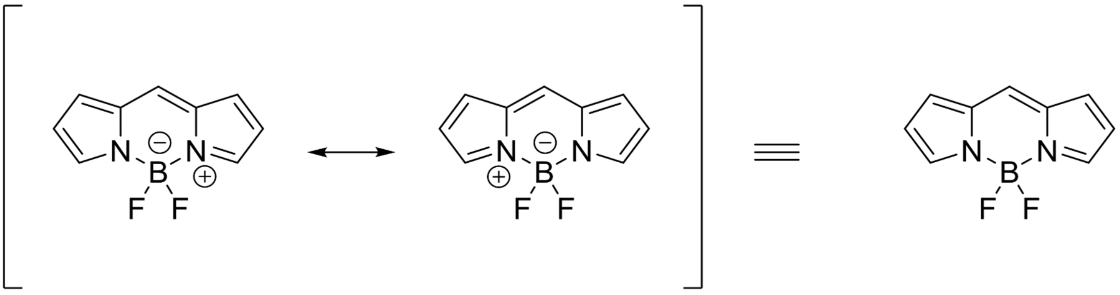

Scheme 2-35: The equivalent resonance structures are generally depicted as an uncharged form.

The single crystal X-ray structure of BODIPY indicates a fused ring based framework with strong π-electron delocalization within the central six-membered and two adjacent five-membered pyrrole rings of the dipyrromethene unit (**Schene 2-36**).[123] This π-electron delocalization is interrupted between both B-N bonds. A deviation from planarity is found for the unsubstituted BODIPY chromophore which exhibits a saddled geometry due to the boron atom deviating from the indacene plane by a 4.8° angle. The average bond length of N1-C3 indicates double bond character, compared with the single-bond character of N1-C4. The molecule displays two slightly different B-F bond distances. The bond angles of N1-B1-N2 and F1-B1-F2 indicate a distorted tetrahedron BF_2N_2 configuration. Although BODIPY resembles a typical monomethine cyanine dye with 6 π-electron delocalized over 5 atoms, the actual fluorophore is found to be isoelectronic with heptamethine cyanines, with 12 π-electron equally distributed over 11 atoms.[124]

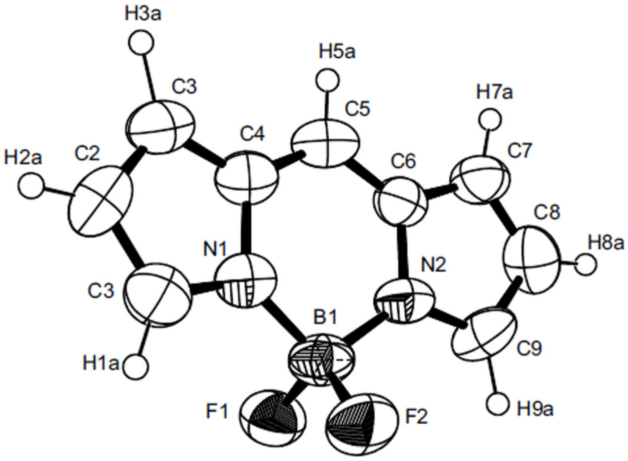

Scheme 2-36: X-ray crystal structure of unsubstituted BODIPY with atom labels and 50% probability displacement ellipsoids.[124]

Substitution at the *meso*-position of the BODIPY has no influence in ground-state characteristics of the BODIPY (absorption and emission remain unaltered) due to the orthogonal geometry of the *meso* substituent and the BODIPY fluorophore, which results in poor electronic conjugation between the two moieties. Conversely, substitution at the α and β positions has a dramatic influence in the spectral properties of the BODIPY. Similarly, aromatic ring fusion of the pyrroles promotes the bathochromic shift of absorption and emission of the BODIPY. A further structural modification involves the exchange of the C-meso with a nitrogen atom, which generates a sub-class of BODIPY dyes commonly called aza-BODIPYs. Due to structure similarity with phthalocyanines, this subclass of BODIPYs could also be referred to as semi-phthalocyanines. The remarkable feature of this dye system is its intense absorption and emission bands in the 650 - 850 nm range.

2.5.2 Synthesis of BODIPYs

Synthetic approaches to the BODIPY framework are generally based on the well-known chemistry of pyrroles and dipyrromethanes, which are synthetic precursors of porphyrins and related macrocyclic compounds. Starting from readily available pyrroles, a variety of dipyrromethene ligands can be obtained, which after complexation with BF_3 in the presence of a non-nucleophilic base, generate the required parent BODIPY fluorophore.

Symmetric BODIPY dyes substituted at the *meso*-position (**Scheme 2-37**) are usually prepared by acid-catalyzed condensation of pyrroles with acid chlorides, anhydrides or aldehydes to generate the dipyrromethene. Alternatively, dipyrromethanes are obtained from aldehydes which are subsequently oxidized to the dipyrromethene. In order to avoid further unwanted polymerizations, the pyrroles have to be substituted at the C-2 position.[125] In the final step, dipyrromethenes are converted to BODIPY dyes by the action of a non-nucleophilic base and $BF_3 \cdot OEt_2$. BODIPY dyes bearing substituents at the *meso*-position often display enhanced stability with respect to their *meso*-unsubstituted counterparts.

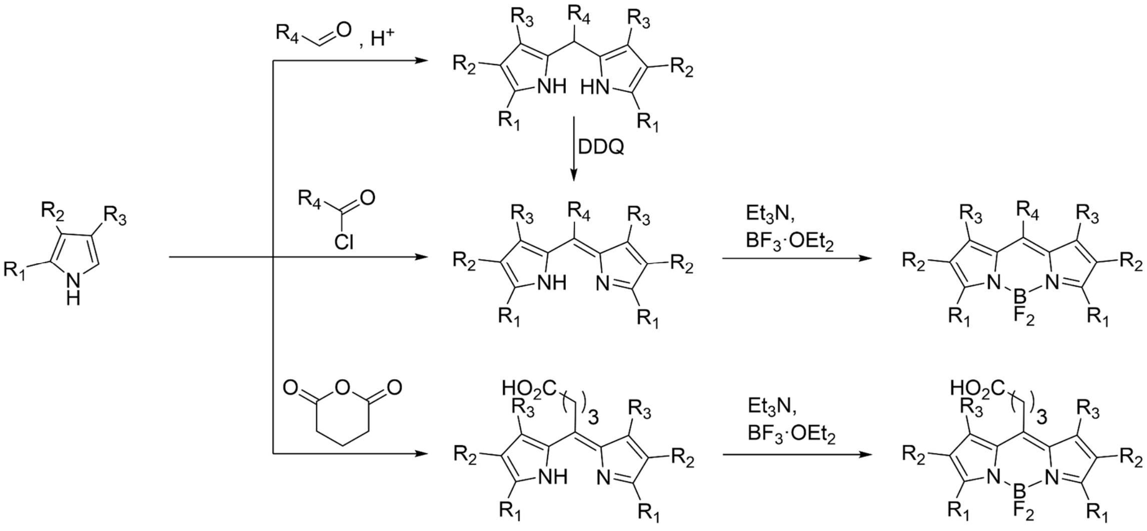

Scheme 2-37: Different synthetic approaches towards symmetric BODIPYs.

Non-symmetric BODIPY dyes, substituted or unsubstituted at the *meso*-position, are usually obtained by the MacDonald coupling, which is an acid-catalyzed condensation of a pyrrole- 2-carbaldehyde with an α-free pyrrole.[126] The desired dipyrromethene is obtained which on complexation with $BF_3 \cdot OEt_2$ in the presence of a base, affords the required BODIPY dye (**Scheme 2-38**). Yields for these reactions are generally very high, but are reduced drastically when an electron-deficient α-free pyrrole is used. Under such conditions, self-condensation of pyrrole-2-carbaldehyde is the favored reaction and yields the undesired symmetric BODIPY as the major product.

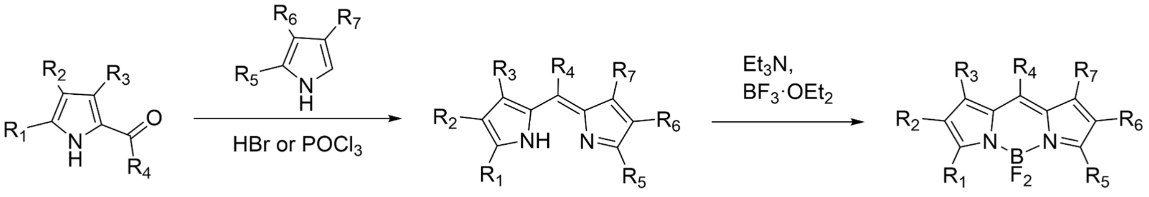

Scheme 2-38: Synthetic approach towards non-symmetrical BODIPYs.

The BODIPY framework can be considered as an electron-poor heteroaromatic compound. Consideration of mesomeric structures confirm the preferred reactivity towards electrophiles at the 2- and 6-positions (**Scheme 2-39**). Only limited electrophilic substitution reactions have been reported including sulfonation, nitration, halogenation and formylation under relatively harsh conditions.[116] Furthermore, the methyl-groups in 3- and 5-positions are acidic enough to react with aldehydes via Knoevenagel condensation to yield the styryl derivatives, which have substantial red-shifted absorption and emission spectra.

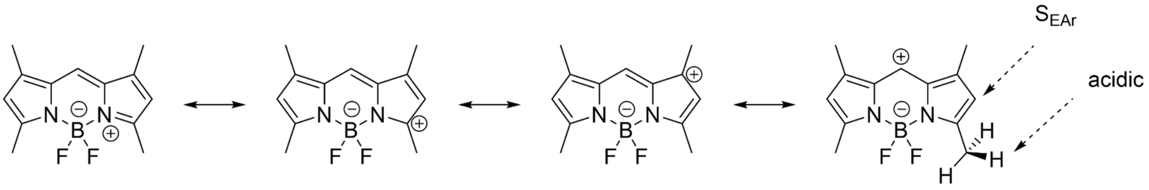

Scheme 2-39: Mesomeric structures of BODIPY. 2- and 6-positions are susceptible towards electrophilic attacks.

A considerable milestone was achieved when it was observed that halogenated BODIPYs at 2- or 5- positions undergo transition metal-catalyzed coupling reactions (Heck, Stille, Suzuki and Sonogashira).[127] Similarly, it was also reported that the presence of good leaving groups such as iodine or chlorine atoms at the 3- and/ or 5-positions enabled BODIPYs to undergo nucleophilic aromatic substitution (S_NAr).[128]

2.5.3 Applications

BODIPYs are among the most promising candidates for fluorescent labels and probes, due to their excellent physicochemical properties and low toxicity. Additionally, they do not significantly influence biological functions, on account of their small molecular size. Numerous BODIPY-based fluorescent labels have been used to target biological compounds such as DNAs, RNAs, nucleotides, amino acids, lipids, polystyrene microspheres, dextran, and proteins.[129] Probes derived from BODIPY are functionalized with reactive ligand/ anchor groups at the end such as carboxylic acids, sulphonic acids, polyethylene glycol, polysaccharides, or oligonucleotides for effective bio-conjugation.[130] Due to their high peak intensity, fluorescent BODIPY probes are among the most readily detectable fluorophores available for various analytical techniques such as gel electrophoresis and DNA sequencing. Oligonucleotide conjugates of BODIPY fluorophores have been used in DNA sequencing as the small molecular fluorophore exhibits a minimal effect on the fragment mobility during electrophoresis.[131]

Due to their small size and ease of modification, they are often employed in the design of selective and sensitive fluorescent chemosensors. These sensors are constructed as fluorophore-spacer-receptor or as intrinsic fluorescent probes, where the receptor is part of the π-electron system of the fluorophore. Fluorophore-spacer-receptor systems operate on the basis of PET or ICT processes. Binding of the analyte (a metal or a proton) to the sensor is monitored by recording the alterations in either the fluorescence intensity or wavelength (**Scheme 2-40**). The binding of a cation usually involves a loss of electron density with a concomitant lowering of the HOMO and LUMO levels of the anchoring-site on the *meso*-group. This perturbation of the reduction potential of the *meso*-group can be exploited by the choice of proper substituents to design a turn On/ Off sensor.[118]

In the case where the receptor is in conjugation with the fluorophore (in α– or β–position), and therefore part of the π-electron system of the BODIPY, a shift of the fluorophore's fundamental transition is expected upon binding. This is rationalized by the diminished donor strength of the receptor upon ligation with a cation, causing a weaker push-pull interaction with the fluorophore and promoting as a result the hypsochromic shift of the emission band (**Scheme 2-41**).[119]

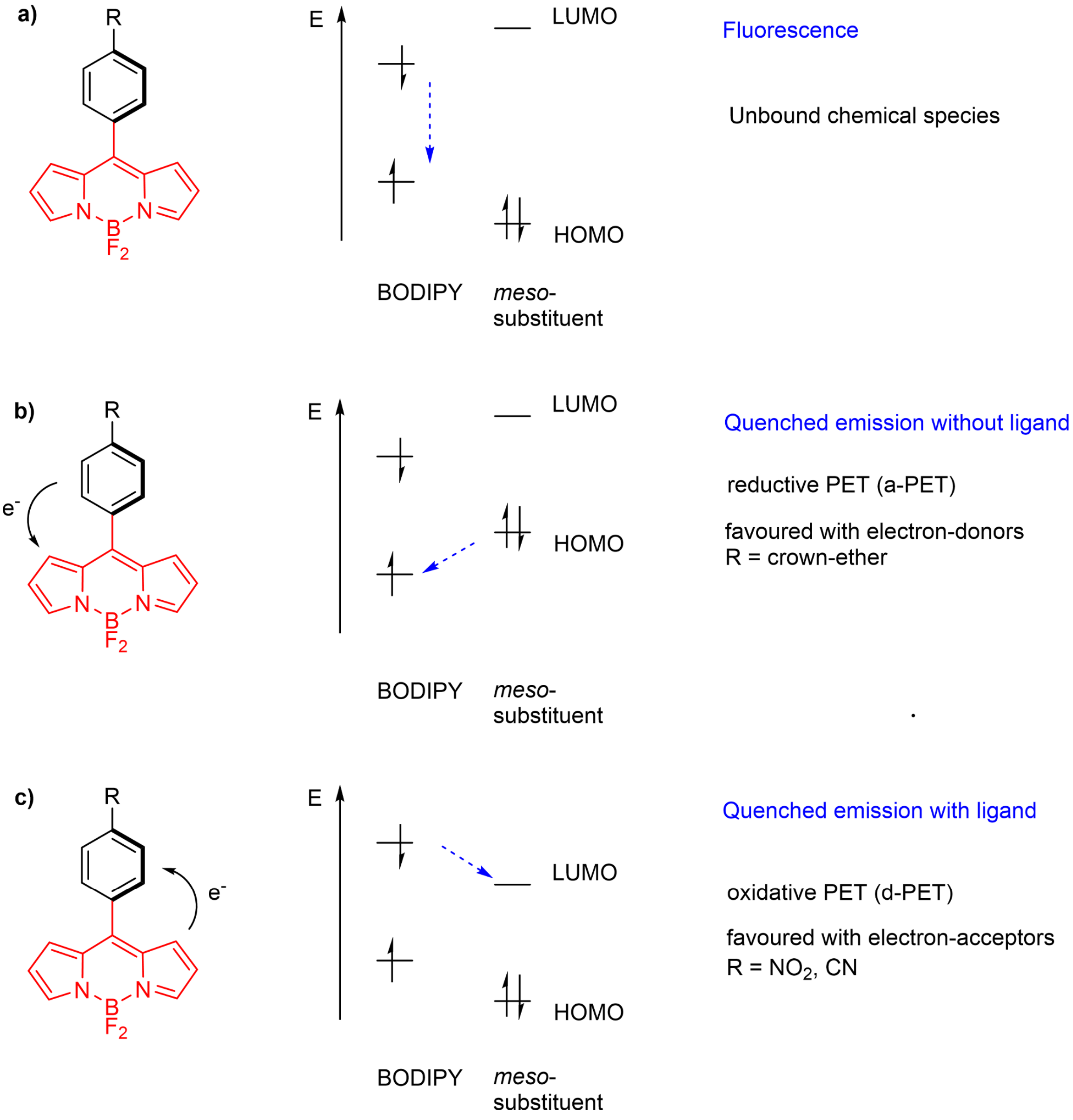
a)
R
N
B
N
F2
E
LUMO
HOMO
BODIPY
meso-
substituent
Fluorescence
Unbound chemical species
b)
R
e-
N
B
N
F2
E
LUMO
HOMO
BODIPY
meso-
substituent
Quenched emission without ligand
reductive PET (a-PET)
favoured with electron-donors
R = crown-ether
c)
R
e-
N
B
N
F2
E
LUMO
HOMO
BODIPY
meso-
substituent
Quenched emission with ligand
oxidative PET (d-PET)
favoured with electron-acceptors
R = NO2, CN

Scheme 2-40: The *meso*-substituent affords a) no significant electronic perturbation, b) electrons to the excited state, and c) a low lying LUMO to accept electrons from the excited state.[118]

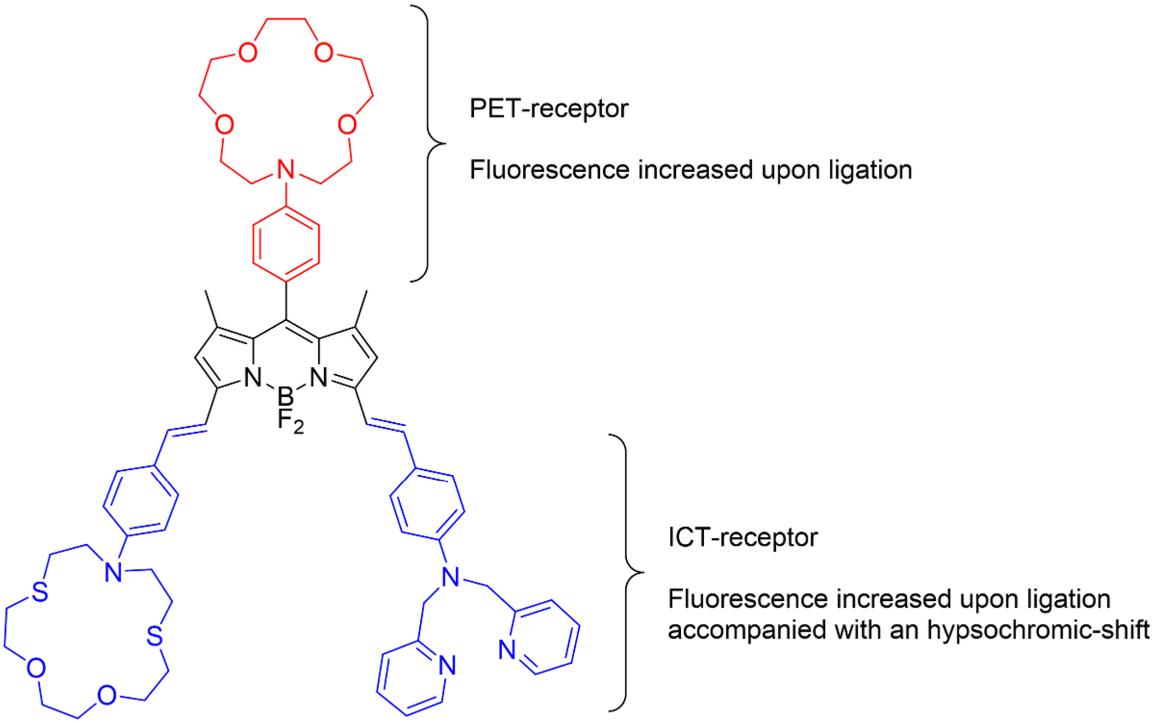
PET-receptor
Fluorescence increased upon ligation
ICT-receptor
Fluorescence increased upon ligation accompanied with an hypsochromic-shift

Scheme 2-41: BODIPY sensor based on PET and ICT fluorescence modulation processes.[119]

2.6 Sensitization

The process of photosensitization has been briefly introduced earlier in Chapter 2.4.1.1, by means of the triplet-triplet energy transfer by the Dexter exchange mechanism. According to the IUPACs golden book definition: “Photosensitization is the process by which a photochemical or photophysical alteration occurs in one molecular entity as a result of initial absorption of radiation by another molecular entity called a photosensitizer. In this process the photosensitizer is not consumed by the reaction.”[132] The proper selection of a sensitizer can be exploited to promote a photochemical reaction in a second molecular entity. As has been previously explained, the substantial distance dependence and the high concentrations required depict a difficult scenario to characterize such a system in an intermolecular regime. Designing a molecular construct, which has at one end a photosensitizer and in close proximity a photoswitch, guarantees the required proximity and orbital overlap to warrant the an effective sensitization. Such a covalently linked dyad facilitates the characterization, enabling to work at low concentration and optical densities below 1.0.

2.6.1 Triarylamine Fluorophores

Triarylamine (TAA) derivatives have been shown to be promising materials for 2PA. TAA is an electron-rich, propeller-shaped molecule exhibiting a C_3 symmetry, thus displaying an octupolar feature.[109] By the introduction of electron-withdrawing groups on the three positions *p* to the central nitrogen, very efficient 2PA fluorophores were recently obtained.[133] Hence, TAA represents an excellent scaffold for 2PA sensitization. TAA possess an easily accessible oxidation potential and readily gives up a nonbonding electron to generate very stable amine cation radicals, which are fundamental to electroluminescent devices.[134]

2.6.1.1 Synthesis of Triarylamines

The classic technique for the construction of triarylamines has been the Ullmann condensation.[135] The reaction entails the condensation of a diphenylamine and an unactivated aryl halide with catalysis by some form of Cu (metal, alloy, Cu (I) or -(II) salt) in the presence of added base. High temperature and extended reaction times are generally needed to secure at best moderate yields. Palladium-catalyzed aromatic amination reactions, as described by both Buchwald and Hartwig,[136] have improved the functional group tolerance of the synthesis of TAA. However, expensive Pd-ligand systems and very strong bases are required. More recently a ligand assisted Ullmann condensation was reported with significant improvements. 1,10-phenanthroline produced significant rate accelerations reaching completion in 5 h in refluxing toluene at 125 °C.[137] This is a temperature significantly lower and a reaction time shorter than the 12 h and 220 °C normally required (**Scheme 2-42**).

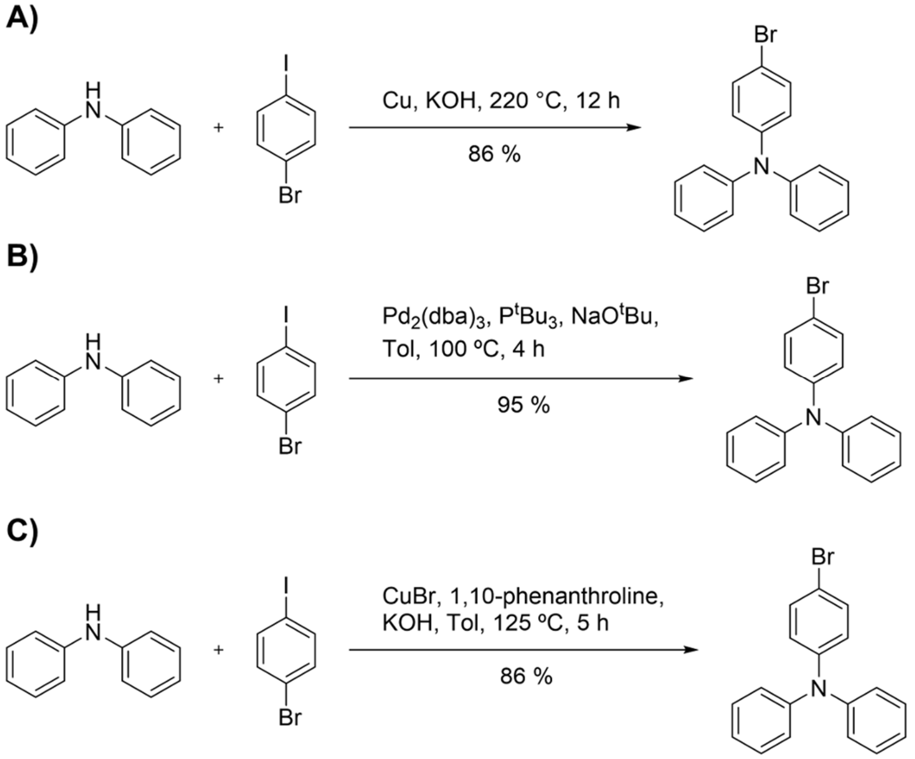

Scheme 2-42: Synthetic protocols for the obtention of TAA. a) Traditional Ullmann condensation, b) Buchwald-Hartwig Pd-catalyzed coupling and c) ligand assisted Ullmann condensation.

2.6.1.2 Photophysical Properties

TAA display strong absorption in the UV range, between 300 - 330 nm and independent of solvent polarity. Derivatives of TAA with EWG and strong CT character resemble also this fingerprint signature (**Scheme 2-43**).[138] Compared to their *N,N*-dialkylamino analogues, the twisted geometry around the nitrogen atom decreases the amino π-donor strength through orbital decoupling and imparts efficient fluorescence properties.[139] In the solid state the twisted geometry prevents the formation of non-radiative π–π aggregates.[140] This emissive behavior starkly contrasts with that reported for their *N,N*-dimethylanilino analogues, known to emit only at low temperatures in rigid matrices. The fluorescence emission can be varied from blue to red changing the nature of the electron-withdrawing substituents, as they readily form very strong CT bands. TAA have fluorescence quantum yields mostly superior to 0.20 and the energy absorbed by the arylamino moieties upon UV excitation is entirely transferred to the emissive ICT excited state as predicted by Kasha's rule.

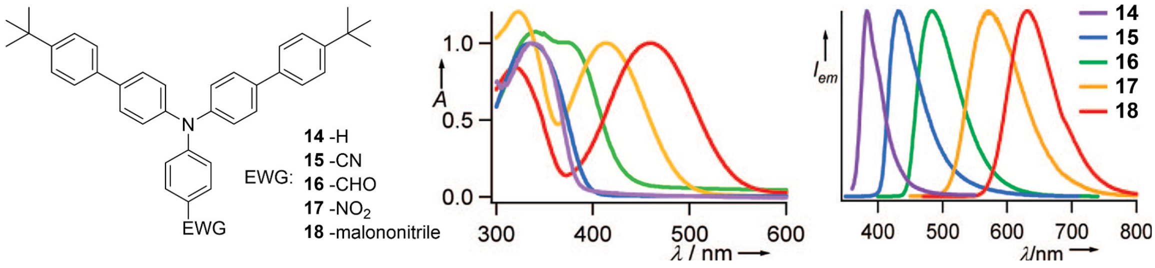

Scheme 2-43: Normalized absorption (middle) and emission (right) spectra (λ_{exc} = 343 nm) of push-pull triarylamine derivatives. CT band can be seen for compounds **16** to **18** (400 - 490nm).[138]

2.6.1.3 Applications

TAA derivatives are largely employed as precursors of small molecule-based functional materials for applications in two-photon bioimaging,[141] organic electronics,[142] optical data storage,[143] and 3D microfabrication.[144] They display a low oxidation potential, which makes them ideal candidates for hole-transport layers in organic LEDs[145] or acid photogenerators upon photoinduced ET for two-photon polymerization.[146]

In a very efficient example of signal amplification, Wu and coworkers employed a 2PA TAA derivative, which was able to transfer an electron upon two-photon excitation to a photoacid generator (NIOTf). The resulting radical anion of NIOTf then cleaved and reacted with the trace water in the polymeric media as well as in net acetonitrile (0.003 wt %) to generate trifluoromethanesulfonic acid, which proceeded to initiate a polymerization reaction and resulting in a substantial signal amplification (**Scheme 2-44**).[147]

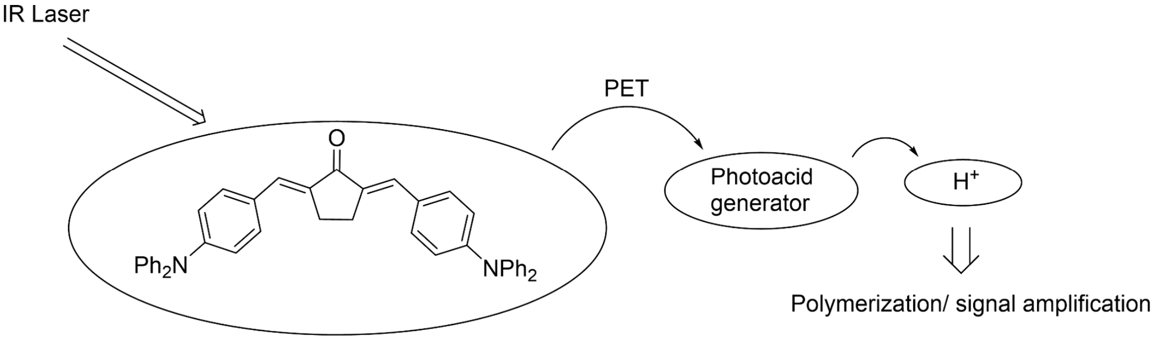

Scheme 2-44: Two-photon sensitized PET from a TAA-dye to a photoacid generator. The reduced photoacid generator cleaves and reacts with trace water to generate protons, which initiate a polymerization.

2.6.2 Ir(III) complexes as Triplett Emitters

Ir (III) complexes are attractive in photochemical applications, because they generally have long-lived excited states and high luminescence efficiencies, increasing the likelihood of either energy or ET occurring prior to radiative or nonradiative decay. Strong spin-orbit coupling leads to efficient intersystem crossing of the singlet excited states to the triplet manifold.[148] The long lifetimes of these excited states are due to the triplet character of this state. Mixing of the singlet and triplet excited states, via spin-orbit coupling, removes the spin-forbidden nature of the radiative relaxation of the triplet state, leading to high phosphorescence efficiencies. Cyclometalated ligands are formally monoanionic and can thus be used to prepare neutral tris-ligand complexes. Furthermore, Ir complexes can be formed with two cyclometalated ligands (*C^N*) and a single monoanionic, bidentate ancillary ligand (LX) (**Scheme 2-45**). The room-temperature phosphorescence quantum yields of these complexes range from 0.1 to 0.6, and their luminescent lifetimes fall between 1 and 14 μs, consistent with emission from a triplet excited state.[149]

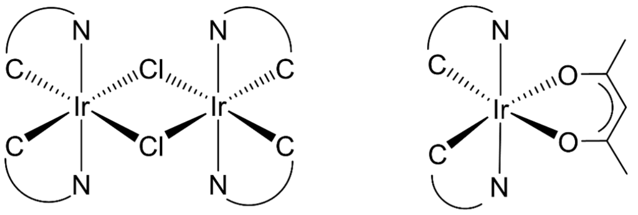

[Ir(C^N)$_2$µ-Cl]$_2$ Ir(C^N)$_2$acac

Scheme 2-45: Coordination geometries of octahedral Ir d^6 complexes with cyclometalated ligands and bridging chlorine (μ-Cl) or a single monoanionic, bidentate ancillary ligand (acetylacetonato).

2.6.2.1 Synthesis of Ir(C^N)$_2$LX Complexes

The common route towards cyclometalated Ir(III) complexes, involves an initial complexation of Ir(III) chloride with the desired ligand in refluxing 2-ethoxyethanol.[150] The product of this reaction is a chloride-bridged dimer, where the Ir center in is octahedrally coordinated by the two bridging chlorides and two cyclometalated *C^N* ligands, with the heterocyclic rings of the ligands in a *trans* configuration.[151] The chloride-bridged dimers can be converted to emissive, monomeric complexes by treating the dimer with a bidentate, anionic secondary ligand (LX), such as acetylacetonate (acac) (**Scheme 2-46**). The complexes are stable in air and can be sublimed in vacuum without decomposition. Analysis by cyclic voltammetry shows that the Ir(*C^N*)$_2$(acac) complexes all undergo a reversible one-electron oxidation; however, no reduction processes were observed in CH_2Cl_2. The oxidation potentials of these complexes vary between 0.8 and 1.0 V (vs Ag/ AgCl). [152]

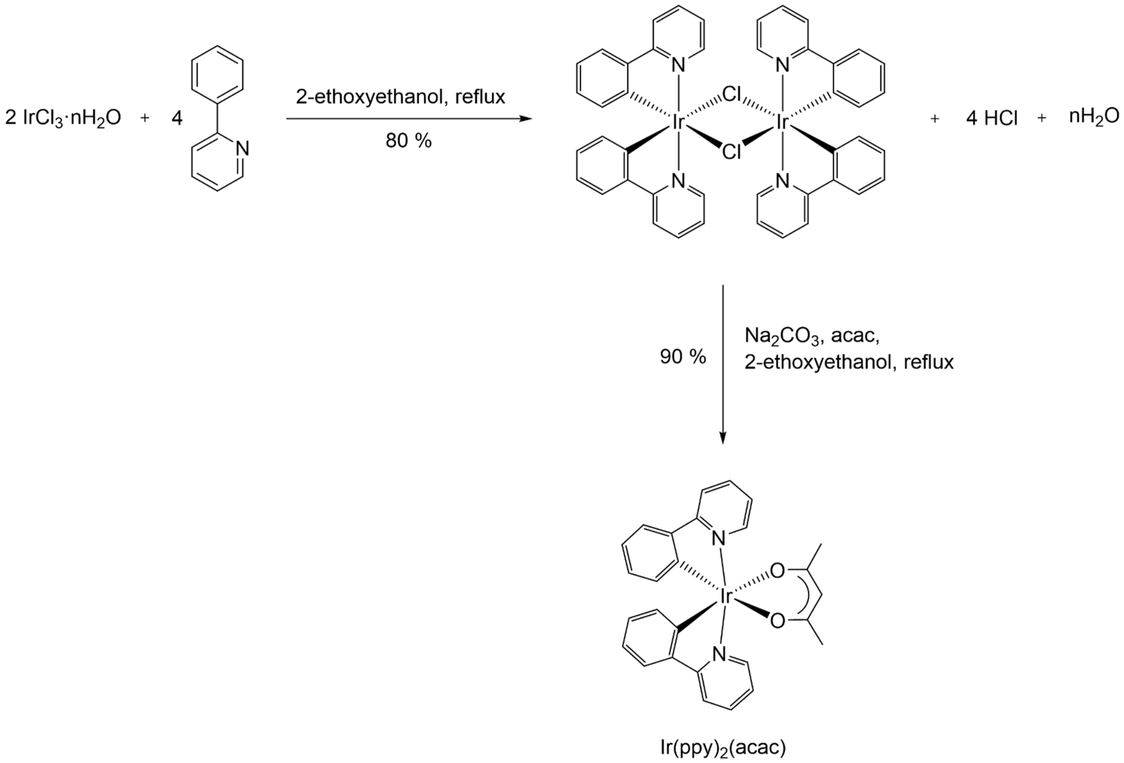
2 IrCl3·nH2O
+
4
N
2-ethoxyethanol, reflux
80 %
Cl
Ir
+
4 HCl
+
nH2O
90 %
Na2CO3, acac,
2-ethoxyethanol, reflux
O
Ir(ppy)2(acac)

Scheme 2-46: Synthetic route towards obtaining Ir(*C^N*)$_2$LX complexes.

2.6.2.2 Photophysical Properties

In the Ir(III) complexes, there are the π- and the excited π^* -orbitals of the organic ligands and the d- and excited d*-orbitals of the central metal atom. In principle four excitations are possible: first of all, a ligand centered (LC) excitation, in this case of π- π^* character, and a metal-to-ligand charge transfer (MLCT) excitation of d- π^* character. Which dominate the emission properties of the complexes (**Scheme 2-47**). The other two possible transitions are a metal-centered (MC) transition of d-d* character and a ligand-to-metal charge transfer (LMCT) transition of π -d* character. However, these excitations are not important, if the d*-orbital lies at high energies.

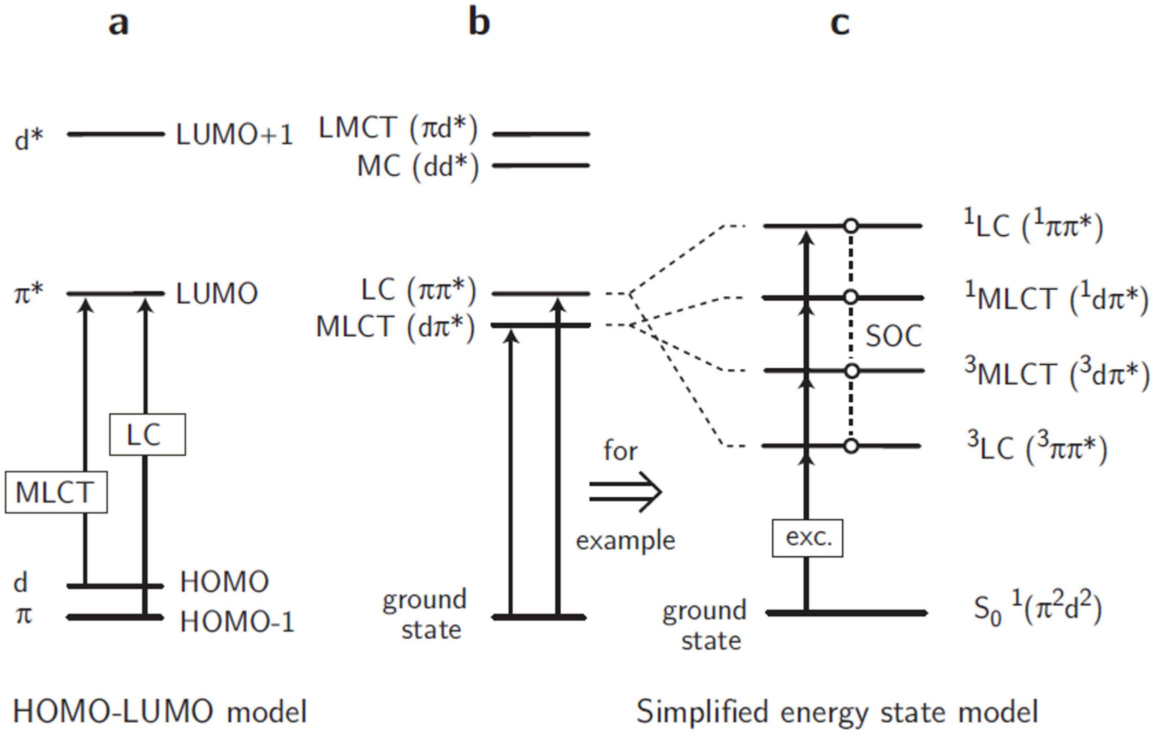
a
b
c
d*
LUMO+1
LMCT (πd*)
MC (dd*)
π*
LUMO
LC (ππ*)
MLCT (dπ*)
LC
MLCT
d
π
HOMO
HOMO-1
ground state
for example
¹LC (¹ππ*)
¹MLCT (¹dπ*)
SOC
³MLCT (³dπ*)
³LC (³ππ*)
exc.
ground state
S₀ ¹(π²d²)
HOMO-LUMO model
Simplified energy state model

Scheme 2-47: a) Simple MO model for an Ir(*C^N*)$_2$LX complex. b) Model for the possible transitions from the ground-state. c) Energy state model including the exchange splitting into singlet and triplet states. The states can experience mixing due to spin-orbit-coupling (SOC).[154]

The spectra of Ir(*C^N*)$_2$LX complexes are characterized by intense bands located in the UV spectral region, between 250 and 350 nm. These bands can be assigned to the allowed $^1(\pi\text{-}\ \pi^*)$ transitions of the C^N ligands. The energies and extinction coefficients for these bands correlate well with the transitions observed for the free ligands. MLCT bands are usually resolved at 410 and 460 nm, with extinction coefficients of 3500 and 2500 L mol^{-1} cm^{-1}, respectively. The spin forbidden ^{3}MLCT at 460 nm gains intensity by mixing with the higher lying ^{1}MLCT transition through the strong spin-orbit coupling of Ir. This mixing is strong enough in these Ir complexes that the formally spin forbidden ^{3}MLCT has an extinction coefficient that is more than half that of the spin-allowed ^{1}MLCT. It has been shown that emission from Ir(*C^N*)$_2$(acac) and Ir*C^N*$_3$ complexes are similar, which emit from MLCT transitions.[153] Changes in the *C^N* ligand in a Ir(*C^N*)$_2$(acac) complex typically have a marked effect on the phosphorescence spectrum (**Scheme 2-48**), while changing the acac ligand leads to a minor shift of 5 nm.

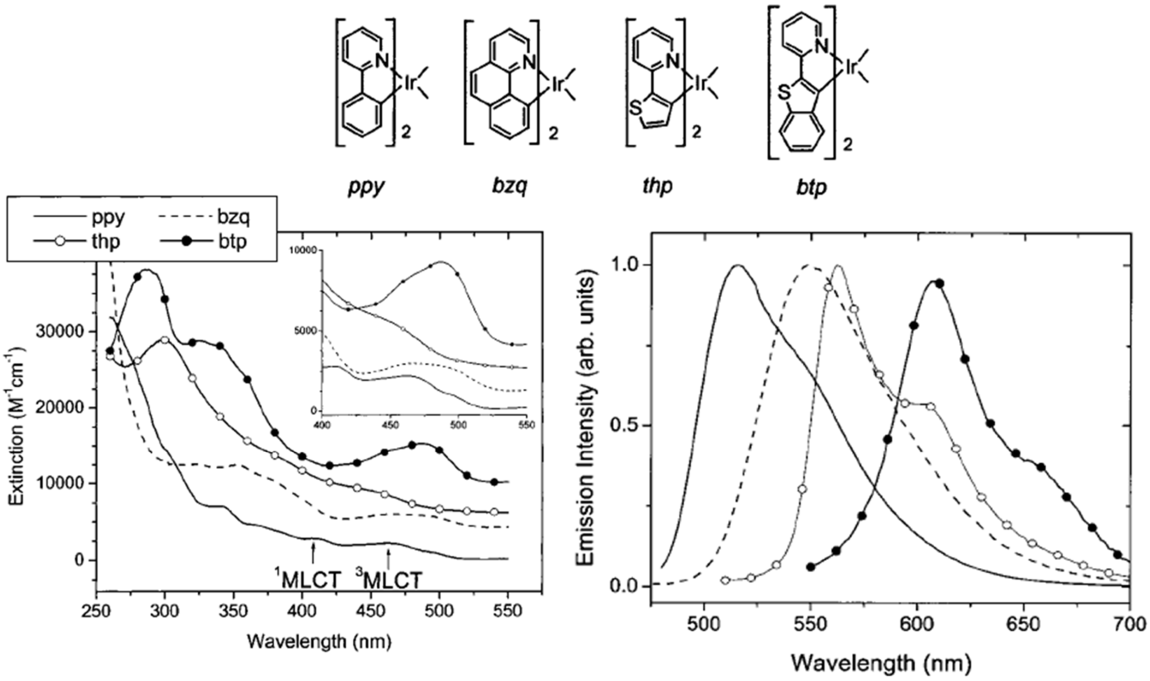

Scheme 2-48: Absorption and emission spectra of Ir(*C^N)*$_2$(acac) complexes. Absorption spectra for the complexes (bottom left). The spectra have been offset for clarity. All four complexes have extinction coefficients of 0.0 at 550 nm. Emission spectra of the same complexes (bottom right).[153]

2.6.2.3 Applications

Ir(III) complexes have been used extensively as photo-catalyzers in preparative chemistry and photoelectrochemistry,[154] as well as photo-sensitizers for dye sensitized solar cells.[155] They have been also successfully employed for electrogenerated chemiluminescence,[156] but the main application is found in the design of doped OLEDs with heavy metal phosphors[157] and triplett harvesting in OLEDs.[158] Efficient red emitting OLEDs have been built both by vacuum deposition[159] and by solution processing.[160] Furthermore, polymeric devices with linkage of the emitter to a polymer host have been also readily obtained.[161]

2.7 Photoswitches as Energy Acceptors

In Chapter 2.1 we have seen that the photoinduced interconversion of one state of a photochromic compound into another is generally accompanied by significant structural and electronic changes. Photoswitchable fluorescent molecules can be assembled by combing photochromic and fluorescent chromophores in a single molecule.[162] In this approach, FRET or PET mechanisms are chosen to reversibly switch the fluorescence emission of the fluorophore. Switching of the fluorescence is carried out by modulating absorption properties or the oxidation/ reduction potentials of the photochromic unit. In a FRET system, the energy of a fluorescence donor molecule is transferred to an acceptor, in this case the photoswitch. Port et al.[163] constructed a photochromic FRET system (**Scheme 2-49**) composed of a fluorescent anthracene fluorophore as a donor and a photochromic fulgimide unit as an acceptor. When the fulgimide moiety is in the open E-form, excitation of the anthracene moiety at 400 nm resulted in fluorescence from the coumarin part. The excited energy is transferred from anthracene to coumarin through E-form fulgimide. Conversely, upon irradiation with 320 nm light, which promotes the photocyclization reaction, the excited energy of anthracene is trapped by the photogenerated C-form fulgimide and the fluorescence is quenched. In this example the fluorescence intensity could be modulated with the photoisomerization.

Tsuchiya reported the synthesis and photoswitching of porphyrin-AB-fluorinatedporphyrin triad (**Scheme 2-50**).[164] In the triad, the nonfluorinated porphyrin can donate electrons to its fluorinated counterpart upon excitation. The distance between the two porphyrin units, however, changes with the state of the AB bridge. The photoinduced isomerization of the AB from *trans* to *cis* decreases separation between the electron donor and the acceptor. As a result, the efficiency of ET increases dramatically and the fluorescence quantum yield drops by 50%. Only after thermal back-isomerization of the AB the original fluorescence is restored.

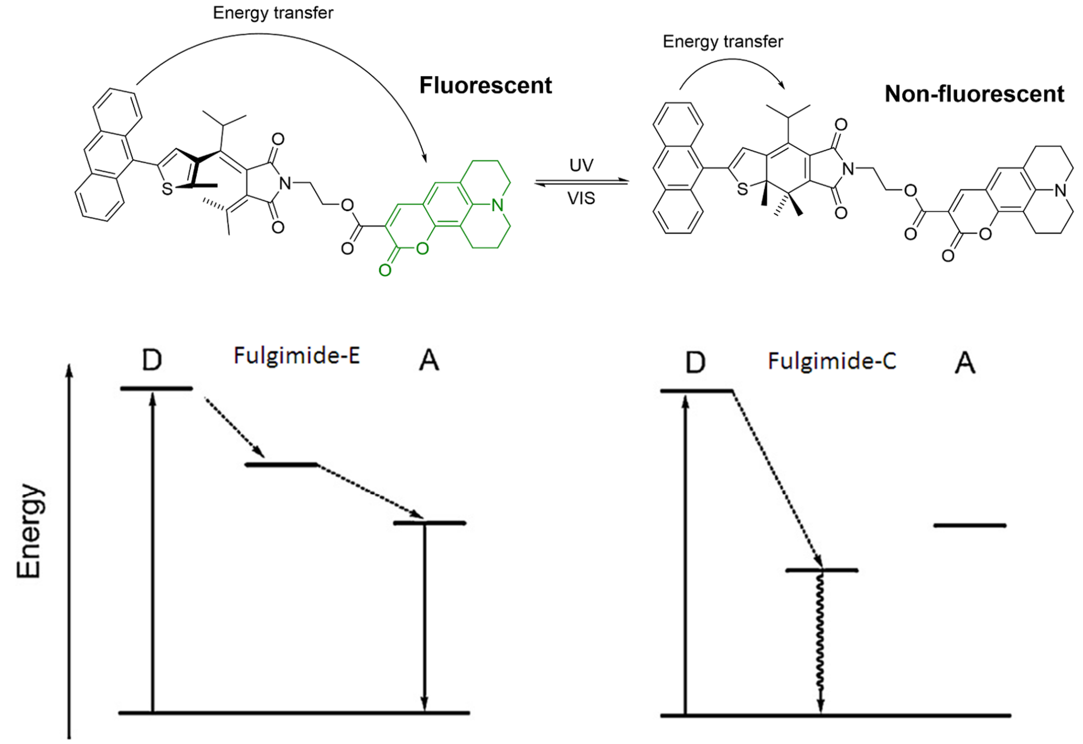

Scheme 2-49: In the open-form, the acceptor level forms the lowest excited state, but in the closed-form the fulgimide part is lowest, trapping the excitation energy of the donor and inhibiting the fluorescence of the coumarin.[163]

The fact that the fluorescence could only be restored after thermal back-isomerization evidences that photochemically it was not possible to address the AB in the *cis*-form. A common issue of such multichromophoric constructs is the loss of photochromic activity. The main difficulty resides in achieving the delicate equilibrium between obtaining the properties resulting from the active coupling of the photoswitch and the fluorophore, and yet at the same time ensuring that the final system retains the intrinsic switching properties of its components. Preserve the spectroscopic identity of the photoswitch and the photochromism is highly challenging, mainly due to energy transfer between the different subunits. The chemical connection between the subunits is thus a critical consideration in the design of multichromophoric compounds because the linker determines the through bond and the through space communication between the components.

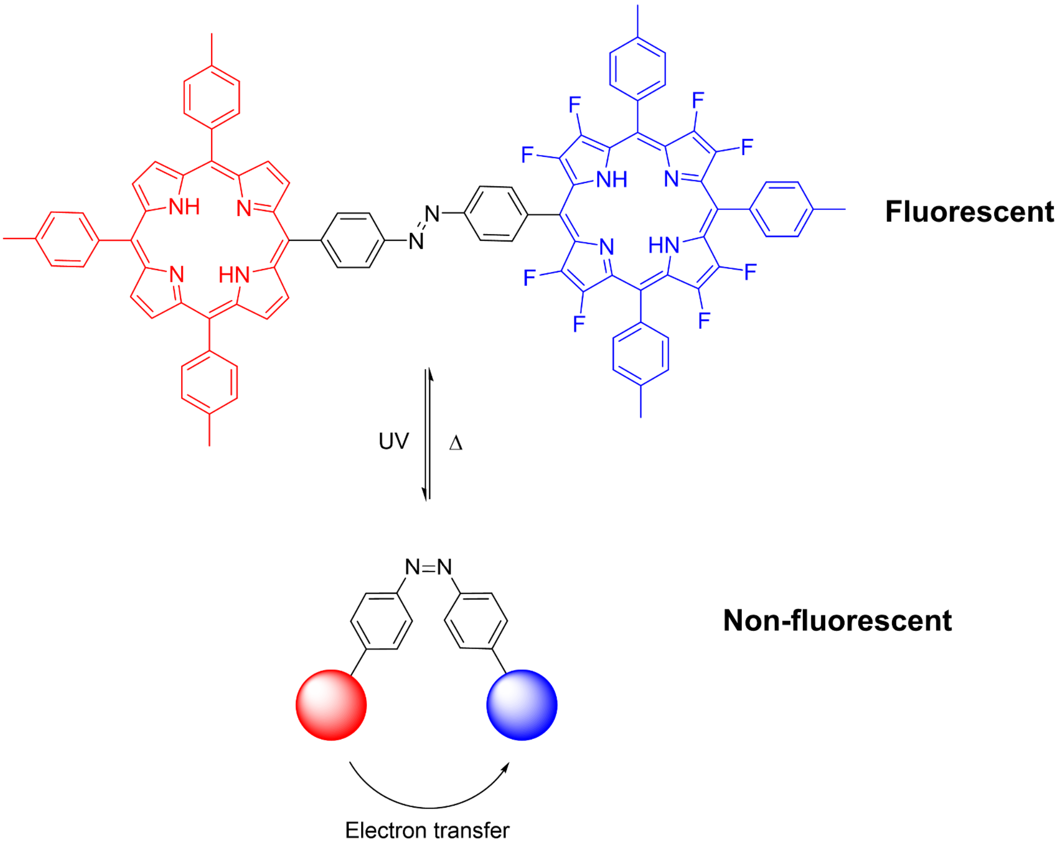

Scheme 2-50: The photoinduced isomerization of the AB activates a PET quenching of the emission of the porphyrin fluorophores.[164]

2.7.1 Fluorescence Modulation with Diarylethenes

Although most DAEs are nonfluorescent in both open- and closed-ring isomers, DAEs having benzo[b]thiophene as the aryl groups exhibit weak fluorescence in both isomers.[165] The open-ring isomer emits blue fluorescence at 420 nm, while the closed-ring isomer exhibits a very weak but distinct emission at 630 nm (Scheme 2-53). However, the fluorescence quantum yields and absorption coefficients of such derivatives are too low to be used in practical applications. To improve the fluorescence property, some fluorophores such as anthracene,[166] 2,4,5-triphenylimidazole,[167] polythiophene,[168] polyphenylene vinylene,[169] metal complexes,[170] fluorescein,[171] rhodamine,[172] napthalimide,[173] and perylenebisimide,[174] were linked with DAE derivatives. When fluorescent chromophores are directly coupled with the DAE unit, the fluorescence quantum yields are reduced and the photochromic reaction quantum yields decrease. The decrease of the cyclization quantum yields is ascribed to the excited energy transfer from the DAE unit to the fluorescent chromophores, while the decrease of the ring opening quantum yield is attributed to elongation of π-conjugation in the closed-ring isomers.[175]

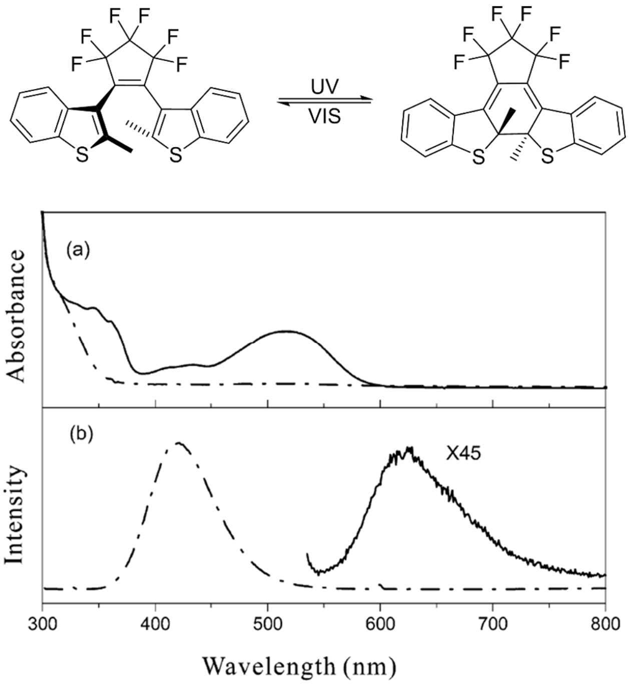

Scheme 2-51: Absorption (middle) and emission (bottom) spectra of benzo[b]thiophene derived DAE. Dashed-line belongs to the open-isomer, solid-line belongs to the PSS of the closed-form.[165]

Bossi et al. designed a fluorescence photoswitching system which is composed of a photochromic DAE and a fluorescent rhodamine-101 chromophore (**Scheme 2-51**).[172] In an ethanol solution, the open-ring isomer shows a relatively high fluorescent quantum yield ($\phi_{Fl} \sim$ 0.52) and a large fluorescence modulation ratio (94%) was achieved upon photocyclization. The fluorescence modulation is effected through FRET from the fluorescent dye to the closed isomers of the photochromic switch. The high FRET efficiency was achieved by maximizing the absorption band overlap of the closed DAE with the emission band of the donor (**Scheme 2-52**). However, the photochromic performance was rather poor, with a cyclization yield of 0.063 and a cycloreversion yield of 0.00022. This diminished photochromic performance was attributed to the fact that most of the irradiation light at 313 nm is absorbed by the fluorophore and hence cannot contribute to photocyclization. The efficiencies of the reverse reaction are nearly unaffected by coupling to Rh101. Interestingly the PSS close to 100% remained unaltered, in comparison with parent-photoswitch, and was the cause for the high fluorescence modulation achieved.

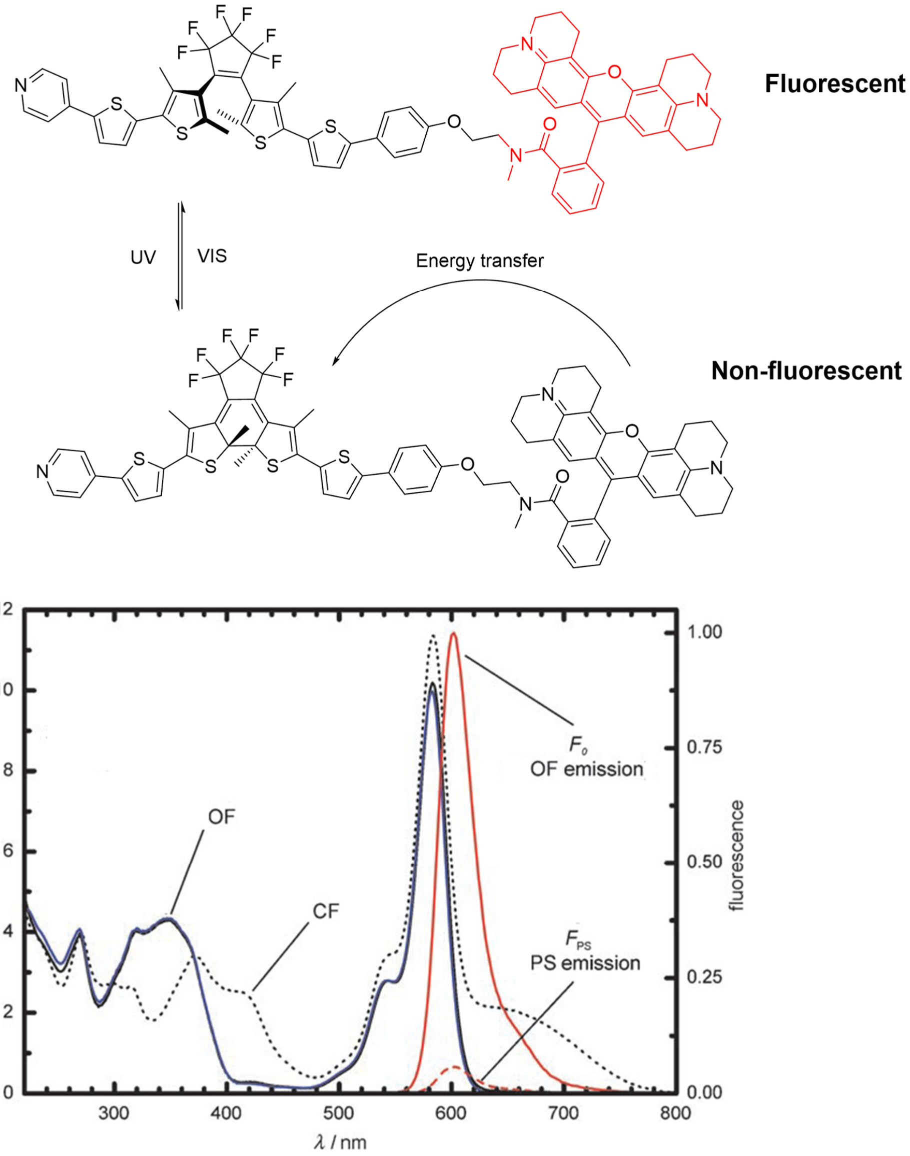
Fluorescent
UV
VIS
Energy transfer
Non-fluorescent
ε/×10⁴ M⁻¹ cm⁻¹
fluorescence
λ / nm
0
2
4
6
8
10
12
0.00
0.25
0.50
0.75
1.00
300
400
500
600
700
800
OF
CF
F0
OF emission
FPS
PS emission

Scheme 2-52: Absorption spectra (left axis) and fluorescence emission (right axis) of the open form (OF; solid red line) and in the photostationary state (PS) under irradiation at 375 nm (dashed red line, 98% closed form (CF)); the different intensities demonstrate the fluorescence modulation.[172]

Similarly, Neckers and coworkers reported the synthesis of a symmetrical DAE-BODIPY dyad, based on FRET modulation of fluorescence emission (**Scheme 2-53**).[176]In this dyad the brightness was extraordinary high due to the presence of two fluorophores per molecule. Additionally, since the BODIPY absorption did not significantly overlap the DAE absorption band in the UV-region, the DAE could be selectively addressed by irradiation at 313 nm. The selective excitation of the DAE endorsed an unaltered photochromism, achieving a cyclization yield of 0.32 and a PSS of 98%. The fluorescence modulation was attained with the large overlap of the BODIPY emission with the absorption band of the DAE in the closed form.

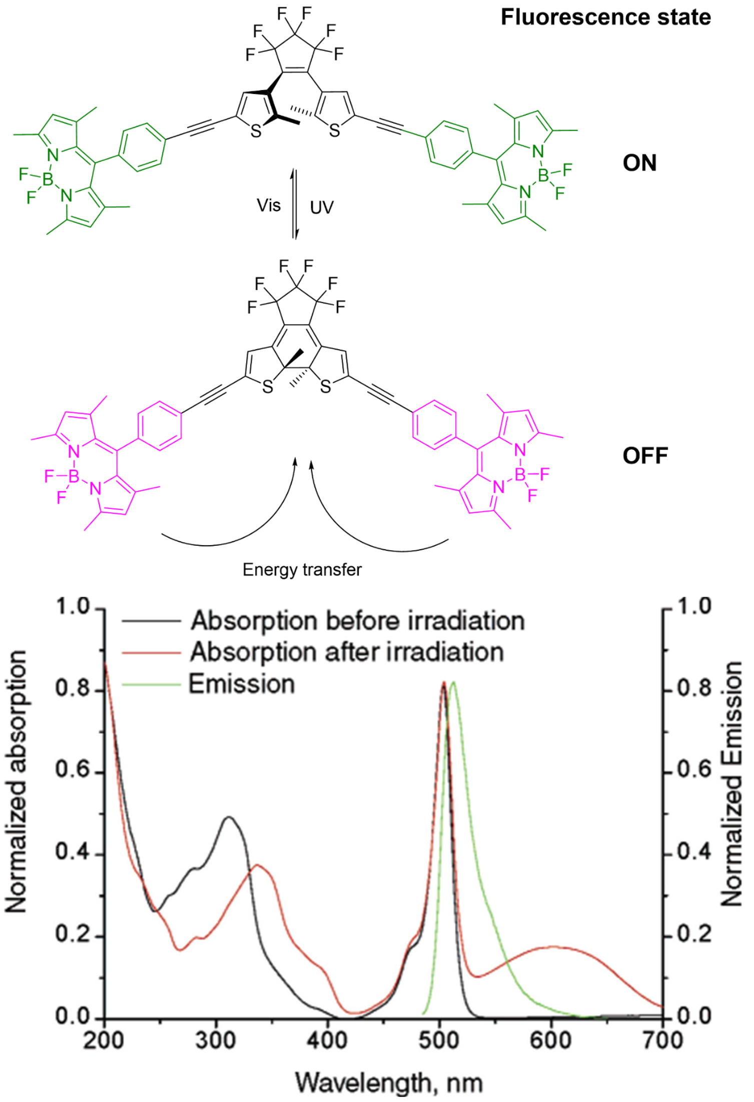

Scheme 2-53: Absorption spectra (left axis) of the open form (solid black line) and in the PSS (solid red line). Fluorescence emission (right axis) of the open form (green solid line); negligible emission was detected for the closed form.[176]

The fluorescence quenching process by energy transfer, although very efficient, has an inherent drawback. The quenching by the intramolecular energy transfer to the closed-ring isomer induces undesirable cycloreversion. To avoid the cycloreversion, it is required to separate the absorption spectra of both isomers of the photochromic unit and the fluorescence spectrum of the fluorophore. For the application to optical memory and super-resolution fluorescence imaging, the fluorescence switching and the probing processes should be decoupled and independently controllable. Under this considerations it is possible to employ PET as the fluorescence quenching mechanism. The group of Würthner designed a DAE-perilenebisimide dyad based on PET fluorescence quenching. The envisioned molecule employed an *S,S*-dioxide DAE derivative as electron acceptor and a fluorescent perylenebisimide chromophore as electron donor to avoid possible spectral overlap (**Scheme 2-54**).[177] By these means, it was possible to modulate the fluorescence emission efficiency form 0.95 in the open form, to just 0.05 in the closed form.

So far all the examples mentioned earlier have a common feature, they are initially in a highly fluorescent form, which upon photoisomerization of the photochromic appendage, promotes the efficient fluorescence quenching. This systems are called turn-Off fluorophores and have been efficiently optimized to avoid the destructive readout in prospective applications. However, a significant signal-to-noise and resolution improvement is expected for systems capable to exhibit turn-On fluorescent properties, besides the fact that modern super-resolution fluorescence microscopy requires an absolutely dark background in the initial state.[178] Such a molecular entity would be initially non-fluorescent and only upon selective activation, the emission could be triggered On.

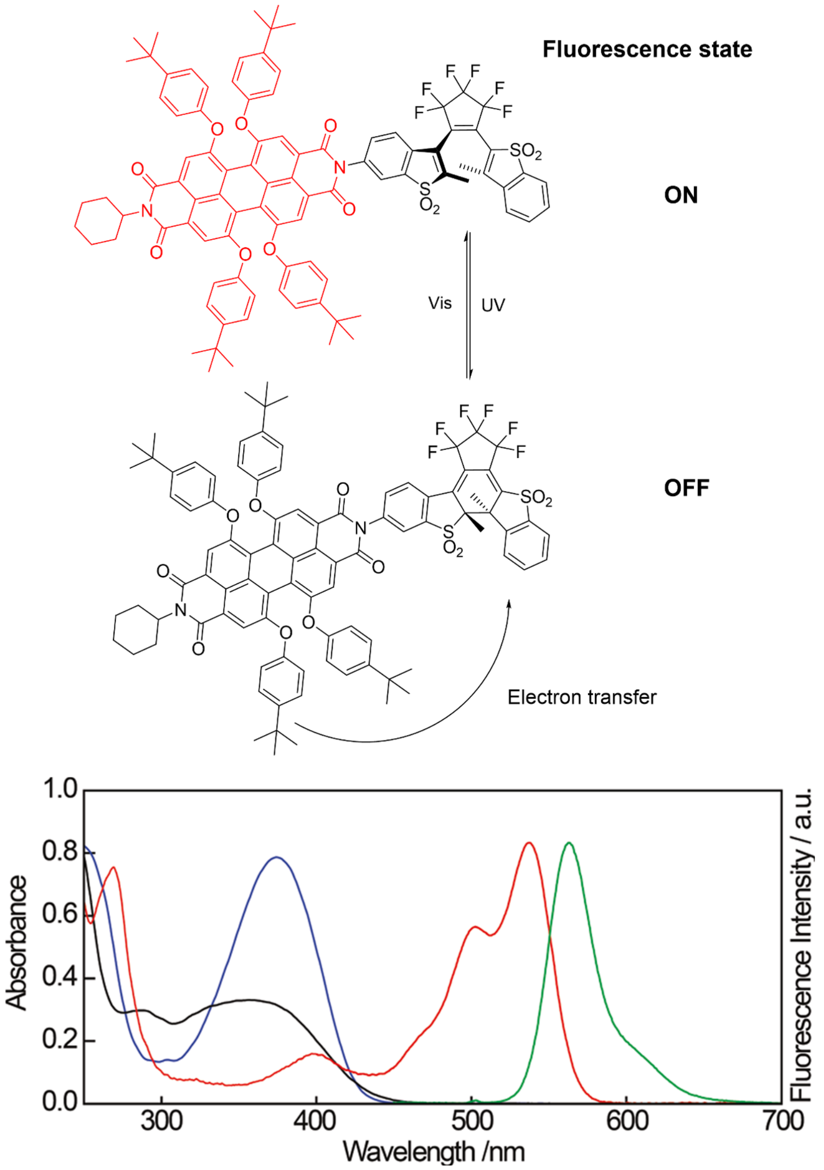

Scheme 2-54: Absorption and fluorescence spectra of each component in 1,4-dioxane. Absorption spectra of the open-ring isomer of DAE (black), the closed-ring isomer of DAE (blue), and the PBI unit (red), and fluorescence spectrum of the PBI unit (green).[177]

State-of-the-art photochromic turn-On fluorophores, depend on the inherent fluorescence of the engineered DAE in the closed state. Irie[179] and Ahn[180] reported on two different DAEs which were intrinsically fluorescent in the closed form (**Scheme 2-55**). However, the fluorescent process and the photochromic reaction compete with each other. Consequently, when the fluorescence quantum yield is high, the photoisomerization reaction is suppressed.

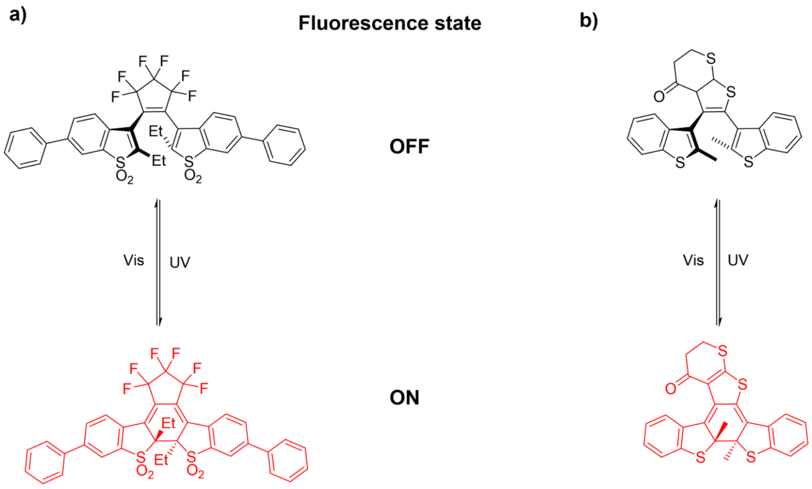

Scheme 2-55: a) Irie's benzo[b]thiophene-1,1-dioxide derived fluorescent DAE;[179] b) Ahn's inherent fluorescent DAE.[180]

Ahn described a DAE which upon cyclization had a fairly high fluorescence at 580 nm (ϕ_{Fl} ~ 0.11). The fluorescence switching contrast was estimated to be ~97:1. Furthermore, the cyclization and cycloreversion quantum yields were determined to be 0.25 and 0.17, respectively. The high fluorescence contrast and excellent reversibility make the compound an excellent fluorescent probe for live cell imaging. In addition, the compound showed no toxicity to cells even in the millimolar concentration range. However, readout promotes the cycloreversion of the DAE.

Likewise, Irie's DAE with benzo[b]thiophene-1,1-dioxide groups had fluorescence quantum yields of the closed ring isomers close to 0.9 undergoing photocyclization reactions with 0.5 yield, to produce yellow closed-ring isomers, which emit brilliant green fluorescence at around 550 nm in 1,4- dioxane (ϕ_{Fl} ~ 0.87) upon excitation with 488 nm light. Nonetheless, the cycloreversion is almost suppressed with a yield of $4 \cdot 10^{-5}$.

It is thus clear that further research has to be performed towards efficient, bright and red-shifted turn-On fluorophores capable to achieve non-destructive readout.

2.7.2 Sensitization and Amplification

In the previous section we have seen how energy transfer can be exploited to modulate fluorescence emission. However, as a consequence the transferred energy from the fluorophore to the photochromic acceptor-unit causes the isomerization of the photoswitch. Energy transfer from a sensitizer to a photoswitch can be exploited to promote the indirect photoisomerization of photoswitches. It has to be noted that this process can be implemented either inter- or intramolecularly. Earlier we have seen the possible sensitizer molecules which range from triplet sensitizers, to two-photon fluorophore, or even upconverting nanoparticles (UCNP). The inherent requisite for sensitization is that the energy donor has to possess the capability of light absorbtion in the visible or even NIR region and transfer the harvested higher excitation energy to the photoswitch, promoting the subsequent isomerization.

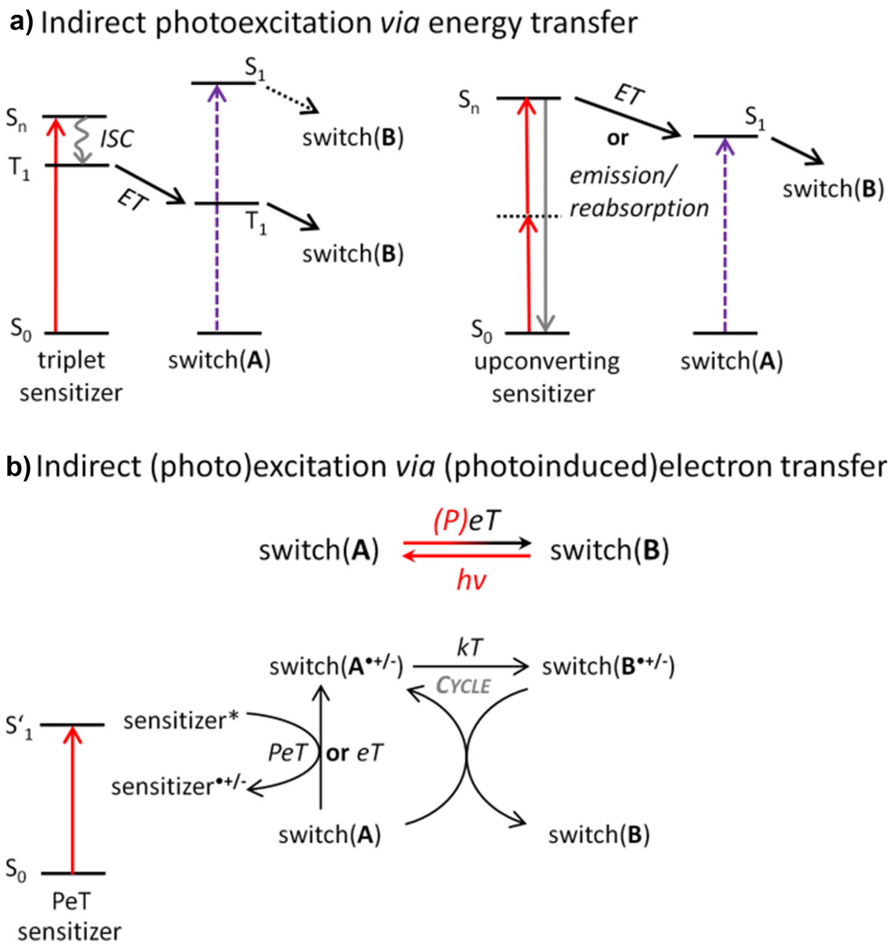
a) Indirect photoexcitation via energy transfer
S_n
T_1
ISC
ET
S_1
T_1
switch(B)
switch(B)
S_0
triplet sensitizer
switch(A)
S_n
ET
or
emission/ reabsorption
S_1
switch(B)
S_0
upconverting sensitizer
switch(A)
b) Indirect (photo)excitation via (photoinduced)electron transfer
switch(A)
(P)eT
hν
switch(B)
switch(A•+/-)
kT
CYCLE
switch(B•+/-)
S'1
sensitizer*
PeT
or eT
sensitizer•+/-
switch(A)
switch(B)
S_0
PeT sensitizer

Scheme 2-56: a) Energy transfer from a triplet (left) or an upconverting (right) sensitizer to the switch. Right: photon upconversion can occur via virtual states in the case of multiphoton antennae or intermediate long-lived excited states in the case of lanthanide-doped nanoparticles). b) Switching involving redox reactions in one direction that can be coupled to a sensitizer, which has been excited with light and initiates the catalytic chain by PET.[181]

Triplet states are lower in energy than their corresponding singlet states, enabling to promote photoisomerization with light of higher wavelength. However, triplet states can only be efficiently populated if intersystem crossing (ISC) is high. By means of the Dexter exchange mechanism triplet sensitizers in close proximity to the photoswitch, can be employed to promote a triplet-triplet energy transfer (**Scheme 2-56a**).[181]

DAEs covalently linked to transition metal complexes undergo efficient ring closure via metal-to-ligand charge-transfer (MLCT) excitation. This process is followed by intersystem crossing, and transfer of the triplet energy to the photoswitch.[170] Intermolecularly this process was also demonstrated using xanthone as an organic sensitizer.[182]

By means of indirect two-photon induced photoisomerization (**Scheme 2-56a**), it is possible to covalently connect a photoswitch and a two-photon fluorophore, whose emission overlaps with the absorption band of the switch in order for FRET to take place. This strategy was used by Zink and coworkers[183] (**Scheme 2-57**) to build mesoporous silica nanoparticles containing both an AB and a two-photon absorbing fluorophore, which could release an encapsulated bioactive compound upon 760 nm irradiation thanks to the *trans→cis* isomerization induced by FRET. The fluorophore was selected for its fluorescence emission, which overlaps with the AB π→π* absorption band. The energy transfer mechanism was assumed from the fluorescence quenching of the fluorophore and implied photoisomerization of the AB, which induced cancer cell death.

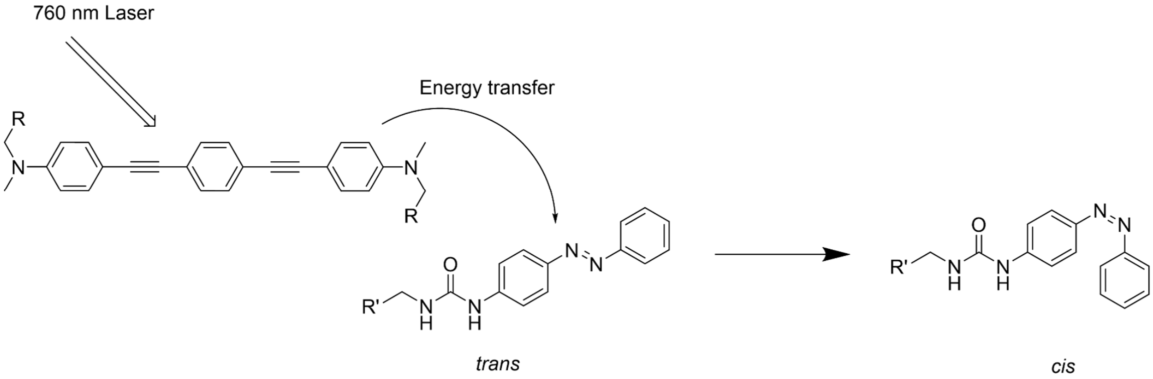

Scheme 2-57: *trans→cis* isomerization of AB with 760 nm light via FRET from a two-photon absorber fluorophore. The system was embedded in mesoporous silica nanoparticles together with a bioactive compound for delivery to cancer cells.[183]

The group of Branda was capable to demonstrate that lanthanide doped upconverting nanoparticles can photoisomerize DAE derivatives with NIR light.[184] Initial absorption of NIR light by the nanoparticle and subsequent emission of UV-light promoted via FRET the photocyclization of the DAE.[185] A more sophisticated design of the nanoparticle (core-shell-shell $NaYF_4$ nanocrystals containing Er^{3+}/ Yb^{3+} and Tm^{3+}/ Yb^{3+} ions doped into separate successive layers) enabled modulation of the emission wavelength by the intensity of the 980 nm excitation light, and thus permitted to fully address the photoisomerization processes of a DAE with NIR light (**Scheme 2-58**).

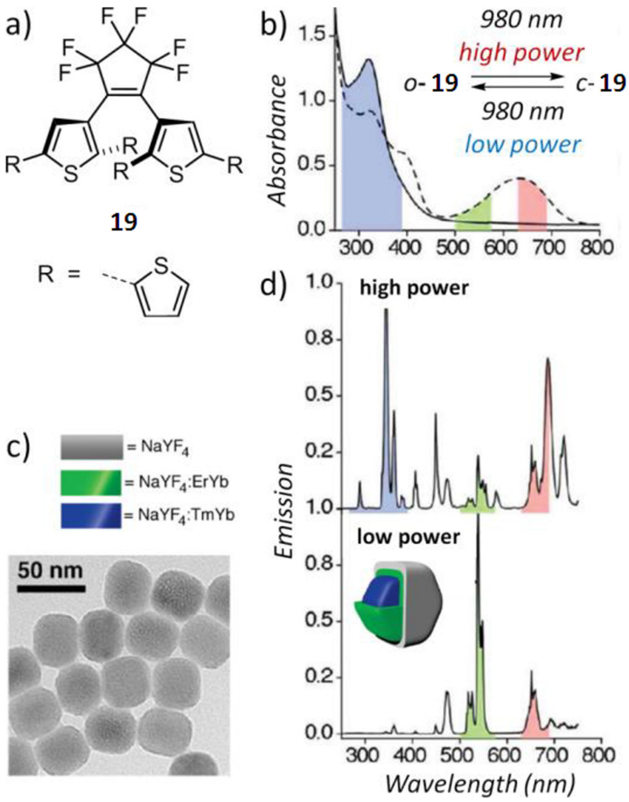

Scheme 2-58: Photoswitchable DAE with 980 nm irradiation. a) Molecular structure and b) UV-vis spectra of DAE derivative **19**.[184] c) Composition and TEM image of the core-shell-shell Tm : Er nanoparticles, which exhibit d) different emission spectra at high (top) and low (bottom) intensity following 980 nm irradiation.

In the last section we have seen that photoswitches can be used to facilitate PET processes, however, the energy stored in an excited sensitizer molecule can also be used to drive an ET to or from the switch. ET can be used to replace UV light induced isomerization by redox catalysis (**Scheme 2-56b**). Switching via oxidation/ reduction of the photoswitch provides the possibility to employ electrons rather than photons for the isomerization. Additionally, it bears also the advantage to amplify the efficiency and sensitivity due to the potential involvement of a catalytic chain reaction (**Scheme 2-16**). Such an amplification mechanism, in which few electron trigger many switching events, has been demonstrated for the ring-opening of some DAE derivatives, for which Kawai et al. could determine net current efficiencies of up to 900%.[186]

The group of Nam exploited the reductive switching with light, by implementing a photoredox catalyst. Following excitation by light a catalytic PET mediated chain promoted the cycloreversion of electron-poor DAEs.[187] Ir(III) complexes were employed as photoredox catalytic sensitizers due to the long-lived triplet excited states, which promoted PET transfer in solution at high concentration (10^{-3} M). A significant improvement of one order of magnitude was achieved in the sensitized cycloreversion process, when compared with the conventional cycloreversion of the DAE (**Scheme 2-59**).

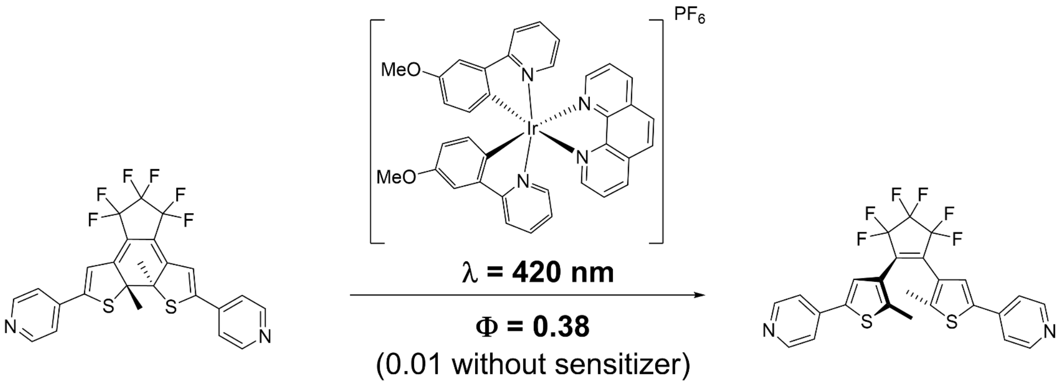

Scheme 2-59: Irradiation at 420 nm, promoted PET from the sensitizer to the DAE, thereby initiating a catalytic cycloreversion cycle. An amplification of one order of magnitude was observed in the overall process in the presence of the sensitzer. ($\Phi = 0.38$ with 20 mol % of catalyst vs. 0.01 without catalyst).[187]

The previous examples demonstrate a stringent limitation of the sensitized switching of photoswitches, imposed by the need of high concentrations for efficient PET or FRET in an intermolecular regime. Furthermore, in principle, quantum yields exceeding unity should be achievable if side reactions during the initiation could be minimized and the catalytic turn over be maximized.

3 Results and Discussion

3.1 Reversibly Photomodulating the Emission of Fluorophore-Photoswitch Dyads

3.1.1 Target Definition

Molecular switches, which undergo efficiently and in a reversible manner a photochemically induced interconversion between two stable isomers, have been widely studied and notoriously improved in the past. Nowadays their accurate and on-demand implementation in more complex molecular entities is possible. Applications arising from such nanoengineered constructs range from optical devices to stimuli-responsive materials. DAEs experience a large increase in conjugation upon photoinduced isomerization with UV-light and possess a high fatigue resistance. These attributes can be exploited to modulate or even unlock secondary functions at the molecular or supramolecular level by using light as a trigger. Among the chemical and physical properties that a molecule can switch, fluorescence is of representative importance since fluorescent molecules can be used as probes for intracellular processes[188] as well as for optical recording materials with fluorescence readout.[189] Furthermore, stable photoswitchable fluorophores are specifically required in novel super-resolution techniques capable of overcoming the diffraction limit of light.[190]

In Chapter 2.7.2 several approaches have been presented, where the selective quenching of fluorescence in compounds bearing a photochromic DAE derivative as the photoswitching unit was achieved. In most fluorophore-photoswitch constructs, either electron or energy transfer is responsible for the modulation, whereat the initial state is strongly emissive while the photoinduced form exhibits a diminished fluorescence. These dyads often termed as *turn-off* fluorescence switches, have detrimental properties inherent to the nature of the mechanism involved in the fluorescence quenching. For instance, if intramolecular energy transfer is chosen for the fluorescence quenching (demanding the spectral overlap of the fluorophore's emission with the closed photoswitch's absorption), during fluorescence readout, the excited energy of the fluorescent chromophore is intramolecularly transferred to the closed-ring isomer and the fluorescent state is quenched.

The process excites the closed-ring isomer of the DAE unit and induces the photochromic back-reaction causing the destructive readout.

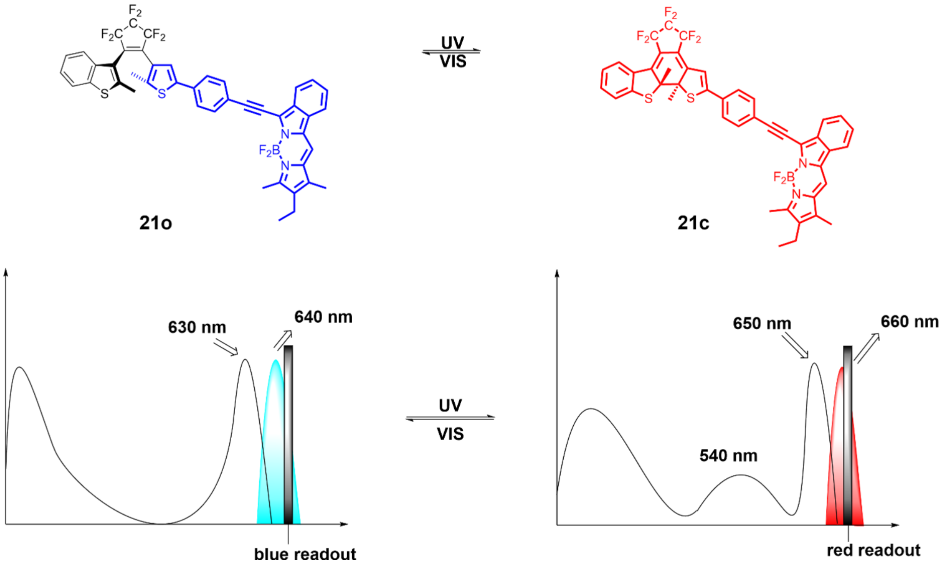

Scheme 3-1: Schematic representation of the bathochromic shift originated by the decrease in the $S_0 \rightarrow S_1$ fluorophore transition with the envisioned dual-fluorescence readout capabilities.

Employing a conjugated bridge to covalently link a fluorophore to a DAE, should upon photoisomerization of the DAE increase the electronic communication between the fundamental states of the dyads components. Such an increased conjugation will diminish the $S_0 \rightarrow S_1$ transition distance in the fluorophore causing a bathochromic shift of the fluorophore’s absorption band (**Scheme 3-1**). Furthermore, if the fluorophore is chosen in such a way that the emission does not overlap the photoswitch’s absorption it can be anticipated that no back-reaction could be induced during readout. In fact, a molecule designed with this working principle could be fluorescent in both the initial and the photoinduced state enabling to reversibly photomodulate the fluorophore’s emission on demand.

3.1.2 Synthesis and Characterization

Compound **21o** was the first synthesized molecular dyad to fulfil and exhibit the targeted behavior outlined in Chapter 3.1.1. Initially synthesized and characterized candidates (**Scheme 3-2**) did not display photochromism and hence will not be described or discussed in this work.[191]

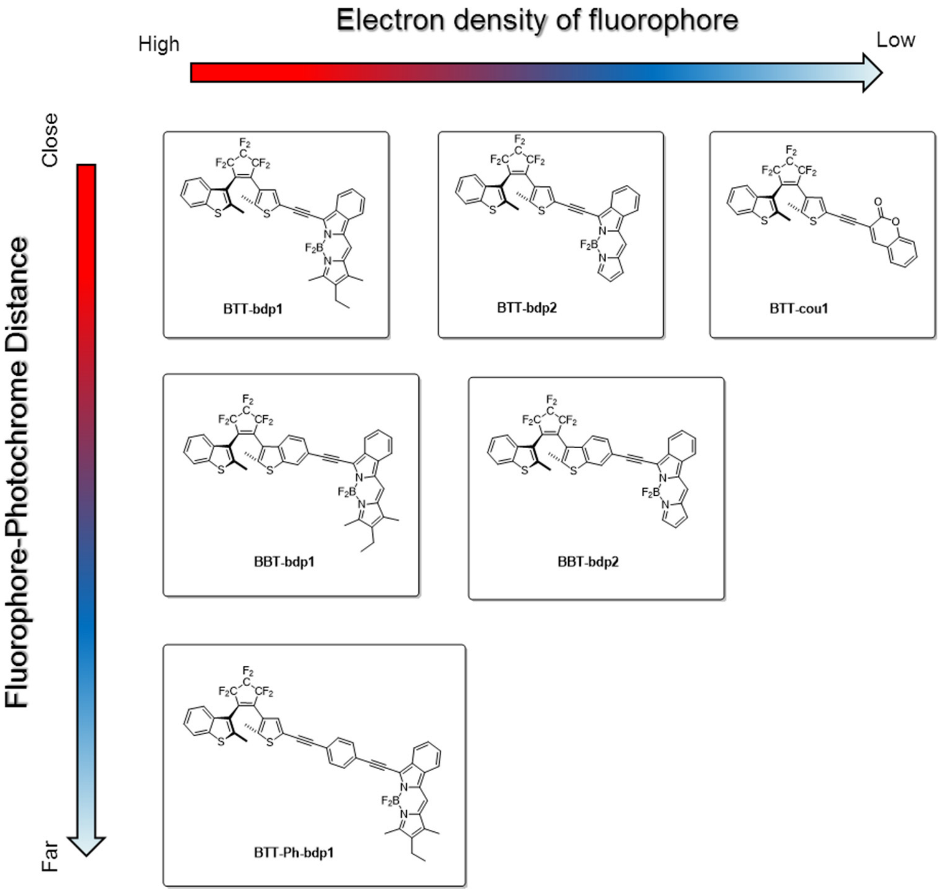
Electron density of fluorophore
High
Low
Fluorophore-Photochrome Distance
Close
Far
BTT-bdp1
BTT-bdp2
BTT-cou1
BBT-bdp1
BBT-bdp2
BTT-Ph-bdp1

Scheme 3-2: Non-photochromic molecular dyads synthesized in the initial stage of this work.

Considering the stringent molecular design, a far-red emitting fluorophore had to be chosen, to avoid overlapping absorption and emission bands in the closed form. With this purpose, a benzo-fused BODIPY dye (**bdp**) which could be covalently linked ensuring conjugation with the DAE was selected (**Scheme 3-3**). Benzo-fused BODIPY dyes enable straightforward non-symmetrical functionalization with nucleophiles or by Pd-catalyzed coupling.[192] The retrosynthesis of the targeted family of dyes evidences the use of inexpensive and readily available materials (**Scheme 3-4**).

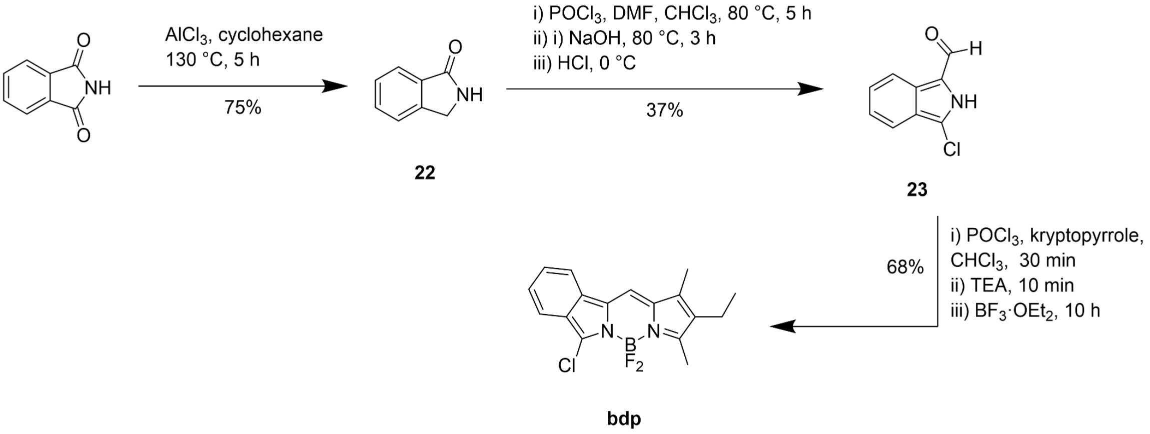
$AlCl_3$, cyclohexane
130 °C, 5 h
75%
i) $POCl_3$, DMF, $CHCl_3$, 80 °C, 5 h
ii) i) NaOH, 80 °C, 3 h
iii) HCl, 0 °C
37%
i) $POCl_3$, kryptopyrrole, $CHCl_3$, 30 min
ii) TEA, 10 min
iii) $BF_3·OEt_2$, 10 h
68%
NH
O
Cl
H
N
B
F_2
22
23
bdp

Scheme 3-3: Synthesis of benzo-fused BODIPY dye **bdp**.

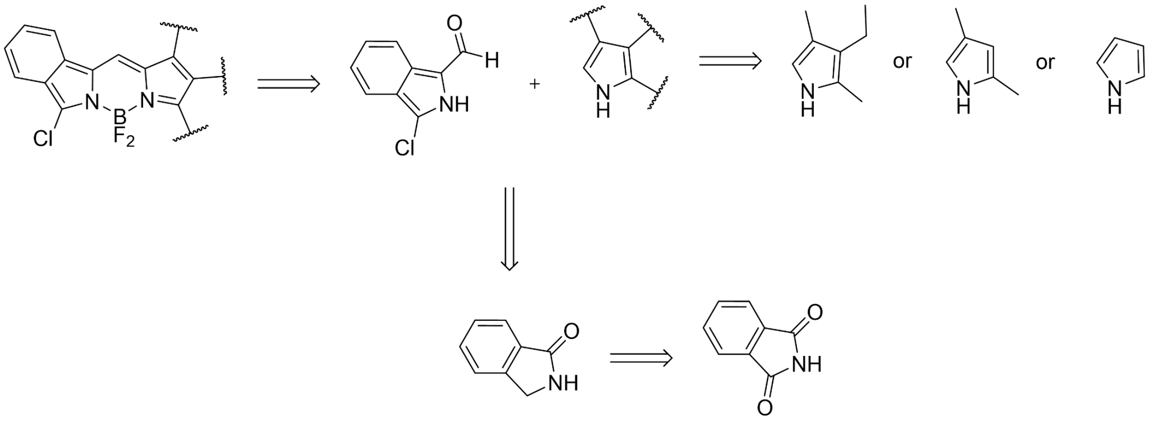
N
B
F_2
Cl
O
H
NH
+
N
H
or
or

Scheme 3-4: Retrosynthetic analysis of the targeted family of BODIPY dyes.

The superacidic reduction of phthalimide, by the addition of 5 eq. of $AlCl_3$ in cyclohexane under elevated pressure in a teflon sealed Schlenck-tube at 120 °C, for 6 h, gave after recrystalization in cyclohexane compound **22** in good yield (75%). The key factor of the reduction is the equilibrium which is established at 120 °C between cyclohexane and methylcyclopentane which in presence of non-anhydrous $AlCl_3$,[193] constitutes the source of hydrogen required for the reduction of phthalimide to isoindolin-1-one **22** (**Scheme 3-5**).

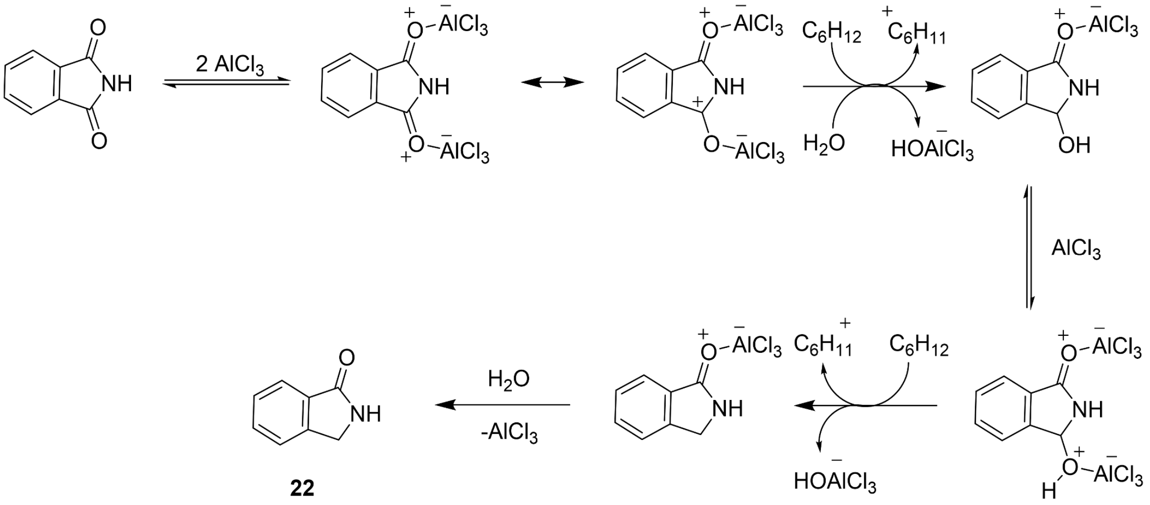
2 AlCl$_3$
AlCl$_3$
C$_6$H$_{12}$
C$_6$H$_{11}$
H$_2$O
HOAlCl$_3$
H$_2$O
-AlCl$_3$
22

Scheme 3-5: Mechanism for the superacidic reduction of phthalimide to isoindolin-1-one.

Under 2:1 Vilsmeier-Haack conditions, chloro-formylation of **22** is performed. Initially, compound **22** undergoes the transformation to Chloroenamine **24** in the presence of DMF and $POCl_3$ in anhydrous $CHCl_3$.[194] The purification by column chromatography over alumina in $CHCl_3$ afforded **24** in the first major greenish fraction. Treatment of **24** with NaOH in EtOH at 70 °C for 3 h, gave after neutralization pure **23** with an overall moderate yield of 37% (**Scheme 3-6**).

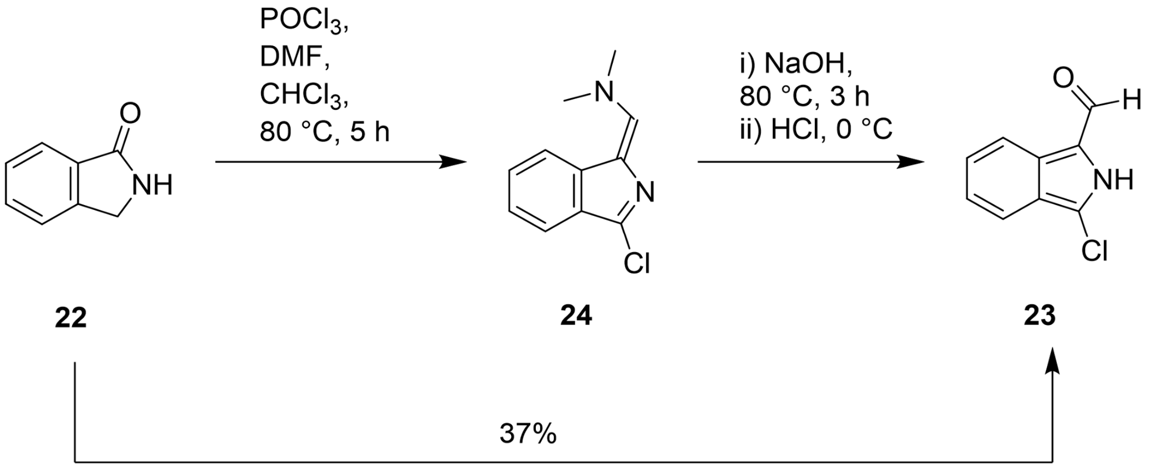
POCl$_3$,
DMF,
CHCl$_3$,
80 °C, 5 h
i) NaOH,
80 °C, 3 h
ii) HCl, 0 °C
22
24
23
37%

Scheme 3-6: Synthesis of chloro-aldehyde precursor for the BODIPY-dyes.

The synthesis of **bdp** could be accomplished by adding kryptopyrrole to a solution prepared from **23** with $POCl_3$ under basic conditions. Final complexation with $BF_3 \cdot Et_2O$

yields after purification by column chromatography, **bdp** in a moderate yield of 57% (**Scheme 3-7**).

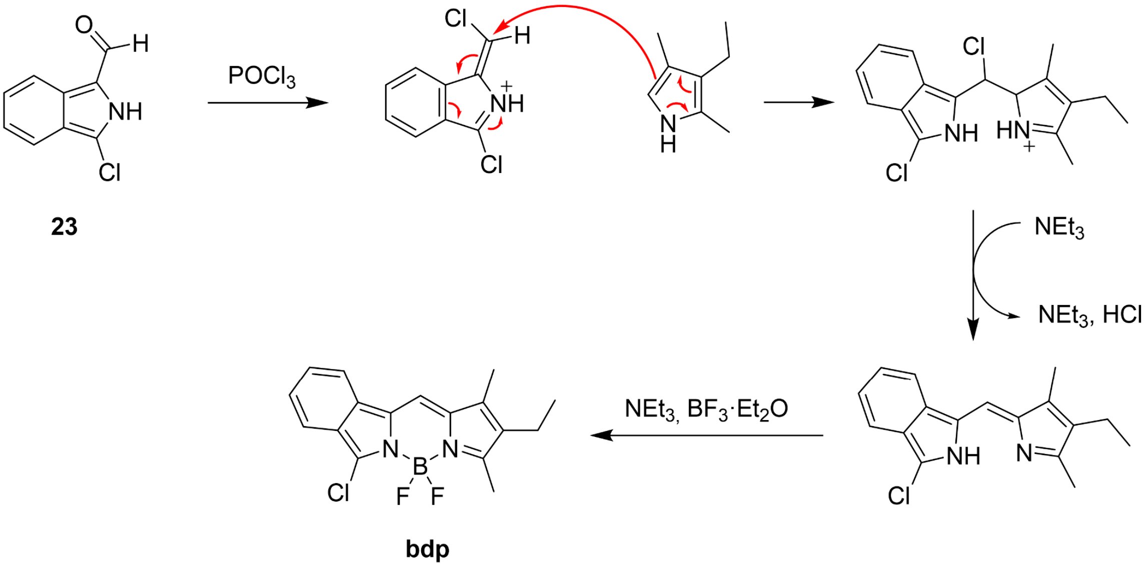

Scheme 3-7: Reaction mechanism for the synthesis of benzo-BODIPY dye **bdp**.

Even though Sonogashira Pd-catalyzed couplings are reported for benzo–fused BODIPY dyes. In the case of BODIPY-Cl substituents, the high temperatures of 80 °C, long reaction times (17 h), basic conditions and the CuI required to proceed to product formation proved to be too harsh to obtain the desired molecular dyad **21o**. The lack of productive coupling was originated by the electron-rich nature of the alkyne bearing coupling partner, which had a thiophene. Instead of Sonogashira coupling only Glasser coupling proceeded during the reaction, obtaining the dimerized alkyne as well as partly decomposed **bdp** (**Scheme 3-8**).

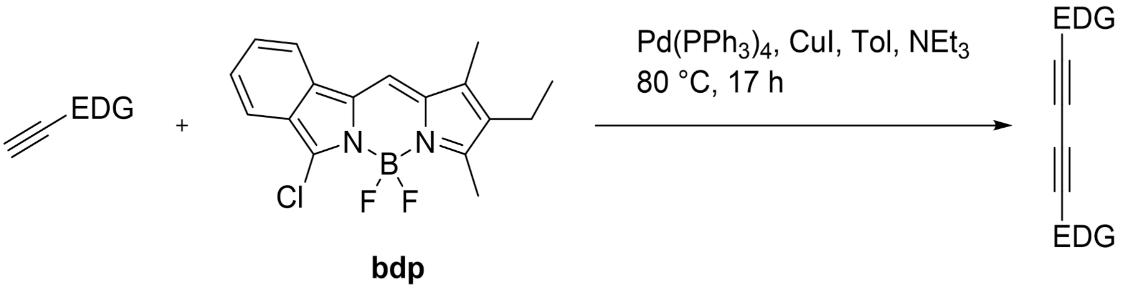

Scheme 3-8: Undesired Glasser-type dimerization of electron-rich alkynes under Sonogashira coupling conditions (EDG = electron-donating group).

To address this synthetic dead-end, several detours were attempted. Namely, the alkyne-bearing unit was exchanged with the BODIPY, to avoid the presence of electron-rich coupling partners (**Scheme 3-9**). Reaction in a teflon sealed tube with 5 eq. of TMSA, $PdCl_2(PPh_3)_2$ and CuI as catalysts in a solvent mixture of anhydrous THF and TEA, heated for 17 h at 70 °C did produce with very poor yields compound **25** (~5%). This was previously observed as it was reported that TMSA is a poor coupling agent with chlorinated-BODIPYs generating multiple side-products.[195] Conversely, using TIPSA in presence of *N*-ethylmorpholine as base and employing a shorter reaction time, was found to significantly improve the yield of the reaction obtaining **26** after purification by column chromatography in acceptable yields (45%).[196] Unfortunately, due to the labile nature of the alkyne-BODIPY, after desilylation with TBAF in THF at room temparture, it was not possible to achieve a subsequent Sonogashira coupling with an aryl-iodide.

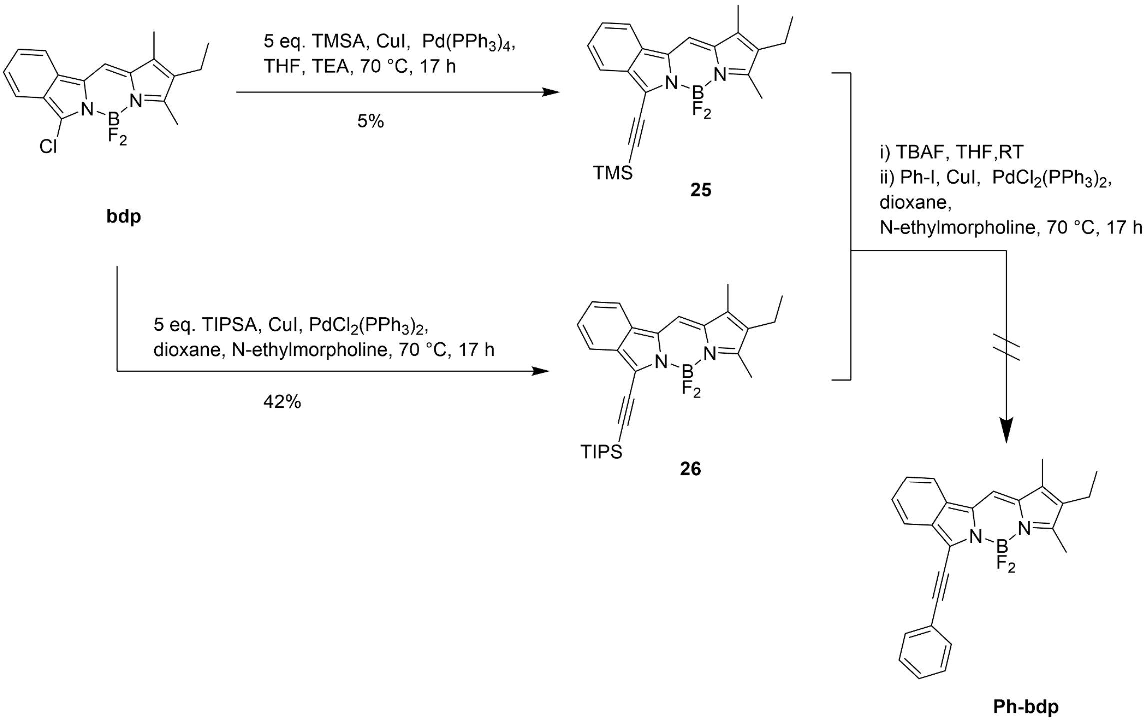
5 eq. TMSA, CuI, Pd(PPh3)4,
THF, TEA, 70 °C, 17 h
5%
Cl
N
B
F2
bdp
5 eq. TIPSA, CuI, PdCl2(PPh3)2,
dioxane, N-ethylmorpholine, 70 °C, 17 h
42%
TMS
25
TIPS
26
i) TBAF, THF,RT
ii) Ph-I, CuI, PdCl2(PPh3)2,
dioxane,
N-ethylmorpholine, 70 °C, 17 h
Ph-bdp

Scheme 3-9: Synthesis of alkyne-BODIPYs and attempted Sonogashira coupling to obtain model compound **Ph-bdp**.

Another detour to solve the synthetic problem, comprised an increase of reactivity in **bdp**. This was achieved by substitution of the chlorine-atom with bromine (**Scheme 3-10**).

The substitution was accomplished by employing the same synthetic protocol as employed towards the obtention of **bdp**, but using $POBr_3$ instead of $POCl_3$ when required.

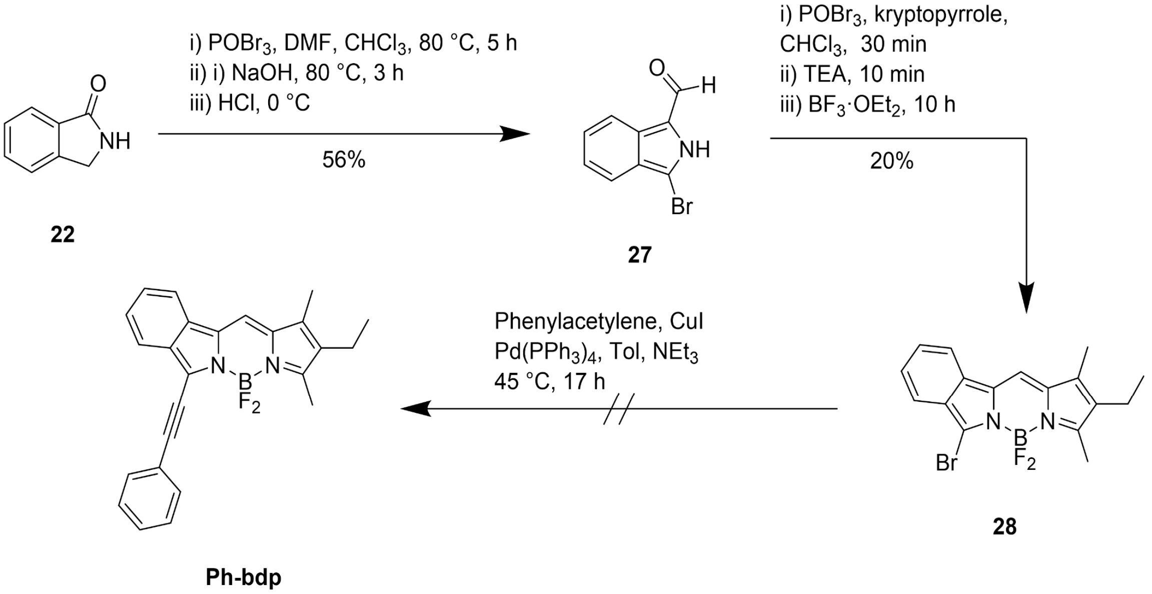
i) POBr3, DMF, CHCl3, 80 °C, 5 h
ii) i) NaOH, 80 °C, 3 h
iii) HCl, 0 °C
56%
i) POBr3, kryptopyrrole, CHCl3, 30 min
ii) TEA, 10 min
iii) BF3·OEt2, 10 h
20%
Phenylacetylene, CuI
Pd(PPh3)4, Tol, NEt3
45 °C, 17 h
O
NH
H
Br
N
B
F2
Br
22
27
28
Ph-bdp

Scheme 3-10: Synthesis of the bromo-derived BODIPY dye **28.**

While the synthesis of the bromo-aldehyde **27** underwent with an increased yield, during purification it was observed that compound **28** was in comparison with other previously synthesized chloro-derived BODIPYs much more labile. During gentle rotavap heating **28** already underwent side-reactions. It was therefore not surprising that the Sonogashira coupling did not proceed to the desired model compound **Ph-bdp**.

The successful alternative was obtained when attempting base-free Pd-catalyzed coupling conditions which avoided the presence of Cu(I) (**Scheme 3-11**).

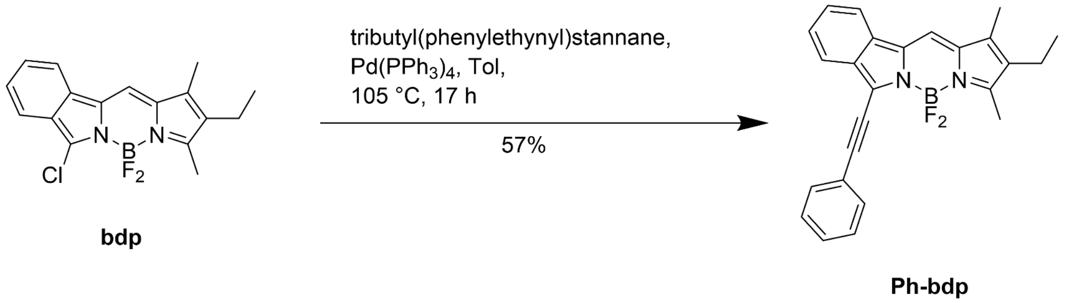
tributyl(phenylethynyl)stannane,
Pd(PPh3)4, Tol,
105 °C, 17 h
57%
N
B
F2
Cl
bdp
Ph-bdp

Scheme 3-11: Successful synthesis of **Ph-bdp** under Cu(I) and base-free conditions.

It is known that ethynyl-stannanes are the most reactive coupling-agents in the Pd-catalyzed Stille-coupling reaction, being able to efficiently couple with unactivated aryl chlorides.[197] Furthermore, Stille-alkynylation has the significant advantage of not producing homo-coupled products, as it is even possible to couple very electron-rich aniline-derived alkynes with aryl-halides in high yields.[198] Additionally, because the Stille-coupling does not require the presence of a base, the reaction conditions show a large functional-group tolerance. The successful coupling was achieved by addition of tributyl(phenylethynyl)stannane to a degased toluene solution of **bdp** in the presence of $Pd(PPh_3)_4$ and allowing to heat at 105 °C for 17 h. After careful extraction with aqueous KF to eliminate unreacted stannane, purification was accomplished by column chromatography obtaining **Ph-bdp** in a relatively high yield (57%).

Once the synthesis and reactivity of the fluorophore was established, focus was set on the photoswitch. Due to the demand of a blue-shifted absorption band in the closed-form no conventional dithienylethene could be employed. The introduction of one benzo[b]thiophene unit as the aryl group was necessary to promote the required hypsochromic shift of the DAE-band. Furthermore, a substantial increase in fatigue resistance is obtained by the substitution of the thiophene moiety with benzo[b]thiophene units. The augmented fatigue resistance can be rationalized due to the inhibition of the formation of photocyclization by-products. The blocking of the 4-position in the thiophene ring with a fused phenyl-ring efficiently suppresses the side-product formation (**Scheme 2-10**). Likewise, to modulate the strength of the coupling between the components in the molecular dyad, a phenyl-ethynylene-spacer was introduced between both moieties. This unit is of upmost importance, since it resembles the precise equilibrium to possibilitate ground-state electronic coupling of the components, without destroying the photochromism of the DAE. The synthesis of **21o** was accomplished in a modular convergent fashion (**Scheme 3-12**), attaching in the final step the BODIPY (**bdp**) to the DAE (**35**) in a sequential desylilation, lithitation, stannilation and final Pd-catalyzed Stille-alkynilation reaction.

The non-symmetrical DAE **35** was obtained by a sequential nucleophilic substitution of octafluorocyclopentene with two different lithiated aryl residues which were obtained as follows. Regioselective dibromination of 2-methylthiophene afforded after vacuum distillation compound **29** in excellent yield (98%). Similarly, the Sonogashira coupling of TIPSA with 4-iodobromobenzene in degased TEA in the presence of CuI and $PdCl_2(PPh_3)_2$ at 40 °C afforded after 3 h of reaction and purification by column chromatography **30** in excellent yield

(99%). Suzuki-coupling of **29** with **30** was achieved sequentially. Initial lithiation of **29** in anhydrous THF at -78 °C with *n*-BuLi, subsequent borylation with $B(OBu)_3$ and final addition of a 2 M solution of Na_2CO_3 followed by degasing with Ar for 15 min enabled the preparation of the solution to which afterwards **30** and $Pd(PPh_3)_4$ were added. The resulting mixture was then submitted to reflux for 17 h and after work-up and purification by column chromatography compound **31** was isolated in good yield (52%).

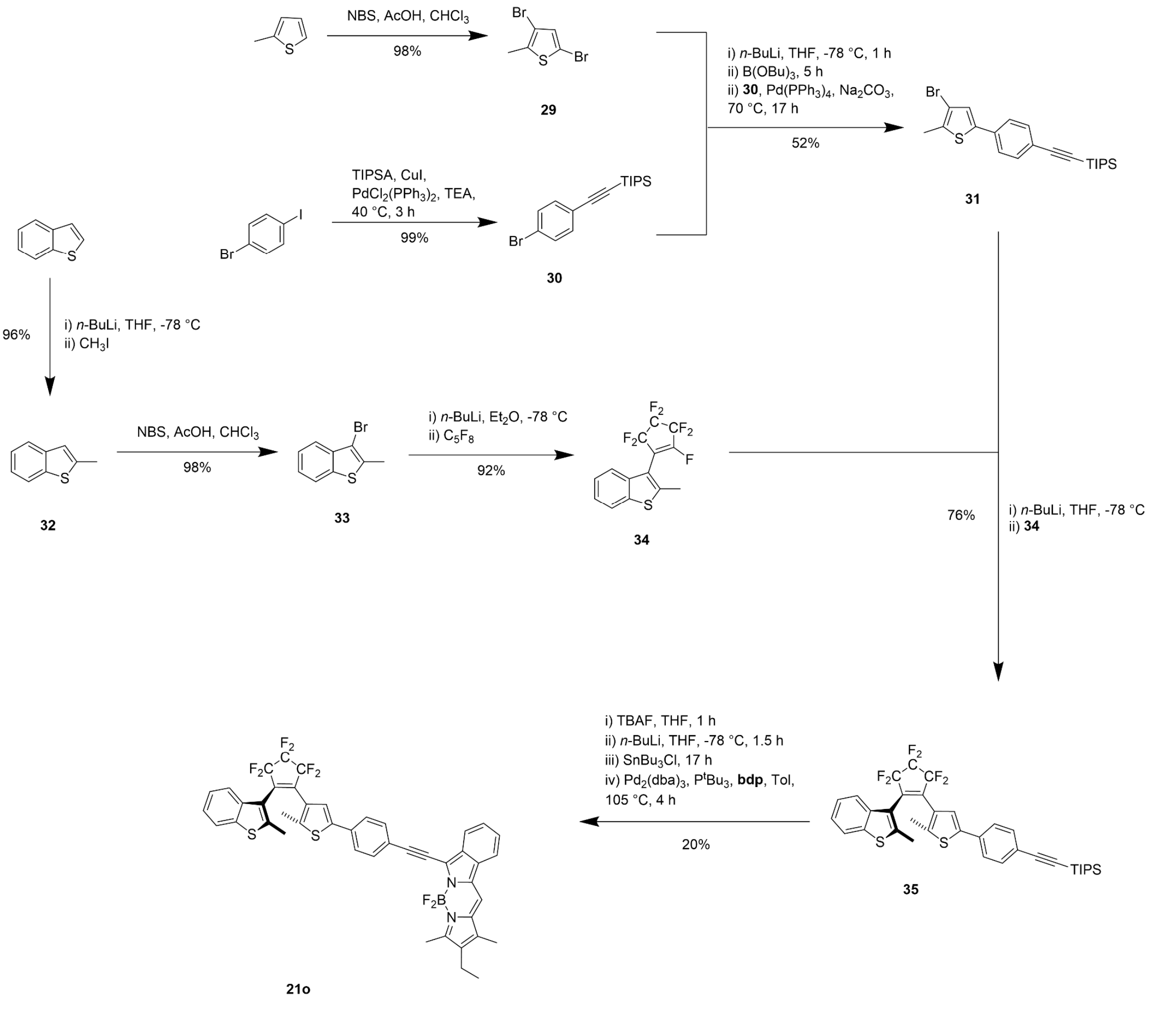
NBS, AcOH, CHCl3
98%
29
TIPSA, CuI,
PdCl2(PPh3)2, TEA,
40 °C, 3 h
99%
30
i) n-BuLi, THF, -78 °C, 1 h
ii) B(OBu)3, 5 h
ii) 30, Pd(PPh3)4, Na2CO3,
70 °C, 17 h
52%
31
TIPS
96%
i) n-BuLi, THF, -78 °C
ii) CH3I
32
NBS, AcOH, CHCl3
98%
33
i) n-BuLi, Et2O, -78 °C
ii) C5F8
92%
34
76%
i) n-BuLi, THF, -78 °C
ii) 34
i) TBAF, THF, 1 h
ii) n-BuLi, THF, -78 °C, 1.5 h
iii) SnBu3Cl, 17 h
iv) Pd2(dba)3, PtBu3, bdp, Tol,
105 °C, 4 h
20%
35
21o

Scheme 3-12: Synthesis of target compound **21o** and precursor DAE **35**.

Benzo[b]thiophene was methylated by the initial lithiation in anhydrous THF at -78 °C with *n*-BuLi, and subsequent addition of CH_3I, the purification was accomplished by column chromatography affording **32** in excellent yield (96%). Regioselective bromination at 3-position was done by addition of NBS in AcOH and $CHCl_3$, which after purification by column chromatography afforded **33** in excellent yield (98%). The synthesis of **34** was vastly optimized compared to previous reports in literature where at least 3 equivalents of the very expensive and volatile octafluorocyclopentane had to be employed.[199] In previous work related to the synthesis of symmetrical DAE precursors (**Scheme 3-2**, **BBT-Ph-bdp1**), it was observed that employing Et_2O instead of THF had a dramatic effect in the formation of the symmetrical DAE, being only able to isolate mono-coupled product although two-fold excess of lithiated 2-methylbenzo[b]thiophene was employed. Therefore, this observation was translated to the directed formation of **34**. In the new modified protocol, an equimolar amount of octafluorocyclopentene and lithitated **33** were employed. Indeed, lithiation of **33** in anhydrous Et_2O at -78 °C with *n*-BuLi, and subsequent addition of one equivalent of octafluorocyclopentene led to the quantitative formation of **34** with an excellent yield after purification by column chromatography of 92%. This newly discovered reaction conditions pave the way for the cost-efficient design of new non-symmetrical DAEs, with exceptional fatigue resistance. The lithiation of **31** in anhydrous THF at -78 °C with *n*-BuLi, and subsequent addition of **34**, afforded after purification by column chromatography non-symmetrical DAE **35** with very good yield (76%). The sequential desilylation with TBAF at room temperature in THF, followed after work-up to the addition of *n*-BuLi in anhydrous THF at -78 °C and subsequent quenching of the lithiated alkyne with $SnBu_3Cl$ enabled the isolation of the alkyne-stannane which was finally brought to dryness and suspended in toluene. The resulting mixture was degased for 15 min and **bdp**, as well as the highly reactive catalyst system composed of $Pd_2(dba)_3$ and P^tBu_3 were added, which upon addition was heated for 4 h at 105 °C. It has to be noted that this catalyst system is immensely more efficient than the use of $Pd(PPh_3)_4$ where the reaction time had to be prolonged for 17 h, additionally conversion to the product is quantitative on hand of UPLC analysis. However, after work-up and purification the isolated yield is reduced due to the acidity of the column chromatography. The dramatic change of color from bright-pink to deep-blue complemented with strong red fluorescence, evidenced the successful coupling reaction, which after purification by column chromatography afforded the target compound **21o** in moderate yield (20%).

Model compound **35** as well as target molecular dyad **21o** show fully reversible photochromism and exhibit appearance of the DAE signature-band in the visible part of the spectrum upon photocyclization (**Figure 3-1**). The photocyclization and cycloreversion quantum yields along with molar absorptivities and composition at the PSS of compounds **21o**, **35** are combined in **Table 3-1** and **Table 3-2**. The absorption spectrum of **35o** in DCM exhibits a broad intense band in the UV region which is ascribed to the π→π* singlet-singlet transition. Upon irradiation with 313 nm, the growth of a band within the 460-650 nm range accompanied with a broad band of smaller intensity between 370-460 nm is observed. The buildup of the long wavelength band was accompanied by a decrease of the intense band centered at 318 nm. The open/ closed isomer ratios in the PSS of **35** were estimated as 15:85 based on the analysis of the NMR spectra. The isomerization quantum yield for the cyclization at 313 nm was of 0.63. The relatively high value can be explained with the establishment of a preferential orientation in solution, favoring the photoactive anti-parallel for. This energetically preferred orientation could be induced by the relative bulkiness of substituents at the thiophene aromatic unit which forces the benzo[b]thiophene unit in an anti-parallel conformation to minimize repulsions. In contrast, upon visible light irradiation at 546 nm, the cycloreversion was inititated with the concomitant raise of the 318 nm band and decrease of the broad visible bands. The determined cycloreversion yield of 0.02 is in the common range for phenyl substituted DAEs.[200] The absorption spectrum of **21o** in DCM exhibits a broad intense band in the UV region which is ascribed to the π→π* singlet-singlet transition. Interestingly the shape is significantly broadened in comparison with **35o** as in the same spectral region the S_0-S_2 transition of the BODIPY fluorophore is located. Furthermore, a comparison of the spectral characteristics of **21o** and **21c** in the UV region, leads to the conclusion that the band originally corresponding to the π→π* transition of the DAE is bathochromically shifted and centered at 378 nm. The same effect is observed for the previously mentioned S_0-S_2 transition of the BODIPY, being red-shifted from 322 nm in **Ph-bdp** to 333 nm in **21o**. The same red-shift is observed for the main $S_0 \rightarrow S_1$ transition of the BODIPY band centered at 624 nm in **Ph-bdp** and 636 nm in **21o**. These spectral-shifts are attributed to the electronic ground-state coupling and elongated π-conjugated system in the dyad, established between the BODIPY-unit and the DAE-unit in the open form. Upon irradiation with 313 nm, the growth of a band within the 400 - 600 nm range accompanied by the raise of an additional sharp band centered at 658 nm and at 330 nm is promoted. The concomitant decrease of the $S_0 \rightarrow S_1$ transition band endorsed to the BODIPY fluorophore centered at 636 nm as well as the π→π* transition of the DAE centered at 378 nm is observed during the cyclization process.

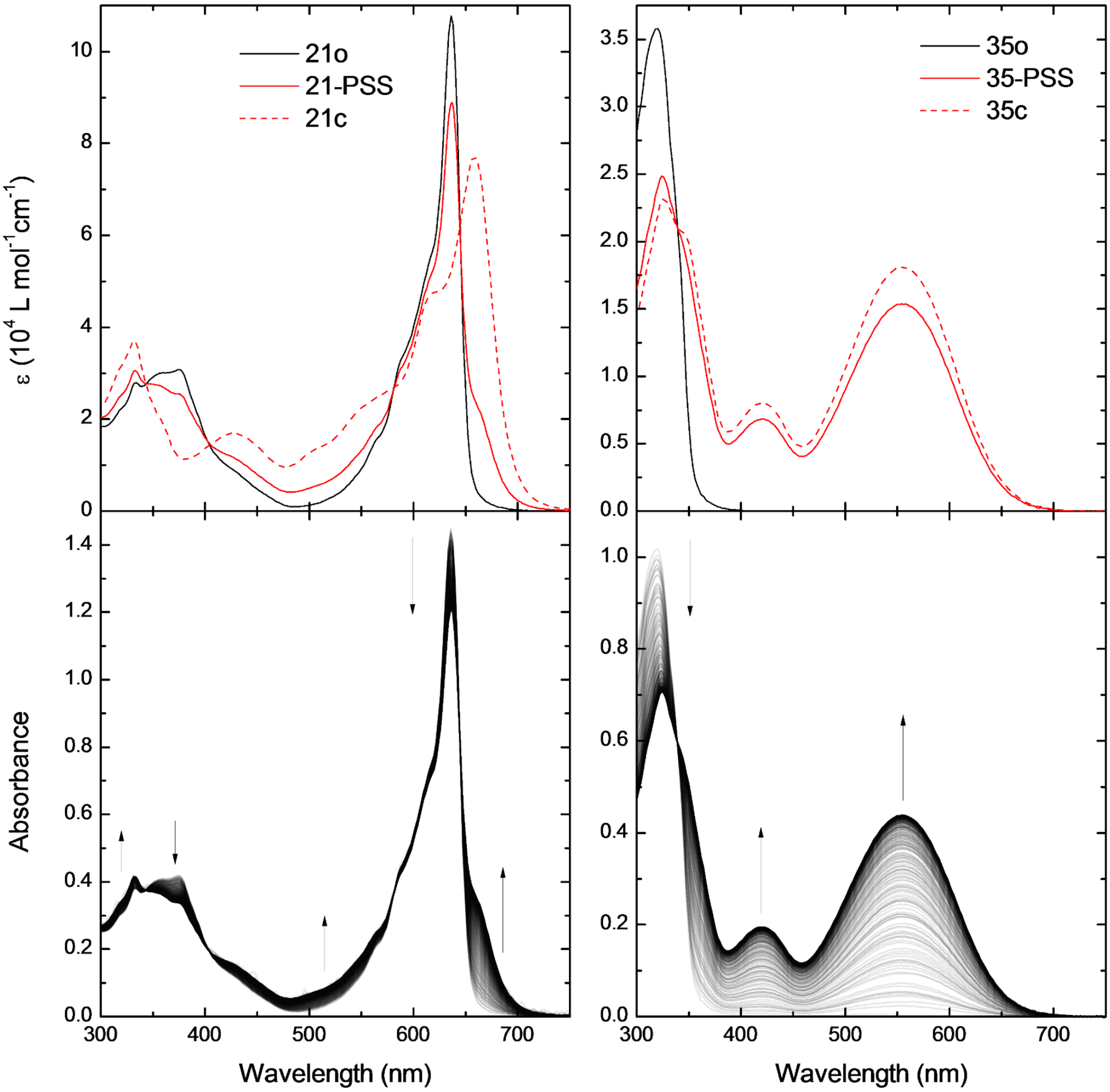

Figure 3-1: UV/vis absorption spectra of **21** (top-left) and **35** (top-right), where the open-form (black line), the PSS (red line) and the simulated pure closed-form (dashed red line) in DCM ($c \approx 10^{-5}$ M) are depicted. Spectral evolution during the course of ring-closure of **21o** (bottom-left) and **35** (bottom-right), induced by irradiation with UV-light (λ_{irr} = 313 nm) at 25 °C.

The open/ closed isomer ratios in the PSS of **21** were estimated as 74:26 in acetonitrile and 56:44 in DCM based on the analysis by ultraperformance liquid chromatography coupled to mass spectrometry detection (UPLC-MS). The isomerization quantum yield for the cyclization at 313 nm was of 0.004. Low values are common for fluorophore-photoswitch molecular dyads, since a large spectral overlap in the UV region imposes a low efficiency to address the electronic transition responsible for the photoisomerization.[172] Upon visible light irradiation at 546 nm, the cycloreversion was initiated with the concomitant raise of the 378 nm band and decrease of the broad visible bands. The determined cycloreversion yield of 0.004 is relatively high for DAEs having an elongated π-system. Although the PSS attained by irradiation of **21o** with 313 nm is rather low, an emerging new band can be distinguished, which is significantly red-shifted to the fluorophore absorption maximum (636 nm). Performing a singular value decomposition (SVD)[a] it was possible to obtain the simulated pure spectrum of **21c**, which was in accordance to the spectra obtained from the UPLC-traces (**Figure 3-2**).

Table 3-1: Molar absorptivities, absorption maxima, composition at the PSS, as well as cyclization and cycloreversion quantum yields of **21** in DCM and MeCN.

	λ_{max} / nm		ε / 10^4 L mol^{-1}cm^{-1}			λ_{irr} / nm	
						313	546
	21o	**21c**	**21o**	**21c**		**o→c**	**c→o**
DCM	636	659	10.80	7.60	ϕ	0.004	0.004
					PSS / %	44	100
MeCN	629	654			ϕ	-	-
					PSS / %	26	100

Table 3-2: Molar absorptivities, absorption maxima, composition at the PSS, as well as cyclization and cycloreversion quantum yields of **35** in DCM.

	λ_{max} / nm		ε / 10^4 L mol^{-1}cm^{-1}			λ_{irr} / nm	
						313	546
	35o	**35c**	**35o**	**35c**		**o→c**	**c→o**
DCM	318	555	3.60	1.80	ϕ	0.63	0.02
					PSS / %	85	100

---

[a] Singular value decomposition (SVD) was performed by Martin Quick of the research group of Prof. Dr. N. P. Ernsting, Humboldt-Universität of Berlin.

The absorption spectrum of the open or closed dyad is not simply the sum of the spectra of the reference BODIPY and **35o/ c**, indicating an electronic coupling between both moieties.The appearance of a red-shifted new band upon photoisomerization evidences a proof of concept for the effect of the increased conjugation in the system upon cyclization.

As was observed for the absorption spectra, the maximum of the emission spectrum of **21o** is bathochromically shifted by 17 nm compared to **Ph-bdp**. This red-shift can be explained with the increased π-system in **21o** compared to **Ph-bdp**, being in agreement with the assumption of the existence of electronic coupling between both moieties in the open-form of the dyad. Additionally, a by 4 nm larger Stokes-shift could be determined for **21o** which is attributed to additional vibrational relaxation prior to the emission. This slightly larger vibrational relaxation might be originated by the augmented freedom degrees of movement of the molecule, since the π-system involved in the emission in **21o** is larger than in **Ph-bdp**. The relative fluorescence quantum yield determined for **Ph-bdp** was of 0.87, which is in line with related BODIPY fluorophores.[192] Interestingly, the relative fluorescence quantum yield of **21o** was slightly lower (0.69), which might be attributed to the fast intramolecular charge transfer process (ICT) from the electron-rich thiophene to the BODIPY acceptor, similar to those previously described in the literature.[201] On the contrary, the emission intensity of **21-PSS** was reduced after irradiation with UV-light. Additionally, even though the overlap of emission and absorption band is negligible, fluorescence quenching is observed upon photocyclization for this compound, which was of 0.44 in DCM (**Figure 3-3**). The extent of fluorescence quenching matches the value obtained for the PSS in this particular solvent and implies that **21c** is non-emissive. The fluorescence emission could be efficiently restored upon cycloreversion by irradiation with visible light at 546 nm. Furthermore, several cycles could be completed without significant appearance of fatigue, highlighting the robustness of the designed molecular dyad.

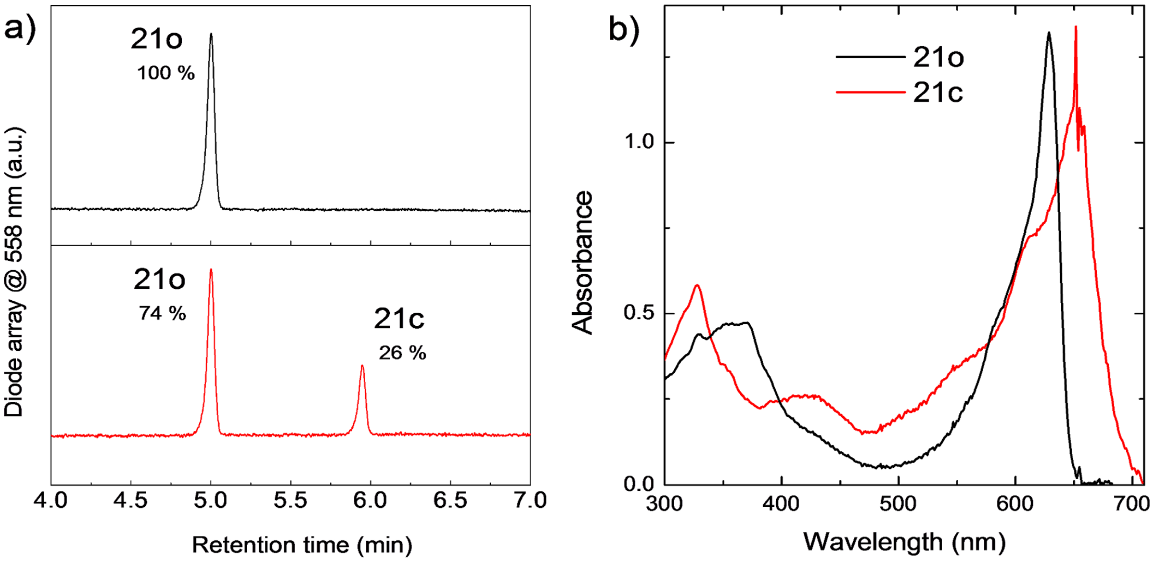

Figure 3-2: a) UPLC-traces of **21o** before irradiation (black line) and after reaching the PSS (red line). b) UV/vis absorption spectra obtained from the UPLC-traces corresponding to the pure open-form **21o** (black line) and the pure closed-form **21c** (red line) in MeCN:H_2O.

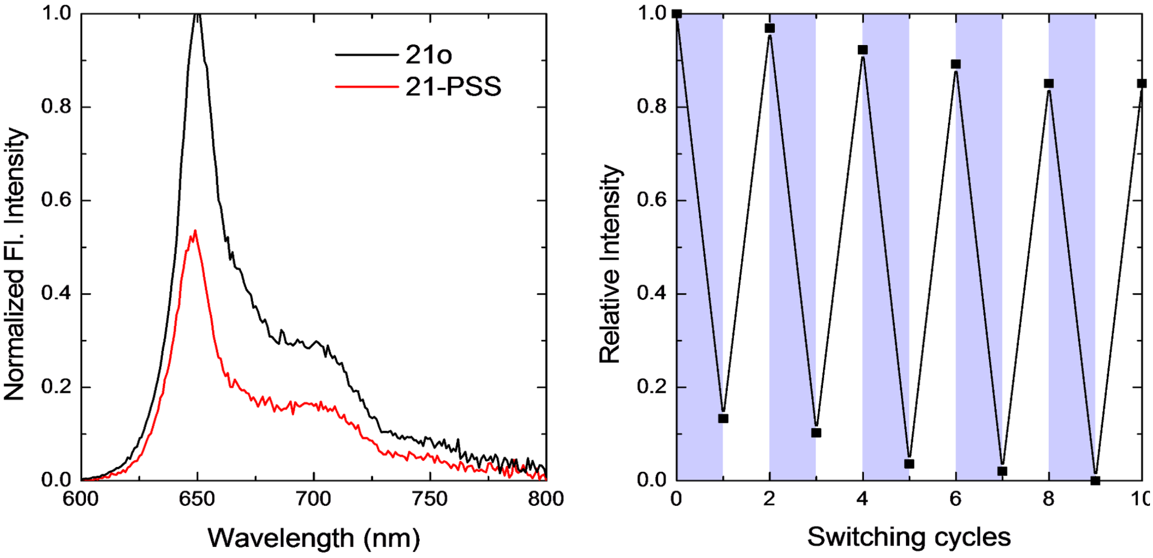

Figure 3-3: Corrected normalized fluorescence emission spectra of **21o** (black line) and in the PSS (red line) obtained in DCM (λ_{exc} = 580 nm, $c \approx 10^{-6}$ M) (left). Relative fluorescence emission intensity upon alternating UV (blue bar) and visible light (whitebar) irradiations to carry out successive switching cycles of **21**(right).

A more concise analysis of the fluorescent properties of **21o** in comparison with the model compound **Ph-bdp** was performed (**Figure 3-4**, **Table 3-3**). With the purpose to evaluate the influence of the cyclized DAE on the fluorescence quenching, the Förster critical distance was calculated employing **Ph-bdp** and **21o** to assess the degree of overlap between the fluorescence emission and the absorption band of **35c**, which was chosen in an approximation as the model compound for the cyclized DAE component of the dyad **21c** (**Figure 3-5**).

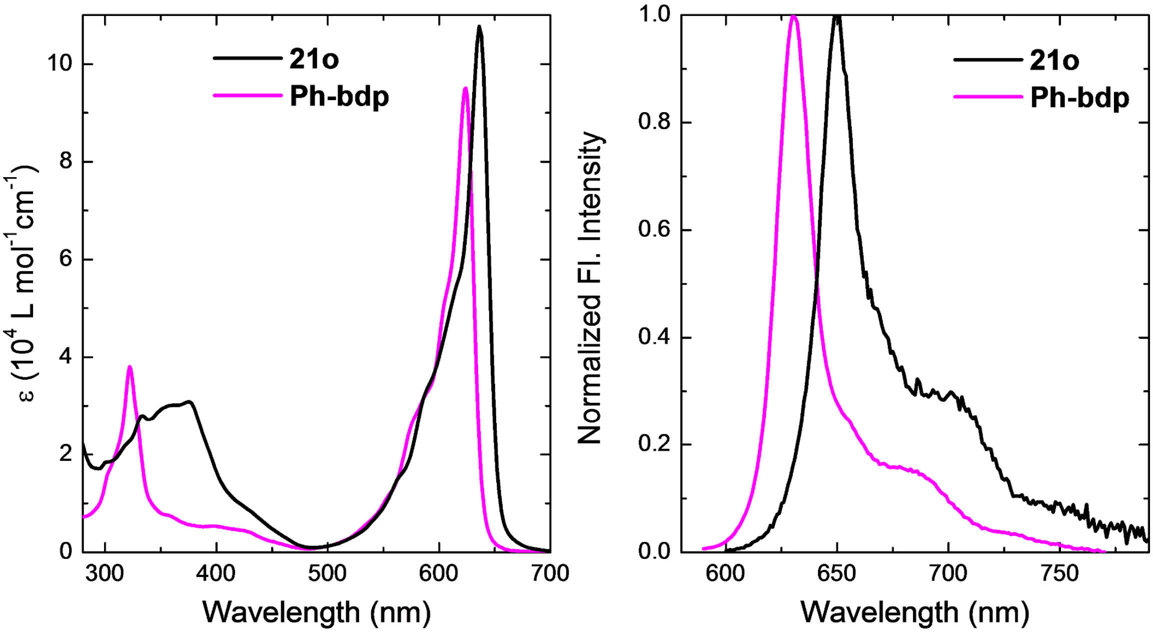

Figure 3-4: UV/vis absorption spectra of **Ph-bdp** (magenta) and **21o** (black) obtained in DCM (c ≈ 10^{-5} M) (left). Corrected normalized fluorescence emission spectra of **Ph-bdp** (magenta) and **21o** (black) obtained in DCM (λ_{exc} = 580 nm, $c \approx 10^{-6}$ M) (right).

Table 3-3: Molar absorptivities, absorption maxima, emission maxima, Stokes shift as well as fluorescence quantum yields and Förster critical distance R_0 of **21** and **Ph-bdp** in DCM.

Compound	ε_{max} / 10^4 L mol^{-1}cm^{-1}	λ_{max} / nm	λ_{em} / nm	Stokes shift / nm	ϕ_{Fl}	Förster distance R_0 / Å
21o	10.80	636	647	11	0.69	36.9
Ph-bdp	9.50	624	630	6	0.90	44.4

The values obtained for the R_0 are very low. Common FRET pairs employed for structural determinations in proteins have values of $R_0 \approx 70$ Å. However, since the distance between donor and acceptor in the dyad is in the range of 10 Å, FRET could be very efficient and it is not surprising that all cyclized molecules are effectively non-emissive. Nonetheless, it has to be considered that the fluorescence emission would be more red-shifted in **21c**, hence, the calculation of the FRET radius is a coarse approximation and probably the poor spectral overlap would be even more pronounced in **21c**, therefore, FRET fluorescence quenching might not be entirely responsible for the completely quenched fluorescence emission of **21c**. To gain further insight into the fluorescence quenching mechanism, cyclic voltammetry (CV)[b] was performed on **21o**, **21c**, **35c** and **Ph-bdp**. Performing CV enabled the determination of the oxidation and reduction potentials, which respectively are related to the HOMO and LUMO levels of the molecule.[202] Knowing the energetic levels of the HOMO and LUMO facilitates the evaluation of a possible PET process involved in the fluorescence quenching. Specifically, it is important to discern if PET is possible from the excited fluorophore to the closed DAE part of the molecule (**Figure 3-6**).

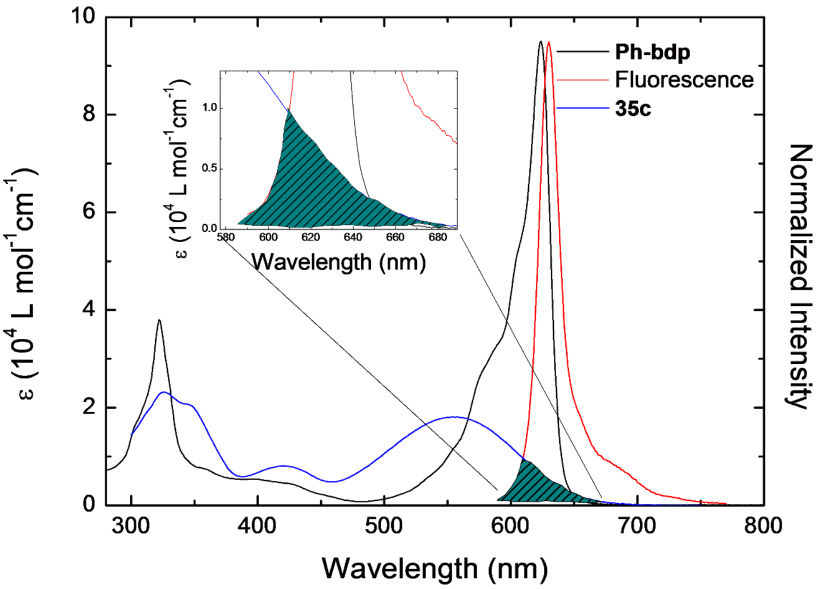

Figure 3-5: Spectral overlap integral (green area, inset enlarged) between model compounds **35c** (blue line) and **Ph-bdp** normalized emission (red line).

---

[b] Cyclic voltammetry measurements were performed by Dr. Lutz Grubert of the research group of Prof. Dr. S. Hecht, Humboldt-Universität zu Berlin.

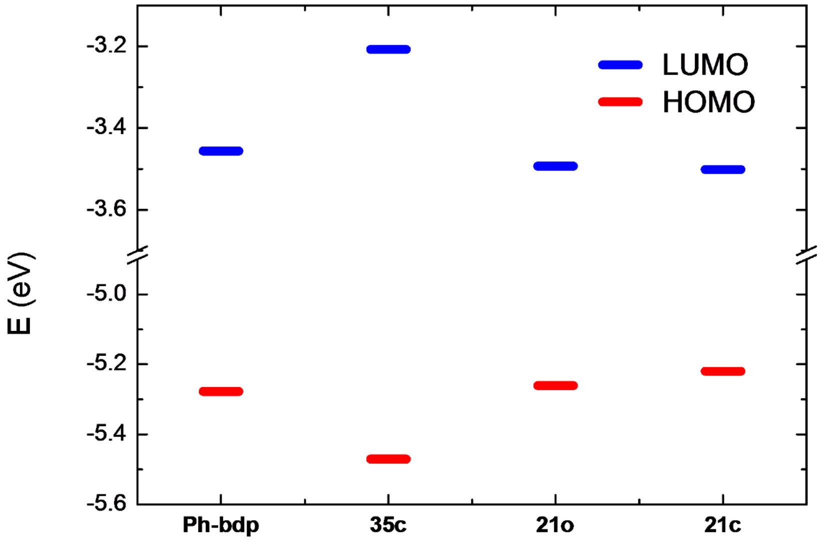

Figure 3-6: Schematic representation of the potential corresponding to the HOMO and LUMO levels determined by CV. Note the slight decrease of the HOMO and LUMO of the dyad upon ring closure.[b]

The determination of the reduction and oxidation potentials evidenced that the HOMO and LUMO were located in the BODIPY-moiety in both the open and closed form of **21**. Furthermore, energetically the LUMO of the DAE (**35c**) is above the LUMO of **21c**. This renders not feasible the hypothesis of a PET from the excited fluorophore-moiety to the DAE-unit. Additionally, due to the reduced gap between HOMO and LUMO of **21c** one further proof is gathered for the effect on the fluorophore imposed by an increase of conjugation upon cyclization.

As it was not possible to fully elucidate the origin of the fluorescence quenching, transient spectroscopy measurements were performed in collaboration with the Goethe-Universität of Frankfurt am Main. These results will be discussed in detail in Chapter 3.1.3. Encouraged by the proof of principle obtained with **21o**, and based on previous findings, where by decoupling DAE component and chromophore, the spectroscopic identity of the individual components was restored,[203] a series of new molecular dyads were designed and synthesized with the objective of achieving full photochromism (**Scheme 3-13**).

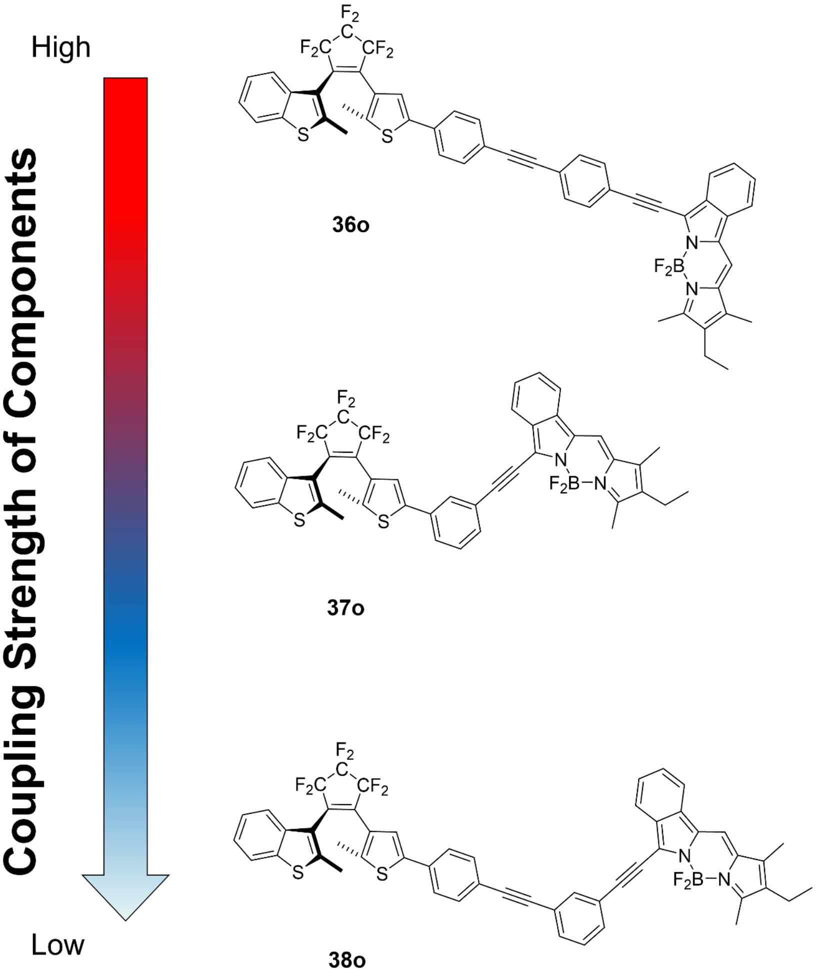

Scheme 3-13: 2nd generation of molecular dyads, designed with a gradual attenuation of coupling-strength between photoswitch and fluorophore.

The synthesis of the DAE precursors for the new molecular dyads was accomplished following a modular approach similar as for **21o** (Scheme 3-14), where in each case the final step of the synthesis comprised the coupling of the stannylalkyne-DAE to the fluorophore **bdp** (**Scheme 3-15**).

The non-symmetrical DAE **42** was obtained by nucleophilic substitution of **34** with a lithiated aryl residue which was obtained as follows. Regioselective Sonogashira coupling of TIPSA with 3-iodobromobenzene in degased TEA in the presence of CuI and $PdCl_2(PPh_3)_2$ at 40 °C afforded after 3 h of reaction and purification by column chromatography **39** in excellent yield (99%). In order to improve the subsequent Pd-catalyzed coupling-reactions with the building-block derived from **39**, bromine was substituted by iodine applying the consecutive lithiation of **39** in anhydrous THF at -78 °C and subsequent quenching with I_2. After purification by column chromatography, compound **40** was obtained in good yield (69%). Suzuki-coupling of **29** with **40** was achieved sequentially. Initial lithiation of **29** in anhydrous THF at -78 °C with *n*-BuLi, following borylation with $B(OBu)_3$ and final addition of a 2 M solution of Na_2CO_3 followed by degasing with Ar for 15 min enabled the preparation of the solution to which afterwards **40** and $Pd(PPh_3)_4$ were added. The resulting mixture was then submitted to reflux for 17 h and after work-up and purification by column chromatography compound **41** was isolated with high yield (82%). The lithiation of **41** in anhydrous THF at -78 °C with *n*-BuLi, and consequent addition of **34**, afforded after purification by column chromatography non-symmetrical DAE **42** with very good yield (74%).

The non-symmetrical DAE **44** was obtained by a sequential desylilation and subsequent Sonogashira coupling. Following this route, homo-coupling of the DAE was observed when employing compound **30**. This observation was ascribed to the reduced reactivity of the bromine-atom and the high tendency of DAE-alkynes to undergo Glasser-coupling due to its electron-rich nature. To circumvent this undesired reactivity, ((4-iodophenyl)ethynyl)trimethylsilane was employed as coupling partner, enabling the possibility to perform the Sonogashira coupling at room temperature due to the increased reactivity of iodine. Indeed, treatment of **35** with TBAF in THF at room temperature, followed by work-up and Sonogashira coupling of the obtained alkyne-DAE with ((4-iodophenyl)ethynyl)trimethylsilane in degased TEA in the presence of CuI and $PdCl_2(PPh_3)_2$ at room temperature, afforded after 3 h of reaction and purification by column chromatography **44** in excellent yield (80%).

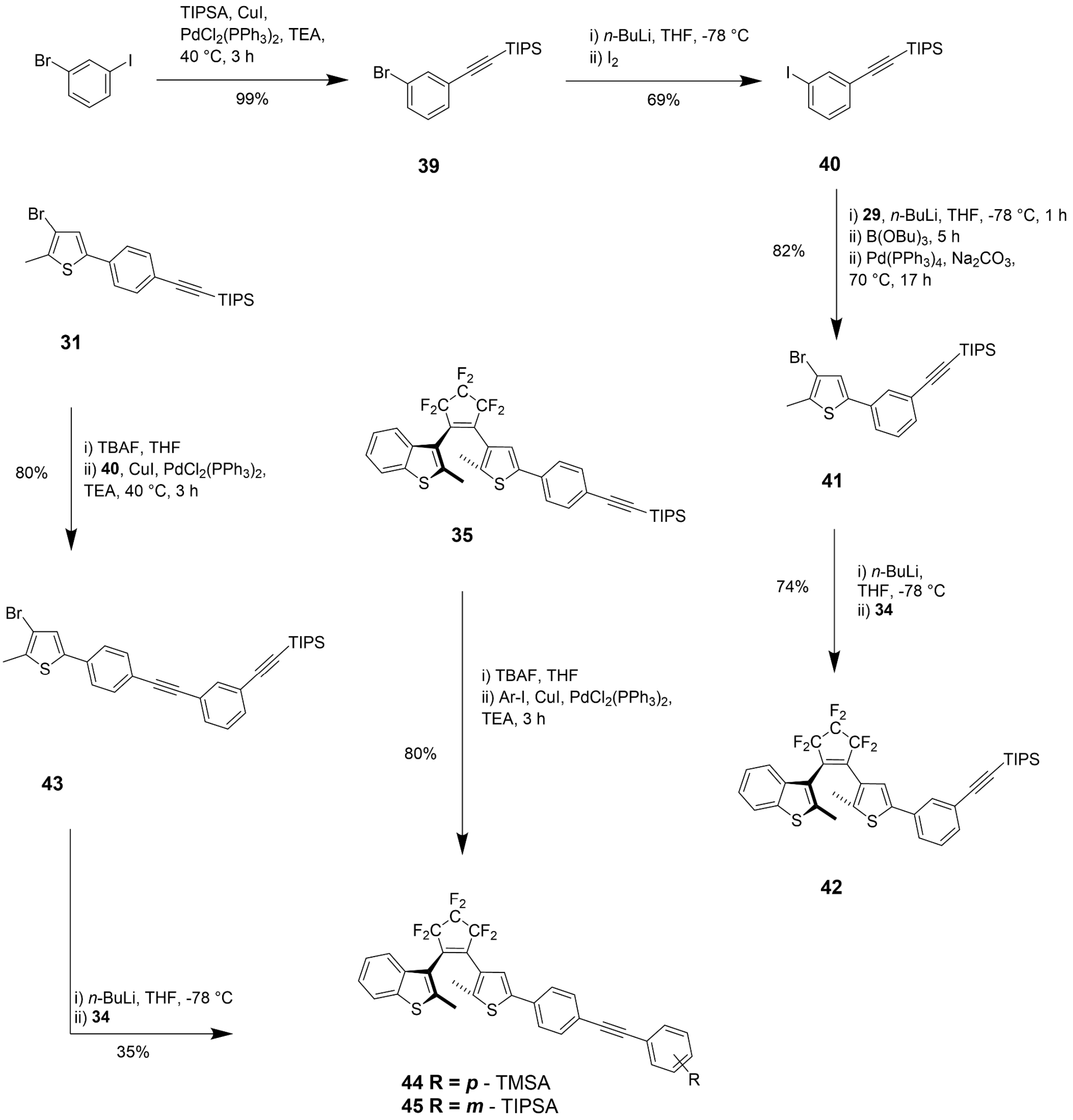
Br
I
TIPSA, CuI,
PdCl2(PPh3)2, TEA,
40 °C, 3 h
99%
Br
TIPS
39
i) n-BuLi, THF, -78 °C
ii) I2
69%
I
TIPS
40
i) 29, n-BuLi, THF, -78 °C, 1 h
ii) B(OBu)3, 5 h
ii) Pd(PPh3)4, Na2CO3,
70 °C, 17 h
82%
Br
S
TIPS
41
i) n-BuLi,
THF, -78 °C
ii) 34
74%
F2
C
F2C
CF2
S
S
TIPS
42
Br
S
TIPS
31
i) TBAF, THF
ii) 40, CuI, PdCl2(PPh3)2,
TEA, 40 °C, 3 h
80%
Br
S
TIPS
43
i) n-BuLi, THF, -78 °C
ii) 34
35%
F2
C
F2C
CF2
S
S
TIPS
35
i) TBAF, THF
ii) Ar-I, CuI, PdCl2(PPh3)2,
TEA, 3 h
80%
F2
C
F2C
CF2
S
S
R
44 R = p - TMSA
45 R = m - TIPSA

Scheme 3-14: Synthesis of precursor DAEs required for the obtention of 2nd generation molecular dyads **36o**, **37o**, **38o**.

The non-symmetrical DAE **45** was obtained by nucleophilic substitution of **34** with a lithiated aryl residue which was obtained as follows. Initial treatment of **31** with TBAF in THF at room temperature, followed by work-up and Sonogashira coupling of the obtained alkyne-DAE with **40** in degased TEA in the presence of CuI and $PdCl_2(PPh_3)_2$ at room temperature, afforded after 3 h of reaction and purification by column chromatography **43** in excellent yield (80%). The lithiation of **43** in anhydrous THF at -78 °C with *n*-BuLi, and subsequent addition of **34**, afforded after purification by column chromatography non-symmetrical DAE **45** with an acceptable yield (35%).

Following the established protocol for **21o**, dyads **36o**, **37o** and **38o** were obtained by the sequential desilylation with TBAF at room temperature in THF, followed after work-up to the addition of *n*-BuLi in anhydrous THF at -78 °C and consequent quenching of the lithiated alkyne with $SnBu_3Cl$ enabled the isolation of the alkyne-stannane which was finally brought to dryness and suspended in toluene. The resulting mixture was degased for 15 min and **bdp**, as well as the highly reactive catalyst system composed of $Pd_2(dba)_3$ and P^tBu_3 were added, which upon addition was heated for 4 h at 105 °C. After purification by column chromatography the target dyads (**36o**, **37o** and **38o**) where obtained in moderate yields (~20%).

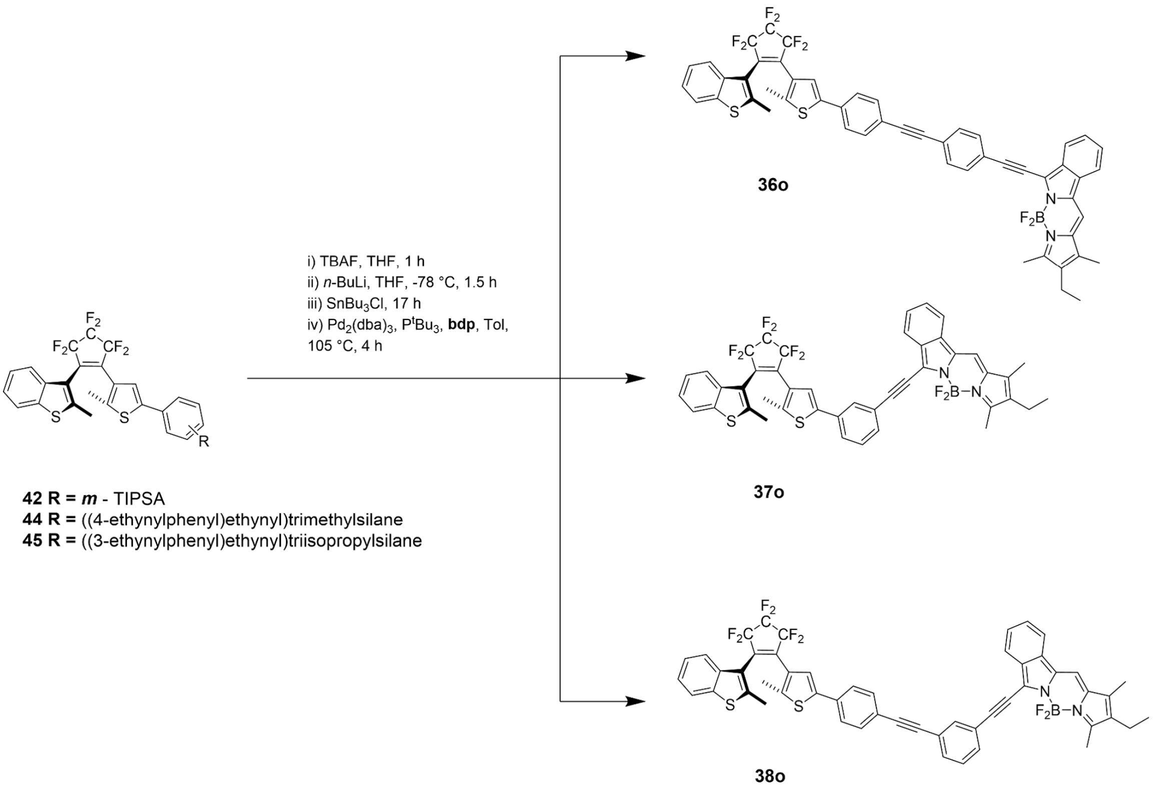
i) TBAF, THF, 1 h
ii) n-BuLi, THF, -78 °C, 1.5 h
iii) SnBu3Cl, 17 h
iv) Pd2(dba)3, PtBu3, bdp, Tol, 105 °C, 4 h
36o
37o
38o
42 R = m - TIPSA
44 R = ((4-ethynylphenyl)ethynyl)trimethylsilane
45 R = ((3-ethynylphenyl)ethynyl)triisopropylsilane

Scheme 3-15: Synthesis of the molecular dyads **36o**, **37o**, **38o**.

Model compounds **42**, **44**, and **45** as well as target molecular dyads **36o**, **37o** and **38o** show fully reversible photochromism and exhibit appearance of the DAE signature-band in the visible part of the spectrum upon photocyclization (**Figure 3-7**, **Figure 3-8**, **Figure 3-9**). The photocyclization and cycloreversion quantum yields along with molar absorptivities and composition at the PSS of compounds **42**, **44**, and **45** as well as target molecular dyads **36o**, **37o** and **38o** are combined in Table 3-4.

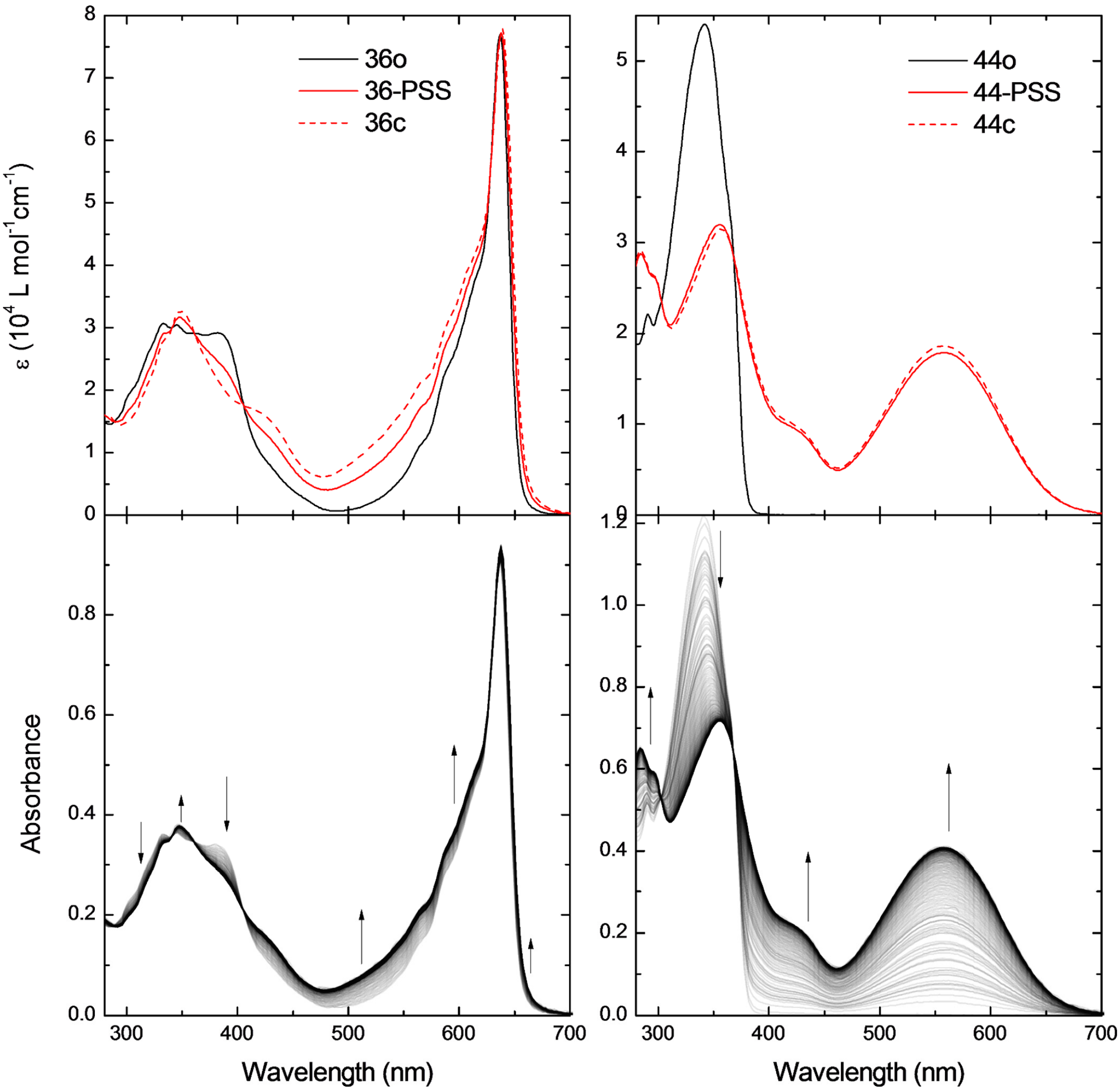

Figure 3-7: UV/vis absorption spectra of **36** (top-left) and **44** (top-right), where the open-form (black line), the PSS (red line) and the simulated pure closed-form (dashed red line) in DCM ($c \approx 10^{-5}$ M) are depicted. Spectral evolution during the course of ring-closure of **36o** (bottom-left) and **44** (bottom-right), induced by irradiation with UV-light (λ_{irr} = 313 nm) at 25 °C.

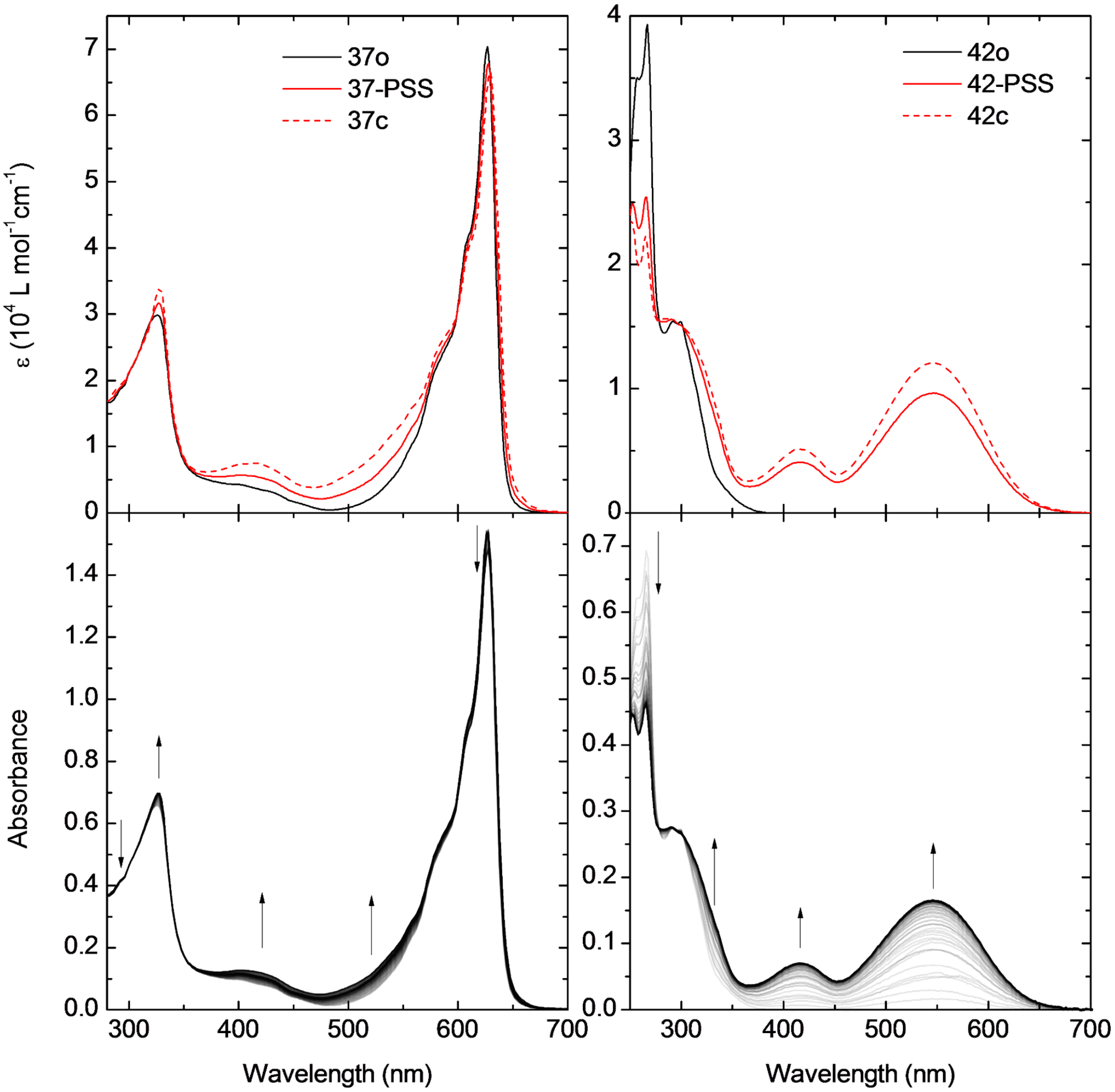

Figure 3-8: UV/vis absorption spectra of **37** (top-left) and **42** (top-right), where the open-form (black line), the PSS (red line) and the simulated pure closed-form (dashed red line) in DCM ($c \approx 10^{-5}$ M) are depicted. Spectral evolution during the course of ring-closure of **37o** (bottom-left) and **42** (bottom-right), induced by irradiation with UV-light (λ_{irr} = 313 nm) at 25 °C.

Contrary to **21o**, upon irradiation of **36o** with 313 nm, a significant amount of the closed isomer **36c** was generated. This observation ratifies that upon electronic decoupling of the components, the spectroscopic identity of each unit is retained, enabling to selectively address each individual component of the dyad. Conversely, since the electronic communication between the fluorophore and the photoswitch is attenuated, no new red-shifted fluorophore-band could be observed upon photocyclization. This assumption is further corroborated with the transient spectroscopy measurements (Chapter 3.1.3).

Table 3-4: Molar absorptivities, absorption maxima, composition at the PSS, as well as cyclization and cycloreversion quantum yields of model compounds **42**, **44**, and **45** as well as target molecular dyads **36o**, **37o** and **38o** in DCM.

Compound	λ_{max} / nm		ε / 10^4 L mol^{-1}cm^{-1}			λ_{irr} / nm	
	open	closed	open	closed		313 **o→c**	546 **c→o**
36	637	638	7.70	7.80	ϕ	0.04	0.01
					PSS / %	60	100
44	342	558	5.40	1.80	ϕ	0.58	0.02
					PSS / %	96	100
37	627		7.00		ϕ	0.014	0.012
					PSS / %	47	100
42	267	546	3.90	1.20	ϕ	0.25	0.02
					PSS / %	80	100
38	627		12.60		ϕ	0.063	0.031
					PSS / %	85	100
45	331	554	4.30	1.60	ϕ	0.30	0.016
					PSS / %	96	100

In the case of **37o**, the ground-state coupling between the DAE and the fluorophore is suppressed. The *meta*-disposition of the components did not prevent a significant overlap of the individual components bands located at the UV-region. Unfortunately, the overlapping band were in the irradiation range where the photochromic reaction is triggered. The overlap originates that the PSS attained in **37o** is low and similar to the PSS determined for **21o**. Prolonged irradiation did not promote any further generation of closed isomer and as was observed for **36c**, no new red-shifted fluorophore-band could be observed upon photocyclization. It could be rationalized that due to the overlap of the absorption bands, upon 313 nm irradiation, photons are employed primarily for the fluorescence emission of the fluorophore (because of the higher oscillator strength at the irradiation wavelength). In a second place photons are absorbed by the open DAE-unit, and promote the cyclization. If this scenario would be accurate, in principle, only longer irradiation times would be necessary to achieve the same PSS as observed for **42**. However, even after prolonge irradiations no significant increase of closed-form was observed. This finding will be described in more detail examining the excited state dynamics upon irradiation (Chapter 3.1.3).

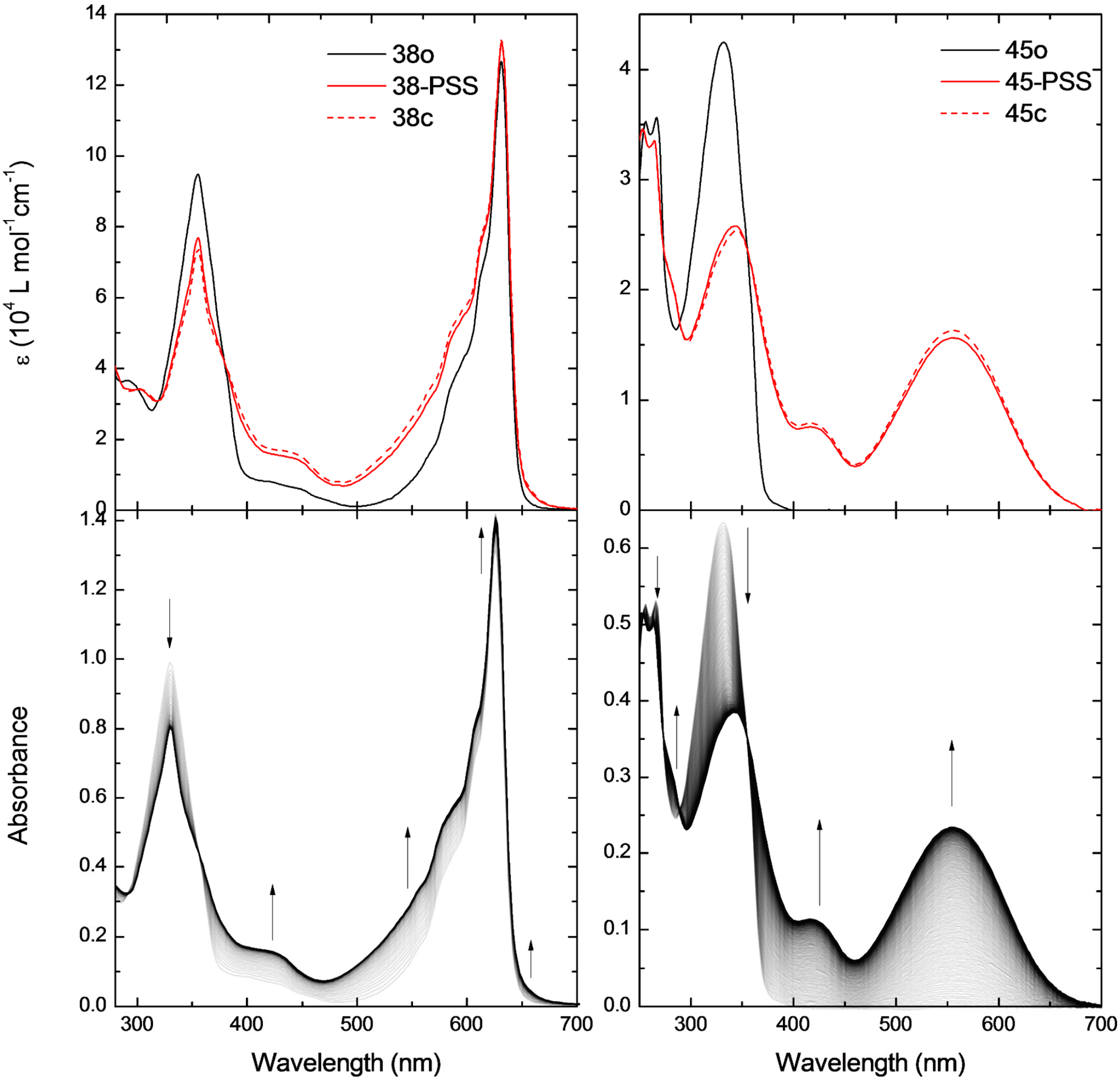

Figure 3-9: UV/vis absorption spectra of **38** (top-left) and **45** (top-right), where the open-form (black line), the PSS (red line) and the simulated pure closed-form (dashed red line) in DCM ($c \approx 10^{-5}$ M) are depicted. Spectral evolution during the course of ring-closure of **38o** (bottom-left) and **45** (bottom-right), induced by irradiation with UV-light (λ_{irr} = 313 nm) at 25 °C.

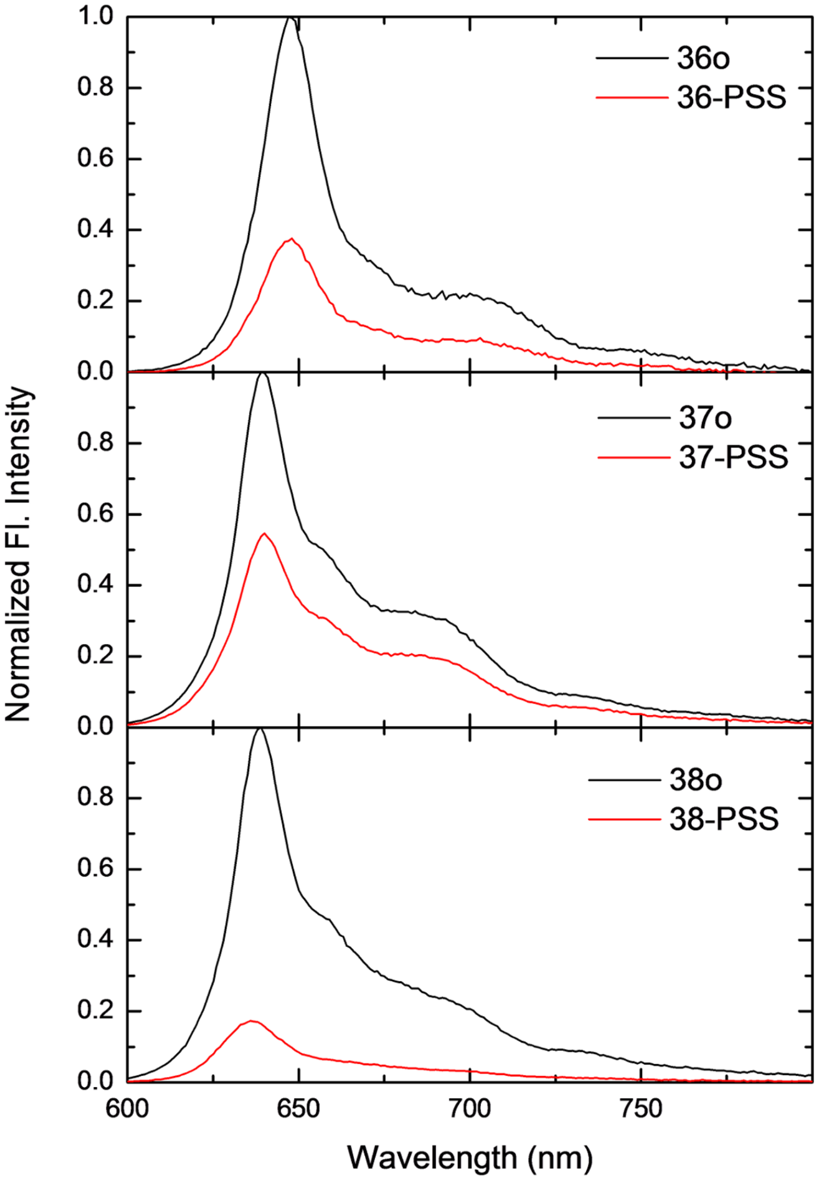

Figure 3-10: Corrected normalized fluorescence emission spectra of **36o** (top, black line), **37o** (middle, black line), and **38o** (bottom, black line), and their respective PSS (red line) obtained in DCM (λ_{exc} = 580 nm, $c \approx 10^{-6}$ M).

The complete decoupling of the components and the mismatched overlap of the band in the UV-region, enabled to improve the switching performance of the DAE achieving a very high PSS in **38o**. Herein, it was possible to selectively address every single component in the UV-region. The results obtained for all four dyads connect the amount of closed molecules with the reduced fluorescence emission of the samples after reaching the PSS (**Figure 3-3**, **Figure 3-10**, **Table 3-3**, **Table 3-5**).

Table 3-5: Molar absorptivities, absorption maxima, emission maxima, Stokes shift as well as fluorescence quantum yields and Förster critical distance R_0 of **36o**, **37o** and **38o** in DCM.

Compound	λ_{max} / nm	ε / 10^4 L mol^{-1}cm^{-1}	λ_{em} / nm	Stokes shift /nm	ϕ_{Fl}	Förster distance R_0 / Å
36o	637	7.70	647	10	0.71	38.2
37o	627	7.00	639	12	0.84	40.4
38o	627	12.60	639	12	0.83	40.3

Since for every dyad the PSS ratio is related to the extent of fluorescence quenching in the closed-form, it can be assumed that the system underlies a very fast and efficient deactivation pathway upon excitation of the closed form. Due to the marginal spectral overlap FRET cannot be the lone cause for the efficient fluorescence quenching. Additionally, triplett quenching should be ruled-out due to the exhaustively degased solutions. Furthermore, HOMO and LUMO levels obtained by CV do not support the possibility of a PET process from the excited fluorophore to the DAE or vice-versa. Therefore, further insight was required to elucidate the nature of the deactivitaion pathways involved in the excited dyads.

3.1.3 Transient Absorption Spectroscopy

As it was mentioned in previous sections, to completely characterize the photophysical properties of the synthesized dyads, transient spectroscopy measurements were performed in collaboration with Felix Schweighöfer.[c] In transient absorption spectroscopy, a fraction of the molecules is promoted to an electronically excited state by means of an excitation (or pump) pulse. Then, a probe pulse is sent through the sample with a delay τ with respect to the pump pulse. A difference absorption spectrum is then calculated, employing the absorption spectrum of the excited sample minus the absorption spectrum of the sample in the ground state (ΔA). By changing the time delay τ between the pump and the probe and recording a ΔA spectrum at each time delay, a ΔA profile as a function of τ and wavelength λ, is obtained. $\Delta A(\tau, \lambda)$. $\Delta A(\tau, \lambda)$ contains information on the dynamic processes that occur in the system such as excited state energy migration, electron and/ or proton transfer processes, isomerization, and intersystem crossing.[204] There are four main contributions to the ΔA spectrum (DAS):

---

[c] The following transient spectroscopy experiments were performed by F. Schweighöfer of the research group of Prof. Dr. J. Wachtveitl, Goethe-Universität Frankfurt am Main.

1. The ground-state bleach (GSB): Ground-state absorption in the excited sample is less than that in the non-excited sample. Consequently, a negative signal in the DAS is observed in the wavelength region of ground state absorption.

2. The stimulated emission (SE): Upon population of the excited state, stimulated emission to the ground state will occur (which will resemble the fluorescence emission) when the probe pulse passes through the excited volume. SE results in an increase of light intensity on the detector, corresponding to a negative ΔA signal.

3. The excited-state absorption (ESA): Upon excitation with the pump beam, optically allowed transitions from the excited states of a chromophore to higher excited states may exist in certain wavelength regions, and absorption of the probe pulse at these wavelengths will occur. Consequently, a positive signal in the DAS is observed in the wavelength region of excited-state absorption.

4. The product absorption: After excitation of the photochemical system, reactions may occur that result in a transient or a long-lived molecular state, such as triplet states, charge-separated states, and isomerized states. The absorption of such a product will appear as a positive signal in the DAS.

Ultrafast transient absorption (TA) spectroscopy was performed on **21** at excitation wavelengths (λ_{exc}) of 600 and 685 nm. At 600 nm both the fluorophore of the open and of the closed dyad can be excited. At 685 nm only the closed isomer of the PSS is addressed. Excitation of the fluorophore in the open dyad results in a long-living TA signal (> 1 ns, **Figure 3-11**) which consists of an excited state absorption (ESA) between 450 and 600 nm and a combination of ground state bleach (GSB) and stimulated emission (SE) at $\lambda > 600$ nm

(**Figure 3-12**). A global fit analysis (of the complete data set) resulted in a main life time of the excited state of 2.6 ns.

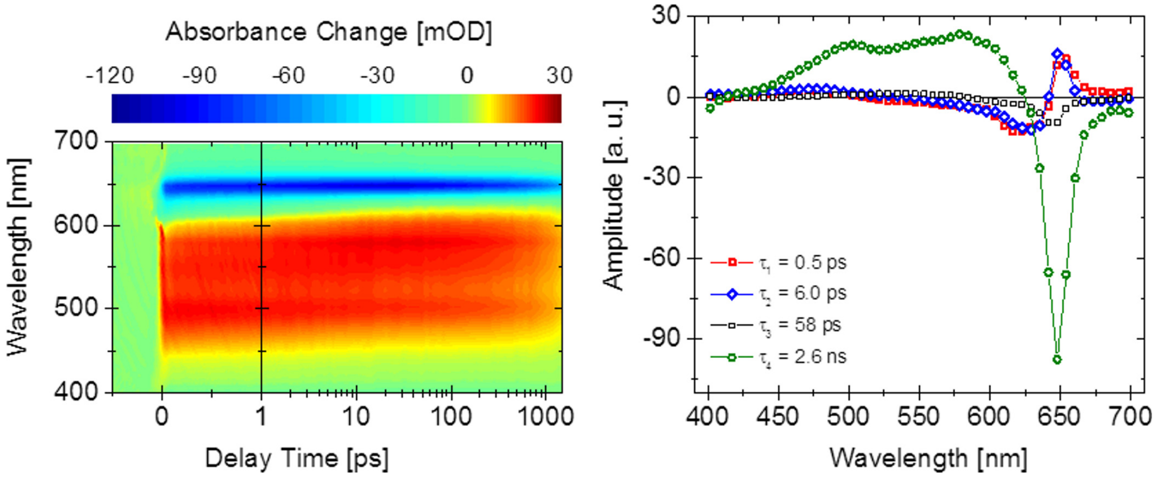

Figure 3-11: TA data of **21o** at λ_{exc} = 600 nm (left), corresponding DAS from global fit analysis (right).[c]

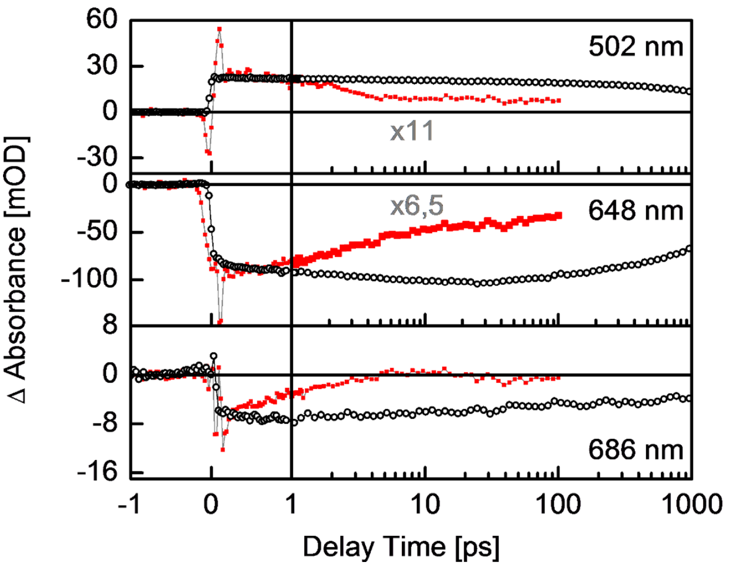

Figure 3-12: Single transient traces at λ_{probe} = 502, 648 and 686 nm of **21o**, excited at 600 nm (black circles) and **21-PSS** excited at 685 nm (red squares).[c]

For the TA measurement of the PSS at λ_{exc} = 685 nm (**Figure 3-13**) a much faster decay of the excited state was observed. The ESA signal (λ_{probe} = 450 - 570 nm) is narrower than in the open isomer and the GSB signal is broader, now ranging from 570 to 700 nm. The main decay took place within the first 10 ps (transient traces at λ_{probe} = 502 and 686 nm,

Figure 3-12). At later delay times a small portion of signal was left which did show the same spectral characteristics as the excited open isomer of the 600 nm measurement. Therefore, it was attributed to excited open isomer of the PSS which could be validated looking at the TA measurement with λ_{exc} = 685 nm of the pure open isomer (TA data, **Figure 3-14**) where as well a negligible amount **21o** was excited.

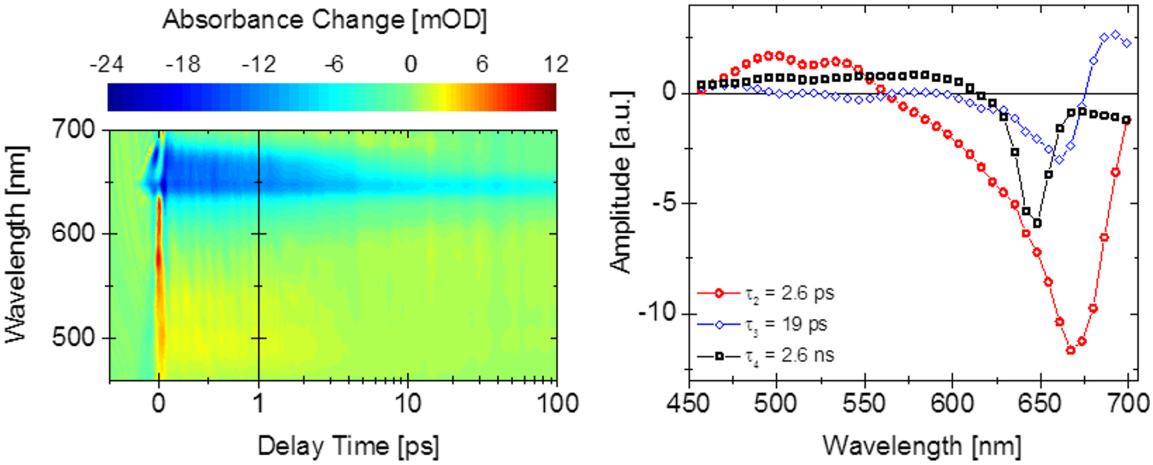

Figure 3-13: TA data of **21-PSS** (left), DAS of **21-PSS** (right) excited at λ_{exc} = 685 nm.[c]

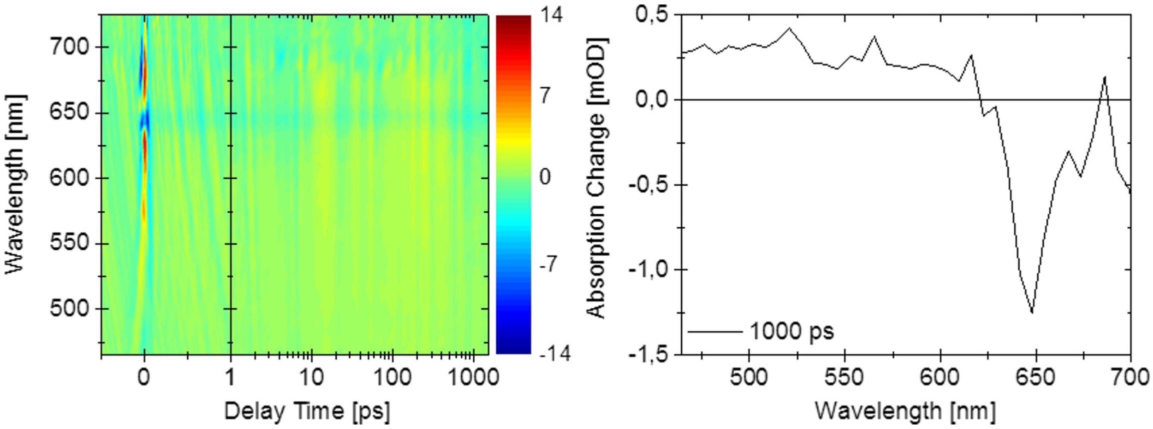

Figure 3-14: TA data λ_{exc} = 685 nm of **21o** (left), DAS at a delay time of 1000 ps (right).[c]

In a global lifetime analysis, four time constants were necessary to describe the data satisfactorily.[205] τ_1 (180 fs, not included) was required to describe a fast process directly after photo excitation. This process was within the time resolution of the experiment (100 fs) and essentially described an ultrafast relaxation in the excited state. The large time constant τ_4 (black line, right **Figure 3-13**) was fixed to a value of 2.6 ns to describe the decay of the part of open isomer within the PSS which was obtained from the measurements of the open isomer excited at 600 nm. Spectra at fixed delay times of both data sets, and the DAS of these two time constants where very similar, which consolidated the assignment. The decay of the main signal is described with the τ_2–DAS (2.6 ps, red line, right **Figure 3-13**) which contributes with large negative amplitudes in the range of the broad GSB signal. The spectral characteristics of this DAS fit well to the steady state absorption spectra of the pure closed isomer. Therefore, this time constant was assigned to the repopulation of the ground state of the closed dyad. The τ_3-DAS (19 ps, blue line, right **Figure 3-13**) with its derivative like shape can be attributed to a cooling process of the closed isomer after relaxation to the electronic ground state, decreasing a slightly red-shifted absorption band. This behavior is already known for other dithienyethene-bodipy conjugates as well as for individual DAEs.[206]

The reference compound **35** was also excited at λ_{exc} = 495 and 600 nm (**Figure 3-15**, **Figure 3-16**). On hand of the TA data, it was confirmed that in the PSS only **35c** is excited at this wavelengths. The TA spectrum of the closed form shows two ESA, one at lower (~500 nm) and one at higher (~670 nm) wavelength. In between is a negative signal, which can be attributed to the GSB of the DAE due to its spectral position. This signal is very weak, so that it is overlaid by the very intense ESA. The signal is very short lived and decays with two main components (τ_2 = 1.1 ps and τ_3 = 6.9 ps, green and red line respectively, left **Figure 3-16**), whereas the decay of the short wavelength ESA is only described by τ_2, while the higher wavelength ESA decays with both components. At longer delay times a very small portion of open isomer is observed as photoproduct, resembling a permanent bleach in the 550 nm region (**Figure 3-17**).[207]

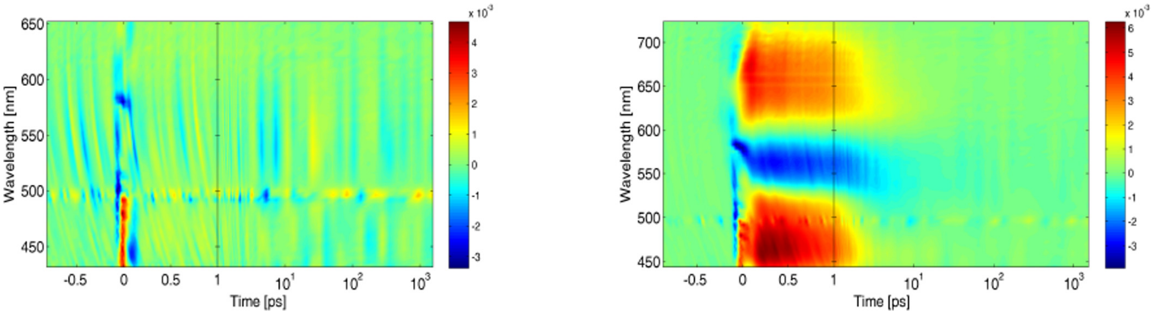

Figure 3-15: TA data λ_{exc} = 495 nm of **35o** (left), **35-PSS** (right).[c]

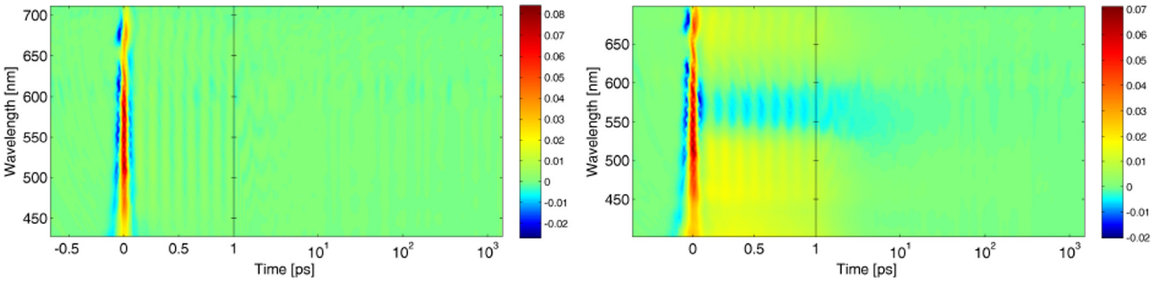

Figure 3-16: TA data λ_{exc} = 600 nm of **35o** (left), **35-PSS** (right).[c]

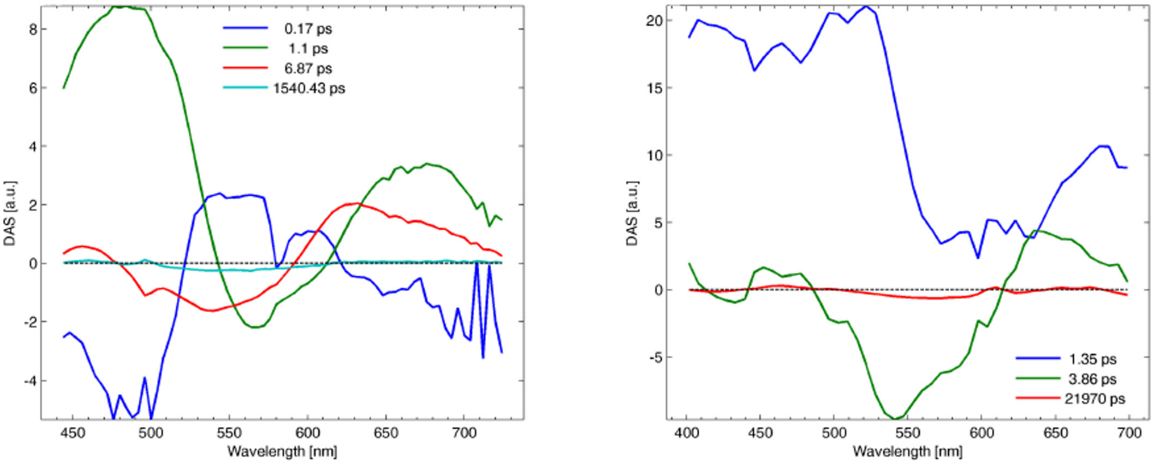

Figure 3-17: DAS of **35-PSS**, excited at λ_{exc} = 495 nm (left), excited at λ_{exc} = 600 nm (right).[c]

Comparison of the relaxation dynamics between the excited **35c** and **21c** allows to identify several similarities. As it was possible to selectively address with 685 nm **21c**, it can be simplified that the fluorophore in conjugation with the DAE, effectively extends the DAE absorption band to the red. All these observations lead to conclude that in the closed dyad the BODIPY and the DAE are electronically coupled. Due to this coupling, they behave as one unit whose relaxation dynamics are comparable to the ones of the pure DAE. The fast non-radiative relaxation proceeds through at least one conical intersection, as it is widely discussed for various DAE.[206] An energy transfer from BODIPY to DAE as another possible relaxation pathway can be ruled out due to the absence of any signals of excited pure DAE. The isomerization to the open dyad is not observed, what is reasonable considering the low quantum yield of ~0.4%.

Furthermore, the results evidenced that upon irradiation at 690 nm, only **21c** could be excited. Once **21c** was in the excited state, the excitation energy followed a non radiative pathway which comprised the deactivation of the molecule to the ground state of **21c** or in the photoisomerization to **21o**. This process took place without any fluorescence emission. Steady-state experiments were conducted to corroborate this observation. Irradiation of compound **21c** with 690 nm ratified the generation of open isomer in a more convenient way than by direct excitation of the DAE-band centered at 546 nm. It has to be noted, that the isomerization yield following 690 nm irradiation (0.004) was equal when performing the irradiation at 565 nm (0.004) or 546 nm (0.004) as would be expected by Kasha's rule. Although recently a wavelength dependency in the cycloreversion isomerization yield was determined for two different DAEs.[208] However, since the BODIPY has a significantly higher oscillator strength than the conventional closed DAE-band, the cycloreversion by excitation of the BODIPY-moiety is faster than the cycloreversion by direct excitation of the DAE-band. This finding is in stark contrast with the general observation that for highly conjugated or push-pull DAEs, whose absorption band is shifted to the red, the cycloreversion process is utterly suppressed.[209]

The dyads **36**, **37** and **38** with the corresponding model compounds (**42**, **44**, and **45**) were also investigated by means of TA spectroscopy. However, they resemble very similar signatures, which differ substantially from **21**. Since **38** had the highest PSS, it will be discussed in more detail, while the TA data of the other dyads will not be mentioned due to the similarity and resulting unnecessary extension of the argument. With **38** irradiations at λ_{exc} = 495 and 630 nm were performed. The TA data at λ_{exc} = 630 nm show a GSB at ~630 nm and an ESA signal between 460 and 580 nm (**Figure 3-18**). A faster decay for the PSS is clearly visible and the difference data (**Figure 3-19**) show a fast decay of BODIPY ESA and GSB with a simultaneous increase of DAE ESA. The fact that signals of excited BODIPY disappear, while simultaneously a signal of excited DAE is appearing, leads to the conclusion that energy is transferred from BODIPY to DAE on a sub ps-timescale. The time constant for the energy transfer step in this case is τ_2 = 200 fs and/ or τ_3 = 1.2 ps.

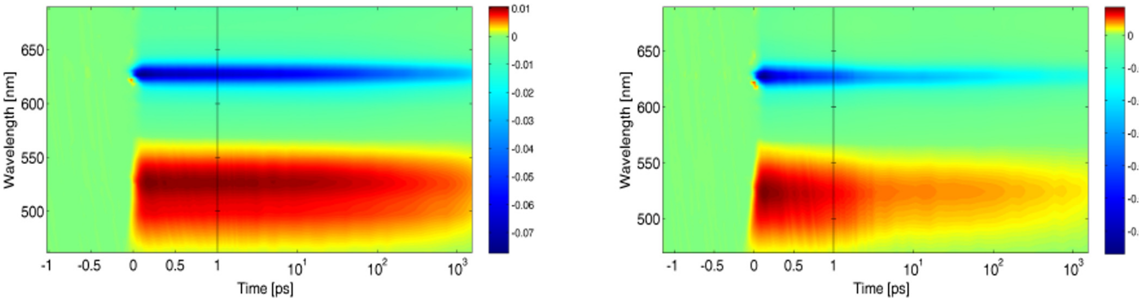

Figure 3-18: TA data λ_{exc} = 630 nm of **38o** (left), **38-PSS** (right).[c]

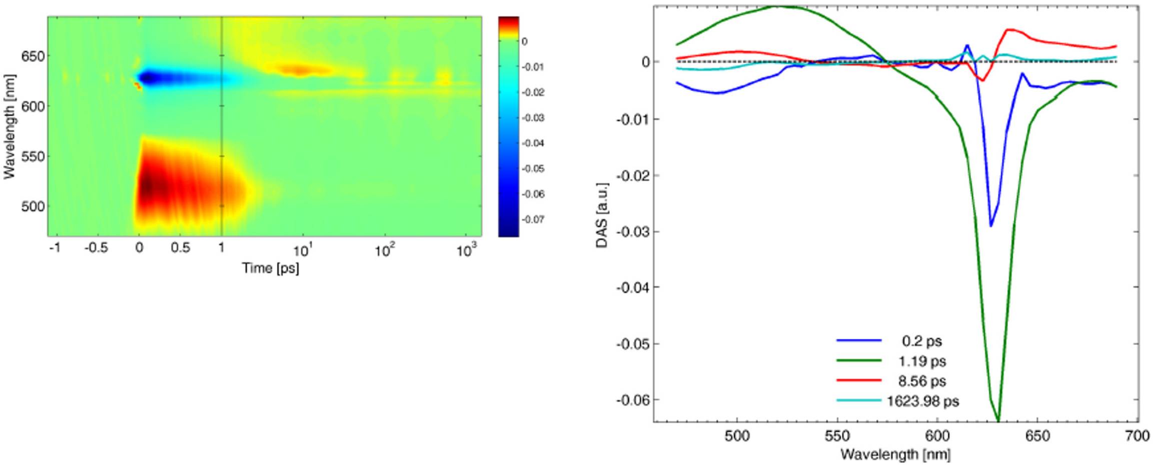

Figure 3-19: TA data difference between **38-PSS** and **38o**, excited at λ_{exc} = 630 nm (left), DAS of corresponding fit (right).[c]

To examine the dynamics of the excited switch, experiments with an excitation wavelength of 505 nm were performed (**Figure 3-20**). At this wavelength, the BODIPY moiety has only a weak absorption, therefore, primarily the DTE is excited. Nevertheless, a direct excitation of the fluorophore could not be avoided completely, which is visible by the negative GSB signal of the BODIPY at ~630 nm. In addition to this signal of direct excited BODIPY, a significantly different signal pattern is observed. It consists of a very weak GSB at λ > 550 nm and two ESA bands, one centered at ~500 nm and the second at λ > 640 nm. This pattern is already known for closed DAE switches and decays within approximately 2 ps. The signal at longer delay times can be assigned to the excited BODIPY in the open dyad by comparing the spectra at 1 ns (**Figure 3-21**) with the one from the directly excited BODIPY. This comparison reveals high similarity, but also shows slight differences (e. g., less absorption at ~560 nm). This might arise from the photoproduct of the cycloreversion reaction, resulting in a residual bleach signal of the closed DAE. TA measurements suggest that the excitation of both parts of the closed molecular dyad leads to EET from the excited to the non-excited moiety. The model resulting from these findings (which also was corroborated with dyads **36** and **37**) is shown in **Scheme 3-16**. It displays the excitation of both parts at different wavelengths, the relaxations to the ground state and the EET between closed switch and BODIPY. Since EET can occur in both directions and the time constants have similar magnitudes, it suggests that an equilibrium between both excited states might be developed. Currently, it is unclear if the life time of the excited states is long enough to reach an equilibrium, especially because the excited DAE underlies a relatively fast relaxation ($\tau_{relax} \approx 7$ ps) to the ground state. Therefore, it can be understood that the build-up of this EET and subsequent equilibration inhibits the fluorescence emission of the BODIPY-unit independently if it was directly or indirectly excited. However, because in the open form of the dyads no such equilibration can take place, the BODIPY can readily emit photons upon excitation.

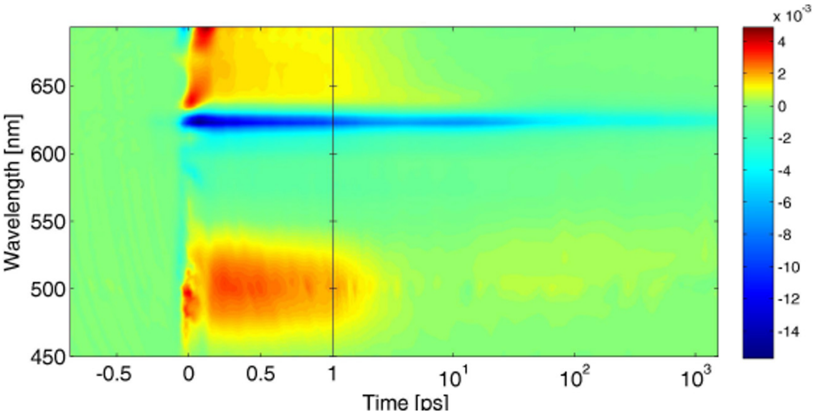

Figure 3-20: TA data of **38-PSS** after photo excitation at λ_{exc} = 505 nm.^{c}

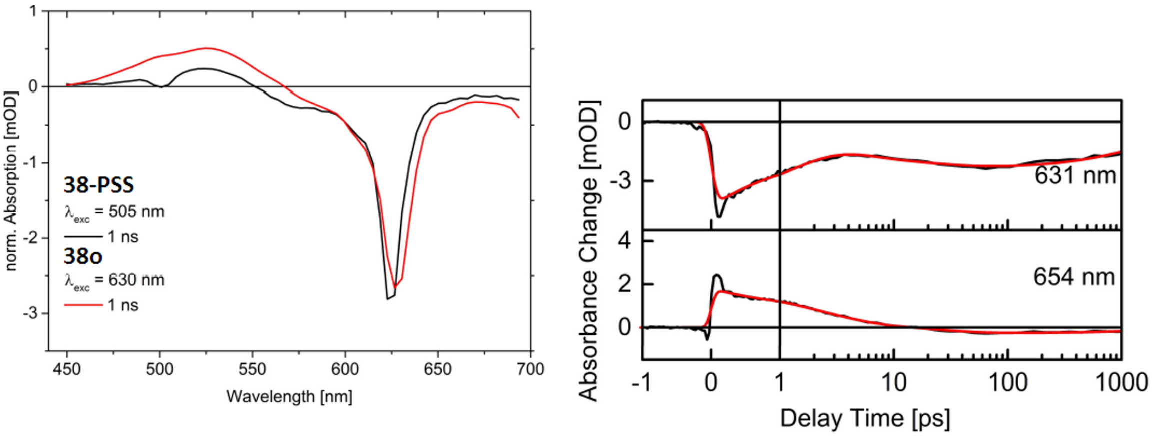

Figure 3-21: Transient absorption spectra at 1 ns, black: after excitation of the BODIPY in **38o**, red: after excitation of the DAE in **38-PSS** (left); single transients of, **38-PSS** (λ_{exc} = 505 nm) at λ_{probe} = 631 nm and 654 nm, an increase of the GSB around 13 ps is clearly visible (631 nm) (right).^{c}

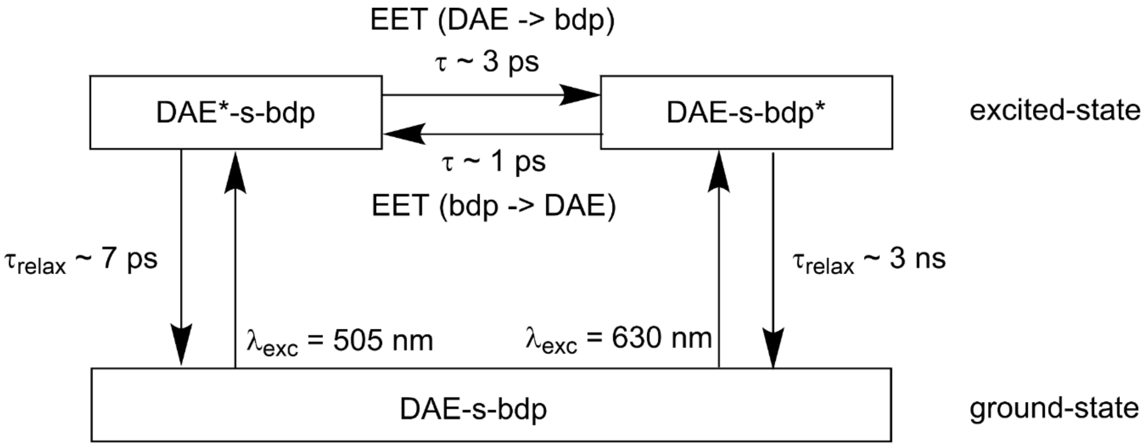

Scheme 3-16: Schematic representation of the processes which take place after excitation of the closed dyads **36c**, **37c** and **38c**.[c]

Furthermore, the fact that no signal of excited DAE can be found in **21-PSS** upon excitation at 685 nm and that the GSB signal looks different to the ones of the other dyads, leads to the conclusion that in this molecule an electronic coupling between fluorophore and DAE exists. This is reasonable due to the shorter bridge length and the linkage via the *p*-position of the phenyl ring. Supported by stationary spectroscopy, it was found that **21c** excited at 685 nm behaved as an improved DAE, whose isomerization efficiency was increased by the higher oscillator strength at the far-red region of the spectrum.

3.1.4 Solubilization in Aqueous Media

Sodium dodecylsulfate (SDS) is an anionic surfactant with amphiphilic properties, having thus a negatively charged hydrophilic region and a neutral single-chain non-polar lipophilic part. SDS has the ability to form very efficiently micelles, once the critical micellar concentration in the solution is reached. A typical micelle in aqueous solution forms an aggregate with the hydrophilic regions in contact with the surrounding solvent, forcing the hydrophobic single-chain regions to the micelle center (**Scheme 3-17**). The difficulty to fill all the volume of the interior of a bilayer, while accommodating the area per head group forced on the molecule by the hydration of the lipid head group, leads to the formation of the micelle. Double-chain amphiphiles such as the saturated dipalmitoylphosphatidylcholine (DPPC) or the unsaturated dioleoylphosphatidylcholine (DOPC) form besides micelles also bilayered structures like vesicles/ liposomes or bilayer sheets. To investigate the feasibility to use **38o** in biological media and its possible applications in fluorescence miscroscopy, the encapsulation of model compound **45** (**Figure 3-22**) and dyad **38** (**Figure 3-23**) in SDS micelles solubilized in water was investigated.

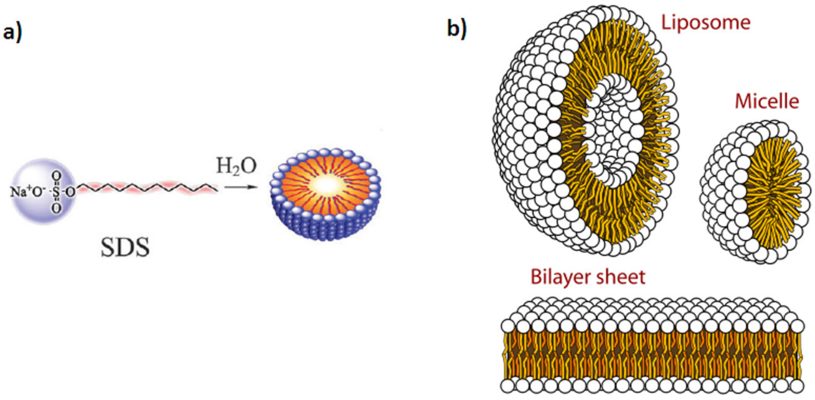

Scheme 3-17: a) Common aggregation behavior of single-chain amphiphiles like SDS in H_2O to form micelles. b) Double-chain amphiphiles in aqueous solutions form micelles, vesicles/ liposomes and bilayer sheets.

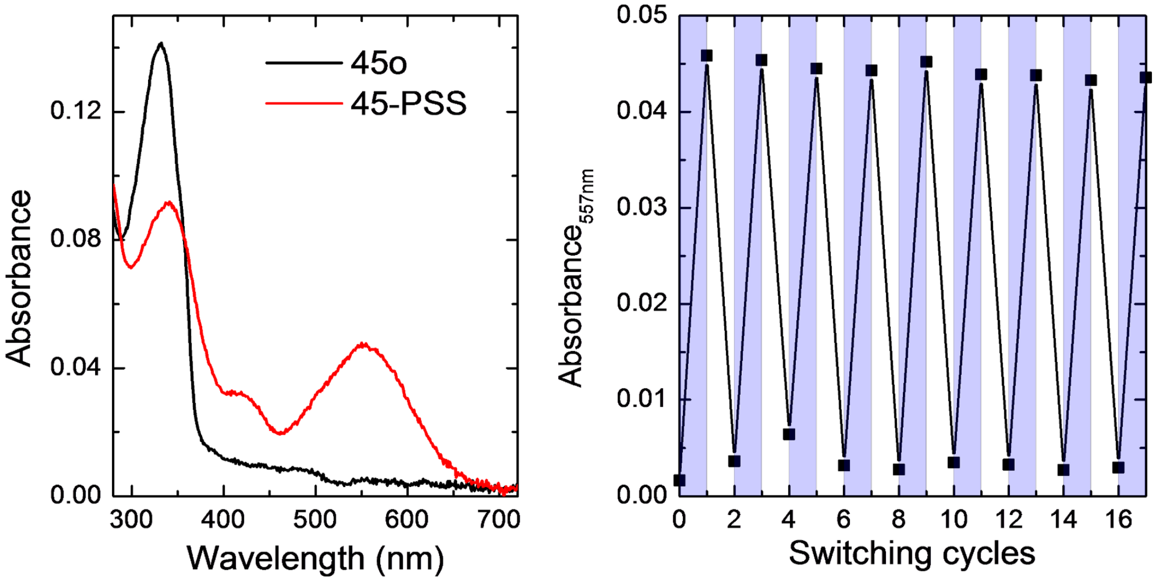

Figure 3-22: Absorption spectra of **45** (black line) and in the PSS (red line) obtained in SDS micelles solubilized in H_2O ($c \approx 10^{-6}$ M) (left). Absorption at $\lambda = 557$ nm upon alternating UV (blue bar) and visible light (white bar) irradiations to carry out successive switching cycles of **45** in the SDS micelles (right).

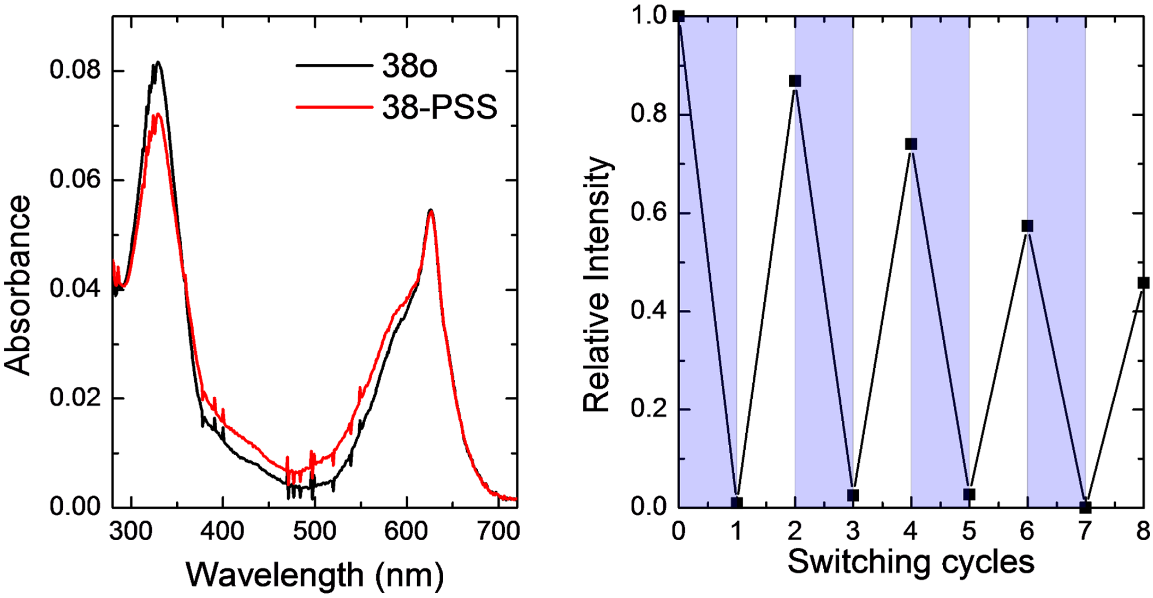

Figure 3-23: Absorption spectra of **38** (black line) and in the PSS (red line) obtained in SDS micelles solubilized in H_2O ($c \approx 10^{-6}$ M) (left). Relative fluorescence intensity upon alternating UV (blue bar) and visible light (white bar) irradiations to carry out successive switching cycles of **38** in the SDS micelles (right).

The encapsulation of the highly hydrophobic **45** in an SDS micelle solubilized in H_2O, was successfully accomplished and it was possible to perform many switching cycles without the appearance of any detectable fatigue. Photoswitching of a DAE derivative that is soluble in physiological media has only been reported in two cases[210,211] and also literature documented examples of water-soluble DAEs are very rare, which normally suffer of significant degradation after each switching cycle.[212] It has been thus proven, that the encapsulation of a fully functional DAE inside a micelle is a very efficient strategy to introduce DAEs in biological media while retaining the photochromic performance. Furthermore, it was also possible to encapsulate and efficiently switch dyad **38** inside of SDS micelles. However, a significant bleach of the fluorescence emission was detected after each switching cycle, this observation is a general issue of fluorophores in aqueous media as they suffer from increased photobleaching. A control experiment employing **Ph-bdp** in SDS micelles subjected to the same irradiation conditions as **38** was performed (**Figure 3-24**). The obtained data evidenced the detrimental effect of UV irradiation on the fluorophore, additionally, a slight bleaching was also observed upon irradiation with visible light. Although in principle the encapsulated fluorophore is protected by the micelle from the surrounding solvent, this colloidal structures are highly dynamic and sporadic contact with polar H_2O

molecules cannot be ruled-out which could enhance the degradation process upon irradiation with UV-light. Since micelles are very small supramolecular aggregates, they are not suited for fluorescence microscopy, due to their small dimensions which difficult their characterization.

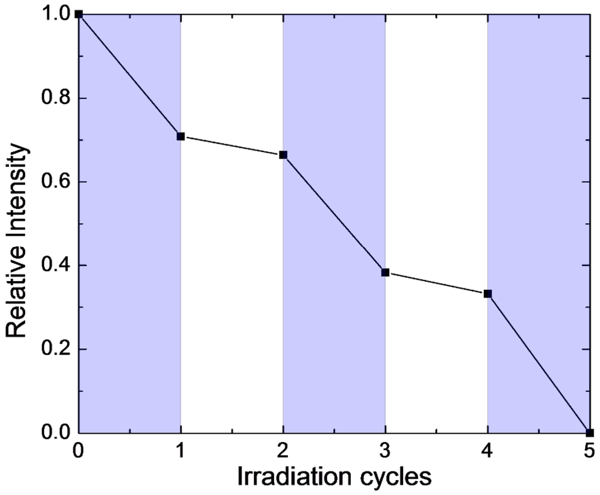

Figure 3-24: Relative fluorescence intensity upon alternating UV (blue bar) and visible light (white bar) irradiations of **Ph-bdp** in the SDS micelles (λ_{exc} = 580 nm).

Nonetheless, encouraged by the successful photochromic activity and the fluorescence modulation obtained for dyad **38** in aqueous media, it was attempted to introduce the dyad inside a vesicle bilayer under biological conditions employing phosphate buffered saline (PBS).[d] For this purpose, giant unilamelar vesicles (GUVs) of DOPC in PBS were prepared by the electroformation method[213] using 1.2 V, 10 Hz for 2 h at room temperature. As contrast for the green fluorescence channel (488 nm) fastDiO (3,3′-dilinoleyloxacarbocyanine perchlorate) was added and for the red channel (635 nm) **38o** was employed (Figure 3-26). Interestingly, when it was attempted to quench the fluorescence emission of **38o** by irradiation with UV-light to promote the cyclization to **38c**, the images obtained for the GUVs were identical as without the UV-light irradiation. To investigate this finding, multilamelar DOPC vesicles in PBS were prepared and were investigated with fluorescence spectroscopy. Here, it was possible to perform switching cycles in the same way as with the SDS micelles. The multilamelar vesicles were therefore investigated by fluorescence microscopy. Unexpectedly though, no fluorescence modulation was observed upon switching cycles.

---

[d] The following fluorescence microscopy and encapsulation experiments in GUVs were performed by Dr. S. Bobone and Dr. S. Chiantia of the research group of Dr. S. Chiantia from the biology department of the Humboldt-Universität zu Berlin.

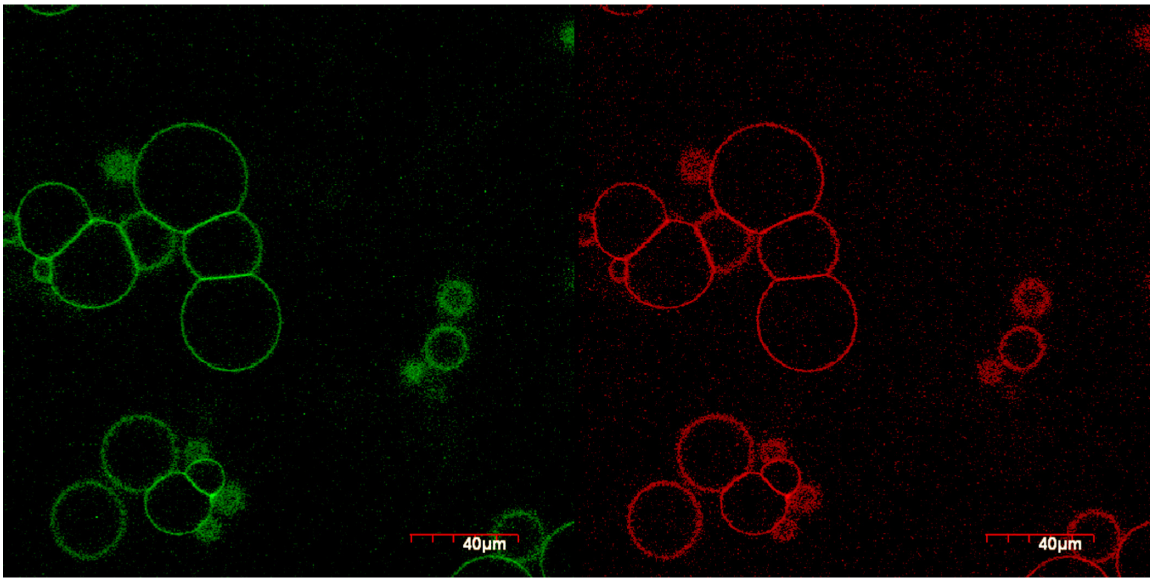

Figure 3-25: Confocal fluorescence microscopy images of DOPC GUVs containing 0.5% fastDiO and 0.5% **38o**. (left) GUV images obtained with the green channel, where only fastDiO emits fluorescence. (right) GUV images obtained with the red channel, where only **38o** emits fluorescence.[d]

The lack of fluorescence modulation of **38** observed with the confocal fluorescence microscope was surprising, since fluorescence modulation of the same sample could be monitored by means of fluorescence spectroscopy upon switching cycles. A deeper look on the observation evidenced that this finding corroborated the TA-spectroscopy data obtained for the dyads **36**, **37** and **38** where an excited state equilibrium is formed independently of the moiety of the dyad irradiated. Being this excited-state equilibrium responsible for the quenching of the fluorescence emission and aditionally causing the cycloreversion. Since confocal fluorescence microscopy employs very powerful laser sources and the GUVs have a very small loading of dyad confined in one unilamelar bilayer it can be anticipated that the excitation beam for the red channel is powerful enough to promote the EET equilibrium in the dyad and therefore stimulate the cycloreversion of the observed sample. The outcome of this process is an absence of fluorescence modulation in the GUVs, in other words, the EET equilibrium promotes the destructive readout of **38c** which is immediately converted to **38o**.

3.2 Sensitized Two-Photon *cis→trans* Isomerization of Azobenzenes

3.2.1 Target Definition

Optimization of AB to efficiently respond to two-photon excitation has been a largely investigated research field. Specifically a lot of efforts have been put in the obtention of AB which are capable to intrinsically perform the *trans→cis* isomerization by means of two-photon excitation. Until now, AB with strong push-pull substitution patterns in the *p*-positions have been studied, which are inherently unfavorable for the generation of *cis*-isomer, because of the very short thermal half-life. Only AB whose thermal stability in the *cis*-form is high can be of relevant significance and therefore push-pull substituents in the *p*-position have to be avoided in the design of two-photon responsive AB. The goal of this Chapter is to investigate if it is possible to circumvent the necessity to employ the AB as the two-photon absorber, but rather use an antenna which gathers the two-photon energy and then transfers it to the AB, subsequently, the sensitized AB should undergo the isomerization process. Since this approach was already proven (**Scheme 2-57**), the goal is to achieve the never reported capability of ABs to isomerize by 2PA from a thermally stable *cis*-form to the *trans*-form and thereby obtain two-photon fully addressable ABs (**Scheme 3-18**).

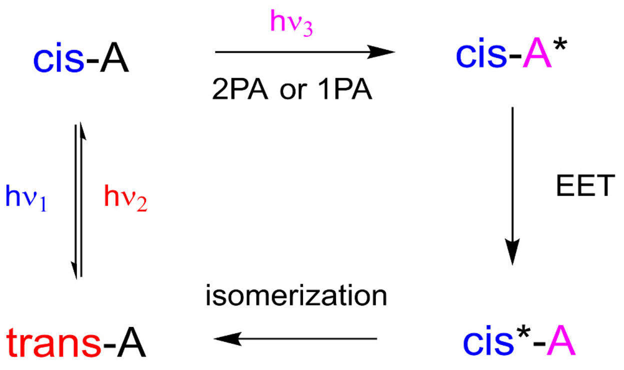

Scheme 3-18: Schematic representation of the sensitized two-photon *cis→trans* isomerization of an AB-antenna dyad.

3.2.2 Synthesis and Characterization

We have seen the superior photochromic and thermal stability of *o*-fluorinated ABs, which have well separated n-π^* bands enabling the possibility to achieve the selective *trans*→*cis* isomerization with visible light ($\lambda > 500$ nm). Furthermore, the thermal half-life of the *cis*-form has been reported to be as high as 2 years at room temperature for certain derivatives. Therefore, this ABs constitute an excellent choice to address the desired molecular properties, because the *cis*-form can be readily produced in high yield with visible light irradiation and is very stable, facilitating the study of *cis*→*trans* sensitized two-photon isomerization. Since triarylamines are excellent 2PA chromophores, an antenna was chosen bearing this moiety. However, further modifications were necessary due to the band overlap which could difficult its selective excitation. With this purpose and in order to achieve the most efficient electronic distribution in the 2PA chromophore, a thiophene-unit was employed to link an additional phenyl-ring, to shift the antennas absorption band to the 380 nm region, where the AB has a minimal oscillator strength. It has to be noted that for triarylamine chromophores, the thiophene-spacer is even more efficient in extending the conjugation length than a double-bond or a triple-bond.[214] This substitution pattern resembles the design of a dipolar 2PA chromophore. The covalent linkage in *m*-position of the AB ensures the spectroscopic identity of each individual component in the ground-state.[215] The depicted molecular dyad as well as the model compounds required for the characterization are shown in **Scheme 3-19**.

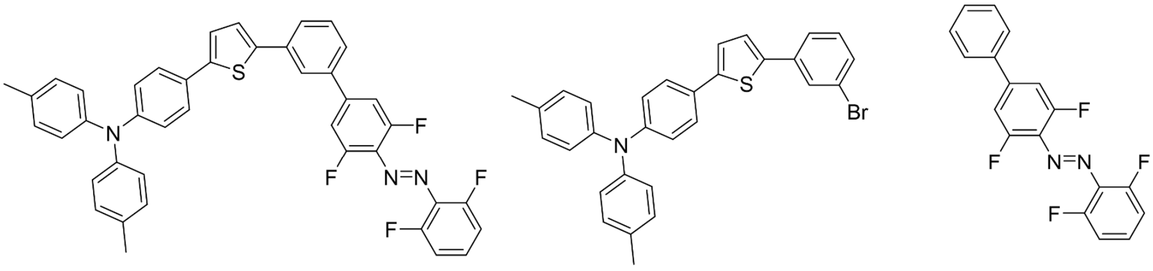

46 **47** **48**

Scheme 3-19: Triarylamine-azo dyad **46** and reference compounds **47** and **48**.

The synthesis of the AB precursors was accomplished following a modular approach (**Scheme 3-20**). Regioselective bromination with NBS in CH_3CN of *o*-difluoroaniline afforded after work-up and purification by column chromatography compound **49** in quantitative yield

(99%). Following the Mills-coupling conditions for the synthesis of non-symmetrical ABs, the electron-poor coupling partner **49** was treated with Oxone^{TM} in a DCM : H_2O mixture overnight. Afterwards, it was isolated and diluted in a toluene : AcOH : TFA mixture (6:6:1) and *o*-difluoroaniline was added. This procedure was modified and adapted to improve the overall yield, which was significantly smaller when only AcOH and TFA were employed. The resulting red mixture was allowed to stir overnight and after work-up and purification by column chromatography compound **50** was obtained with an excellent yield (93%). The optimized conditions offered a vast improvement, specifically, when employing electron-poor nucleophiles like *o*-difluoroaniline. For comparison, when neat AcOH with TFA was used the yields of **50** never reached more than 5% of isolated yield. The synthesis of model compound **48** was accomplished by sequential lithiation of phenylbromide in anhydrous THF at -78 °C followed by borylation with $B(^iOPr)_3$ and final addition of a 2 M solution of Na_2CO_3 followed by degasing with Ar for 15 min enabled the preparation of the solution to which afterwards **50** and $Pd(PPh_3)_4$ were added. The resulting mixture was then submitted to reflux for 17 h and after work-up and purification by column chromatography compound **48** was isolated with excellent yield (91%).

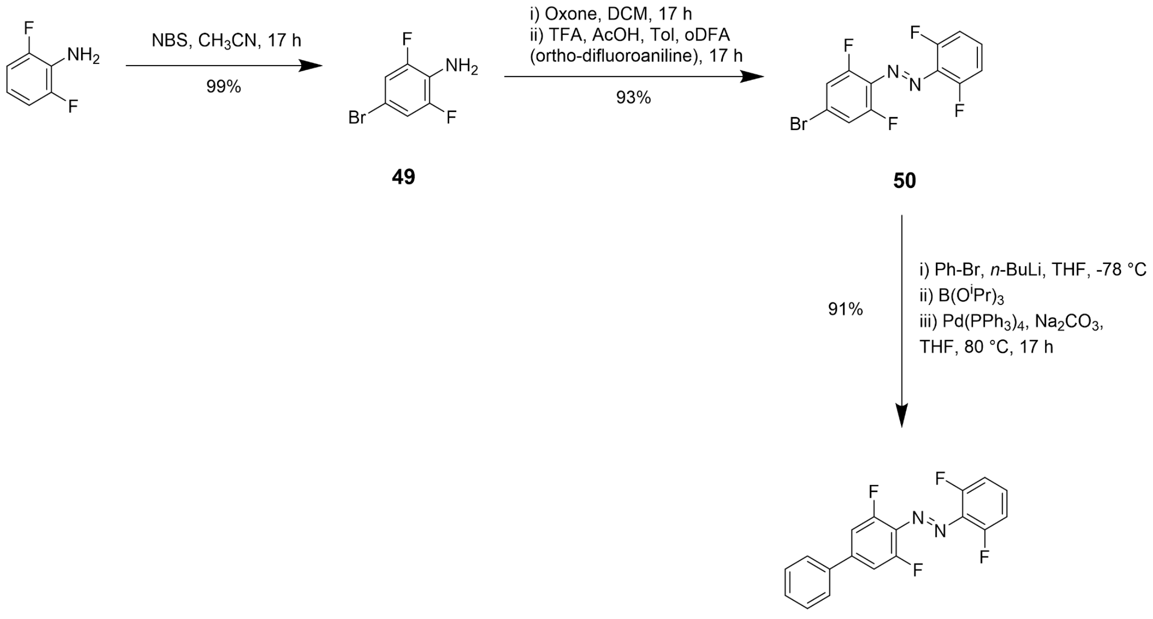

49

50

48

Scheme 3-20: Synthesis of AB precursors and model compound **48**.

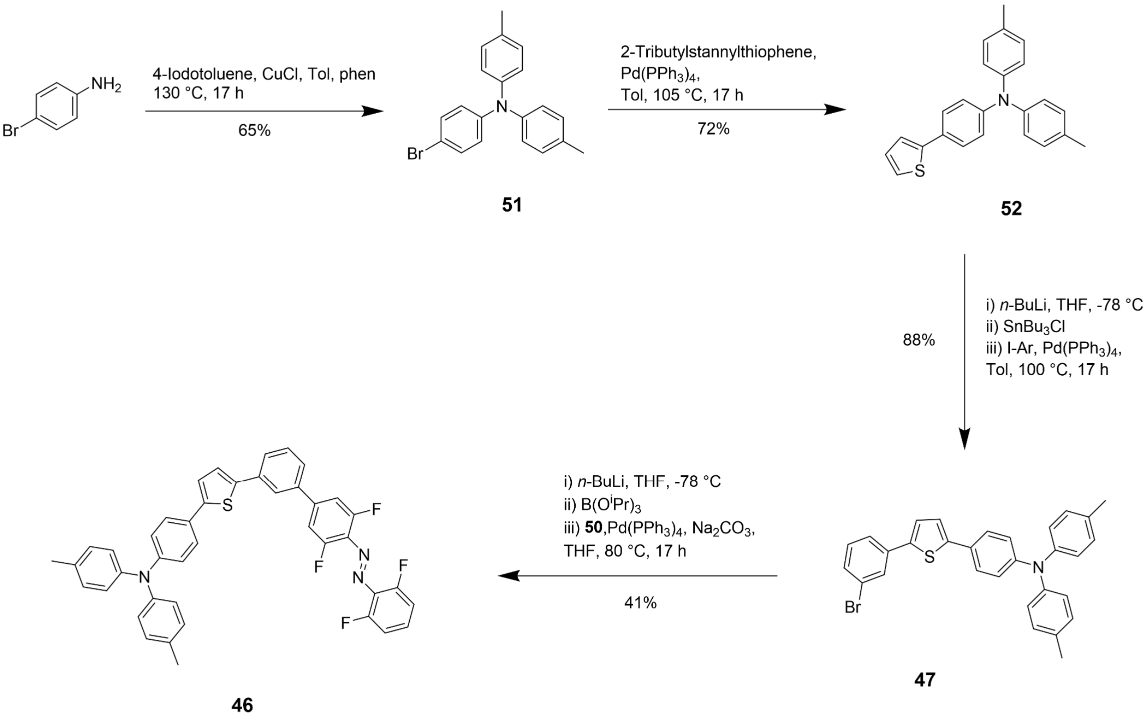

NH2
Br
4-Iodotoluene, CuCl, Tol, phen
130 °C, 17 h
65%
51
2-Tributylstannylthiophene,
Pd(PPh3)4,
Tol, 105 °C, 17 h
72%
52
i) n-BuLi, THF, -78 °C
ii) SnBu3Cl
iii) I-Ar, Pd(PPh3)4,
Tol, 100 °C, 17 h
88%
47
i) n-BuLi, THF, -78 °C
ii) B(OiPr)3
iii) 50,Pd(PPh3)4, Na2CO3,
THF, 80 °C, 17 h
41%
46

Scheme 3-21: Synthesis of antenna precursors and molecular dyad **46** as well as model compounds **47**.

The synthesis of the antenna and the molecular dyad (Scheme 3-21) was achieved in a convergent modular approach. Triarylamine **51** was obtained by the Ullmann-type ligand-assisted Cu-catalyzed coupling of 4-iodotoluene to 4-bromoaniline in refluxing toluene at 130 °C for 17 h, which afforded after work-up and purification by column chromatography compound **51** in good yield (65%). The Stille-coupling of 2-tributylstannylthiophene to compound **51** in toluene at 105 °C for 17 h, afforded after work-up and purification by column chromatography compound **52** in good yield (72%). Initial lithiation of **52** in anhydrous THF at -78 °C with *n*-BuLi, following stannilation with $SnCl(Bu)_3$ and subsequent solvent evaporation and dilution in dry degased toluene enabled the preparation of the solution to which afterwards 3-bromoiodobenzene and $Pd(PPh_3)_4$ were added. The resulting mixture was then submitted to reflux for 17 h and after work-up and purification by column chromatography compound **47** was isolated with very good yield (88%). The targeted molecular dyad **46** was obtained by Suzuki-coupling between borylated **47** and **50**. Initial lithiation of **47** in anhydrous THF at -78 °C with *n*-BuLi, following borylation with $B(^iOPr)_3$ and final addition of a 2 M solution of Na_2CO_3 followed by degasing with Ar for 15 min enabled the preparation of the solution to which afterwards **50** and $Pd(PPh_3)_4$ were added. The resulting mixture was then submitted to reflux for 17 h and after work-up and purification by column chromatography compound **46** was isolated with moderate yield (41%).

Model compound **47** as well as target molecular dyad **46** show fully reversible photochromism and exhibit very high *cis*-form content in the PSS obtained upon vis-light irradiation (**Figure 3-26**). The thermal half-lives, along with molar absorptivities and composition at the PSS of compounds **46** and **48** in *n*-hexanes and acetonitrile are combined in **Table 3-6**.

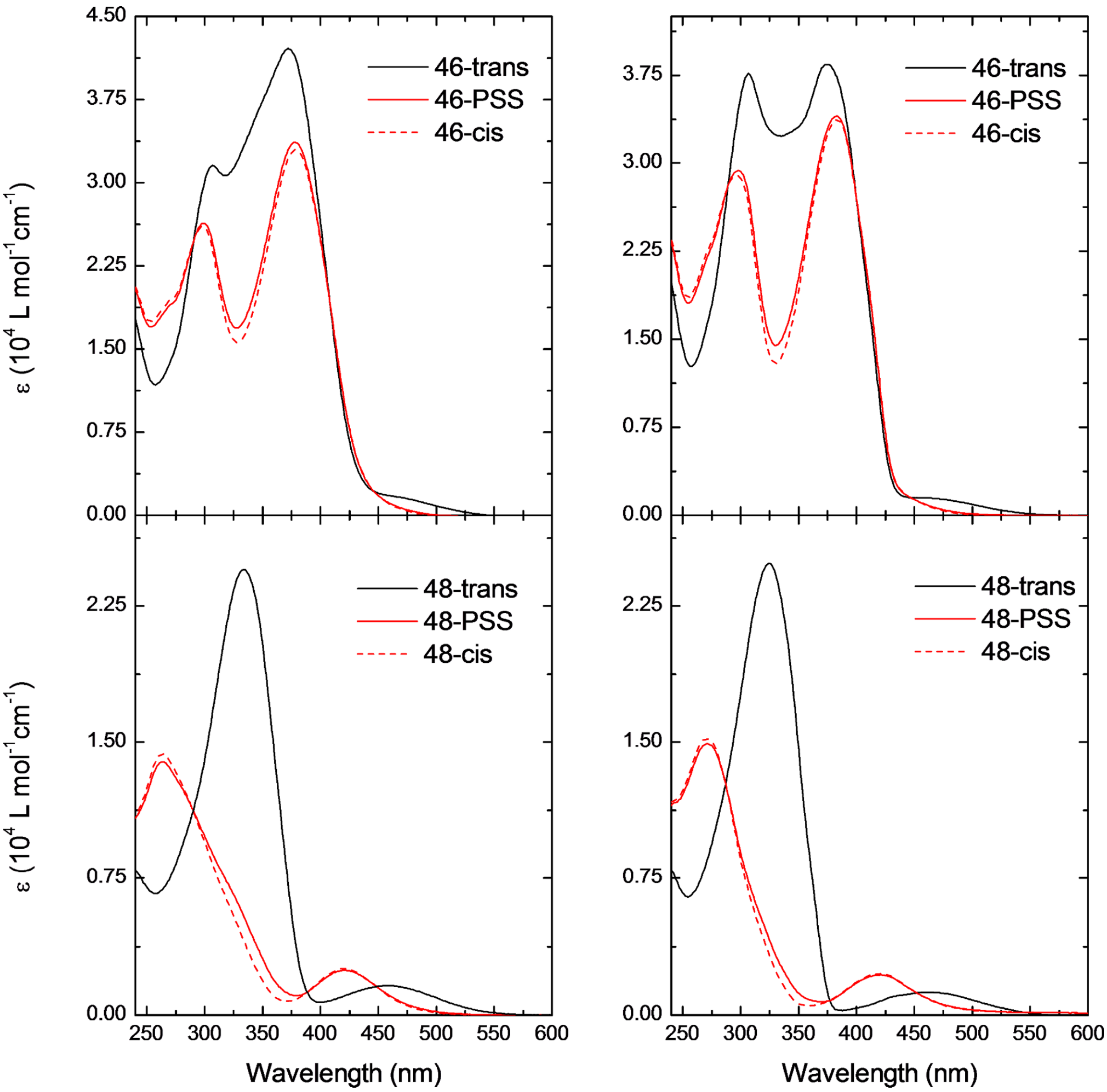

Figure 3-26: UV/vis absorption spectra of **46** (top) and **48** (bottom), where the *trans*-form (black line), the PSS (red line) and the simulated pure *cis*-form (dashed red line) in

acetonitrile (left) and *n*-hexanes (right) (c ≈ 10^{-5} M) are depicted. PSS induced by irradiation with vis-light (λ_{irr} > 500 nm) at 25 °C.

Table 3-6: Molar absorptivities, absorption maxima, composition at the PSS, as well as thermal half-lives and thermal isomerization rates of **46** and **48** in *n*-hexanes (hex) and acetonitrile (ACN).

	Solvent	λ_{max} / nm		ε / 10^4 L mol^{-1}cm^{-1}		$\tau_{1/2}$[a] (298K)/ days	k(298K)[a] / h^{-1}	PSS[b]
		trans	*cis*	*trans*	*cis*			λ > 500nm
46	hex	374	383	3.80	3.40	522	5.5 x 10^{-5}	8% *trans* 92% *cis*
	ACN	372	378	4.20	3.30			
48	hex	324	271	2.50	1.50	48	6.0 x 10^{-4}	4% *trans* 96% *cis*
	ACN	334	263	2.50	1.40			

[a] Calculated in DMSO. [b] Calculated in acetonitrile.

Upon irradiation with green light (λ > 500 nm) the n→π* band of the *trans*-form is selectively addressed enabling to achieve very high PSSs in both compounds **46** and **48**, with similar values as for the previously reported *o*-fluorinated ABs.[72] It can be thus assumed, that the *m*-linked antenna to the AB has no electronic influence over the n→π* band of the AB, ensuring the possibility to selectively address by selective irradiation the individual components of the molecular dyad **46**. Furthermore, it was observed that **48** exhibited a significant solvatochromism when increasing the solvent polarity. Interestingly, when increasing the polarity from *n*-hexanes to acetonitrile, solvatochromism only caused the bathochromic-shift of the π→π* band, while the n→π* band remained unaltered in both solvents. Consequently, the solvatochromism of **48** promoted a significant shape-change of the UV-vis spectrum in compound **46**. However, the PSS upon green light irradiation was unchanged due to the negligible solvent influence on the n→π* band. It has to be noted that the antenna itself (**47**, **Figure 3-28**) did not display noteworthy solvatochromism in the absorption spectrum upon increasing solvent polarity. In contrast to the similar spectroscopic properties, the kinetic study of **46** and **48** evidenced substantial thermodynamic differences between both compounds, as can be seen on the markedly higher rate constant and more than ten-times higher thermal half-life of **46**. To gain further insight, according to Eyring's theory[216] and employing the van't Hoff and the Arrhenius plots the thermodynamic parameters for thermal *cis→trans* isomerization were determined for **46** and **48** (**Figure 3-27**, **Table 3-7**).

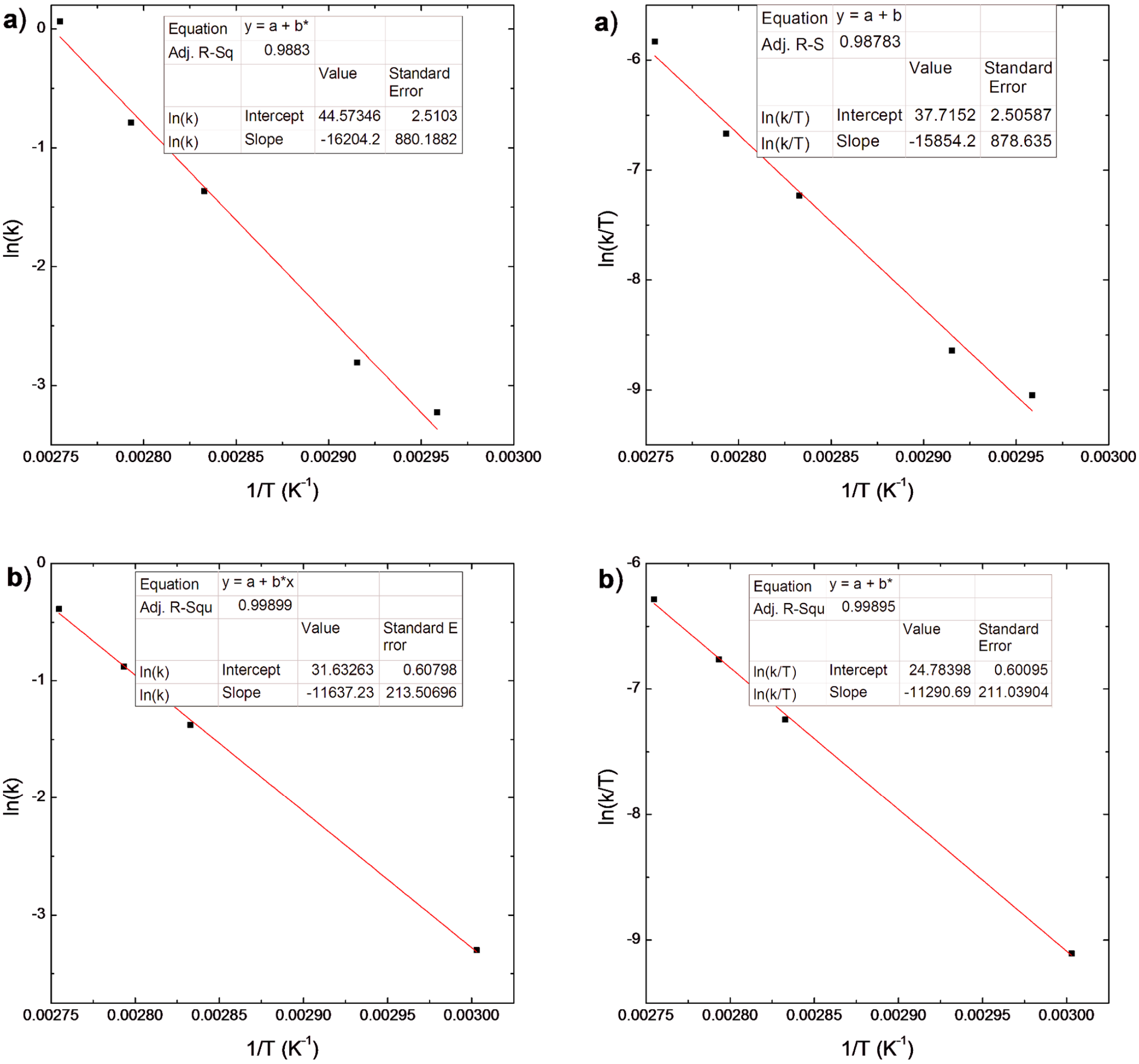

Equation	y = a + b*		
Adj. R-Sq	0.9883		
		Value	Standard Error
ln(k)	Intercept	44.57346	2.5103
ln(k)	Slope	-16204.2	880.1882

Equation	y = a + b		
Adj. R-S	0.98783		
		Value	Standard Error
ln(k/T)	Intercept	37.7152	2.50587
ln(k/T)	Slope	-15854.2	878.635

Equation	y = a + b*x		
Adj. R-Squ	0.99899		
		Value	Standard E rror
ln(k)	Intercept	31.63263	0.60798
ln(k)	Slope	-11637.23	213.50696

Equation	y = a + b*		
Adj. R-Squ	0.99895		
		Value	Standard Error
ln(k/T)	Intercept	24.78398	0.60095
ln(k/T)	Slope	-11290.69	211.03904

Figure 3-27: (a) Thermal **46-*cis*** → **46-*trans*** isomerization in DMSO: Arrhenius plot (left), van’t Hoff plot (right). (b) Thermal **48-*cis*** → **48-*trans*** isomerization in DMSO: Arrhenius plot (left), van’t Hoff plot (right).

On hand of all experimental thermodynamic parameters it can be assumed that since compound **46** is more voluminous and has more freedom degrees of movement, the thermal barrier involved in the *cis→trans* isomerization is higher than for **48**. Consequently, the isomerization rate and thermal half-life of **46** is higher than for **48**, which requires less activation energy to isomerize thermally from the *cis*- to the *trans*-form.

Table 3-7: Experimental activation energies E_a, Eyring activation free energies $\Delta G^{\ddagger}$, enthalpies $\Delta H^{\ddagger}$, and entropies $\Delta S^{\ddagger}$ calculated from Arrhenius and van't Hoff plots for compounds **46** and **48** in DMSO.

Compound	E_a / kJ·mol^{-1}	$\Delta H^{\ddagger}$ / kJ·mol^{-1}	$\Delta S^{\ddagger}$ / J·mol^{-1}·K^{-1}	$\Delta G^{\ddagger}$ / kJ·mol^{-1}
46	134.72	131.81	-46.02	145.53
48	96.75	93.87	-33.09	103.74

To rationalize the impact on the photochemical properties of the coupling of the AB with **47**, the fluorescence spectra and relative fluorescence quantum yields of **46** and **47** were determined (**Figure 3-28**, **Figure 3-29**, **Table 3-8**). Furthermore, the 2PA properties of **47** were investigated (Chapter 3.2.3). As have been earlier mentioned, **47** did not exhibit significant solvatochromism in the UV-vis absorption spectra upon varying solvent polarity. However, a significant solvent effect could be observed in the fluorescence emission.

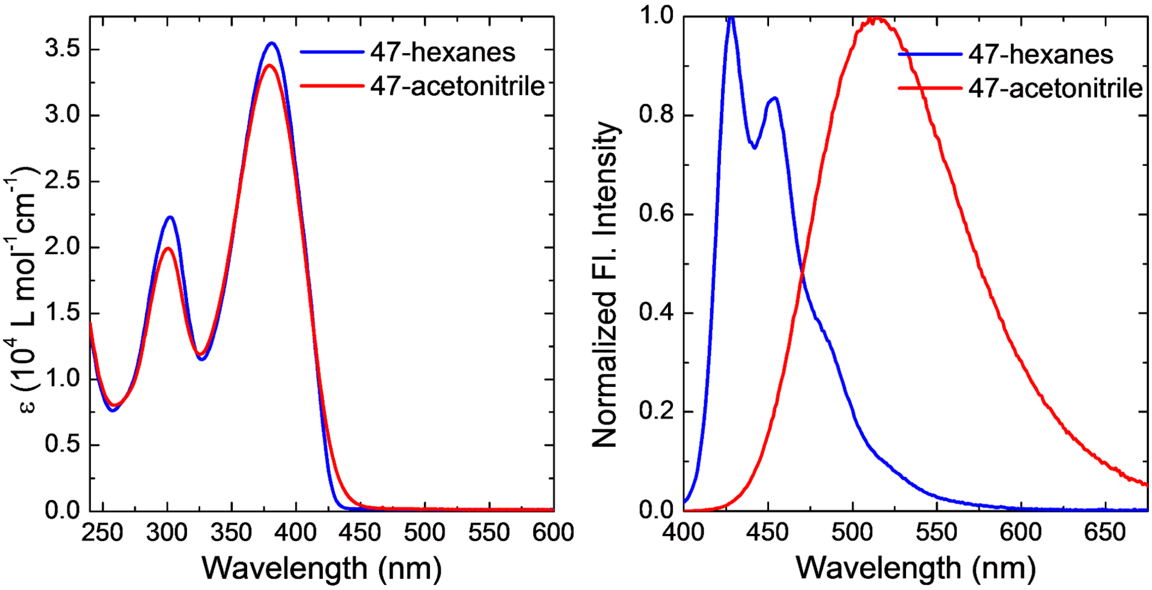

Figure 3-28: UV/vis absorption spectra of **47** obtained in *n*-hexanes (blue-line) and acetonitrile (red line) ($c \approx 10^{-5}$ M) (left). Corrected normalized fluorescence emission spectra

of **47** obtained in *n*-hexanes (blue line) and acetonitrile (red line) (λ_{exc} = 348 nm, $c \approx 10^{-6}$ M) (right).

Table 3-8: Molar absorptivities, absorption maxima, emission maxima, Stokes shift as well as fluorescence quantum yields of **46** and **47** in *n*-hexanes and acetonitrile. No emission difference was observed upon photoisomerization of **46**.

	Solvent	λ_{max} / nm		ε / 10^4 L mol^{-1}cm^{-1}		λ_{em} / nm	Stokes shift /nm	ϕ_{Fl}
		trans	*cis*	*trans*	*cis*			
46	hex	374	383	3.80	3.40	432	58	3.9×10^{-3}
	ACN	372	378	4.20	3.30	498	127	2.6×10^{-3}
47	hex	381		3.60		429	48	0.12
	ACN	379		3.40		515	136	0.27

The fluorescence band of **47** in acetonitrile is red-shifted relative to that in *n*-hexanes by 86 nm, due to polar solvation in acetonitrile. Note also the different band-shape of the absorption and emission spectra in *n*-hexanes. The emission band is relatively narrow, whereas the absorption band remains broad and smooth (without structure). The band-shape of an electronic transition is known to be determined by Franck-Condon factors of optically active vibrational modes, which in turn depend on molecular geometry. Thus, the observed difference between the absorption and emission spectra indicates a change of the equilibrium molecular geometry after $S_0 \rightarrow S_1$ optical excitation. The solvent dependent fluorescence quantum yield will be discussed in more detail with transient spectroscopy (Chapter 3.2.3). Attention has to be focused on the severely quenched fluorescence emission of **46** which has a fluorescence quantum yield two orders of magnitude lower than **47** and is almost undetectable by the experimental conditions employed. These findings endorse the possibility of EET from the antenna to the AB. An evaluation of the Förster critical distance (R_0) and FRET efficiency (E) was made for ***cis*-46** and ***trans*-46** (**Table 3-9**). Although the R_0 values are rather low, the distances between the donor and the acceptor in the dyad are considerably smaller, hence, FRET is a possible explanation for the lower fluorescence quantum yield of **46**.

Table 3-9: Förster critical distance R_0 obtained from the overlap of emission and absorption spectra as well as FRET efficiencies E calculated for **46** in the respective *cis*- and *trans*-forms obtained in *n*-hexanes (hex) and acetonitrile (ACN).

	Förster distance R_0 / Å		*E*	
	ACN	hex	ACN	hex
***trans*-46**	13.3	24.4	0.99	0.97
***cis*-46**	13.0	24.1	-	-

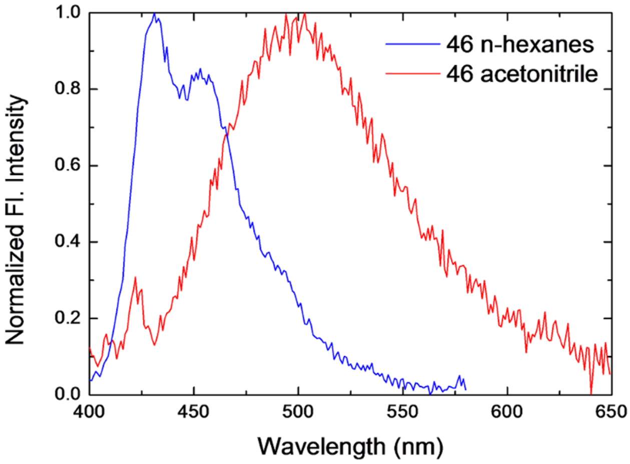

Figure 3-29: Corrected normalized fluorescence emission spectra of **46** obtained in *n*-hexanes (blue-line) and acetonitrile (red line) (λ_{exc} = 348 nm, $c \approx 10^{-6}$ M).

The influence of the antenna in the photophysical performance was also measured. With this purpose the isomerization quantum yields for **46** and **48** at four different wavelengths were determined (**Table 3-10**). ABs are known to photoisomerize with higher quantum yields when excited to the S_1 state ($n\rightarrow\pi^*$ transition) than to the S_2 state ($\pi\rightarrow\pi^*$ transition).[57] This behavior represent an example for the violation of Kasha's rule, in which it is implied that photoisomerization is independent of the excitation wavelength as it always proceeds from the same lowest excited-state. As such, the obtained results are not in full agreement with this observation.

Table 3-10: Quantum yields of isomerization of **46** and **48**, measured in acetonitrile (ACN) and *n*-hexanes (hex) at four different wavelengths (330, 380, 440, and 510 nm).

Compound	excitation	$\phi_{trans \rightarrow cis}$		$\phi_{cis \rightarrow trans}$	
		ACN	hex	ACN	hex
46	S_0-S_2 (330nm)	0.06	0.12	0.15	0.21
	$\lambda_{47\mathrm{max}}$ (380nm)	0.02	0.08	0.20	0.38
	S_0-S_1 (440nm)	0.07	0.16	0.22	0.08
	S_0-S_1 (510nm)	0.16	0.10	-	-
48	S_0-S_2 (330nm)	0.16	0.16	0.10	0.09
	$\lambda_{47\mathrm{max}}$ (380nm)	0.19	0.14	0.18	0.09
	S_0-S_1 (440nm)	0.16	0.16	0.37	0.43
	S_0-S_1 (510nm)	0.22	0.19	-	-

Quantum yields for the *trans→cis* isomerization following red-edge n→π* band excitation (510 nm) were determined to be slightly higher for both **46** and **48**, than the values obtained through the π→π* transition (330 nm) for the same compounds. Additionally, isomerization quantum yields following n→π* band excitation (510 nm) are higher in acetonitrile than in *n*-hexanes. The quantum yield for the *trans→cis* isomerization following π→π* excitation of **46** was measured to be 0.06 while in the case of **48** it was 0.16. A remarkable observation was made for the case of **48**, as apparently *trans→cis* isomerization following π→π* (330 nm) and n→π* (440 nm) have the same efficiency, opposed to the conventional case in ABs, where the isomerization yield following S_1 excitation is higher. Furthermore, excitation at the red-edge of the n→π* band (510 nm) led to a higher isomerization yield. The apparent wavelength dependent isomerization quantum yield upon excitation of the same n→π* band was not reported by Gauglitz on unsubstituted AB.[24] Although he determined an isomerization yield of 0.20 with 405 nm irradiation and of 0.22 with 436 nm, he also established a significantly higher error on the 436 nm measurement imposed by the smaller extinction coefficient of the AB and higher associated experimental uncertainty. But, the effect was not as pronounced as in **46** and is attributed to an increasing error source upon the determination of longer wavelength quantum yields due to the decreasing absorption of the n→π* band of the AB. An additional error source is the different actinometer employed. Ferrioxalate actinometry is not suited for wavelength determinations above ~450 nm, therefore, a different actinometer was employed for the determination of I_0 at 510 nm (Aberchrome 670).[e,217] The reverse *cis→trans* isomerization at 440 nm is quite efficient for **48**, with quantum yields of around 0.4, but significantly lower for **46**. Interestingly, excitation at the absorption maximum of the antenna (380 nm) promotes the very fast and efficient *cis→trans* isomerization in **46** (**Figure 3-30**), with a quantum yield of up to 0.38 in *n*-hexanes. The same excitation in the opposite direction is subject to other concomitant processes, having a lower isomerization quantum yield of 0.08 in *n*-hexanes. On the opposite, excitation (380 nm) for the *cis→trans* isomerization of **48** leads to a significantly lower PSS content although the quantum yield is comparable in both directions. Over the course of the *cis→trans* isomerization following 380 nm irradiation of **46** and **48**, differential spectra were calculated, observing the same spectral-shape evolution. The obtained differential spectra further support that the antenna and the AB components are completely electronically decoupled in the ground-state. Furthermore, it was possible to attribute the photoisomerization process of **46** solely to the the AB-chromophore. Nonetheless, since isomerization quantum yields depend on the excited state energy surfaces and a straightforward explanation is not possible for the divergencies between the values of **46** and **48**, transient spectroscopy was performed on these compounds (Chapter 3.2.3).

The almost negligible fluorescence emission of **46**, the high isomerization yields upon *cis→trans* isomerization following 380 nm excitation of **46** and relatively poor *trans→cis* isomerization yields following the same irradiation, the absence of electronic coupling between the AB and the antenna, and the significantly higher PSS ratios obtained from the irradiation at 380 nm compared with **48**, enforce the possibility of excited-state interaction between the dyad components in **46**. The antenna mediated isomerization also

---

[e] I_0-value at λ_{irr} = 436 nm obtained using Aberchrome 670 was 16 % lower than the value obtained using ferrioxalate under identical irradiation conditions. This demonstrates the uncertainty when comparing quantitative photochemical measurements using different actinometers.

promotes an increase in the efficiency of the *cis→trans* conversion, which could be caused either by EET or by PET. In Chapter 2.3.4 the electrochemical properties of ABs were presented and it is possible to speculate with a PET process from the antenna to *cis*-AB causing the very fast electrochemical *cis→trans* isomerization. This process could explain the relatively low *trans→cis* isomerization yields upon 380 nm irradiation as all the *cis*-AB generated by the direct absorption would be converted back by the photons absorbed at 380 nm by the antenna, which would promote the PET forcing the AB to isomerize back to the *trans*-form. The interplay of both processes could explain the lower isomerization yield in **46** for the *trans→cis* isomerization as compared with **48**. However, it has to be considered that when FRET and Dexter-type ET are competing, if there is spectral overlap, the transfer occurs by FRET.[78] This statement is only true in the long-range regime. If both processes compete in short-ranges (~6 Å), then it was experimentally proven that the Dexter mechanism prevails.[218] The net result of Dexter transfer is identical to the Förster mechanism but does not require significant oscillator strength on the part of the acceptor. Consequently, Dexter transfer can be effective in a wider range of chemical systems being also more difficult to determine unambiguously.[219] As a result, Dexter transfer is often the default mechanism assumed in systems containing weakly absorbing acceptors for which a charge-separated species is not detected.

In **46** the possibility of a Dexter-type electron exchange mechanism is realistic due to the very small donor and acceptor distance, which are effectively fused. Furthermore, electronic-coupling in the excited-state is to be expected in *m*-linked conjugates,[215] and has been previously reported as relatively efficient.[220] Excited-state coupling would permit the wavefunction overlap required in the Dexter electron exchange mechanism. Similarly, it can be estimated that if Dexter-type electron-exchange and PET are competing, and a spectral overlap between donor and acceptor exists, the Dexter mechanism would be the preferential cause for the transfer of energy. It has to be noted that distinguishing between Dexter transfer and PET represents a commonly encountered and sometimes intractable problem in excited-state chemistry.[221] Summarizing, it can be roughly predicted that in a competing scenario, the mechanistic excited-state energy transfer preference for long-distances is FRET > Dexter > PET, and for short-distances Dexter > FRET > PET.

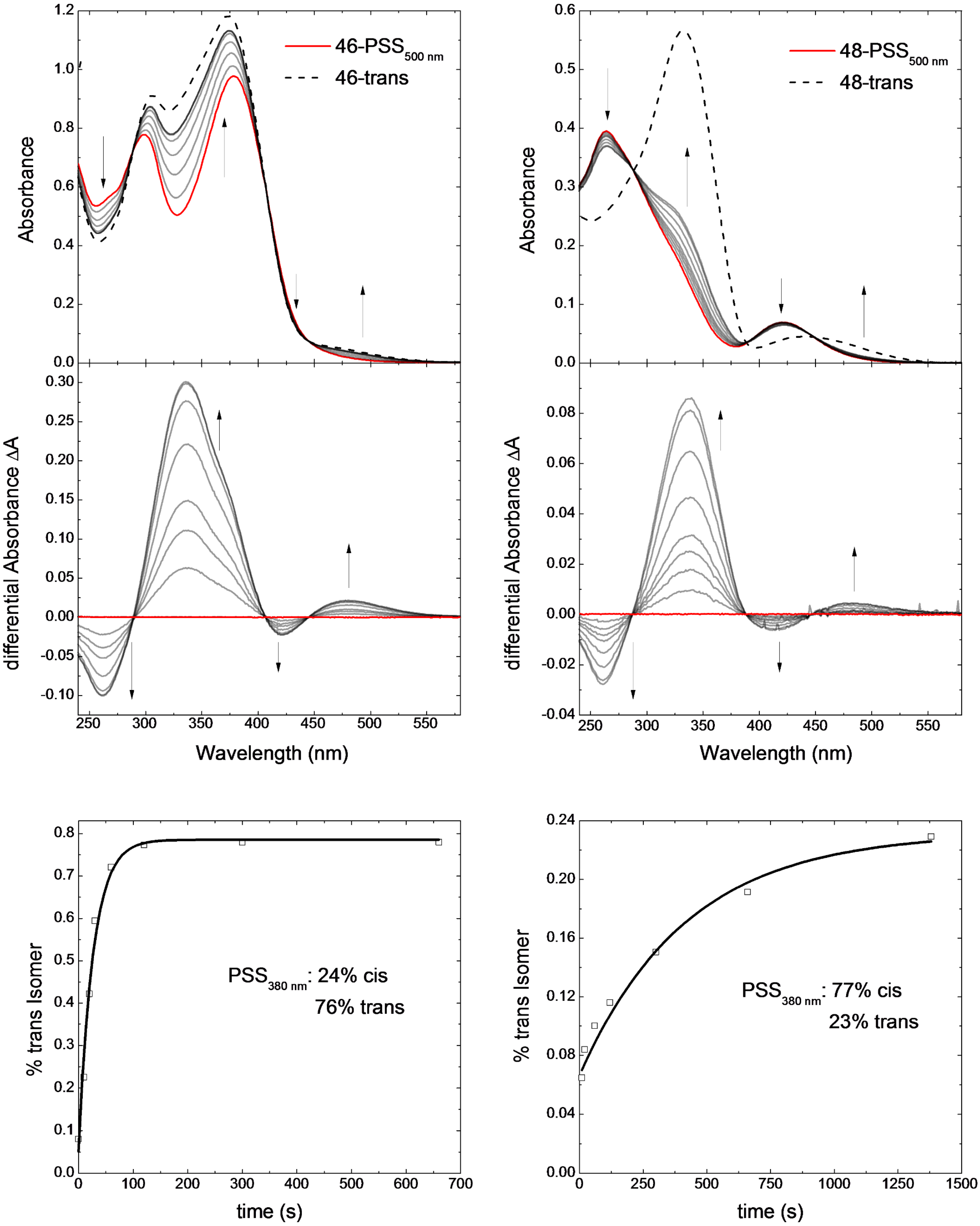

Figure 3-30: Spectral evolution during the course of *cis→trans* isomerization induced by irradiation with UV-light (λ_{irr} = 380 nm) at 25 °C of **46** (left) and **48** (right), where the *trans*-form (dotted-line) and the PSS of the *cis*-form (red line) in acetonitrile ($c \approx 10^{-5}$ M) are depicted (top). Differential spectral evolution during the course of *cis→trans* isomerization

of **46** (left) and **48** (right) (middle). *trans*-form content evolution versus 380 nm irradiation time in seconds for **46** (left) and **48** (right) in acetonitrile (bottom).

Having established the one-photon photochemistry of compounds **46** and **48**, the two-photon photochemistry was probed. With this purpose the *trans→cis* isomerization of **48** by 660 nm irradiation with a focused laser-beam and the sensitized *cis→trans* isomerization of **46** by 750 nm irradiation with a focused laser-beam were monitored by UPLC. Herein, it was possible to establish the precise isomer formation as a function of two-photon irradiation time (**Figure 3-31**).

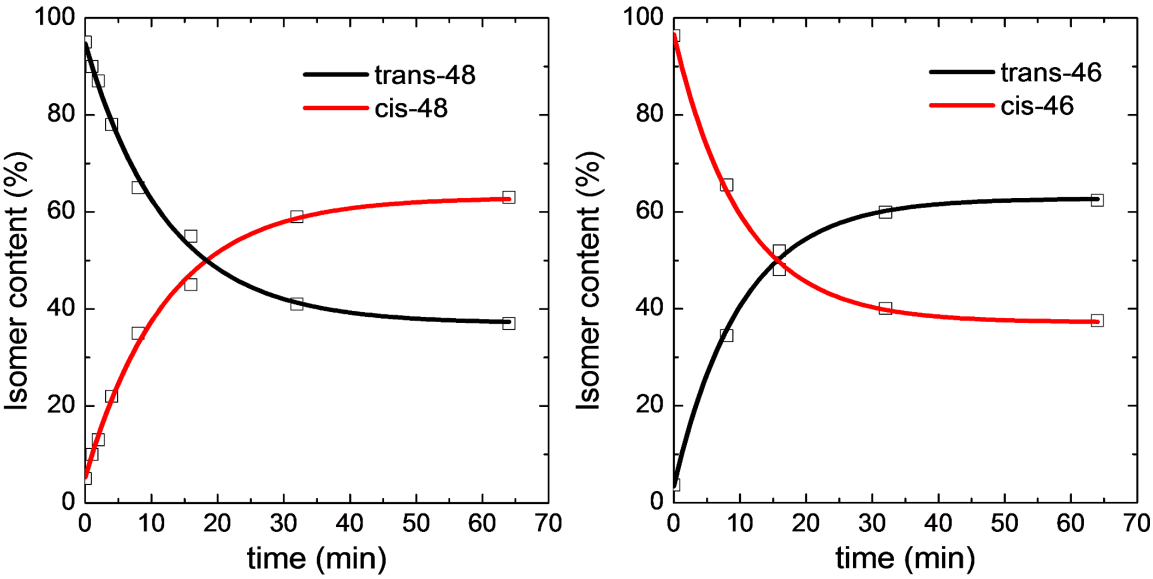

Figure 3-31: Time course of two-photon *trans→cis* photoisomerization of **48** (λ_{irr} = 660 nm, $c \approx 10^{-3}$ M, E_p = 8 μJ) (left), and two-photon sensitized *cis→trans* photoisomerization of **46** (λ_{irr} = 750 nm, $c \approx 10^{-4}$ M, E_p = 8 μJ) (right) as monitored by UPLC. The concentration of the *trans*-isomer (black line) and *cis*-isomer (red line) are expressed as a percent of the total compound in the mixture.

Interestingly, for both compounds the PSS which is established by two-photon irradiation is slightly lower than the one observed for the corresponding one-photon irradiation. This deviance might be caused by decomposition of the compound upon prolonged high intensity pulsed irradiation. Unfortunately, the decomposition products could not be detected by the UPLC measurements. Confirmation that the observed photoisomerization was induced by 2PA was provided by the fact that it must obey the square-law energy dependence.[222] The initial rates of photoisomerization were monitored for compounds **46** and **48** as a function of laser intensity. The initial rate of photoisomerization shows a nonlinear dependence upon laser intensity, and the logarithmic plot has a slope close to 2 in both cases, which is characteristic of a two-photon process (**Figure 3-32**).

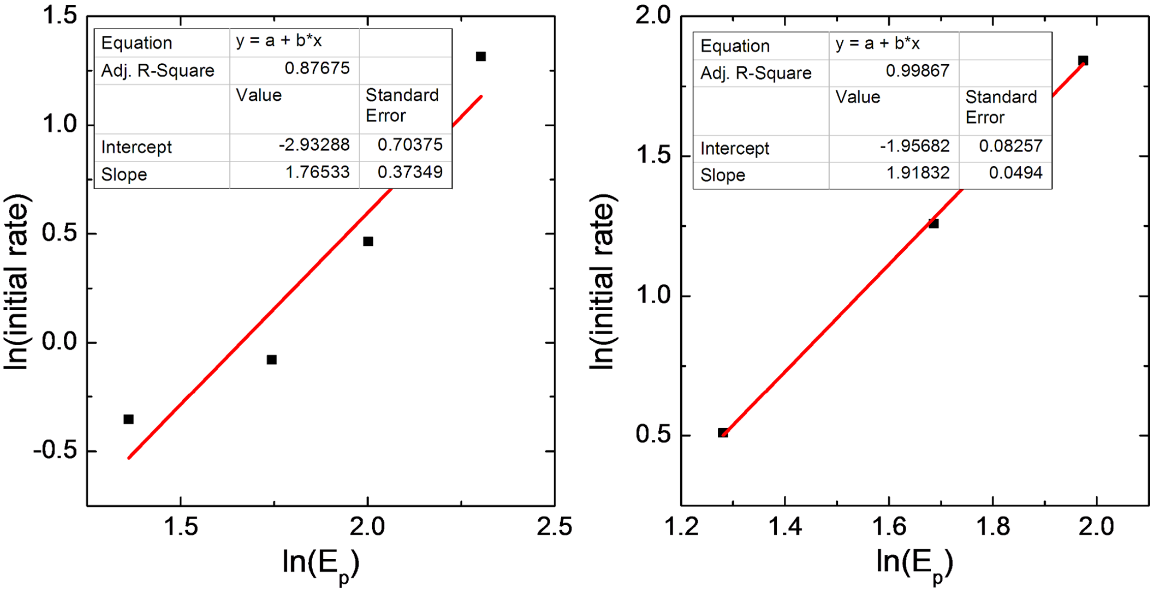

Equation	y = a + b*x	
Adj. R-Square	0.87675	
	Value	Standard Error
Intercept	-2.93288	0.70375
Slope	1.76533	0.37349

Equation	y = a + b*x	
Adj. R-Square	0.99867	
	Value	Standard Error
Intercept	-1.95682	0.08257
Slope	1.91832	0.0494

Figure 3-32: Dependence of the initial rate of ***cis*-48** isomer formation (left) on the average laser power at 660 nm, or ***trans*-46** isomer formation (right) on the average laser power at 750 nm as monitored by UPLC.

The ln-ln plot of initial rate vs power for **46** has a slope of 1.92 in accordance with the predicted slope for a two-photon process of 2. However, for **48** the slope is of 1.77. This nonconformity from the ideal value has been previously reported and is ascribed to competing processes, such as saturation or photobleaching.[223] It has to be noted that the solution of **48** ($c \approx 10^{-3}$ M) was one order of magnitude more concentrated than the one of **46** ($c \approx 10^{-4}$ M), which further empowers the possibility of augmented excited-state saturation during the course of the experiment.

To gain further insight in the sensitization process in **46** and confirm the involvement of a PET mechanism, the electrochemical characterization by CV of compounds **46**, **47** and **48** was performed. The obtained cyclic voltamograms determined that all compounds exhibit fully reversible one electron oxidations and reductions (**Figure 3-33**, **Table 3-11**). Likewise, the reduction potential of **47** (out of range) is higher than **48**, meaning that the LUMO of the antenna is much higher in energy, permitting a possible PET fluorescence quenching mechanism in **46** upon 380 nm excitation. Under this assumption the antenna would act as electron donor, and the *cis*-AB as the acceptor.

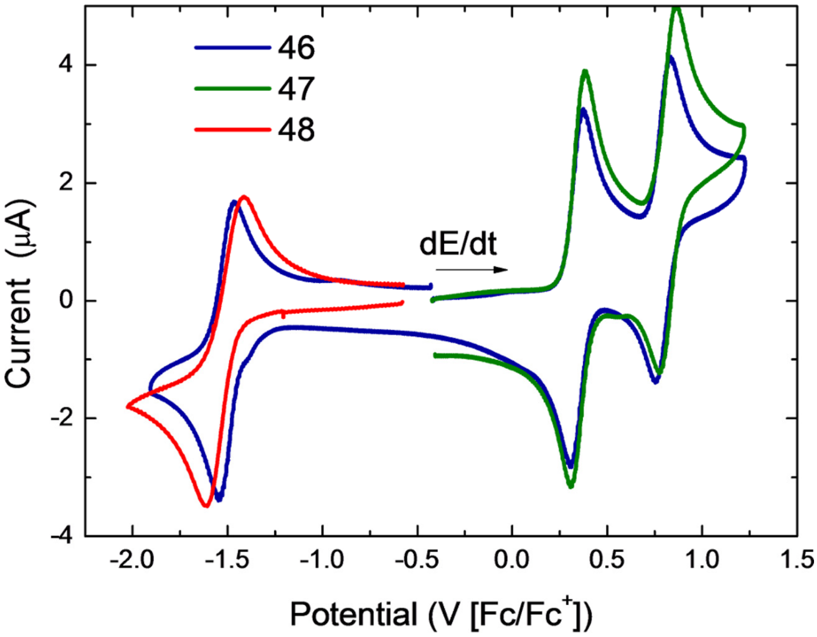

Figure 3-33: Cyclic voltammetry of **46** (blue line), **47** (green line) and **48** (red line) in acetonitrile 0.1 M Bu_4NPF_6.[b]

The potential of the first fully reversible oxidation process of the reference compound **47** is equal to the first oxidation process of **46**. Similarly, the second fully reversible oxidation process of **47** at 0.86 V is only 30 mV higher as the one observed in **46**, therefore, it can be assumed that the electron-poor fluorinated AB has in the *m*-position even a smaller electron-withdrawing effect than the bromine at the same position in **47**. The first fully reversible reduction process of the reference AB compound ***trans*-48** is at -1.61 V and only slightly lower by 70 mV than the first reduction process of ***trans*-46**. Meaning that there is a slight electron-withdrawing effect exhorted by the antenna, which decreases the overall distribution of electron density in the AB-moiety and promotes a subtle diminishment of the reduction potential in ***trans*-46** as compared with ***trans*-48**.

Table 3-11: Anodic and cathodic peak potentials of **46**, **47** and **48**, determined by cyclic voltammetry in acetonitrile. All values are reported against the ferrocene/ferrocenium redox couple as external standard.

Compound	E_p^{a1} / V	E_p^{a2} / V	E_p^{c1} / V
***trans*-46**	0.37	0.83	-1.54
47	0.37	0.86	-
***trans*-48**	-	-	-1.61

When the cyclic voltammetry of compounds ***cis*-46** and ***cis*-48** was performed, only the cathodic peaks, which correspond to the pure *trans*-form were detected. Following Hapiot's methodology,[74] very fast scan rates were employed combined with spectroelectrochemistry (SEC), to record the spectral evolution upon increasing applied negative potential of ***cis*-48** (**Figure 3-34**) and ***cis*-46** (**Figure 3-35**). As can be seen in the left inset of **Figure 3-34**, at lower negative potentials there is a small reduction process (inset, red line) which once is initiated at very low current values, converts the AB solution in a catalytical cascade of events quantitatively into ***trans*-48**. Afterwards, a further increase of the applied negative potential promotes the reduction of the electrochemically generated ***trans*-48** to the radical-anion (right inset, **Figure 3-34**, blue-line), with the corresponding spectral signature-bands appearing at 442 nm and 575 nm. The same behavior was observed for ***cis*-46**, meaning that electrochemical reduction of the AB-*cis* moiety in **46** is a catalytic process which is possible to promote under an applied negative potential at the conditions employed in the SEC and CV measurements. Since the HOMO and LUMO levels enable a possible PET from the excited antenna to the ground-state of the *cis*-AB moiety, this mechanism could explain the observed photophysical properties of compound **46** upon 380 nm excitation.

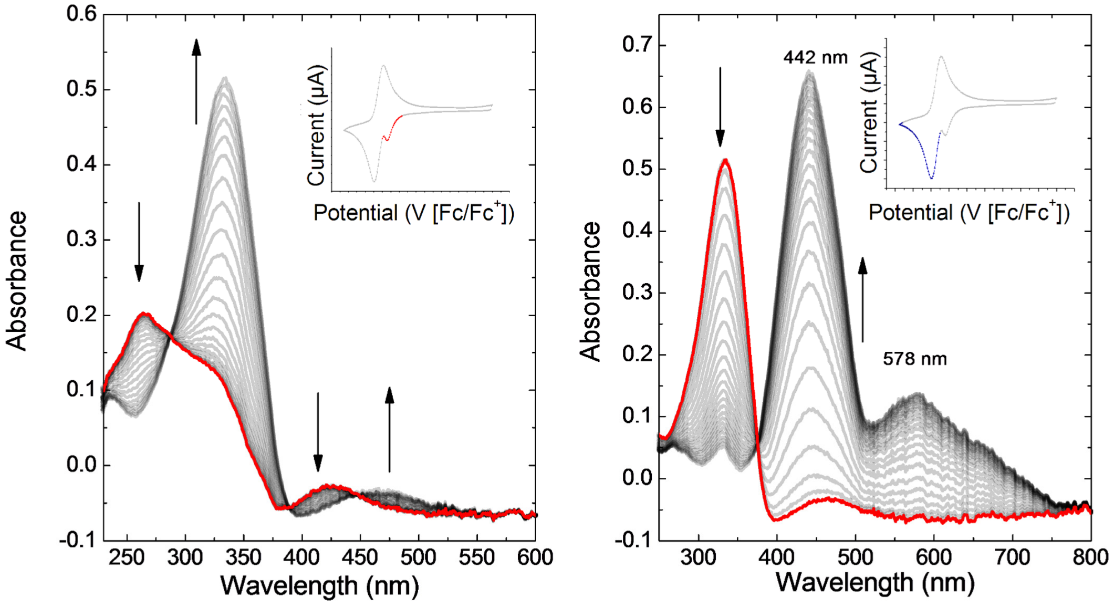

Figure 3-34: Spectral evolution starting from a ***cis*-48** enriched solution (red line) in acetonitrile 0.1 M Bu_4NPF_6 upon increasing applied negative potential corresponding to inset red line (left). Continued spectral evolution after electrochemical isomerization of ***cis*-48→*trans*-48** (red line) upon increasing applied negative potential corresponding to inset blue line (right).[b]

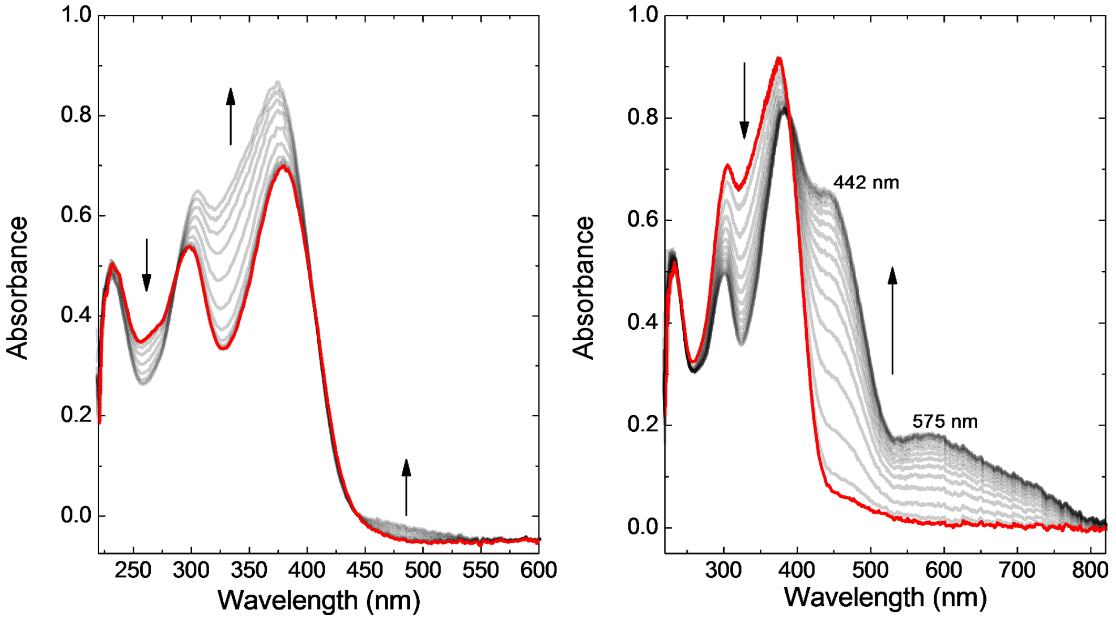

Figure 3-35: Spectral evolution starting from a ***cis*-46** enriched solution (red line) in acetonitrile 0.1 M Bu_4NPF_6 upon increasing applied negative potential (left). Continued

spectral evolution after electrochemical isomerization of ***cis*-46→*trans*-46** (red line) upon increasing applied negative potential (right).[b]

3.2.3 Transient Absorption Spectroscopy

Characterization of the photophysical properties by means of transient spectroscopy measurements were performed in collaboration with Dr. Sergey A. Kovalenko.[f] Herein, as part of the results of this work a new methodology was developed to measure transient spectra of molecules by two-photon excitation and determine their absolute 2PA cross-section $\sigma^{(2)}$. Since the main objective of this project was to demonstrate the two-photon sensitized *cis→trans* isomerization of **46**, a comprehensive study of the TA spectra of the reference compounds **47** and **48** is first needed with one-photon and then with two-photon excitation. Once the behavior of each component was understood, the dyad could be examined first by one-photon and then by two-photon excitation.

TA spectra of **47** upon 2-photon excitation are shown in **Figure 3-36**. Note that the 2-photon energy ($2\nu_P$ = 26596 cm^{-1}) is nearly equal to that of 1-photon (ν_P = 26316 cm^{-1}), implying that the two states are very close in energy. Consider *n*-hexanes first. The most important spectral changes occur for delays *t* = 0.4 - 64 ps (top left). During that time interval the bleach signal remains nearly constant, while SE and ESA rise on a picosecond timescale. This behavior is very different from that observed upon 1-photon excitation. At the same time in acetonitrile, the spectral evolution between 0.3 - 4 ps (top right) is quite similar to that under 1-photon excitation. There the evolution in the red can again be interpreted as a red-shift of SE due to solvation. Coming back to *n*-hexanes, it is worth to mention that the SE band is two times less intense than the bleach, unlike in the 1-photon case where the two bands are of the same intensity. After *t* = 100 ps (middle) the signal decays in both solvents on a 1 ns scale, similar to 1-photon excitation.

---

[f] The following transient spectroscopy experiments were performed by Dr. Sergey A. Kovalenko of the research group of Prof. Dr. N. P. Ernsting, Humboldt-Universität zu Berlin.

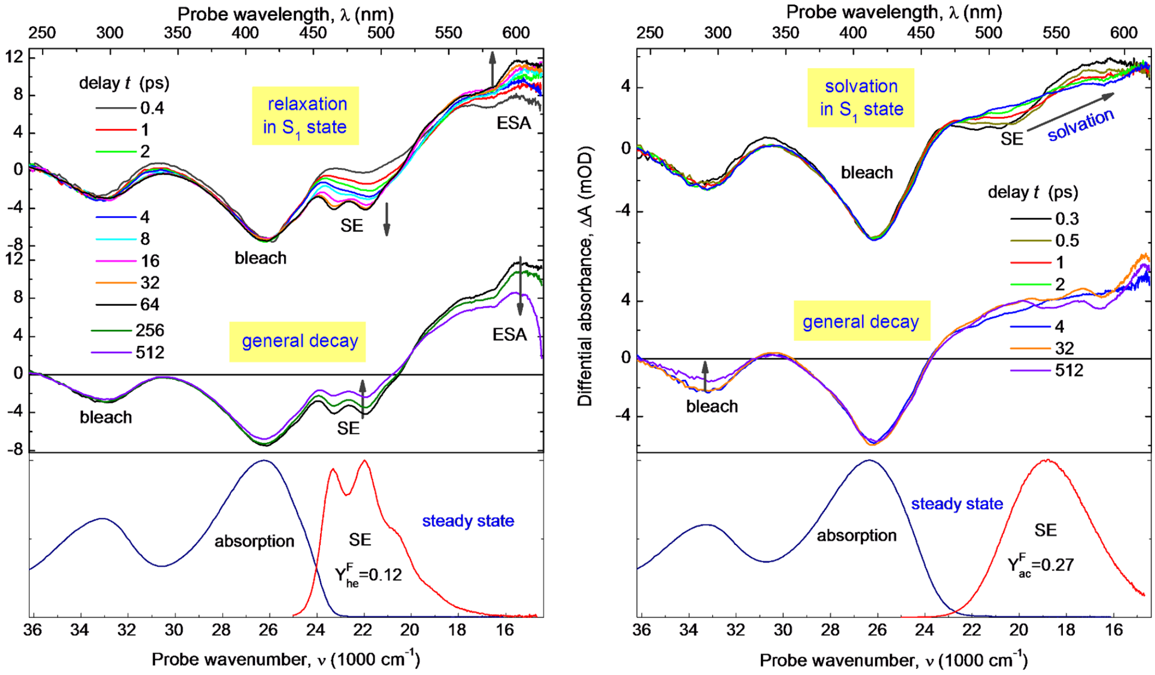

Figure 3-36: TA spectra of **47** in solution upon 2-photon excitation, λ_P = 752 nm, E_p = 7.6 μJ, a_P = 150 μ. In *n*-hexanes for delays *t* = 0.4-64 ps (top left) the bleach is constant in time, whereas SE and ESA rise in intensity on a picosecond scale. In acetonitrile for *t* = 0.3-4 ps (top right) the evolution is dominated by solvation, similar to the 1-photon case. After 100 ps (middle) the signal decays in both solvents. The lowest panels show stationary absorption and SE spectra.[d]

Until now, 2-photon excitation is assumed to be responsible for the TA signal, neglecting higher-order contributions. If this is the case, it can be checked with with pump energy dependence (**Figure 3-37**). Herein it the TA spectra in *n*-hexanes under nonlinear excitation with pump energies E_1 = 4.8 μJ, E_2 = 6.5 μJ, E_3 = 9.0 μJ are depicted (left). The corresponding signal ratios ($\Delta A_2 / \Delta A_1$), ($\Delta A_3 / \Delta A_1$) are displayed at right, with grey lines representing expected values for 2-photon excitation. At low energies $E_p \leq 6$ μJ the agreement is good, at least in the region of the main bleach band, around 27000 cm^{-1}. Hence the 2-photon contribution dominates higher-order nonlinearities. However, for $E_p \geq 6$ μJ deviations become evident indicating 3- and 4-photon contributions. Next interesting feature of the spectra at left is that the relaxation behavior looks similar for three pumping energies E_i. At the same time, with increasing E_i the SE band becomes substantially weaker than the bleach band. This suggests that the molecules excited with 3- or 4-photons do not reach the S_1 surface, but follow a different relaxation path.

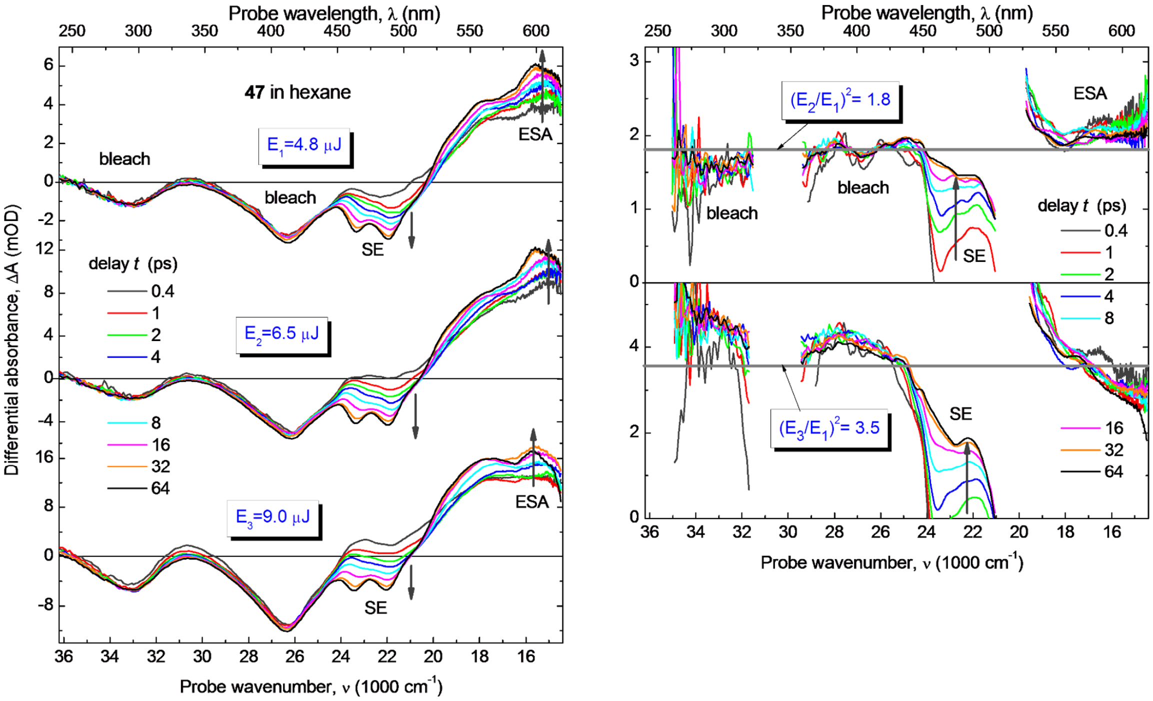

Figure 3-37: (left) TA spectra ΔA_1, ΔA_2, ΔA_3 in *n*-hexanes upon nonlinear (λ_P = 752 nm) excitation with pump energy E_1 = 4.8 µJ, E_2 = 6.5 µJ, E_3 = 9.0 µJ. (right) Spectral dependent signal ratios (ΔA_2 / ΔA_1), (ΔA_3 / ΔA_1), with grey lines indicating the expected ratio for 2-photon excitation. The 2-photon contribution dominates the TA signal for $E_P \leq 6$ µJ. In that case higher-order nonlinearities can be neglected. Hence the vibrational cooling, which may contribute after 2- or 4-photon excitation, should be negligible. The observed rise of SE and ESA is probably related with relaxation over a barrier within the S_1 surface (from one to another local energy minimum).[d]

Derived from this work, the relationship between the cross-section $\sigma^{(2)}$ and the bleach $\Delta A_{bl}^{(2)}$ was established, which opens the way for absolute measurements. The $\sigma^{(2)}$ determined for the 2PA antenna **47** was of 20 GM and confirms the nonlinear behavior of **47** which was further proven by the pump energy dependence.

TA spectra of ***trans*-48** upon 1-photon and 2-photon π→π* (330 or 640 nm, $S_0 \rightarrow S_2$) excitation are shown in **Figure 3-38**. Early delays, *t* = 0.10 - 1.00 ps, reveal ultrafast decay in the red and growth in the blue, with an isosbestic point at λ = 440 nm. The observed ultrafast evolution on a 0.1 ps scale is reasonably associated with the $S_n \rightarrow S_1$ relaxation.[224] Interestingly, the subsequent S_1 evolution is similar from that upon the direct n→π* (S_1)

excitation. ESA 1 and ESA 2 (at 377 and 411 nm) can be still recognized. For 2-photon excitation, the ESA bands are more diffused and their relaxation is slower. Interestingly the ESA 1 band seems to be significantly more intense as with 1-photon excitation. Additionally, although energetically the S_2 energy surface should be addressed by 2-photon excitation, it is not possible to identify a neat $S_2 \rightarrow S_1$ relaxation within the first 1 ps. Late spectra in the bleach region are consistent with the isomerized ***cis*-48** product. In addition, there are other products absent under 1-photon excitation. These additional products resemble the ESA 2 band in the case of *n*-hexanes and acetonitrile, however, it seems more pronounced in the latter case.

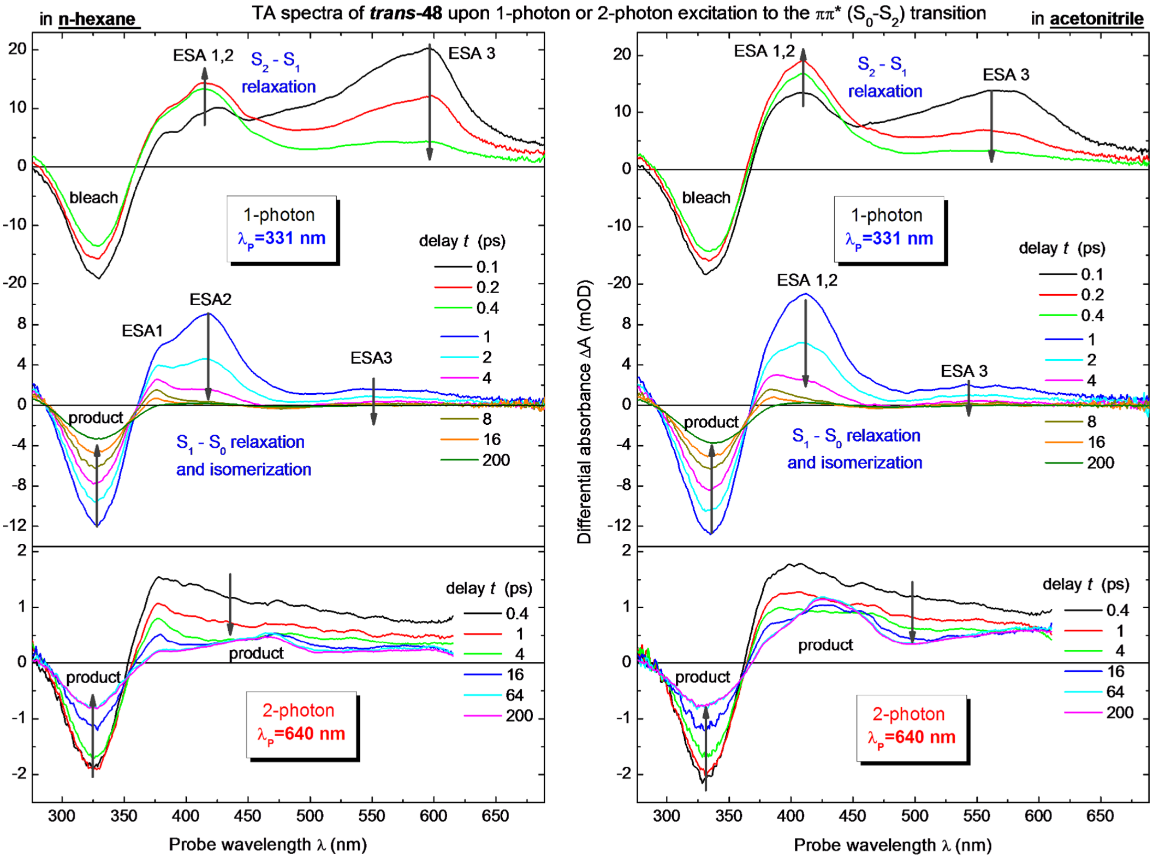

Figure 3-38: TA spectra of ***trans*-48** in *n*-hexanes and acetonitrile upon ($S_0 \rightarrow S_2$) excitation. With 1-photon excitation (λ_P = 331 nm) one observes first $S_2 \rightarrow S_1$ relaxation (top), and then $S_1 \rightarrow S_0$ relaxation and isomerization (middle). With 2-photon excitation (λ_P = 640 nm, bottom) the ESA bands are more diffused and their relaxation is slower. Late spectra in the bleach region are consistent with the isomerization products. In addition there are other products absent under 1-photon excitation.[d]

To confirm that the 2-photon *trans*→*cis* isomerization was a nonlinear process, a concentrated solution of ***trans*-48** in *n*-hexanes was irradiated (λ_P = 660 nm) with a focused laser beam. The conversion depending on laser focusing and irradiation time was monitored by UPLC (**Figure 3-39**). Herein it was possible to confirm the generation of *cis*-isomer even after only 15 min with a strongly focused beam. It was even possible to isomerize **48** with a weakly focused laser source by 2-photon excitation.

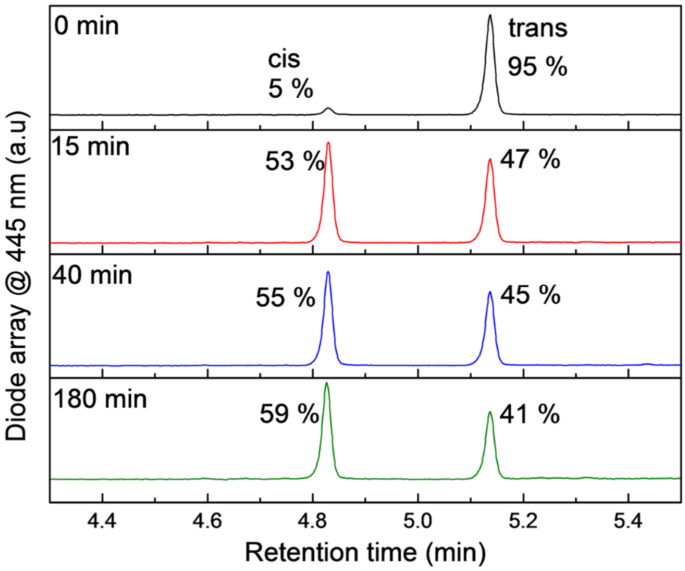

Figure 3-39: UPLC traces of samples taken after different irradiation times with 2-photon excitation (E = 10 μJ, λ_P = 660 nm, 1 cm path length, $c \approx 10^{-3}$ M). No irradiation (black line). 15 min irradiation with strongly focused laser beam (red line). 40 min irradiation with moderately focused laser beam (blue line). 180 min irradiation with a weakly focused laser beam (green line).

Having understood and determined the main behavior and spectroscopic signatures of **47** and ***trans* -48** upon 1-photon and 2-photon irradiation, TA spectra of ***trans*-46** upon 1-photon λ = 442 nm (S_0-S_1) excitation were obtained and are presented in **Figure 3-40**. Between pump-probe delays $0.1 \leq t \leq 1.0$ ps (top) the bleach decay is negligible compared to ESA 2 that reflects mainly an excited-state evolution. After t = 1 ps (middle) the bleach recovery corresponds to $S_1 \rightarrow S_0$ relaxation and *trans*→*cis* isomerization. The late bleach spectrum at 512 ps is due to *cis* (positive) and *trans* (negative) contributions with the additional contribution of residual excited TAA component, and therefore can be roughly fitted by their difference absorption ($A_c - A_t$), as shown at the bottom. The contribution is originitad by partial absorption of the TAA at the irradiation wavelength and is confirmed by the weak SE in the late spectra.

Considering the evolution in *n*-hexanes in more detail (left). At t = 0.10 ps (black spectrum) there are two main contributions which can be assigned on hand of the reference compounds **47** and **48**. There is the characteristic bleach component of the AB centered at ~330 nm with a negligible decay compared to the ESA 2 which is in this case not equal to the ESA 1. The difference arises from the TAA contribution to the bleach at ~380 nm accompanied with SE which overlaps the ESA 1 as well as the ESA from the TAA which grows in intensity from $0.1 \leq t \leq 1.0$ ps. The added processes cause an overall contribution to the ESA 1 which results in an almost negligible excited-state evolution from $0.1 \leq t \leq 1.0$ ps. After t = 1 ps (middle) the bleach recovery corresponds to S_1-S_0 relaxation and *trans-cis* isomerization. Herein the contribution to the bleach and ESA of the TAA is negligible and remains as residual excitation after the isomerization. The late bleach spectrum at 512 ps is due to *cis* (positive) and *trans* (negative) contributions with the additional influence of residual excited triarylamine component. Interestingly, there is a larger extent of excited TAA in acetonitrile as compared with *n*-hexanes. This finding is in accordance with the determined *trans→cis* isomerization yield in *n*-hexanes, which is 0.16 vs. 0.07 in acetonitrile. The isomerization yield is rationalized with the fact that the antenna is excited more extensively in acetonitrile, thus decreasing the number of photons available for the AB to absorb and promote the isomerization. This assumption is confirmed by the larger bleach region centered at ~380 nm in acetonitrile (right) which is attributed to the TAA component of **46**.

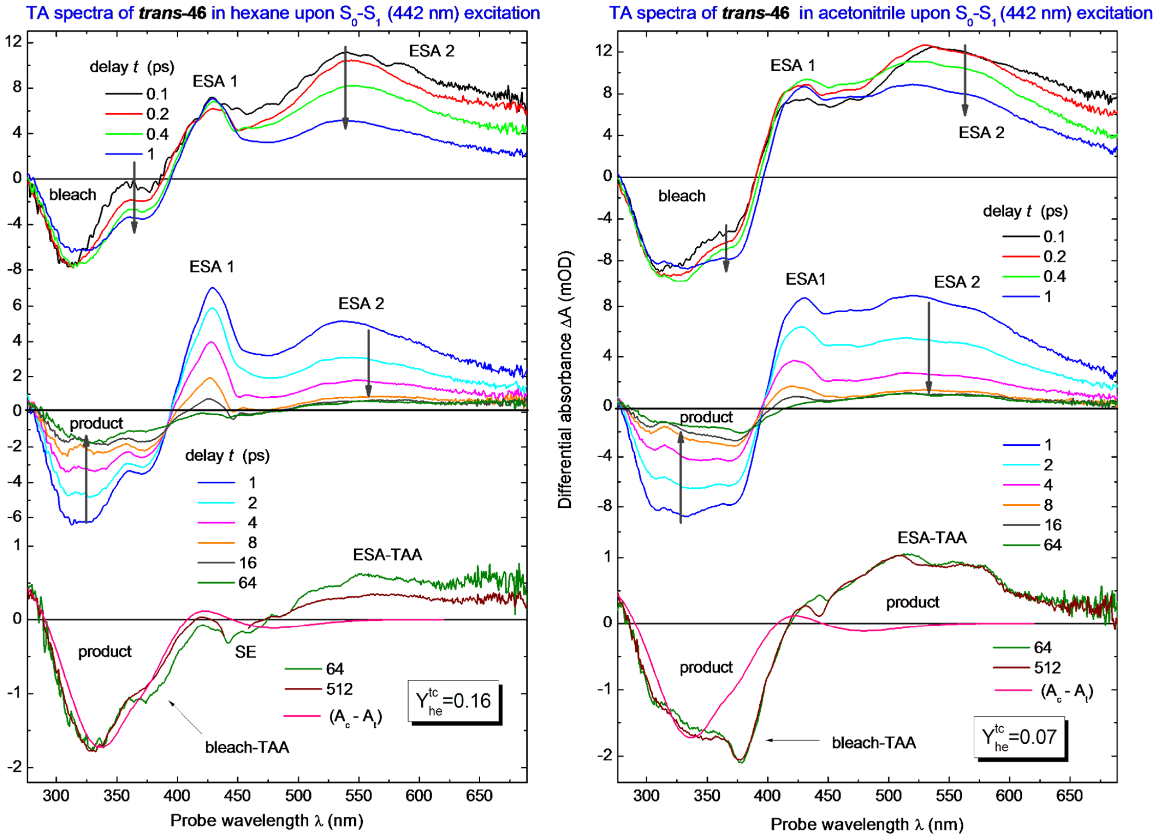

Figure 3-40: TA spectra of ***trans*-46** upon 1-photon $S_0 \rightarrow S_1$ excitation ($\lambda_P = 440$ nm) Between pump-probe delays $0.1 \leq t \leq 1.0$ ps (top) the bleach decay is negligible compared to ESA that reflects mainly an excited-state evolution. After *t* = 1 ps (middle) the bleach recovery corresponds to $S_1 \rightarrow S_0$ relaxation and *trans*→*cis* isomerization.[d]

Upon irradiation at the λ_{max} of **47** (380 nm) a distinct behavior was observed. TA spectra of ***trans*-46** in *n*-hexanes and acetonitrile upon $S_0 \rightarrow S_2$ (380 nm) excitation were obtained (**Figure 3-41**). Opposed as with 440 nm irradiation, the bleach signal resembles the TAA component with characteristic minima at 380 nm and 306 nm at *t* < 1 ps. The bleach signal decreases afterwards and is again resolved at 330 nm at *t* = 1 ps. This process, which is more pronounced in *n*-hexanes, could be attributed to an energy transfer from the excited TAA to the AB. An early evolution (t < 1 ps, top) reflects mainly $S_2 \rightarrow S_1$ relaxation. It has to be noted that ESA signature corresponds mainly to the TAA component as can be seen by comparison with **47**. Later (t > 1 ps) the ESA decay and bleach recovery are concomitant indicating $S_1 \rightarrow S_0$ relaxation and isomerization. A product was observed at very long time (t = 512 ps) in the bleach region. Interestingly, in *n*-hexanes at 16 ps and later one sees decaying SE (~450 nm) which is similar to that from **47**. The residual bleach corresponds as in the case with 440 nm excitation to TAA bleach and the ESA is accordingly also assigned to this fragment. Hence the relaxation path branches in two: the majority of excited molecules follow the AB path, but in few of them the excitation is localized at the TAA-unit and they relax accordingly.

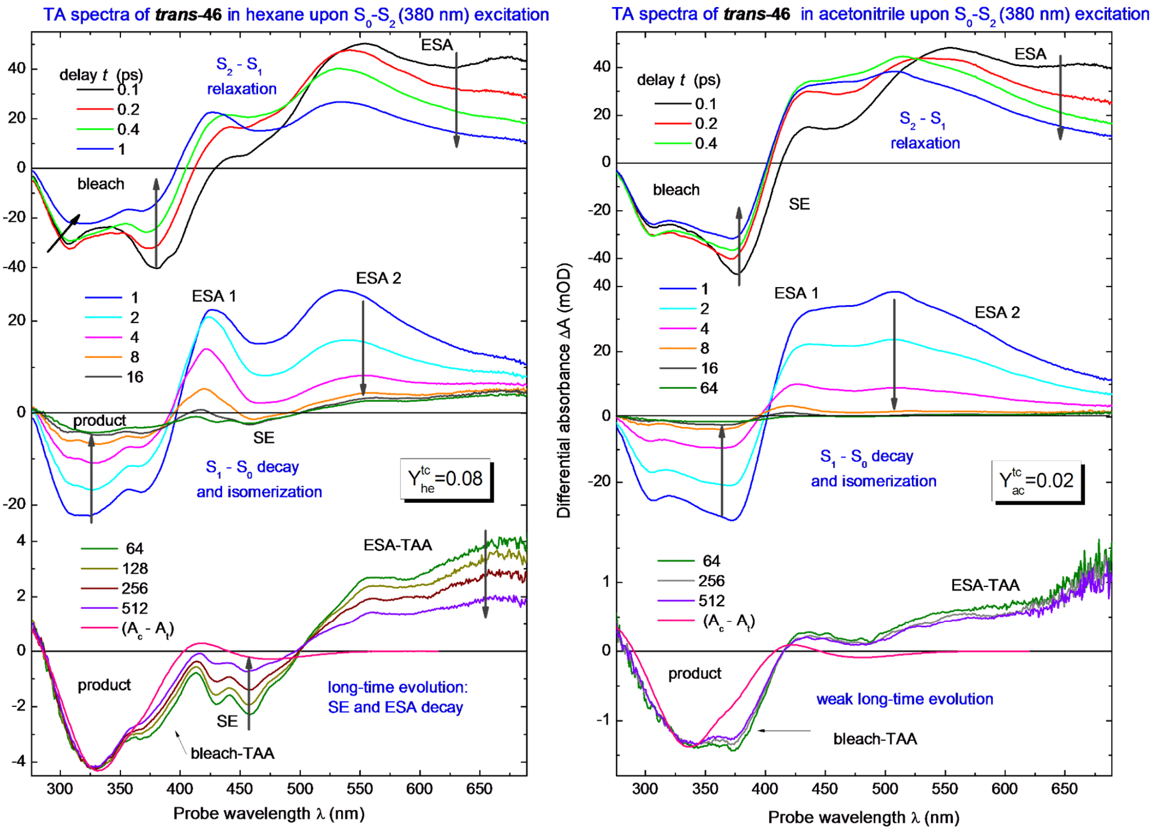

Figure 3-41: TA spectra of ***trans*-46** in *n*-hexanes and acetonitrile upon $S_0 \rightarrow S_2$ (380 nm) excitation. An early evolution (t < 1 ps, top) reflects mainly $S_2 \rightarrow S_1$ relaxation Later (t > 1 ps) the ESA decay and bleach recovery are concomitant indicating $S_1 \rightarrow S_0$ relaxation and isomerization.[d]

Figure 3-42 shows the TA spectra of ***cis*-46** upon n→π* ($S_0 \rightarrow S_1$, 442 nm) excitation which show very similar evolution to unsubstituted ***cis*-48**. Herein isomerization products are already observed after 0.4 ps. However, there is a significant ESA contribution of the TAA in the red. It is interesting that as observed with ***trans*-46**, ESA 1 is almost not resolved and exhibits a negligible decay compared to ESA 2. The difference arises from the TAA contribution to the bleach at ~380 nm accompanied with SE which overlaps the ESA 1 as well as the ESA from the TAA which grows in intensity from $0.1 \leq t \leq 1.0$ ps. The added processes cause an overall contribution to the ESA 1 which results in an almost negligible excited-state evolution from $0.1 \leq t \leq 1.0$ ps. After *t* = 1 ps (middle) the bleach recovery corresponds to $S_1 \rightarrow S_0$ relaxation and *cis→trans* isomerization. Herein, the contribution to the bleach and ESA of the TAA is negligible and remains as residual excitation after the isomerization. The late bleach spectrum at 512 ps is due to *trans* (positive) and *cis* (negative) contributions with the additional contribution of residual excited triarylamine component. Interestingly, there is a larger extent of excited TAA in acetonitrile as compared with *n*-hexanes. Nevertheless, as can be seen on the late bleach spectra the determined *cis→trans* isomerization yield in *n*-hexanes is lower, with 0.08 vs. 0.22 in acetonitrile. This observation is not fully understood because it does not follow the observed trend that isomerizations of **46** and **48** are higher in *n*-hexanes than in acetonitrile. Furthermore, it seems that the absorption of the TAA component is larger in acetonitrile, thus diminishing slightly the amount of photons available for the AB to absorb and should consequently exhibit a lower isomerization yield. Since this is not the case, an investigation on the excited state energy surfaces would be necessary to rationalize this finding. However, the large amount of atoms in the molecule render the computational simulation of the system extremely time consuming for the level of accuracy required.

Upon irradiation at the λ_{max} of **47** (380 nm) a distinct behavior was observed. TA spectra of ***cis*-46** in *n*-hexanes and acetonitrile upon $S_0 \rightarrow S_2$ (380 nm) excitation were obtained (**Figure 3-43**). An early evolution (*t* < 1 ps, top) reflects mainly ESA relaxation, however, $S_2 \rightarrow S_1$ and $S_1 \rightarrow S_0$ relaxation are not well separated (or the $S_2 \rightarrow S_1$ relaxation is too fast). It has to be noted that ESA signature corresponds mainly to the TAA component as can be seen by comparison with **47**. An important observation is the lack of appearance of isomerization product at early times, which is opposed to the behavior observed for ***cis*-46** following $n \rightarrow \pi^*$ excitation. Later (*t* > 1 ps) the ESA decay and bleach recovery are concomitant indicating $S_1 \rightarrow S_0$ relaxation and isomerization. A product evolution is seen at *t* = 2 ps in the bleach region as a positive signal. A detailed look to the case in *n*-hexanes evidences a visibly resolved ESA 1 band corresponding to the AB component. The decay of the ESA 1 band with the associated product formation indicates that upon 380 nm excitation at the beginning (t < 1 ps) only TAA is excited, from *t* > 1 ps the excitation energy is transferred to the S_1 of the *cis*-AB component which immediately isomerizes accordingly. Although a similar ESA decay and parallel *cis→trans* isomerization process is found for the ***cis*-48** $\pi \rightarrow \pi^*$ excitation case, the dynamics are significantly different, being the product evolution almost completed at t = 8 ps for ***cis*-46**, whereas in ***cis*-48** product evolution proceeds until t = 200 ps. This important difference is also tangible with the divergent isomerization yields of *cis*→*trans* isomerization in *n*-hexanes for **46** (0.38) and **48** (0.09). Again, in *n*-hexanes at 16 ps and later one sees decaying SE (~450 nm) which is similar to that from **47**. The residual bleach corresponds as in the case with 440 nm excitation to TAA bleach and the ESA is accordingly also assigned to this fragment. As seen in the earlier cases, relaxation path branches in two: the majority of excited molecules follow the AB path, but in few of them the excitation is localized at the TAA-unit and they relax accordingly.

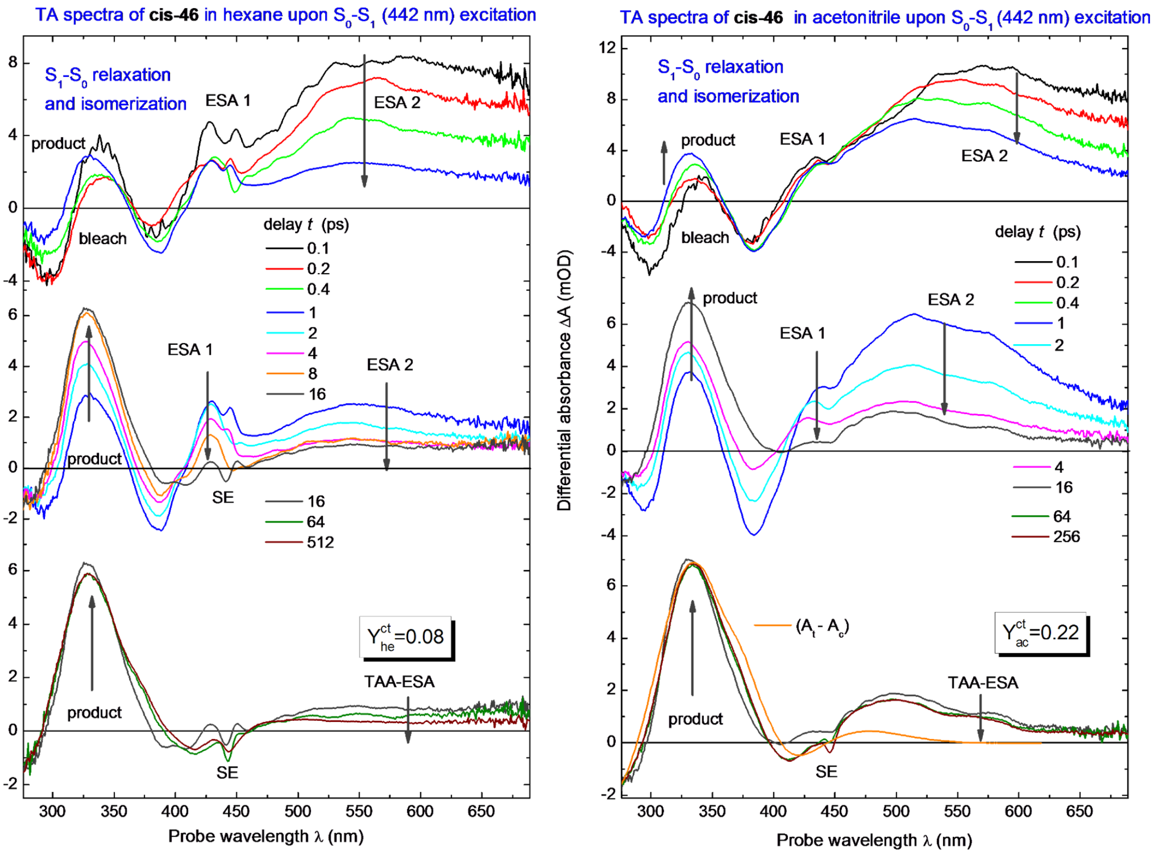

Figure 3-42: TA spectra of ***cis*-46** upon 1-photon $S_0 \rightarrow S_1$ excitation (λ_P= 440 nm). Between pump-probe delays $0.1 \leq t \leq 1.0$ ps (top) the bleach decay is negligible compared to ESA that reflects mainly an excited-state evolution. Herein, isomerization products are already observed after 0.4 ps. After t = 1 ps (middle) the bleach recovery corresponds to $S_1 \rightarrow S_0$ relaxation and *cis*→*trans* isomerization. The contribution is originated by partial absorption of the TAA at the irradiation wavelength and is confirmed by the weak SE and residual bleach in the late spectra.[d]

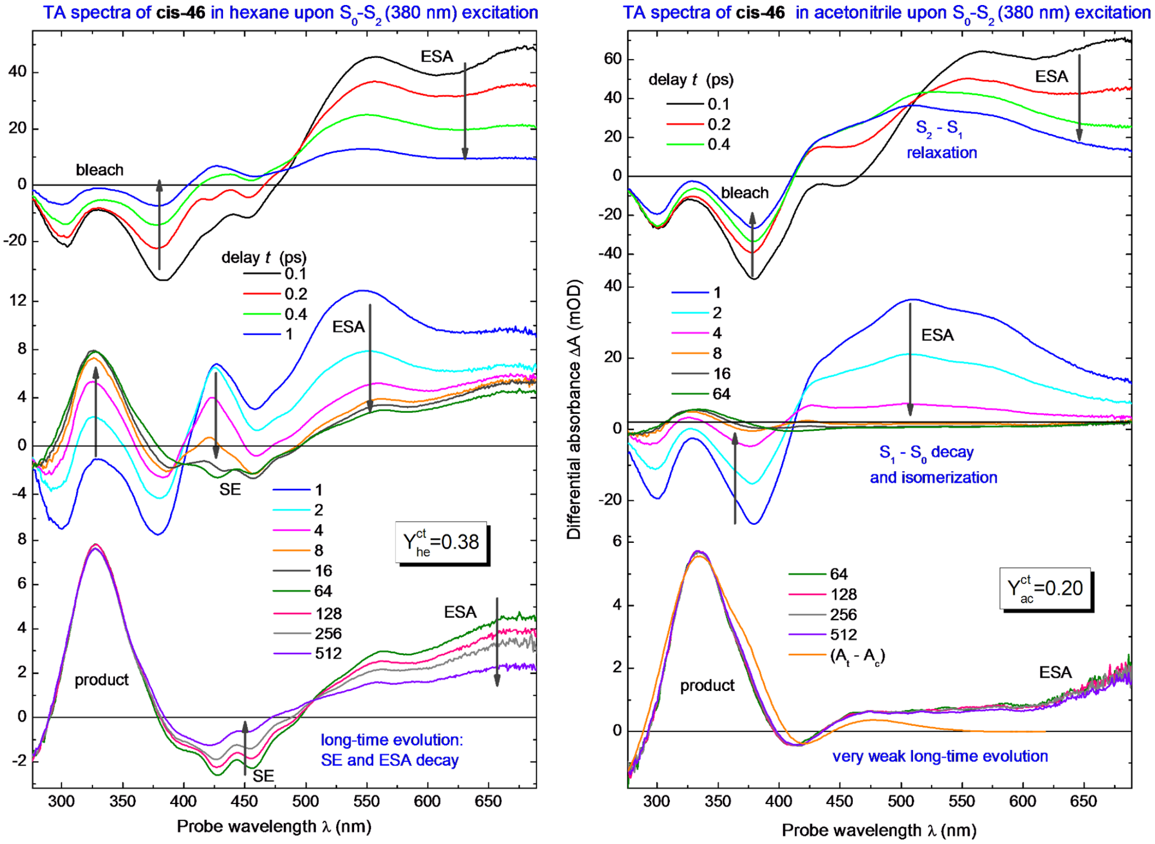

Figure 3-43: TA spectra of ***cis*-46** in *n*-hexanes and acetonitrile upon $S_0 \rightarrow S_2$ (380 nm) excitation. Here, $S_2 \rightarrow S_1$ and $S_1 \rightarrow S_0$ relaxation are not well separated (or the $S_2 \rightarrow S_1$ relaxation is too fast). In *n*-hexanes fluorescence from the TAA-unit is observed, similar to the *trans* case (**Figure 3-41**). The bleach signal at late time is now positive as it is proportional to the difference absorption ($A_t - A_c$).[d]

On hand of these results, it seems straightforward to assign the increase of isomerization yield in **46** originated by the efficient and very fast (sub picosecond scale) energy transfer from the TAA to the AB. During the transfer of energy, it was not possible to detect the appearance of ESA bands which could be assigned to charged species. Furthermore, polar solvents did not influence the formation of such species, but rather diminished the isomerization yield. It is generally assumed, that PET increases in efficiency with solvent polarity, due to the larger stabilization of the charge separated species, while FRET is not influenced by the solvent. The observed isomerization yield decrease in polar solvents is unclear, but it might be indicative of an underlying competing phenomenon associated with the very weak long-time evolution. Therefore, due to the close proximity of components, strong excited-state coupling, neglectable spectral overlap and absence of charged species even in polar solvents, it can be assumed that the transfer of energy is governed by a Dexter-type exchange mechanism.

Once the energy transfer from the TAA to the AB component was confirmed, the 2-photon excitation of **46** was studied. In **Figure 3-44** the TA spectra of ***cis*-46** upon 1-photon and 2-photon $\pi \rightarrow \pi^*$ (380 or 750 nm, $S_0 \rightarrow S_2$) excitation as well as of **47** are represented (lower frames). Early delays, *t* = 0.40 - 4.00 ps, reveal a slow overall bleach recovery and ESA decay. The ESA bands are more diffused and their relaxation is slower with 2-photon excitation. The ESA 1 band can be easily identified at ~377 nm which is indicative of an energy transfer from the TAA to the AB. Furthermore, under 2-photon excitation no SE could be detected, which confirms the hypothesis of an energy transfer to the AB component. Similarly as with **48**, the S_2 energy surface should be addressed by 2-photon excitation, but it is not possible to identify a neat $S_2 \rightarrow S_1$ relaxation within the first 1 ps. Late spectra in the bleach region are consistent with the isomerized ***cis*-46** product. Similarly as with 1-photon excitation, the amount of product is much larger in *n*-hexanes. In addition, there are other products absent under 1-photon excitation. These additional products resemble the ESA 2 band, and comparison with the bleach indicates that a considerable amount of energy is still at the TAA component after 600 ps. This behavior is consistent with the slower relaxation dynamics and bleach recovery observed for **47** and **48** upon 2-photon excitation.

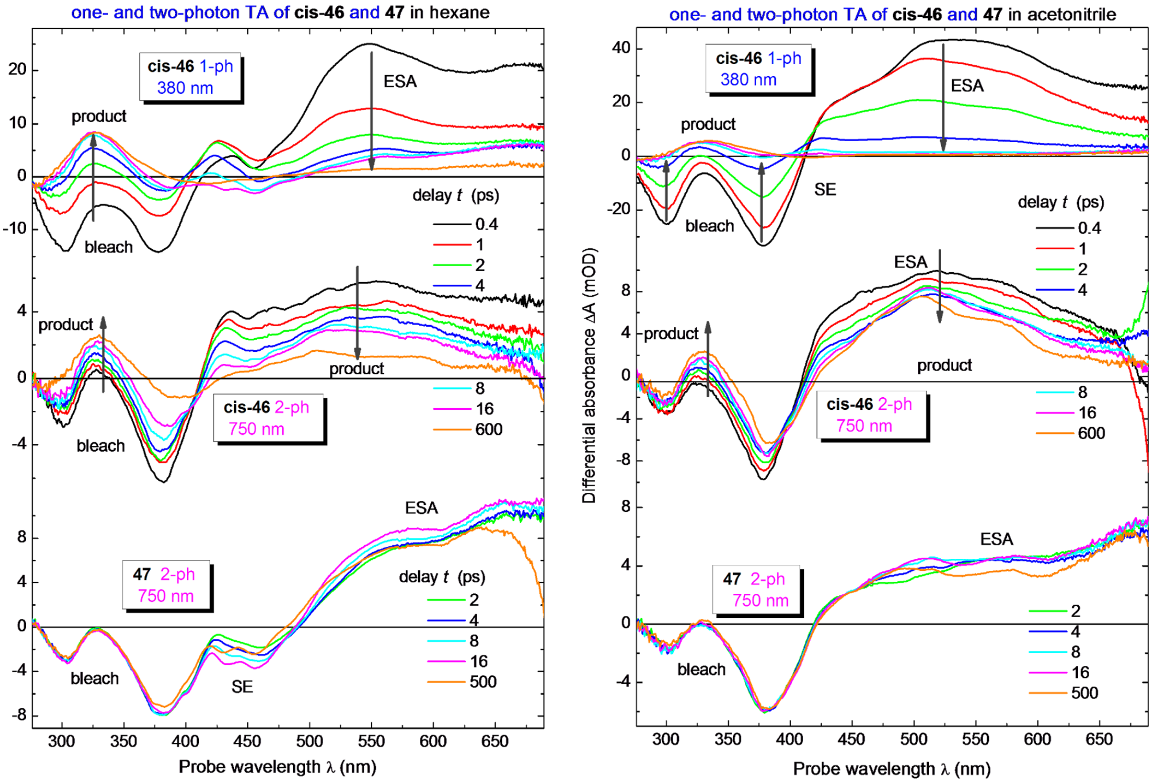

Figure 3-44: 1- and 2-photon excited TA spectra of ***cis*-46** and **47** in *n*-hexanes and acetonitrile. The products (from ***cis*-46**) in the bleach and ESA regions are clearly different upon 1- and 2-photon excitation, as evidenced by the bleach and ESA region.[d]

The square power dependece (**Figure 3-32**) verified that the 2-photon sensitized *cis*→*trans* isomerization was successfully accomplished. In this particular system, the process seems to be more efficient in nonpolar solvents. The absence of charged species and negligible amounts of SE allow to conclude that the transfer of excitation energy proceeds from the sensitizer to the AB by a Dexter-type mechanism. The transfer of energy is an ultrafast process which promotes the complete isomerization of the AB almost within the first 16 ps, whereas **48** required 200 ps. With 2-photon excitation the overall process is slower, and again in *n*-hexanes a faster relaxation dynamic is observed as compared with acetonitrile. Interestingly, under 2-photon excitation a substantial amount of excitation energy remains on the antenna, which is not transferred to the AB. Further studies should be performed with flash photolysis to investigate the slower component of the excited-state dynamics.

3.3 PET mediated *cis→trans* Isomerization of Azobenzenes

3.3.1 Target Definition

Derived from the findings of the preceding Chapter and motivated by the catalytical electrochemical isomerization of ABs observed for compound **48** when performing the SEC and CV, the goal of this project is to achieve the amplification of a light stimulus by coupling the absorption of photons with an electrochemical cascade reaction by means of a PET mediated step. By irradiation of a covalently linked triplet-sensitizer to an electron-deficient AB it can be anticipated that a PET process from the excited donor to the lower lying acceptor will take place. Concomitant formation of the radical-anion centered at the AB in the *cis*-form immediately triggers the electrochemical isomerization to the *trans*-form. If the newly formed *trans*-isomer of the charge-separated species is stable enough, ideally, a second neutral molecule in the *cis*-form could act as electron acceptor, promoting an additional intermolecular electrochemical-isomerization and thus initiating a catalytic cascade. In theory, this process could be rationalized with photoisomerization yields greater than 1.0, as one photon is capable to effectively promote more than one photochemical event (**Scheme 3-22**).

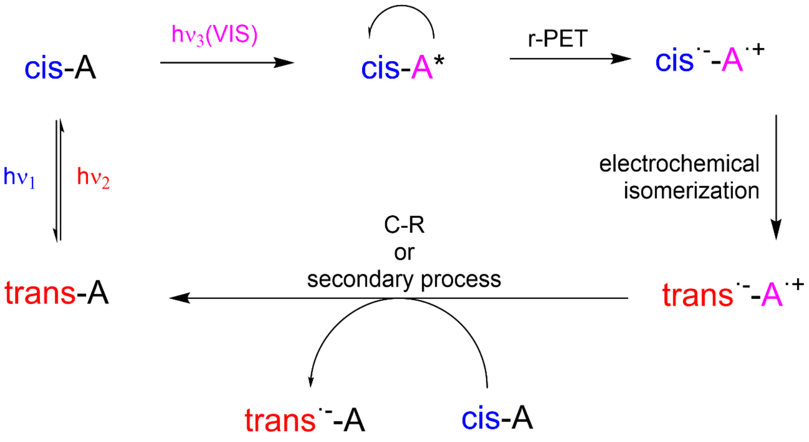

Scheme 3-22: Schematic representation of the PET mediated *cis→trans* isomerization of an AB-antenna dyad.

3.3.2 Synthesis and Characterization

To warrant the possibility of a PET process, no other relaxation pathways could be competing, therefore, no spectral overlap of the emission and the absorption can occur. EET is a faster process than PET hence the molecule prefers this deactivation pathway, rather than evolving as consequence of PET into a charge-separated state. It is also of significance that to promote an efficient PET process the lifetime of the excited donor should be as long-lived as possible in an intermolecular scenario. With this purpose a long-lived phosphorescent triplett-emitter derived form Ir(III) was chosen. Furthermore, to modulate the charge-separation and charge-recombination rates, it is important to favor the initial charge-separation while the charge-recombination is attenuated. Considering these requirements *m*-phenyleneethynylene spacers have demonstrated good performance.[220] Finally, due to the benefitial photophysical and electrochemical properties an *o*-fluorinated AB was chosen as the photochromic electron-poor acceptor. The depicted molecular dyad as well as the model compounds required for the characterization are shown in **Scheme 3-23**.

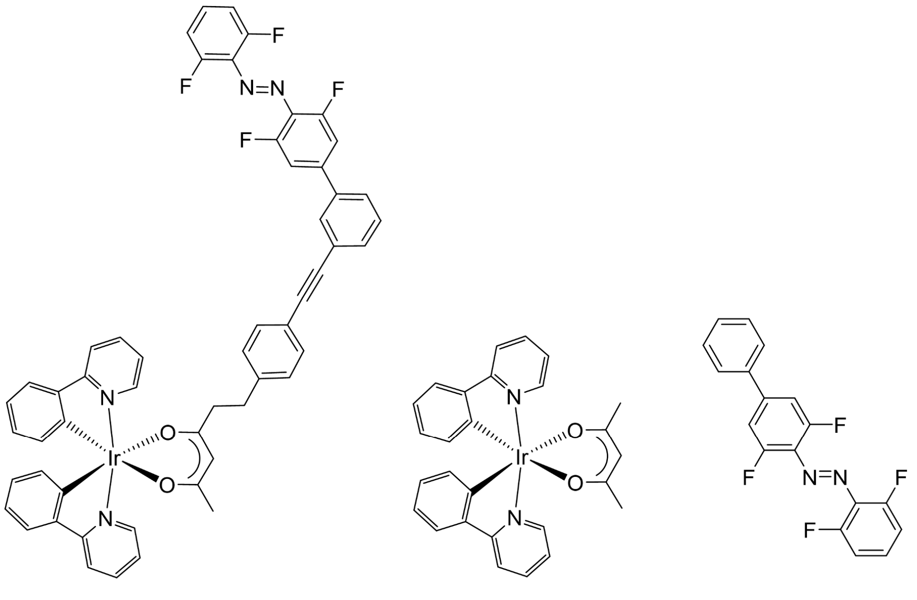

53

54

48

Scheme 3-23: Ir(ppy)$_2$acac-azo dyad **53** and reference compounds **54** and **48**.

The synthesis of **53** was accomplished by a final complexation step of the acac-AB ligand **57** (**Scheme 3-24**) to the commercially available $[\{Ir(\mu\text{-}Cl)(ppy)_2\}_2]$ chloride-bridged dimer (**Scheme 3-25**).

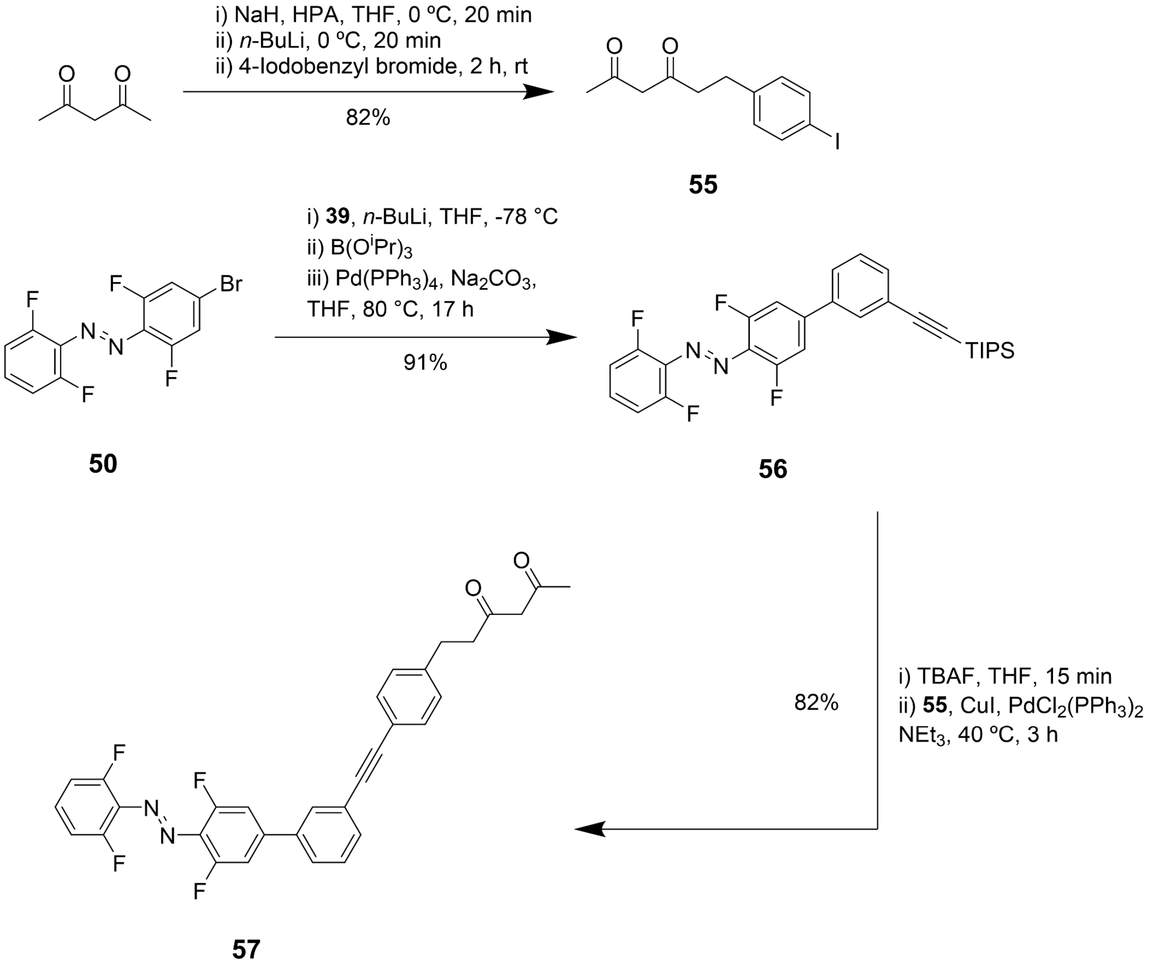
i) NaH, HPA, THF, 0 °C, 20 min
ii) n-BuLi, 0 °C, 20 min
ii) 4-Iodobenzyl bromide, 2 h, rt
82%
55
i) 39, n-BuLi, THF, -78 °C
ii) B(OiPr)3
iii) Pd(PPh3)4, Na2CO3, THF, 80 °C, 17 h
91%
50
56
TIPS
i) TBAF, THF, 15 min
ii) 55, CuI, PdCl2(PPh3)2 NEt3, 40 °C, 3 h
82%
57

Scheme 3-24: Synthesis of AB ligand **57**.

The synthesis of the AB ligand was accomplished following a modular approach. Regioselective nucleophilic addition of acetylacetone to 4-iodobenzyl bromide was achieved by the stepwise formation of the disodiumenolate of acetylacetone with NaH in anhydrous THF at 0 °C assisted by hexamethylphosphamide (HPA), which promotes the subsequent fast metal exchange with *n*-BuLi at the 1-position. Addition of 4-iodobenzyl bromide gave after work-up and purification by column chromatography compound **55** in very good yield (82%). The synthesis of intermediate **56** was accomplished by sequential lithiation of **39** in anhydrous THF at -78 °C followed by borylation with $B(^iOPr)_3$ and final addition of a 2 M solution of Na_2CO_3 followed by degasing with Ar for 15 min enabled the preparation of the solution to which afterwards **50** and $Pd(PPh_3)_4$ were added. The resulting mixture was then submitted to reflux for 17 h and after work-up and purification by column chromatography compound **56** was isolated with excellent yield (91%). Treatment of **56** with TBAF in THF at room temperature, followed by work-up and Sonogashira coupling of the obtained alkyne-AB with **55** in degased TEA in the presence of CuI and $PdCl_2(PPh_3)_2$ at room temperature afforded after 3 h of reaction and purification by column chromatography **57** in excellent yield (82%).

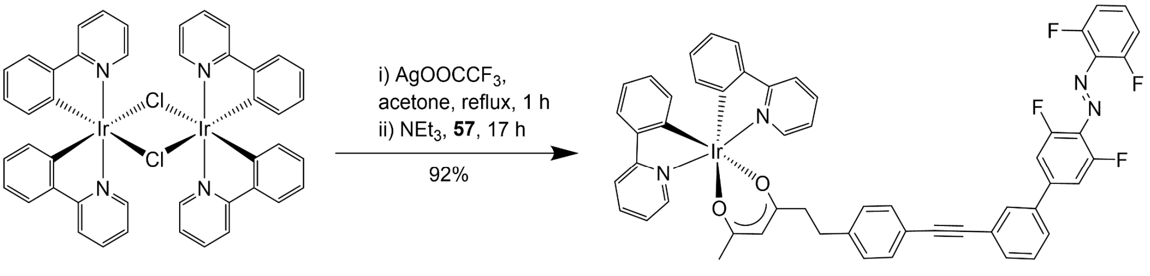

53

Scheme 3-25: Synthesis of target molecular dyad **53**.

To increase the reactivity of the Ir(III) center towards **57**, the commercial dimeric species of [{Ir(*μ*-Cl)(ppy)$_2$}$_2$] was treated with $AgOOCF_3$ in anhydrous acetone at reflux for 17 h under Ar atmosphere. As consequence of this procedure the complex lost the dimeric form and the chlorine atoms were substituted by -$OOCF_3$. The solution was filtered and washed several times with acetone to eliminate the precipitated AgCl, and then **57** under basic conditions was added. After 17 h at room temperature, TLC analysis showed quantitative completion of the reaction. After work-up, purification was performed by an initial column chromatography in Al_2O_3, followed by separation of minor Ir(III) impurities by gel permeation chromatography (GPC) and a final clean-up by column chromatography in Al_2O_3 with additional recrystallization from PE which yielded compound **53** in excellent yield (92%).

The target molecular dyad **53** shows fully reversible photochromism and exhibits very high *cis*-form content in the PSS obtained upon vis-light irradiation (**Figure 3-45**). The absorptivities and composition at the PSS of compounds **53** in acetonitrile are depicted in **Table 3-12**.

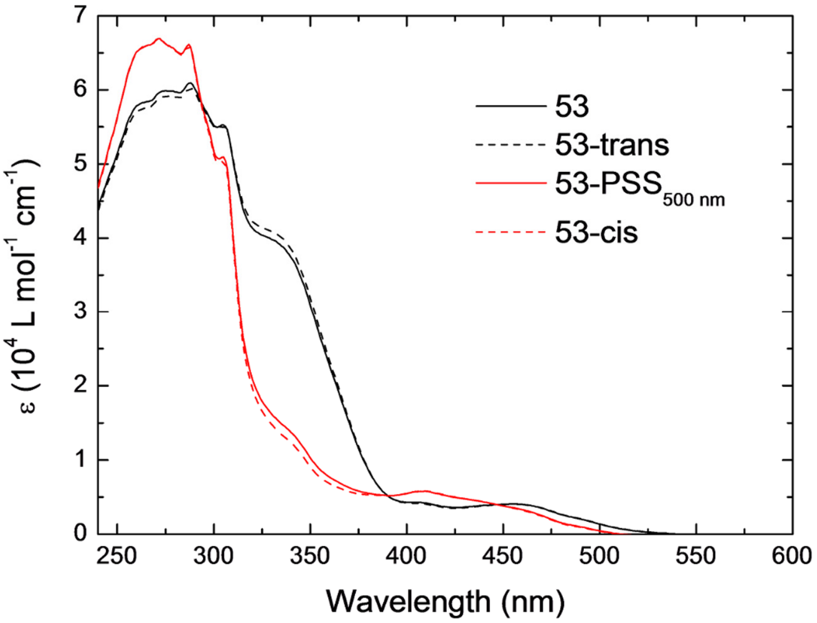

Figure 3-45: UV/vis absorption spectra of **53** as obtained from synthesis (black line), the *trans*-form (dashed black line), the PSS (red line) and the simulated pure *cis*-form (dashed red line) in acetonitrile ($c \approx 10^{-5}$ M) are depicted. PSS induced by irradiation with vis-light (λ_{irr} > 500 nm) at 25 °C.

Table 3-12: Molar absorptivities, absorption maxima of AB-moiety and composition at the PSS at different irradiation wavelengths of **53** in acetonitrile.

	λ_{max} / nm		ε / 10^4 L mol^{-1}cm^{-1}		PSS	PSS
	trans	*cis*	*trans*	*cis*	λ > 500nm	λ = 380nm
53	336	272	3.98	6.69	5% *trans* 95% *cis*	53% *trans* 47% *cis*

Upon irradiation with green light (λ > 500 nm) the n→π* band of the *trans*-form is selectively addressed enabling to achieve a very high PSSs in compound **53**, with similar values as for the previously reported *o*-fluorinated ABs.72 It can be thus assumed, that the Ir(III)-antenna has no electronic influence over the n→π* band of the AB, ensuring the possibility to selectively address with light the individual components of the molecular dyad **53**. Since the overlap of the absorption spectra between the AB and the Ir(III) complex is severe in the UV region, it is difficult to assign the proper transitions of **53**. However, because the coupling did not influence the electronic properties of the AB moiety, we can assume that the assigned transitions for **54** will be in the same spectral region for **53** (**Figure 3-46**). The observed transitions are assigned in accordance with the literature[149] and in analogy to the assignments of $Ir(ppy)_3$.[225] Strong transitions in the region below ~310 nm are assigned to allowed $^1(\pi\text{-}\ \pi^*)$ transitions of the ligands and therefore are largely ligand centered (LC). The maximum is observed at 258 nm ($3.9\cdot10^4$ $L\cdot mol^{-1}\cdot cm^{-1}$). They correspond to singlet ground state S_0 to ^1LC transitions. On the other hand, the transitions occurring longer than 320 nm with the maximum at 340 nm ($0.9\cdot10^4$ $L\cdot mol^{-1}\cdot cm^{-1}$) and a shoulder at 407 nm ($0.4\cdot10^4$ $L\cdot mol^{-1}\cdot cm^{-1}$) result from S_0 to ^1MLCT (metal-to-ligand-charge transfer) transitions mainly of Ir5d-(ppy)π^* character. The weakly manifesting shoulder between 440 nm and 480 nm with a maxima at 463 nm ($0.2\cdot10^4$ $L\cdot mol^{-1}\cdot cm^{-1}$) correspond to ^3MLCT states. The fact that the absorption into the lowest triplet state T_1 is observed, is remarkable and indicative of an MLCT admixture to this state, typical of $Ir(ppy)_n$ complexes. Thus, in analogy to similar compounds, the emissive state is assigned to be dominantly of ^3LC character with small ^1MLCT admixtures starting at 480 nm and having the emission maximum at 526 nm. Interestingly, the emissive intensity of the complex was severely influenced by the coupling of the AB (right, **Figure 3-46**). The emission was quenched by almost 60% in compound **53** as compared with **54**, whereas the emission band shape prevailed.

Following the same approach as in the preceding Chapter, the excitation at the ^1MLCT region of the antenna (380 nm) promotes the very fast and efficient *cis→trans* isomerization in **53** which was quantified by UPLC (**Figure 3-47**), with a quantum yield of 0.28 in acetonitrile. The same excitation (380 nm) for the *cis→trans* isomerization of **48** leads to a significantly lower PSS content with a quantum yield of 0.20 in acetonitrile. Over the course of the *cis→trans* isomerization following 380 nm irradiation of **53** and **48**, differential spectra were calculated, observing a very similar spectral-shape evolution (**Figure 3-48**). The obtained differential spectra further corroborate that the antenna and the AB components are completely electronically decoupled in the ground-state and that the photoisomerization of **53** only influences the AB-chromophore, as observed for **48**.

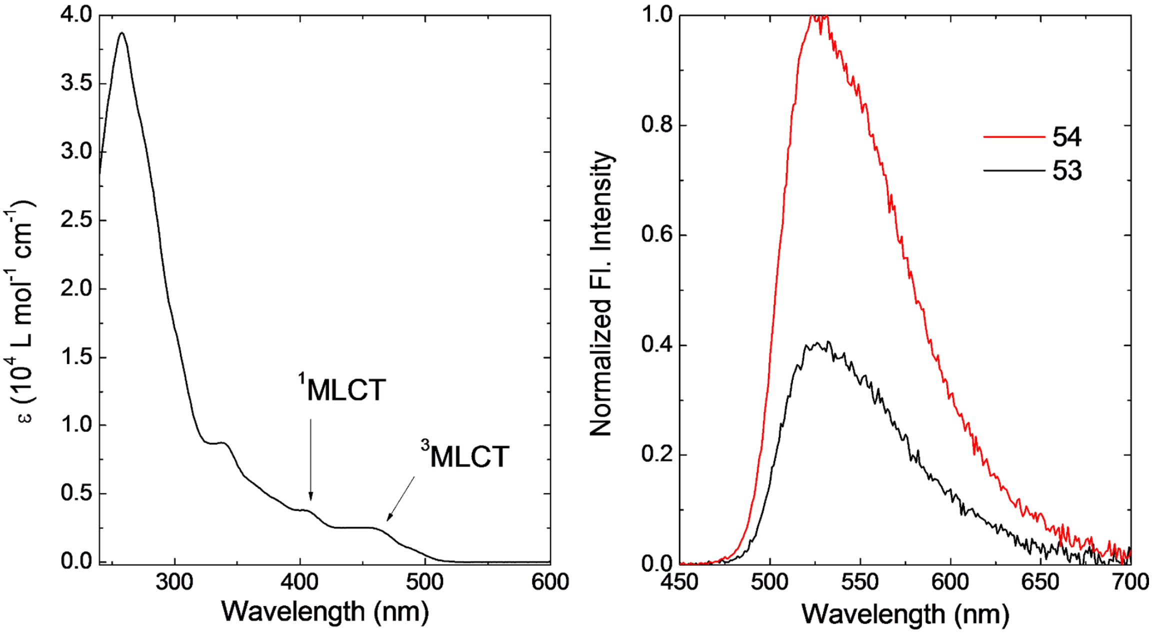

Figure 3-46: UV/ vis absorption spectra of **54** obtained in acetonitrile ($c \approx 10^{-5}$ M). The band at ~400 nm can be assigned to ^{1}MLCT and the band centered at ~460 nm to the ^{3}MLCT transition(left). Corrected normalized fluorescence emission spectra of **54** (red line) and **53** (black line) obtained in acetonitrile (λ_{exc} = 380 nm, $c \approx 10^{-6}$ M) at 25 °C (right).

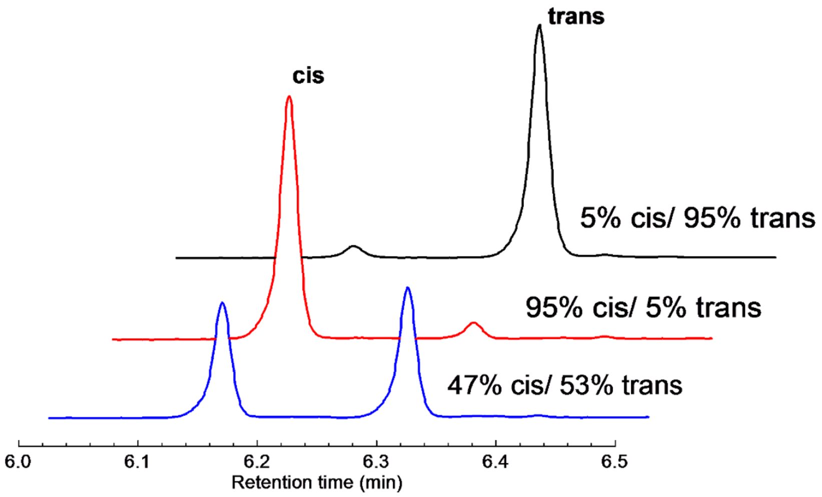

Figure 3-47: UPLC-traces of **53** before irradiation (black line), after reaching the PSS with λ > 500 nm (red line) and after reaching the PSS by irradiation with 380 nm of the *cis*-enriched solution.

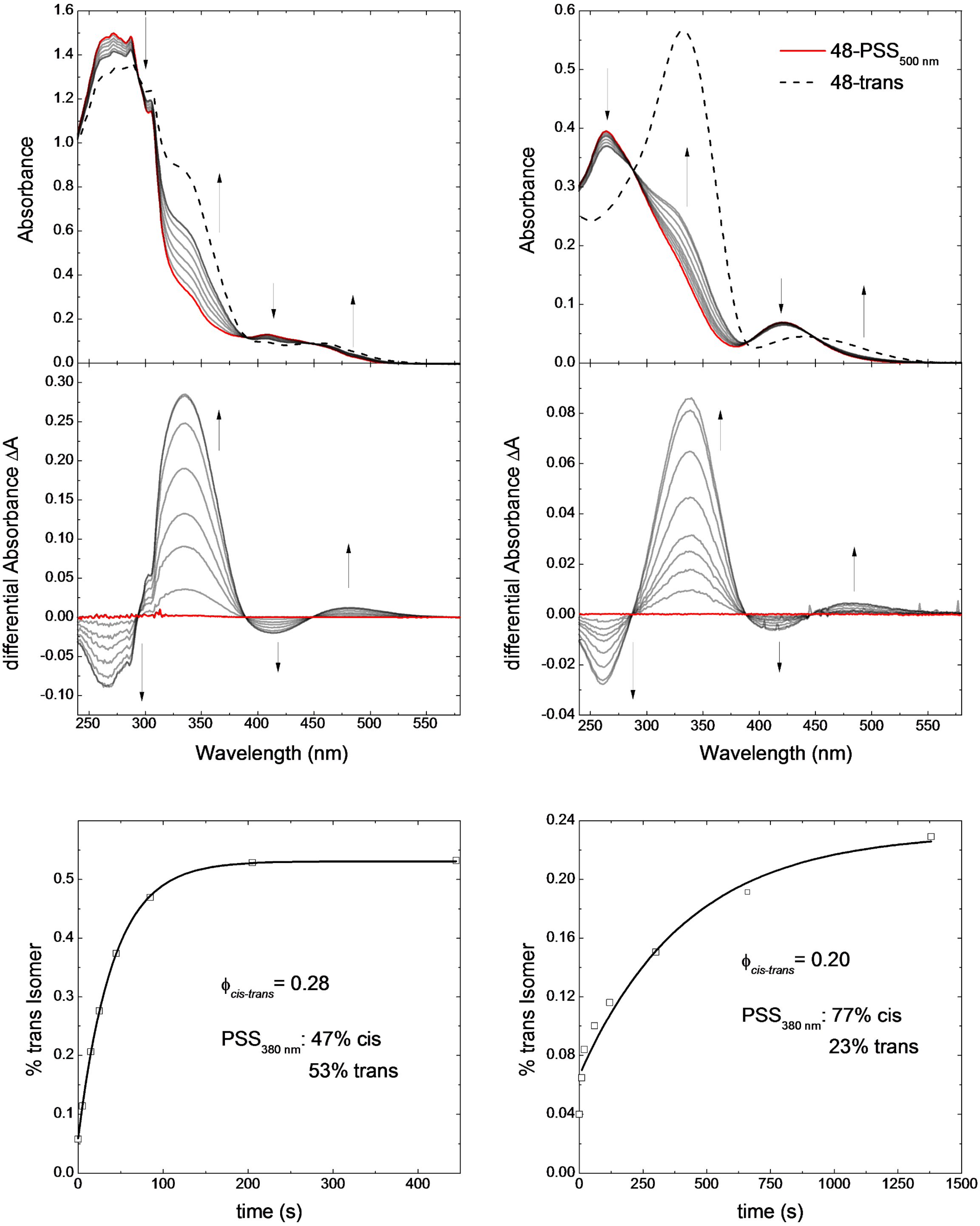

Figure 3-48: (top) Spectral evolution during the course of *cis*→*trans* isomerization induced by irradiation with UV-light (λ_{irr} = 380 nm) at 25 °C of **53** (left) and **48** (right), where the *trans*-form (dotted-line) and the PSS of the *cis*-form (red line) in acetonitrile ($c \approx 10^{-5}$ M) are depicted. (middle) Differential spectral evolution during the course of *cis*→*trans*

isomerization of **53** (left) and **48** (right). (bottom) *trans*-form content evolution versus 380 nm irradiation time in seconds for **53** (left) and **48** (right) in acetonitrile.

To confirm the possible PET process, the electrochemical characterization by CV of compounds **53**, and **54** was performed. The obtained cyclic voltammograms determined that all compounds exhibit fully reversible one electron oxidations and reductions (**Figure 3-49**, **Table 3-13**). Likewise, the reduction potential of **54** is considerably higher than **48**, meaning that the LUMO of the antenna is much higher in energy, permitting a possible PET fluorescence quenching mechanism in **53** upon ^{1}MLCT excitation. However, the obtained reduction potential which is assigned to the LUMO level is only an approximation as probably the ET proceeds from the excited triplet-state T_1 which has a much larger decay half-time than the S_1. Additionally, the S_1 which is determined by cyclic voltammetry would be poorly populated by ^{1}MLCT excitation due to the large ISC. Under the assumption that ET could proceed from the T_1-state, the antenna would act as an electron donor, and the *cis*-AB as the acceptor.

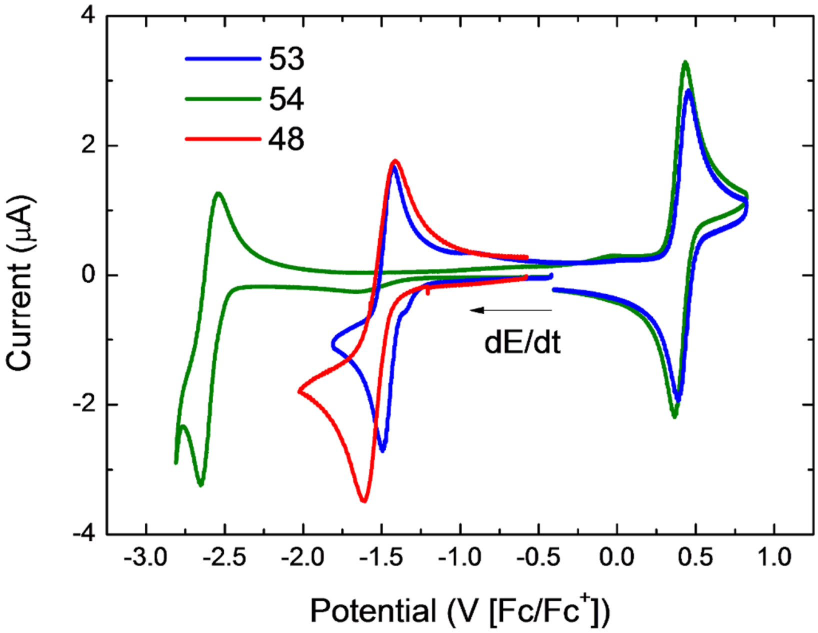

Figure 3-49: Cyclic voltammetry of **53** (blue line), **54** (green line) and **48** (red line) in acetonitrile 0.1 M Bu_4NPF_6.[b]

The potential of the first fully reversible oxidation process of the reference compound **54** is equal to the first oxidation process of **53**, consequently, it can be assumed that the electron-poor fluorinated AB has no electronic influence on the Ir(III) antenna. Upon covalent coupling of compound **54** with the AB, the first reversible reduction of compound **53** has a potential similar to the one observed for **48**. The new positively shifted reduction can be ascribed to the AB component and effectively influences the LUMO of the dyad, which is localized on the AB. The first fully reversible reduction process of the reference AB compound ***trans*-48** is at -1.61 V and negatively shifted by 130 mV in comparison with the first reduction process of ***trans*-53**. Herein, it can be assumed that there is an electron-withdrawing effect exhorted by the tolane spacer between the antenna and the AB, which decreases the overall distribution of electron density in the AB-moiety and promotes a diminishment of the reduction potential in ***trans*-53** as compared with ***trans*-48**.

Table 3-13: Anodic and cathodic peak potentials of **53**, **54** and **48**, determined by cyclic voltammetry in acetonitrile. All values are reported against the Fc/ Fc$^+$ redox couple as external standard.

Compound	E_p^{a1} / V	E_p^{c1} / V
***trans*-53**	0.44	-1.48
54	0.43	-2.65
***trans*-48**	-	-1.61

When the cyclic voltammetry of compound ***cis*-53** was performed, only the cathodic peak which correspond to the pure *trans*-form was detected. Following Hapiot's methodology and as performed in Chapter 3.2.2, very fast scan rates were employed combined with SEC, to record the spectral evolution upon increasing applied negative potential of ***cis*-53** (**Figure 3-50**). As can be seen in the left inset of **Figure 3-34**, at lower negative potentials, there was a small reduction process (inset, red line) which once is initiated at very low current values, converts the AB solution in a catalytical cascade of events quantitatively into ***trans*-53**. Afterwards, a further increase of the applied negative potential promotes the reduction of the electrochemically generated ***trans*-53** to the radical-anion (right inset, **Figure 3-50**, blue line), with the corresponding spectral signature-bands appearing at 442 nm and 575 nm. The same behavior was observed for the reference compound ***cis*-48** (**Figure 3-34**), meaning that electrochemical reduction of the *cis*-AB moiety in **53** is a catalytic process which is possible to promote under an applied negative potential at the conditions employed in the SEC and CV measurements. Since the HOMO and LUMO levels enable a possible PET from the excited antenna to the ground-state of the *cis*-AB moiety, this mechanism could explain the observed photophysical properties of compound **53** upon 380 nm excitation.

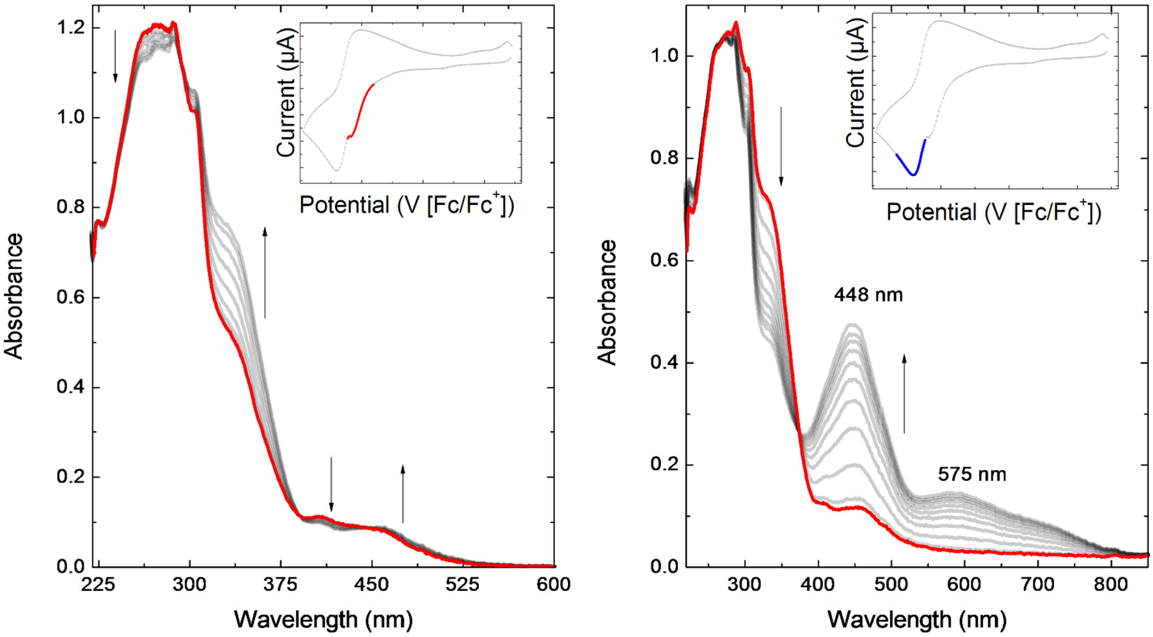

Figure 3-50: Spectral evolution starting from a ***cis*-53** enriched solution (red line) in acetonitrile 0.1 M Bu_4NPF_6 upon increasing applied negative potential corresponding to inset red line (left). Continued spectral evolution after electrochemical isomerization of ***cis*-53→*trans*-53** (red line) upon increasing applied negative potential corresponding to inset blue line (right).[b]

A thorough investigation of the PET mediated formation of the *cis→trans* isomerization of **53** by means of transient spectroscopy has not yet been conducted. The prospected study could shed light in the dynamics involved upon direct excitation of the Ir(III) sensitizer, and allow to discern if there are ET processes involved in the generation of the *trans*-form with the concomitant formation of radical species. The formed radical anion of the *cis*-AB would be very short living and probably not detectable, however, once the electrochemical isomerization proceeds, the signature of the *trans*-AB radical anion should resemble the signature bands observed at 448 nm and 575 nm which could be assigned to the spectra obtained by SEC. The limiting factor of this process is the charge-recombination reaction which could severely influence the half-life of the *trans*-AB radical anion.

4 Conclusions and Outlook

4.1 Reversibly Photomodulating the Emission of Fluorophore-Photoswitch Dyads

As described in Chapter 3.1, a novel set of molecular dyads was designed and synthesized with distinct properties. A largely improved synthetic protocol towards the design of non-symmetrical DAEs was developed and excellent fatigue resistance and photochromic properties (even in aqueous media) of easy functionalizable DAEs were achieved. On hand of compound **21**, it was possible to demonstrate that it is a promising strategy to exploit the electronic properties of DAEs to modulate the fluorophore $S_0 \rightarrow S_1$ transition which thereby lowers the band gap of the whole molecular dyad. A guideline was established for the perilous task of designing fluorophore-photoswitch dyads and the multiple considerations which are required to achieve functional photochromic compounds. Furthermore, the unprecedented red-shift and increase of the photochromic efficiency of the closed form of a DAE was achieved by effectively extending the conjugation length of the closed DAE. This observation is in stark contrast to previously reported DAEs, where a red-shift of the closed DAE band, by means of push-pull systems or an extended π-system, led to the severe suppression of the photochromic performance of the DAE. This property is rationalized with the fact that **21c** behaves as an individual molecule rather than a dyad with two distinctive addressable units. Therefore, the exceptionally high oscillator strength of the fluorophore promotes the efficient cycloreversion in the 680 nm region, which proceeds faster than with conventional 546 nm irradiation of the DAE. Further studies should be focused on the implementation of this design principle with photoswitches possesing poor cycloreversion yields to unleash far-red highly efficient photochromism. Possible applications could be also exploited in the design of DAEs with precisely tailored HOMO-LUMO gaps.

Ground-state electronic decoupling of the photoswitch and the fluorophore as in **36**, **37** and **38**, restored gradually the full photochromic performance of the DAE enabling to achieve high PSSs. It was also observed that contrary to the common design guidelines of turn-Off fluorescent switches, an almost negligible red-edge spectral overlap of DAE absorption band with fluorophore emission band is sufficient to completely quench the fluorescence of the fluorophore in the closed form of the dyad. Transient spectroscopy measurements assisted in differentiating the appearance of a yet unknown excited-state equilibration process between DAE and fluorophore in the closed form of the dyad.

The photochromic performance of the dyads was successfully studied in aqueous and biological media, which proved to be excellent inside of SDS micelles and DOPC GUVs. Fluorescence miscroscopy measurements of **38** highlighted the importance of shunning FRET processes as the fluorescence quenching mechanism. In order to achieve truly functional non-destructive fluorescent switches for imaging applications in biology or material sciencies, FRET has to be avoided since the irradiation intensity required for microscopy measurements is high enough to promote the quantitaive FRET mediated cycloreversion of the DAE component of the dyad. In this context, the contribution of this work is significant and will lead to the obtention of turn-On non-destructive fluorescent dyads. In this scenario, unpublished progress was achieved relying on the findings of this work and employing PET as the fluorescence quenching mechanism of the dyad (**Scheme 4-1**).

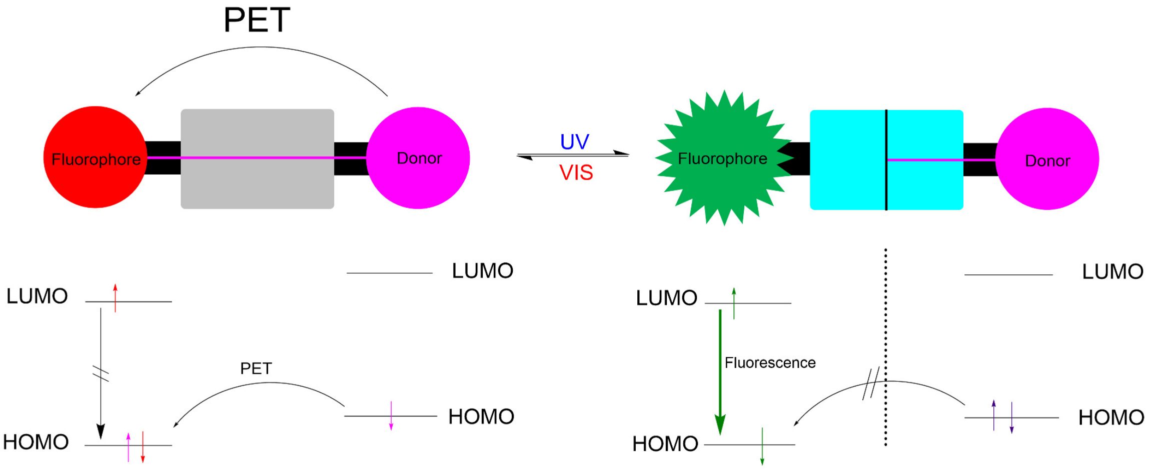

Scheme 4-1: Schematic representation of a photoswitch-fluorophore-donor triad incorporating light-gated trun-On fluorescence with non-destructive readout. (left) In the open form, the DAE (grey rectangle) favours the electronic coupling of the electron donor and the fluorophore, resulting in no fluorescence emission upon excitation of the fluorophore. (right) In the closed form the DAE decouples the donor and the fluorophore, enabling upon excitation of the fluorophore the fluorescence emission.

The compound envisioned with this design principle is depicted in Scheme 4-2. This conceptually improved approach would improve the molecular dyad towards attaining non-destructive readout and would also guarantee the fluorophore's performance in the closed form of the DAE, as it is not in conjugation with the DAE. Additionally, to avoid any possible FRET process, the benzo[b]thiophene and thiophene units of the DAE would be oxidizied to the corresponding sulfones. This oxidation promotes an increase in the thermal stability of the closed isomer as well as the hypsochromic-shift of the absorption band.

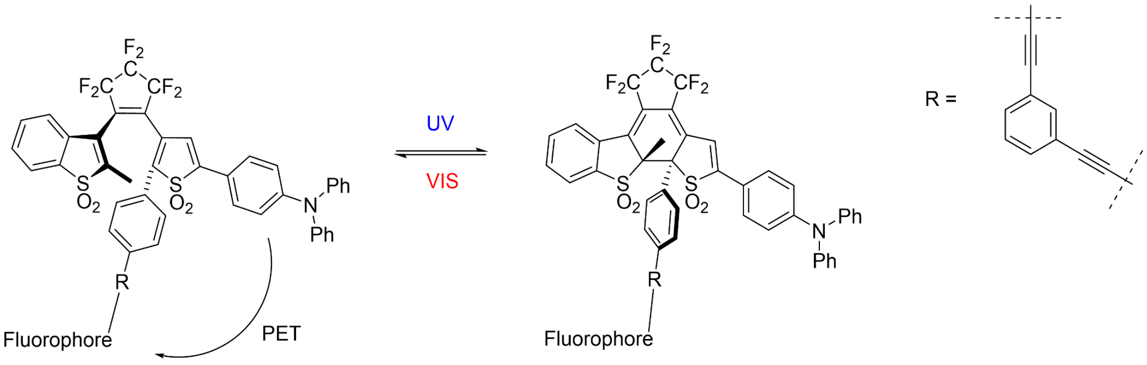
F2
F2C
CF2
S
O2
S
O2
N
Ph
Ph
R
Fluorophore
PET
UV
VIS
F2
F2C
CF2
S
O2
S
O2
N
Ph
Ph
R
Fluorophore
R =

Scheme 4-2: Proposed structural framework, where the fluorophore could be a benzo-fused BODIPY.

4.2 Sensitized Two-Photon *cis→trans* Isomerization of Azobenzenes

Summarizing the results presented in Chapter 3.2, the succesfull synthesis of a novel triarylamine-AB molecular dyad **46** was accomplished. The photochemical properties of this compound was studied as well as the electrochemical behavior, to elucidate the mechanism responsible for the highly efficient *cis→trans* isomerization of the AB component of the dyad upon excitation of the triarylamine band of the compound (380 nm). A significant difference in the PSS ratio and required time to reach it was moreover observed, as well as a four-fold increase in the isomerization yield for the same process in *n*-hexanes as compared with the reference compound **48**. The considerably quenched fluorescence emission of **46** in comparison with **47** and the determined redox potentials motivated the study of the excited-state dynamics by means of TA spectroscopy. The results obtained in collaboration with Dr. S. Kovalenko supported the photophysical properties observed by stationary measurements and pointed towards an energy transfer process from the excited TAA to the ground-state *cis*-AB. Subsequent isomerization of the AB component explained the antenna mediated *cis→trans* isomerization of **46** upon 380 nm irradiation. Furthermore, it was proven that this process was also possible by two-photon irradiation at 750 nm. A combined examination of the TA spectra and the SEC confirmed the lack of appearance of any charged species upon excitation, even in highly polar acetonitrile. Consequently, it can be postulated that the energy transfer from the TAA to the *cis*-AB in **46** is governed by a short-range strongly coupled Dexter-type mechanism. Since TAA are known to have large $\sigma^{(2)}$, as a partial result of this work, a procedure was developed to determine absolute $\sigma^{(2)}$, which was determined to be of 20 GM for reference compound **47**. Furthermore, the investigation of **48** by TA spectroscopy led to the significant observation that this AB does not violate Kasha's Rule having the same *trans→cis* isomerization quantum yield upon S_0-S_1 or S_0-S_2 excitation. Additionally, it was proven that the dipolar structure and broken symmetry of **48** led to a significant increase of the $\sigma^{(2)}$, rendering this AB as inherently two-photon responsive. This remarkable feature is of imperative significance, due to the thermally very stable *cis*-form and very small dimensions of the molecule. Isomerization experiments upon 660 nm irradiation with a focused laser beam corroborated the isomerization of highly concentrated solutions by two-photon irradiation.

The main objective of this project was satisfactorily proven, being possible to promote the sensitized *cis→trans* isomerization by means of two-photon excitation of the TAA. The initial intention of an AB completely addressable with visible-light by one-photon or two-photon excitation was thus accomplished. As consequence of the extraordinary long thermal half-life of ***cis*-46** it could be conceivable to quantitatively convert an ensemble of molecules into the *cis*-form by vis-light irradiation, and by means of highly focused two-photon excitation only isomerize to the *trans*-form a very specific subset of molecules. This fully reversible process could be achieved with subdiffraction resolution and only employing visible light sources which could be efficiently exploited in conjunction with biopharmacology and drug-release systems.

Prospective work will be focused on the optimization of the $\sigma^{(2)}$ of the TAA antenna, to increase the subdiffraction resolution of the system. Solid-state two-photon studies should be performed, blending **46** in a polymer matrix. These experiments would help to evaluate the feasibility of the envisioned solid-state subdiffraction resolution in the isomerization process. Additionally, the fascinating possibility to include **46** in smart drug release systems could be highly interesting, due to the likelihood of attaining extremily high spatial and temporal resolution as well as an extraordinary tissue penetration depth.

4.3 PET Mediated *cis→trans* Isomerization of Azobenzenes

In Chapter 3.3 the successful synthesis of a novel AB bidentate ligand and it's efficacious complexation to yield the first reported AB-Ir(III) complex **53** was reported. The photochemical properties of this compound were studied as well as the electrochemical behavior. A highly efficient *cis→trans* isomerization of the AB component of the dyad upon excitation of the ^{1}MLCT band of the compound was determined. Preliminary results evidence the possibility of a PET process evolving from the initial excitation of the Ir(III) complex, which by ISC advances into the long-lived T_1 state. From the T_1 it can be understood, that on hand of the reduction potentials of the molecule, ET to the *cis*-AB component in the ground state proceeds. Upon reduction of the *cis*-AB the radical anion immediately evolves to the *trans*-AB. Unfortunately, the so formed *trans*-AB radical anion seems not to be long lived enough to promote an intermolecular cascade of isomerizations, which would lead to the amplification of the initially employed photon to excite the Ir(III) component of the dyad. It is thus clear that to achieve the significant amplification of the initiating light stimulus, an equilibrium between the charge recombination and the diffusion has to be attained. If the charge recombination is slow, diffusion of the radical anion in the solution could lead to a productive collision with a neutral *cis*-AB molecule, which will act as intermolecular electron acceptor. Once the productive collision has taken place, a new *trans*-AB radical anion is electrochemically formed, which could collide with a further neutral *cis*-AB molecule, leading to the propagation and amplification of a cascade of isomerizations in the solution.

To overcome the inherent drawback of the fast charge recombination process in a molecular dyad, a straightforward strategy is to increase the concentration in the solution with the aim to increase the collision probability with another radical anion before the charge recombination can proceed. It could be also conceivable to enlarge the separation between the PET sensitizer and the AB implementing spacers which would only favour the charge separation process, such as paracyclophanes or more *m*-phenyleneethynylene units. A more elegant approach would be to increase the density of AB units per sensitizer molecule. This can be accomplished in the solid state, either blending the molecules inside a conductive polymer matrix or, even more advantageously, merging the components as repeated constituents to form a functional side-chain polymer (**Scheme 4-3**).

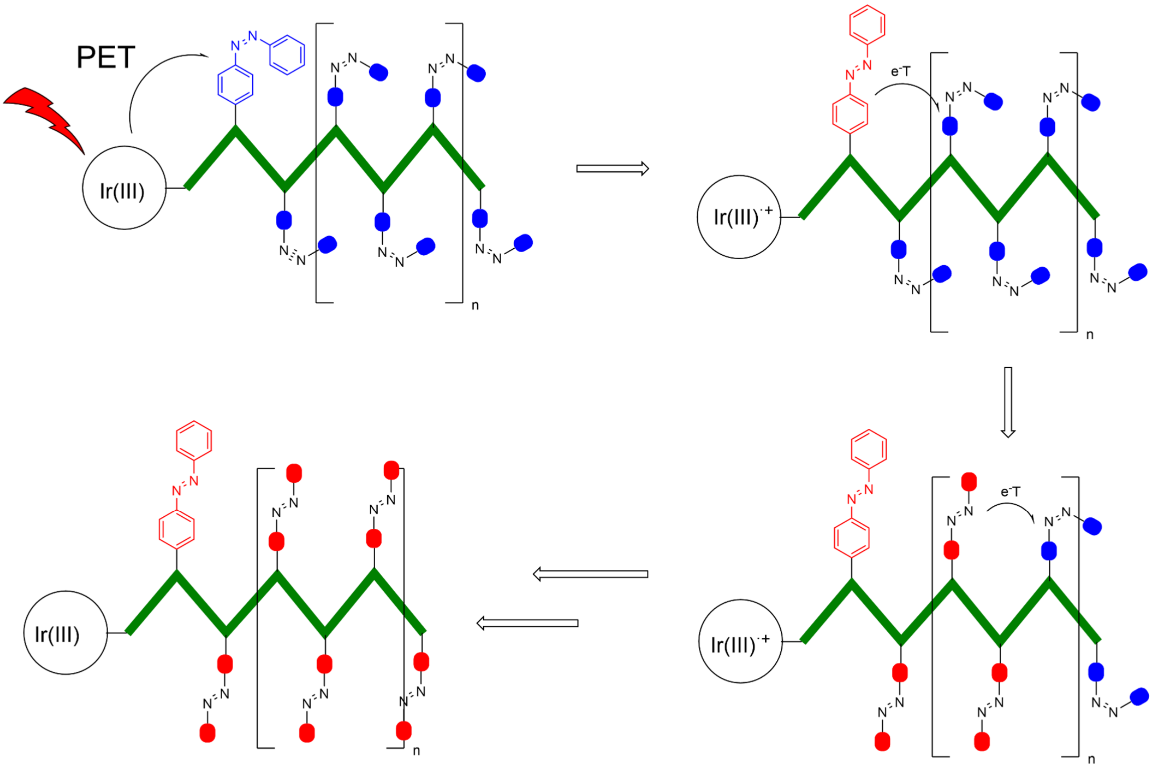

Scheme 4-3: Schematic representation of a polymeric backbone, decorated with AB sidechains. Upon irradiation of the Ir(III) complex, a PET process is initiated to the closest *cis*-AB. After isomerization to the *trans*-form, the ET propagates along the backbone isomerizing the rest of cis-ABs to the *trans*-form. The functional Ir(III) initiator was employed in the polymerization process to ensure the high AB : Ir(III) ratio in the polymer.

To undertake the synthesis of the previously described sidechain polymer, the polymerization step is of fundamental importance, because the initiator will be the PET sensitizer. Prototypical conditions which could lead to the successful synthesis of the envisioned polymer can be found in the atom transfer radical polymerization (ATRP) or the anionic ring opening polymerization (AROP). Herein, the Ir(III) complex would be decorated with an alcohol (for the AROP) or as an ester of the α-bromoisobutiric acid (ATRP). The most straightforward monomer source could be an AB derivative with a vinyl or methacrylate group (ATRP) or an epoxide (AROP). Application of the standard polymerization procedures would lead to the envisioned functional polymer. The applications of such a polymer are tremendous since it comprises the conversion of a catalytic amount of light into an amplified quantitative isomerization of a polymeric AB ensemble. The translation of nanoscopic alteration into macroscopic property modulation could be easily achieved through the conversion and amplification of light stimuli into mechanical work. The generated work could be harvested by confining the *cis*-AB polymer between two plates which upon light irradiation would be converted to the *trans*-form generating a visible macroscopic change caused by the distance modulation of the plates (**Scheme 4-4**).

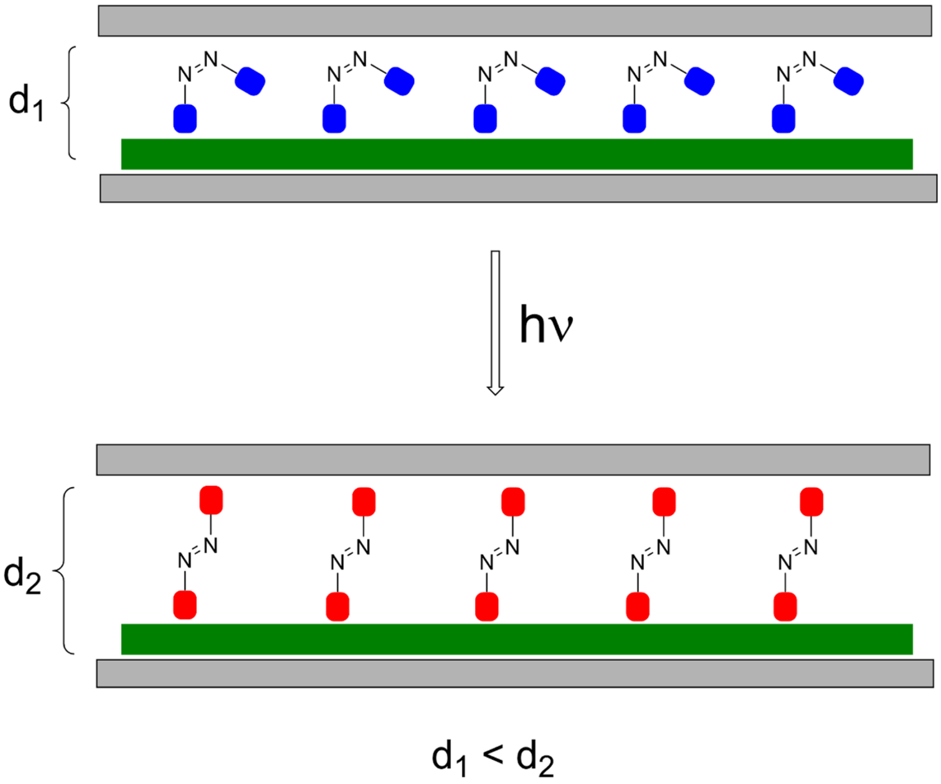

Scheme 4-4: Schematic representation of the *cis*-AB polymer, which is converted to the *trans*-form by a catalytic amount of light. The macroscopic change is the increase of distance between the plates.

Further applications could be imagined in the coating of surfaces, whose properties such as hydrophobicity, could be modulated with a meager amount of light irradiation due to the photoinduced fast electrochemical *cis*-*trans* isomerization of the polymer. Furthermore, an interesting feature of the projected system is the introduction of directionality in the process. Once the *trans*-form is electrochemically generated due to the thermodynamics of the process, the ET can only proceed in the direction where more *cis*-AB is encountered. This process has several analogies to the directional electron transport chain, which nature exploits in photosynthesis.

5 Experimental Section

5.1 Materials and Methods

5.1.1 Analytical Instrumentation

NMR spectra were recorded on a 500 MHz (125 MHz for ^{13}C, 470 MHz for ^{19}F) Bruker AVANCE II 500 spectrometer or on a 300 MHz (75 MHz for ^{13}C, 282 MHz for ^{19}F) Bruker AVANCE II 300 spectrometer at 25 °C using residual protonated solvent signals[226] as internal standards (^1H: $\delta(CDCl_3)$ = 7.26 ppm, $\delta(CD_2Cl_2)$ = 5.32 ppm; ^{13}C: $\delta(CDCl_3)$ = 77.16 ppm, $\delta(CD_2Cl_2)$ = 53.84 ppm) or $CFCl_3$ as external standard for ^{19}F-spectra ($\delta(CFCl_3)$ = 0 ppm). Multiplicities are abbreviated as follows: singlet (s), doublet (d), triplet (t), quadruplet (q), quintet (quint), multiplet (m), and broad (br). Ultrahigh-performance liquid chromatography/ mass spectrometry (UPLC/ MS) was performed on a Waters Acquity UPLC equipped with a Waters LCT Premier XE Mass detector for high-resolution MS (HR-MS, ESI^+-ionization) and with Waters Alliance systems (consisting of a Waters Separations Module 2695, a Waters Diode Array Detector 996 and a Waters Mass Detector ZQ 2000). Electrochemical measurements were carried out using a HEKA-Elektronik PG310 potentiostat or an Autolab PGSTAT128N and an Ava Spec-2048x14 spectrometer equipped with an Avalight-DH-SBAL lamp. TLC was performed on Merck Silica Gel 60 F254 TLC plates with a fluorescent indicator employing 254 nm UV-lamp for visualization. Preparative GPC was performed on a LC-9210NEXT preparative recycling GPC (Japan Analytical Industry).

5.1.2 Chemicals and Solvents

Solvents and commercial starting materials were used as supplied. All reactions requiring inert gas atmosphere were performed under Ar atmosphere. The solvents were dried before use, if necessary, employing an Innovative Technologies solvent purification system (multi-unit micro series). All experiments involving light-sensitive compounds were carried out in the dark under red light. Technologies solvent purification system (multi-unit micro series). Silica gel for chromatography (0.035–0.070 mm, 60 Å) was used for column chromatography. The petroleum ether (PE) used had a boiling range of 40-60 °C.

5.2 Synthesis and Characterization Data

Diarylethene-BODIPY Dyad (21o):

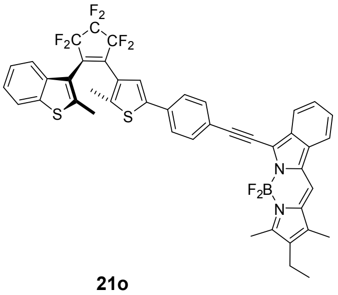

21o

To a solution of **35** (0.10 g, 0.15 mmol, 1 equiv.) in dry THF (30 mL), TBAF (0.18 mL, 0.18 mmol, 1.2 equiv.) was added. The resulting solution was stirred for 15 min at room temperature. TLC analysis showed completion of the reaction. The mixture was then diluted with Et_2O and washed with sat. NH_4Cl solution and H_2O. The organic layer was then dried over $MgSO_4$ and concentrated under reduced pressure. The residue was then dissolved in dry THF (30 mL) and cooled to -78 °C. Subsequently, *n*-BuLi (0.08 mL, 0.18 mmol, 1.2 equiv.) was added and the solution was left stirring at that temperature for 1 h. Then $SnCl(Bu)_3$ (0.05 mL, 0.18 mmol, 1.2 equiv.) was added and left stirring 2 h slowly reaching room temperature. Afterwards the mixture was then diluted with Et_2O and washed with brine and H_2O. The organic layer was then dried over $MgSO_4$ and concentrated under reduced pressure. The residue was then dissolved in dry toluene (5 mL) and the resulting solution was deoxygenated by letting bubble Ar for 15 min. To the deoxygenated solution, **bdp** (0.05 g, 0.15 mmol, 1.0 equiv.), $Pd_2(dba)_3$ (0.01 g, 0.012 mmol, 0.08 equiv.) and P^tBu_3 (0.03 mL, 0.024 mmol, 0.16 equiv.) were added. Finally the solution was heated for 4 h at 105 °C. TLC analysis showed completion of the reaction. It was then proceeded to dilute the solution with Et_2O, and washed once with brine (100 mL). The organic layer was dried over $MgSO_4$ and concentrated under reduced pressure. It was then purified by column chromatography over silica gel (PE : DCM, 1:1) yielding 0.05 g (20%) of **21o** as a dark blue solid. **^{1}H-NMR (300 MHz, CD_2Cl_2):** δ (ppm) = 7.87 (dt, $^3J_{H,H}$ = 8.2 Hz, $^4J_{H,H}$ = 0.9 Hz, 1 H, CH_{ar}), 7.82 (dt, $^3J_{H,H}$ = 8.2 Hz, $^4J_{H,H}$ = 0.9 Hz, 1 H, CH_{ar}), 7.79 – 7.75 (m, 1 H, CH_{ar}), 7.69 – 7.63 (m, 2 H, CH_{ar}), 7.56 (d, $^3J_{H,H}$ = 7.1 Hz, 1 H, CH_{ar}), 7.51 – 7.47 (m, 2 H, CH_{ar}), 7.47 – 7.43 (m, 1 H, CH_{ar}), 7.40 – 7.31 (m, 4 H, CH_{ar}), 7.30 (d, $^3J_{H,H}$ = 3.3 Hz, 1 H, CH_{ar}), 2.55 (s, 3 H, CH_3), 2.41 (q, $^3J_{H,H}$ = 7.6 Hz, 2 H, CH_2), 2.34 (s, 3 H, CH_3), 2.22 (s, 3 H, CH_3), 1.99 (s, 3 H, CH_3), 1.08 (t, $^3J_{H,H}$ = 7.6 Hz, 3 H, CH_3). **^{19}F-NMR (282 MHz, CD_2Cl_2):** δ (ppm) = -109.31

(s, 2 F, *CF₂*), -110.25 (q, *J* = 264.4 Hz, 2 F, *CF₂*), -132.48 (q, *J* = 264.4 Hz, 2 F, *CF₂*), -144.14 (dd, $^1J_{B,F}$ = 61.5 Hz, $^2J_{F,F}$ = 30.2 Hz, 2 F, *BF₂*). **^{13}C-NMR (75 MHz, CD_2Cl_2):** δ (ppm) = 157.72, 143.42, 141.29, 140.96, 140.85, 138.74, 138.50, 138.22, 134.53, 133.97, 133.46, 133.24, 132.97, 129.83, 129.45, 128.77, 126.11, 125.78, 125.36, 124.96, 124.28, 123.90, 122.54, 122.41, 121.70, 120.38, 119.44, 118.20, 116.23, 110.41, 104.77, 72.41, 17.60, 15.15, 15.08, 14.63, 13.07, 9.66. **HRMS (ESI$^+$):** *m/z* = 814.204 (calcd. 814.190 for $[C_{44}H_{31}BF_8N_2S_2]^+$).

Isoindolin-1-one (22):

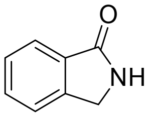

22

Phthalimide (58.852 g, 400 mmol) was added to a suspension of $AlCl_3$ (266.68 g, 2.0 mol, 5 equiv.) in cyclohexane (320 mL). The mixture was heated at 130 °C for 5 h (shaking the reaction vessel periodically to ensure mixture of components) until a red and a transparent phase were formed, then it was cooled to room temperature. The mixture was afterwards cautiously poured over ice and extracted with DCM. The organic phase was dried over $MgSO_4$, filtered and concentrated under reduced pressure. It was then dissolved in DCM and cyclohexane. Afterwards the DCM was evaporated and **22** was then allowed to slowly precipitate from cyclohexane obtaining 39.92 g of a yellow solid with 75% yield. **^{1}H-NMR (300 MHz, $CDCl_3$):** δ (ppm) = 7.92-7.46 (m, 4 H, *CH_{ar}*), 6.52 (b, 1 H, *NH*), 4.48 (s, 2 H, *CH₂*). **^{13}C-NMR (75 MHz, $CDCl_3$):** δ (ppm) = 172.7, 143.9, 132.3, 131.7, 128.0, 123.6, 123.3, 46.0. **HRMS (ESI$^+$):** *m/z* = 134.061 (calcd. 134.060 for $[C_8H_8NO]^+$).

3-Chloro-2H-isoindole-1-carbaldehyde (23):

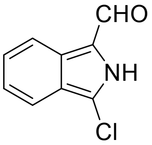

23

A mixture of dry dimethylformamide (2.31 mL, 30.04 mmol, 2 equiv.) and anhydrous DCM (20 mL) was cooled to 0 °C. Subsequently, a solution of $POCl_3$ (2.74 mL, 30.04 mmol, 2 equiv.) in anhydrous DCM (20 mL) was added dropwise at this temperature. A solution of **22** (2.0 g, 15.02 mmol, 1 equiv.) in anhydrous DCM (20 mL) was then added dropwise at 0 °C. The deep brown mixture was refluxed for 5 h and cooled. DCM (16 mL) was added and, at 0 °C, aqueous NaOH (5 M) was added until reaching pH 8. The organic layer was washed three times with water and dried ($MgSO_4$). The product was concentrated, and chromatographed on alumina with chloroform as eluent. The first major fraction (greenish) was collected and the solvent removed to give the chloroenamine intermediate **24** as a greenish solid. This intermediate was refluxed for 3 h in ethanol (210 mL) containing aqueous NaOH (4 M, 17 mL). The solution was neutralized with 2 M HCl at 0 °C, and extracted with $CHCl_3$. The organic layer was washed with $NaHCO_3$ and then with brine, dried over $MgSO_4$ and evaporated. Yield 1.0 g (37%) of a gray solid. **^{1}H-NMR (300 MHz, $CDCl_3$):** δ (ppm) = 9.42 (s, 1 H, *CHO*), 7.71-7.61 (m, 4 H, CH_{ar}). **HRMS (ESI$^+$):** *m/z* = 179.989 (calcd. 179.010 for $[C_9H_6ClNO]^+$).

7-Chloro-2-ethyl-5,5-difluoro-1,3-dimethyl-*5H*-4l^4,5l^4-pyrrolo[1',2':1,6][1,3,2]diazaborinino[4,3-*a*]isoindole (bdp):

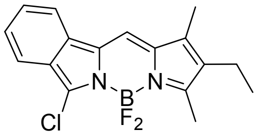

bdp

To a solution of **23** (0.79 g, 4.4 mmol) in 10 mL of dry $CHCl_3$ was added 3-ethyl-2,4-dimethylpyrrole (0.53 mL, 3.96 mmol, 0.9 eq.) in 1 mL of dry $CHCl_3$ and $POCl_3$ (0.40 mL, 4.4 mmol, 1 eq.) in 1 mL of dry $CHCl_3$, respectively, at 0 °C under Ar. The reaction mixture was stirred for 30 min, and Et_3N (6.1 mL, 44.0 mmol, 10 eq.) was added into the reaction mixture. The mixture was further stirred for 10 min, then $BF_3{\cdot}OEt_2$ (6.03 mL, 48.4 mmol, 11 eq.) was added through a syringe. The reaction mixture was left stirring for 10 h, poured into 50 mL of water, and extracted with 30 mL of $CHCl_3$. Organic layers were combined, washed with $NaHCO_3$, brine and dried over $MgSO_4$. The solvent was removed under vacuum. The crude product was purified by chromatography (silica gel, PE : DCM = 2:1), to give the desired compound **bdp** as a purple powder in 68% yield (1.0 g). **^{1}H-NMR (300 MHz, $CDCl_3$):** δ (ppm) = 7.78-7.68 (m, 2 H, CH_{ar}), 7.47 (t, $^3J_{H,H}$ = 7.36, 1 H, CH_{ar}), 7.31 (t, $^3J_{H,H}$ = 7.36, 1 H, CH_{ar}), 7.28 (s, 1 H, CH_{ar}), 2.53 (s, 3 H, CH_3), 2.39(q, $^3J_{H,H}$ = 7.42, 2 H, CH_2), 2.21 (s, 3 H, CH_3), 1.08 (t, $^3J_{H,H}$ = 7.42, 3 H, CH_3). **^{13}C-NMR (75 MHz, $CDCl_3$):** δ (ppm) = 140.44, 139.94, 134.44, 132.54, 130.22, 125.74, 121.72, 119.02, 116.51, 110.14, 29.85, 17.42, 14.71, 9.64. **^{19}F-NMR (282.38 MHz, $CDCl_3$):** δ (ppm) = -145.05 (dd, $^1J_{B,F}$ = 61.5 Hz, $^2J_{F,F}$ = 30.2 Hz, 2 F, BF_2). **HRMS (ESI$^+$):** *m/z* = 332.058 (calcd. 332.109 for $[C_{17}H_{16}BClF_2N_2]^+$).

2-Ethyl-5,5-difluoro-1,3-dimethyl-7-((trimethylsilyl)ethynyl)-*5H*-4l^4,5l^4-pyrrolo[1',2':1,6][1,3,2]diazaborinino[4,3-*a*]isoindole (25):

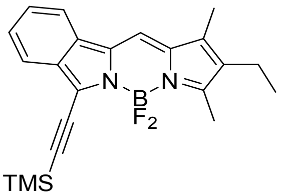

25

To a screw-sealed Schlenk flask were added **bdp** (61 mg, 0.2 mmol), $Pd(PPh_3)_2Cl_2$ (22 mg, 3 mmol%), and CuI (13 mg, 7 mmol%) in 15 mL of dry THF, Et_3N (10 mL) and TMSA (110 µL, 1.0 mmol, 5 equiv.) were added through a syringe into the mixture, respectively. The mixture was stirred at 75 °C for 17 h, cooled to room temperature, and filtrated through Celite, then the cake was washed with DCM (3x20 mL). Solvent was removed under vacuum. The crude product was purified by chromatography (silica gel, PE : DCM, 4:1) to give the desired compound **25** as dark blue solid in 9% yield (10 mg). **^{1}H-NMR (300 MHz, $CDCl_3$):** δ (ppm) = 8.07 (d, $^3J_{H,H}$ = 8.28 Hz, 1 H, *CH$_{ar}$*), 7.80 (d, $^3J_{H,H}$ = 8.28 Hz, 1 H, *CH$_{ar}$*), 7.45 (t, $^3J_{H,H}$ = 7.06 Hz, 1 H, *CH$_{ar}$*), 7.35-7.29 (m, 2 H, *CH$_{ar}$*), 2.53 (s, 3 H, *CH$_3$*), 2.41 (q, $^3J_{H,H}$ = 7.43 Hz, 2 H, *CH$_2$*), 2.22 (s, 3 H, *CH$_3$*), 1.09 (t, $^3J_{H,H}$ = 7.43 Hz, 3 H, *CH$_3$*), 0.27 (s, 9 H, *CH$_3$*). **^{19}F-NMR (282.38 MHz, $CDCl_3$):** δ (ppm) = -140.96- -141.31 (dd, $^1J_{B,F}$ = 61.5 Hz, $^2J_{F,F}$ = 33.5 Hz, 2 F, *BF$_2$*). **HRMS (ESI$^+$):** *m/z* = 394.062 (calcd. 394.180 for $[C_{22}H_{25}BF_2N_2Si]^+$).

2-Ethyl-5,5-difluoro-1,3-dimethyl-7-((triisopropylsilyl)ethynyl)-*5H*-4l^4,5l^4-pyrrolo[1',2':1,6][1,3,2]diazaborinino[4,3-*a*]isoindole (26):

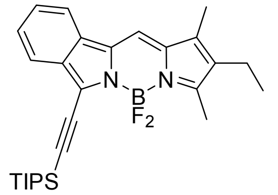

26

To a screw-sealed Schlenk flask were added **bdp** (100 mg, 0.3 mol), $Pd(PPh_3)_4$ (6 mg, 3 mol%), and CuI (4 mg, 7 mol%) in 15 mL of dry dioxane, *N*-ethylmorpholine (10 mL) and TIPSA (336 µL, 1.5 mmol, 5 equiv.) were added through a syringe into the mixture, respectively. The mixture was stirred at 75°C for 17 h, cooled to room temperature, and filtrated through Celite, then the cake was washed with DCM (3x20 mL). Solvent was removed under vacuum. The crude product was purified by chromatography (silica gel, PE : DCM, 4:1) to give the desired compound **26** as dark blue solid in 35% yield (50 mg). **^{1}H-NMR (300 MHz, $CDCl_3$):** δ (ppm) = 7.77-7.71 (m, 2 H, CH_{ar}), 7.39 (t, $^3J_{H,H}$ = 8.10 Hz, 1 H, CH_{ar}), 7.30 (t, $^3J_{H,H}$ = 8.10 Hz, 1 H, CH_{ar}), 7.24 (s, 1 H, CH_{ar}), 2.54 (s, 3 H, CH_3), 2.39 (q, $^3J_{H,H}$ = 7.60 Hz, 2 H, CH_2), 2.21 (s, 3 H, CH_3), 1.22 (m, 21 H), 1.08 (t, $^3J_{H,H}$ = 7.60 Hz, 3 H, CH_3). **^{19}F-NMR (282.38 MHz, $CDCl_3$):** δ (ppm) = -125,83 (dd, $^1J_{B,F}$ = 61.5 Hz, $^2J_{F,F}$ = 18.6 Hz, 2 F, BF_2). **HRMS (ESI$^+$):** *m/z* = 478.310 (calcd. 478.282 for $[C_{28}H_{37}BF_2N_2Si]^+$).

3-Bromo-2H-isoindole-1-carbaldehyde (27):

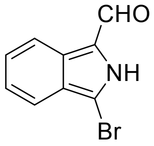

27

A mixture of anhydrous dimethylformamide (2.31 mL, 30.04 mmol, 2 equiv.) and anhydrous DCM (20 mL) was cooled to 0 °C. Subsequently, a solution of $POBr_3$ (8.61 g, 30.04 mmol, 2 equiv.) in anhydrous DCM (20 mL) was added dropwise at this temperature. A solution of **22** (2.0 g, 15.02 mmol, 1 equiv.) in anhydrous DCM (20 mL) was then added dropwise at 0 °C. The deep brown mixture was refluxed for 17 h and cooled. DCM (16 mL) was added and, at 0 °C, aqueous NaOH (5 M) was added until reaching pH 8. The organic layer was washed three times with water and dried ($MgSO_4$). The product was concentrated, and chromatographed on alumina with chloroform. The first major fraction (greenish) was collected and the solvent removed to give the chloroenamine intermediate **6** as a discoloured solid. This intermediate was refluxed for 3 h in ethanol (210 mL) containing aqueous sodium hydroxide (4 M, 17 mL). The solution was neutralized with 2 M HCl at 0 °C, and extracted with $CHCl_3$. The organic layer was washed with $NaHCO_3$ and then with brine, dried over $MgSO_4$ and evaporated. Yield 1.0 g (56%) of a brown solid. **^{1}H-NMR (300 MHz, CD_2Cl_2):** δ (ppm) = 9.74 (s, 1 H, CH_{ar}), 8.05-7.15 (m, 4 H, CH_{ar}). **HRMS (ESI$^+$):** *m/z* = 223.958 (calcd. 222.960 for $[C_9H_6BrNO]^+$).

7-Bromo-2-ethyl-5,5-difluoro-1,3-dimethyl-*5H*-4l^4,5l^4-pyrrolo[1',2':1,6][1,3,2]diazaborinino[4,3-*a*]isoindole (28):

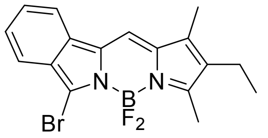

28

To a solution of **27** (0.45 g, 2.0 mmol) in 10 mL of dry $CHCl_3$ was added 3-ethyl-2,4-dimethylpyrrole (0.24 mL, 1.80 mmol, 0.9 equiv.) in 1 mL of dry $CHCl_3$ and $POBr_3$ (0.57 g, 2.0 mmol, 1 equiv.) in 1 mL of dry $CHCl_3$, respectively, at 0 °C under Ar. The reaction mixture was stirred for 30 min, and Et_3N (2.77 mL, 20.0 mmol, 10 equiv.) was added into the reaction mixture. The mixture was further stirred for 10 min, then $BF_3{\cdot}OEt_2$ (2.74 mL, 22.0 mmol, 11 equiv.) was added through a syringe. The reaction mixture was left stirring for 10 h, poured into 50 mL of water, and extracted with 30 mL of $CHCl_3$. Organic layers were combined, washed with $NaHCO_3$, brine and dried over $MgSO_4$. Solvent was removed under vacuum. The crude product was purified by chromatography (silica gel, PE : DCM, 2:1), to give the desired compound **28** as a purple powder in 20% yield (0.14 g). **^{1}H-NMR (300 MHz, $CDCl_3$):** δ (ppm) = 7.85-7.77 (m, 2 H, *CH$_{ar}$*), 7.53 (t, $^3J_{H,H}$ = 8.10 Hz, 1 H, *CH$_{ar}$*), 7.44 (s, 1 H, *CH$_{ar}$*), 7.35 (t, $^3J_{H,H}$ = 8.10 Hz, 1 H, *CH$_{ar}$*), 2.51 (s, 3 H, *CH$_3$*), 2.39(q, $^3J_{H,H}$ = 7.42 Hz, 2 H, *CH$_2$*), 2.22 (s, 3 H, *CH$_3$*), 1.19 (t, $^3J_{H,H}$ = 7.42 Hz, 3 H, *CH$_3$*). **^{13}C-NMR (75 MHz, $CDCl_3$):** δ (ppm) = 144.54, 139.94, 134.44, 132.54, 130.99, 126.66, 124.42, 119.82, 118.44, 117.24, 29.85, 17.46, 14.50, 9.67. **^{19}F-NMR (282.38 MHz, $CDCl_3$):** δ (ppm) = -141.58 (dd, $^1J_{B,F}$ = 61.5 Hz, $^2J_{F,F}$ = 31.1 Hz, 2 F, *BF$_2$*). **HRMS (ESI$^+$):** *m/z* = 376.058 (calcd. 377.034 for $[C_{17}H_{16}BBrF_2N_2]^+$).

2-Ethyl-5,5-difluoro-1,3-dimethyl-7-(phenylethynyl)-*5H*-4l^4,5l^4-pyrrolo[1',2':1,6][1,3,2]diazaborinino[4,3-*a*]isoindole (Ph-bdp):

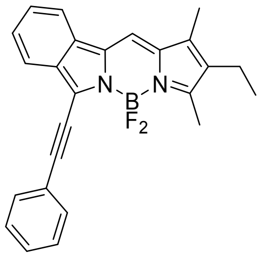

Ph-bdp

Compound **bdp** (25 mg, 0.075 mmol), tributyl(phenylethynyl)stannane (30 mg, 0.075 mmol, 1 equiv.) and $Pd(PPh_3)_4$ (13 mg, 0.011 mmol 15 mol%) were stirred under an Ar inert gas atmosphere in dry toluene (2 mL) at 105 °C for 17 h. The solvent was removed in vacuo. The residue was purified by flash chromatography (PE/DCM 2:1) obtaining 0.017 g of a blue solid, yield 57%. **^{1}H-NMR (300 MHz, CD_2Cl_2):** δ (ppm) = 7.89 (dt, $^3J_{H,H}$ = 8.1 Hz, $^4J_{H,H}$ = 0.9 Hz, 1 H, CH_{ar}), 7.83 (dt, $^3J_{H,H}$ = 8.1 Hz, $^4J_{H,H}$ = 0.9 Hz, 1 H, CH_{ar}), 7.74 – 7.67 (m, 2 H, CH_{ar}), 7.51 – 7.41 (m, 4 H, CH_{ar}), 7.39 – 7.31 (m, 2 H, CH_{ar}), 2.54 (s, 3 H, CH_3), 2.41 (q, $^3J_{H,H}$ = 7.6 Hz, 2 H, CH_2), 2.23 (s, 3 H, CH_3), 1.08 (t, $^3J_{H,H}$ = 7.42 Hz, 3 H, CH_3). **^{19}F-NMR (282.38 MHz, CD_2Cl_2):** δ (ppm) = -144.25 (dd, $^1J_{B,F}$ = 61.5 Hz, $^2J_{F,F}$ = 30.9 Hz, 2 F, BF_2). **HRMS (ESI$^+$):** *m/z* = 398.157 (calcd. 398.177 for $[C_{25}H_{21}BF_2N_2]^+$).

3,5-Dibromo-2-methylthiophene (29):

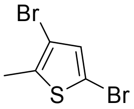

29

N-bromosuccinimide (35.58 g, 0.2 mol) was dissolved in AcOH:$CHCl_3$ (1:1, 500 ml). A solution of 2-methylthiophene (9.82 g, 0.1 mol) in AcOH (100 mL) was added dropwise to the suspension at room temperature, and the mixture was stirred for an additional 17 h. The resulting mixture was poured into a mixture of PE (500 mL) and water (500 mL) and the layers were separated. The organic layer was washed with 1 M NaOH (500 mL) and brine (500 mL) successively, and dried over anhydrous $MgSO_4$. Filtration and evaporation gave after purification by silica plug in PE 26.06 g of **29** (98% yield) as a pale yellow liquid. **^{1}H-NMR (300 MHz, $CDCl_3$):** δ (ppm) = 6.85 (s, 1 H, CH_{ar}), 2.33 (s, 3 H, CH_3). **^{13}C-NMR (75 MHz, $CDCl_3$):** δ (ppm) = 136.0, 131.9, 108.7, 108.5, 14.8.

((4-Bromophenyl)ethynyl)triisopropylsilane (30):

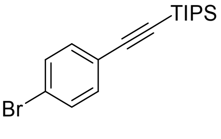

30

To a solution of 1-bromo-4-iodobenzene (14.99 g, 53.0 mmol) in degassed Et_3N (100 mL) was added CuI (0.25 g, 1.33 mmol, 0.025 eq.), $PdCl_2(PPh_3)_2$ (1.86 g, 2.65 mmol, 0.05 eq.) and TIPSA (13.08 mL, 58.3 mmol, 1.1 eq.). Subsequently the mixture was heated at 40 °C for 17 h. The reaction was monitored by TLC, and upon completion the brown mixture was then dissolved in PE and passed through a celite plug. The solvent was then evaporated. Final residue was purified through a silica gel column using PE as eluent. Removal of solvent from the main fraction yielded a colourless oil. Yield 18.76 g, 99%.**^{1}H-NMR (300 MHz, $CDCl_3$):** δ (ppm) = 7.48 – 7.41 (m, 2 H, *CH$_{ar}$*), 7.36 – 7.30 (m, 2 H, *CH$_{ar}$*), 1.12(s, 21 H). **HRMS (ESI$^+$):** *m/z* = 337.946 (calcd. 338.089 for $[C_{17}H_{25}BrSi]^+$).

((4-(4-Bromo-5-methylthiophen-2-yl)phenyl)ethynyl)triisopropylsilane (31):

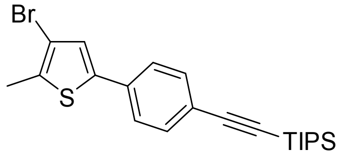

31

To a solution of **30** (3.95 g, 11.7 mmol, 1.0 equiv.) in 100 mL anhydrous THF under Ar at -78 °C was added *n*-BuLi (5.85 mL, 12.87 mmol, 1.1 equiv.) and left stirring at that temperature for 1 h. Then $B(OBu)_3$ (3.47 mL, 12.87 mmol, 1.1 equiv.) was added and left stirring overnight slowly reaching room temperature. Afterwards a 2 M Na_2CO_3 (19.31 mL, 38.61 mmol, 3.3 equiv.) solution was added and the resulting solution was deoxygenated by letting bubble Ar for 15 min. To the deoxygenated solution, **29** (3.0 g, 11.7 mmol, 1.0 equiv.) and the $Pd(PPh_3)_4$ (1.08 g, 0.94 mmol, 0.08 equiv.) catalyst were added. Finally the solution was refluxed for 17 h at 80 °C. TLC analysis showed completion of the reaction. It was then proceeded to dilute the solution with Et_2O, and wash once with brine (100 mL). The organic layer was dried over $MgSO_4$ and concentrated under reduced pressure. It was then purified by column chromatography over silica gel (PE) yielding 3.64 g (63%) of a white solid. **^{1}H-NMR (300 MHz, CD_2Cl_2):** δ (ppm) = 7.45 (s, 4 H, *CH$_{ar}$*), 7.15 (s, 1 H, *CH$_{ar}$*), 2.41 (s, 3 H, *CH$_3$*), 1.12 (s, 21 H). **^{13}C-NMR (75 MHz, CD_2Cl_2):** δ (ppm) = 139.37, 138.93, 133.34, 131.69, 124.67, 122.49, 121.31, 115.10, 108.53, 91.55, 18.79, 15.06, 11.69. **HRMS (ESI$^+$):** *m/z* = 331.059 (calcd. 434.090 for $[C_{22}H_{29}BrSSi]^+$).

2-Methylbenzo[b]thiophene (32):

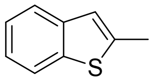

32

To a solution of benzo[b]thiophene (3.47 mL, 29.0 mmol) in dry THF, was added dropwise *n*-BuLi (14.5 mL, 31.9 mmol, 1.1 equiv.) at -78°C under Ar atm. The mixture was stirred at -78 °C for 1h and then CH_3I (1.81 mL, 29.0 mmol, 1.0 equiv.) was added. Afterwards it was allowed to reach room temperature and it was stirred for 1 h. The mixture was poured into water and extracted with Et_2O. The organic layer was then dried over $MgSO_4$ and it was concentrated under reduced Pressure. Further purifications were not necessary, obtaining 3.95 g of compound **32** as white crystals with 92% yield. **^{1}H-NMR (300 MHz, $CDCl_3$):** δ (ppm) = 7.75 (m, $^3J_{H,H}$ = 7.78 Hz, 1 H, *CH_{ar}*), 7.66 (m, $^3J_{H,H}$ = 7.32 Hz, 1 H, *CH_{ar}*), 7.31 (ddd, $^3J_{H,H}$ = 7.78 Hz, $^3J_{H,H}$ = 7.09 Hz, $^4J_{H,H}$ = 1.15 Hz, 1 H, *CH_{ar}*), 7.26 (s, 1 H, *CH_{ar}*), 7.25 (ddd, $^3J_{H,H}$ = 7.32 Hz, $^3J_{H,H}$ = 7.09 Hz, $^4J_{H,H}$ = 1.40 Hz, 1 H, *CH_{ar}*), 2,60 (d, $^4J_{H,H}$ = 1.12 Hz, 3 H, *CH_3*).

3-Bromo-2-methylbenzo[b]thiophene (33):

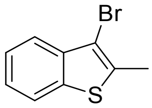

33

To a 0 °C cooled solution of **32** (3.91 g, 26.4 mmol) in AcOH:$CHCl_3$ (1:1, 75 mL), was added N-bromosuccinimide (4.84 g, 27.19 mmol, 1.03 eq.). It was allowed to stir for 17 h. To the mixture was added a sat. solution of $Na_2S_2O_3$. Then it was extracted in DCM and washed with $NaHCO_3$ and H_2O. The organic layer was then dried over $MgSO_4$ and concentrated under reduced Pressure. It was then purified by column chromatography in PE obtaining 5.69 g of **33** as yellow crystals, yield 95%. **^{1}H-NMR (300 MHz, $CDCl_3$):** δ (ppm) = 7.73 (m, $^3J_{H,H}$ = 7.50 Hz, 1 H, *CH_{ar}*), 7,72 (m, $^3J_{H,H}$ = 7.44 Hz, 1 H, *CH_{ar}*), 7.42 (ddd, $^3J_{H,H}$ = 7.50 Hz, $^3J_{H,H}$ = 7.29 Hz, $^4J_{H,H}$ = 1.03 Hz, 1 H, *CH_{ar}*), 7.33 (ddd, $^3J_{H,H}$ = 7.44 Hz, $^3J_{H,H}$ = 7.29 Hz, $^4J_{H,H}$ = 1.19 Hz, 1 H, *CH_{ar}*), 2.57 (s, 3 H, *CH_3*).

3-(2-Fluoro-3,3,4,4,5,5-hexafluorocyclopent-1-en-1-yl)-2-methylbenzo[b]thiophene (34):

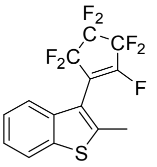

34

To a solution of **33** (1.76 g, 7.75 mmol) in dry Et_2O at -78 °C was added *n*-BuLi (3.70 mL, 8.14 mmol, 1.05 equiv.) and left stirring for 1 h. Then C_5F_8 (1.04 mL, 7.75 mmol, 1.0 equiv.) was added and the mixture was allowed to slowly reach room temperature for 17 h. The mixture was then diluted with Et_2O and washed with brine and H_2O. The organic layer was dried over $MgSO_4$ and evaporated. Final residue was purified through a silica gel column using PE as eluent. Removal of solvent from the main fraction yielded off-white crystals. Yield 2.4 g, 92%. **^{1}H-NMR (300 MHz, $CDCl_3$):** δ (ppm) = 7.87 – 7.74 (m, 1 H, *CH$_{ar}$*), 7.55 – 7.45 (m, 1 H, *CH$_{ar}$*), 7.45 – 7.32 (m, 2 H, *CH$_{ar}$*), 2.53 (s, 3 H, *CH$_3$*). **^{19}F-NMR (282 MHz, $CDCl_3$):** δ (ppm) = -107.05 (m, 2 F, *CF$_2$*), -118.22 (m, 2 F, *CF$_2$*), -124.53 (s, 1 F, *CF*), -129.69 (m, 2 F, *CF$_2$*). **^{13}C-NMR (75 MHz, $CDCl_3$):** δ (ppm) = 144.27, 138.40, 138.34, 125.31, 124.92, 122.33, 121.76, 121.73, 114.49, 14.82. **HRMS (ESI$^+$):** *m/z* = 340.016 (calcd. 340.014 for $[C_{14}H_7F_7S]^+$).

((4-(4-(3,3,4,4,5,5-Hexafluoro-2-(2-methylbenzo[b]thiophen-3-yl)cyclopent-1-en-1-yl)-5-methylthiophen-2-yl)phenyl)ethynyl)triisopropylsilane (35o):

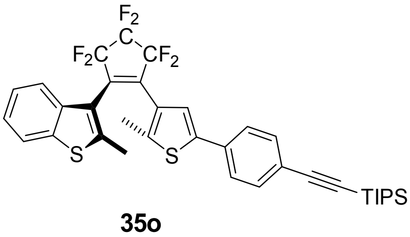

35o

To a solution of **31** (2.17 g, 5.0 mmol, 1.0 equiv.) in 100 ml anhydrous THF under Ar at -78 °C was added *n*-BuLi (2.39 mL, 5.25 mmol, 1.05 equiv.) and left stirring at that temperature for 1 h. Then **34** (1.96 g, 5.75 mmol, 1.15 equiv.) was added and left stirring for 2 h slowly reaching room temperature. TLC analysis showed completion of the reaction. The mixture was then diluted with Et_2O and washed with brine and H_2O. The organic layer was dried over $MgsO_4$ and evaporated. Final residue was purified through a silica gel column

(Pe : DCM, 8:1). Removal of solvent from the main fraction yielded **35o** as an oil. 2.60 g (76%). **^{1}H-NMR (300 MHz, CD_2Cl_2):** δ (ppm) = 7.79 – 7.73 (m, 1 H, *CH_{ar}*), 7.54 (d, *J*=7.0, 1 H, *CH_{ar}*), 7.45 – 7.39 (m, 2 H, *CH_{ar}*), 7.39– 7.34 (m, 2 H, *CH_{ar}*), 7.34 – 7.29 (m, 1 H, *CH_{ar}*), 7.20 (s, 1 H, *CH_{ar}*), 2.32 (s, 3 H, *CH_3*), 1.95 (s, 3 H, *CH_3*), 1.11 (s, 21 H). **^{19}F-NMR (282 MHz, CD_2Cl_2):** δ (ppm) = -109.34 (m, 2 F, *CF_2*), -110.31 (q, *J* = 280.21 Hz, 2 F, *CF_2*), -132.56 (q, *J* = 262.71 Hz, 2 F, *CF_2*). **^{13}C-NMR (75 MHz, CD_2Cl_2):** δ (ppm) = 143.41, 143.01, 141.61, 138.84, 138.64, 133.50, 132.94, 125.73, 125.59, 125.44, 125.04, 123.50, 123.34, 122.60, 122.46, 120.55, 107.09, 92.54, 18.93, 15.19, 15.08, 11.83. **HRMS (ESI$^+$):** *m/z* = 674.190 (calcd. 674.856 for $[C_{36}H_{36}F_6S_2Si]^+$).

((4-(4-(3,3,4,4,5,5-Hexafluoro-2-(2-methylbenzo[b]thiophen-3-yl)cyclopent-1-en-1-yl)-5-methylthiophen-2-yl)phenyl)ethynyl)triisopropylsilane (35c):

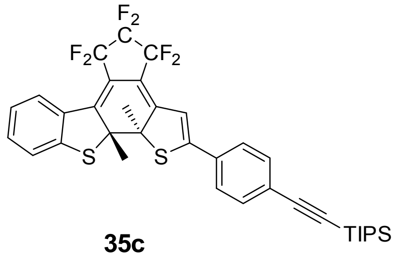

35c

35o was dissolved in an NMR tube in CD_2Cl_2 and irradiated with a 313 nm UV-lamp for 20 min. **^{1}H-NMR (300 MHz, CD_2Cl_2):** δ (ppm) = 7.80 – 7.77 (m, 1 H, *CH_{ar}*), 7.58 – 7.48 (m, 4 H, *CH_{ar}*), 7.30 – 7.22 (m, 2 H, *CH_{ar}*), 7.16 – 7.11 (m, 1 H, *CH_{ar}*), 6.77 (m, 1 H, *CH_{ar}*), 2.06 (s, 6 H, *CH_3*), 1.17 – 1.03 (m, 21 H). **^{19}F-NMR (282 MHz, CD_2Cl_2):** δ (ppm) = -103.71 (d, *J* = 256.7 Hz, 1 F, *CF_2*), -103.85 (d, *J* = 256.7 Hz, 1 F, *CF_2*), -120.33 (d, *J* = 264.2 Hz, 1 F, *CF_2*), -122.64 (d, *J* = 261.1 Hz, 1 F, *CF_2*), -128.14 (d, *J* = 252.7 Hz, 1 F, *CF_2*), -138.16 (d, *J* = 252.0 Hz, 1 F, *CF_2*).

Diarylethene-BODIPY Dyad (36o):

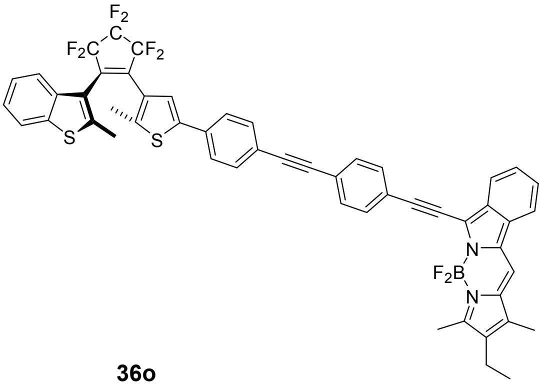

36o

To a solution of **44** (0.15 g, 0.15 mmol, 1 equiv.) in dry THF (30 mL), TBAF (0.18 mL, 0.18 mmol, 1.2 equiv.) was added. The resulting solution was stirred for 15 min at room temperature. TLC analysis showed completion of the reaction. The mixture was then diluted with Et_2O and washed with sat. NH_4Cl solution and H_2O. The organic layer was then dried over $MgSO_4$ and concentrated under reduced pressure. The residue was then dissolved in dry THF (30 mL) and cooled to -78 °C. Subsequently, *n*-BuLi (0.08 mL, 0.18 mmol, 1.2 equiv.) was added and the solution was left stirring at that temperature for 1 h. Then $SnCl(Bu)_3$ (0.05 mL, 0.18 mmol, 1.2 equiv.) was added and left stirring 2 h slowly reaching room temperature. Afterwards the mixture was then diluted with Et_2O and washed with brine and H_2O. The OL was then dried over $MgSO_4$ and concentrated under reduced pressure. The residue was then dissolved in dry toluene (5 mL) and the resulting solution was deoxygenated by letting bubble Ar for 15 min. To the deoxygenated solution, **bdp** (0.05 g, 0.15 mmol, 1.0 equiv.), $Pd_2(dba)_3$ (0.01 g, 0.012 mmol, 0.08 equiv.) and P^tBu_3 (0.03 mL, 0.024 mmol, 0.16 equiv.) were added. Finally the solution was heated for 4 h at 105 °C. TLC analysis showed completion of the reaction. It was then proceeded to dilute the solution with Et_2O, and washed once with brine (100 mL). The organic layer was dried over $MgSO_4$ and concentrated under reduced pressure. It was then purified by column chromatography over silica gel (Pe : DCM, 4:1). Removal of solvent from the main fraction yielded **36o** as a dark blue solid. 0.03 g (22%). **^{1}H-NMR (300 MHz, CD_2Cl_2):** δ (ppm) = 7.88 (d, $^3J_{H,H}$ = 8.1 Hz, 1 H, CH_{ar}), 7.83 (d, $^3J_{H,H}$ = 8.2 Hz, 1 H, CH_{ar}), 7.79 – 7.74 (m, 1 H, CH_{ar}), 7.72 – 7.66 (m, 2 H, CH_{ar}), 7.62 – 7.29 (m, 12 H, CH_{ar}), 7.26 (s, 1 H, CH_{ar}), 2.56 (s, 3 H, CH_3), 2.41 (q, $^3J_{H,H}$ = 7.6 Hz, 2 H, CH_2), 2.33 (s, 3 H, CH_3), 2.23 (s, 3 H, CH_3), 1.96 (s, 3 H, CH_3), 1.09 (t, $^3J_{H,H}$ = 7.6 Hz, 3 H, CH_{ar}). **^{19}F-NMR (282 MHz, CD_2Cl_2):** δ (ppm) = -109.30 (s, 2 F, CF_2), -110.27 (q, *J* = 263.4 Hz, 2 F, CF_2), -132.29 (q, *J* = 245.6 Hz, 2 F, CF_2), -144.16 (dd, $^1J_{B,F}$ = 61.2 Hz,

$^2J_{F,F}$ = 29.8 Hz, 2 F, BF_2). **^{13}C-NMR (75 MHz, CD_2Cl_2):** δ (ppm) = 157.75, 143.40, 143.11, 141.42, 138.72, 138.50, 138.46, 134.71, 133.92, 133.68, 133.41, 132.58, 132.38, 132.08, 129.43, 128.78, 126.15, 125.73, 125.67, 125.34, 124.94, 124.59, 123.53, 122.52, 122.49, 120.49, 119.45, 116.31, 110.41, 110.38, 104.48, 92.16, 90.64, 84.04, 17.61, 15.14, 15.04, 14.62, 13.11, 9.68. **HRMS (ESI$^+$):** *m/z* = 914.232 (calcd. 914.222 for $[C_{52}H_{35}BF_8N_2S_2]^+$).

Diarylethene-BODIPY Dyad (37o):

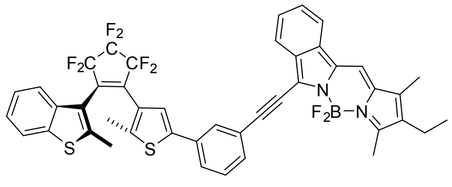

37o

To a solution of **42** (0.24 g, 0.36 mmol, 1.2 equiv.) in dry THF (30 mL), TBAF (0.42 mL, 0.42 mmol, 1.4 equiv.) was added. The resulting solution was stirred for 15 min at room temperature. TLC analysis showed completion of the reaction. The mixture was then diluted with Et_2O and washed with sat. NH_4Cl solution and H_2O. The organic layer was then dried over $MgSO_4$ and concentrated under reduced pressure. The residue was then dissolved in dry THF (30 mL) and cooled to -78 °C. Subsequently, *n*-BuLi (0.17 mL, 0.36 mmol, 1.2 equiv.) was added and the solution was left stirring at that temperature for 1 h. Then $SnCl(Bu)_3$ (0.10 mL, 0.36 mmol, 1.2 equiv.) was added and left stirring 2 h slowly reaching room temperature. Afterwards the mixture was then diluted with Et_2O and washed with brine and H_2O. The organic layer was then dried over $MgSO_4$ and concentrated under reduced pressure. The residue was then dissolved in dry toluene (5 mL) and the resulting solution was deoxygenated by letting bubble Ar for 15 min. To the deoxygenated solution, **bdp** (0.10 g, 0.3 mmol, 1.0 equiv.), $Pd_2(dba)_3$ (0.02 g, 0.024 mmol, 0.08 equiv.) and P^tBu_3 (0.05 mL, 0.048 mmol, 0.16 equiv.) were added. Finally the solution was heated for 4 h at 105 °C. TLC analysis showed completion of the reaction. It was then proceeded to dilute the solution with Et_2O, and washed once with brine (100 mL). The organic layer was dried over $MgSO_4$ and concentrated under reduced pressure. It was then purified by column chromatography over silica gel (Pe : DCM, 4:1). Removal of solvent from the main fraction yielded **37o** as a dark blue solid. 0.05 g (20%).**^{1}H-NMR (300 MHz, CD_2Cl_2):** δ (ppm) = 7.89 (dt, $^3J_{H,H}$ = 8.2 Hz, $^4J_{H,H}$ = 0.9 Hz, 1 H, CH_{ar}), 7.83 (dt, $^3J_{H,H}$ = 8.2 Hz, $^4J_{H,H}$ = 0.9 Hz, 1 H, CH_{ar}), 7.79 – 7.75 (m, 2 H, CH_{ar}), 7.64 – 7.55 (m, 2 H, CH_{ar}), 7.51 – 7.28 (m, 8 H, CH_{ar}), 2.56 (s, 3 H, CH_3), 2.40 (q, $^3J_{H,H}$ = 6.9 Hz, 2 H, CH_2), 2.35 (s, 3 H, CH_3), 2.22 (s, 3 H, CH_3), 1.98 (s, 3

H, *CH3*), 1.08 (t, $^3J_{H,H}$ = 6.9 Hz, 3 H, *CH$_{ar}$*). **^{19}F-NMR (282 MHz, CD_2Cl_2):** δ (ppm) = -109.29 (s, 2 F, *CF$_2$*), -110.24 (q, *J* = 338.2 Hz, 2 F, *CF$_2$*), -132.48 (q, *J* = 245.6 Hz, 2 F, *CF$_2$*), -144.14 (dd, $^1J_{B,F}$ = 61.7 Hz, $^2J_{F,F}$ = 30.6 Hz, 2 F, *BF$_2$*). **^{13}C-NMR (75 MHz, CD_2Cl_2):** δ (ppm) = 157.70, 143.43, 143.03, 141.00, 138.74, 138.48, 134.66, 134.13, 133.91, 133.42, 131.72, 129.67, 129.42, 128.95, 128.65, 127.03, 126.10, 125.58, 125.35, 124.95, 123.69, 123.32, 122.53, 122.38, 120.41, 119.46, 116.42, 110.41, 110.38, 104.02, 82.54, 17.60, 15.18, 15.02, 14.62, 13.09, 9.67. **HRMS (ESI$^+$):** *m/z* = 814.196 (calcd. 814.190 for $[C_{44}H_{31}BF_8N_2S_2]^+$).

Diarylethene-BODIPY Dyad (38o):

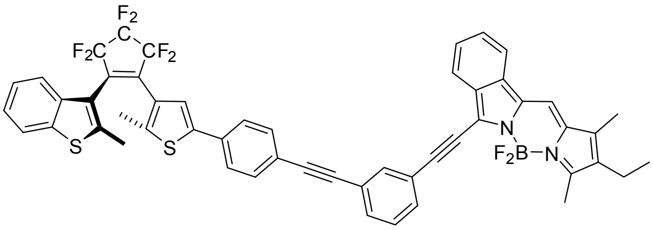

38o

To a solution of **45** (018 g, 0.23 mmol, 1.15 equiv.) in dry THF (30 mL), TBAF (0.24 mL, 0.24 mmol, 1.2 equiv.) was added. The resulting solution was stirred for 15 min at room temperature. TLC analysis showed completion of the reaction. The mixture was then diluted with Et_2O and washed with sat. NH_4Cl solution and H_2O. The organic layer was then dried over $MgSO_4$ and concentrated under reduced pressure. The residue was then dissolved in dry THF (30 mL) and cooled to -78 °C. Subsequently, *n*-BuLi (0.11 mL, 0.24 mmol, 1.2 equiv.) was added and the solution was left stirring at that temperature for 1 h. Then $SnCl(Bu)_3$ (0.07 mL, 0.24 mmol, 1.2 equiv.) was added and left stirring 2 h slowly reaching room temperature. Afterwards the mixture was then diluted with Et_2O and washed with brine and H_2O. The organic layer was then dried over $MgSO_4$ and concentrated under reduced pressure. The residue was then dissolved in dry toluene (5 mL) and the resulting solution was deoxygenated by letting bubble Ar for 15 min. To the deoxygenated solution, **bdp** (0.07 g, 0.20 mmol, 1.0 equiv.), $Pd_2(dba)_3$ (0.015 g, 0.016 mmol, 0.08 equiv.) and P^tBu_3 (0.03 mL, 0.032 mmol, 0.16 equiv.) were added. Finally the solution was heated for 4 h at 105 °C. TLC analysis showed completion of the reaction. It was then proceeded to dilute the solution with Et_2O, and washed once with brine (100 mL). The organic layer was dried over $MgSO_4$ and concentrated under reduced pressure. It was then purified by column chromatography over silica gel (Pe : DCM, 4:1). Removal of solvent from the main fraction yielded **38o** as a dark blue solid. 0.04 g (22%). **^{1}H-NMR (300 MHz, CD_2Cl_2):** δ (ppm) = 7.93

-7.88 (m, 1 H, CH_{ar}), 7.87 – 7.82 (m, 2 H, CH_{ar}), 7.80 – 7.75 (m, 1 H, CH_{ar}), 7.71 – 7.65 (m, 1 H, CH_{ar}), 7.61 – 7.28 (m, 12 H, CH_{ar}), 7.26 (s, 1 H, CH_{ar}), 2.57 (s, 3 H, CH_3), 2.43 (q, $^3J_{H,H}$ = 7.6 Hz, 2 H, CH_2), 2.34 (s, 3 H, CH_3), 2.25 (s, 3 H, CH_3), 1.96 (s, 3 H, CH_3), 1.09 (t, $^3J_{H,H}$ = 7.6 Hz, 3 H, CH_3). **^{19}F-NMR (282 MHz, CD_2Cl_2):** δ (ppm) = -109.35 (s, 2 F, CF_2), -110.32 (q, J = 270.6 Hz, 2 F, CF_2), -132.39 (q, J = 241.1 Hz, 2 F, CF_2), -144.21 (dd, $^1J_{B,F}$ = 61.2 Hz, $^2J_{F,F}$ = 29.8 Hz, 2 F, BF_2). **HRMS (ESI$^+$):** *m/z* = 914.232 (calcd. 914.222 for $[C_{52}H_{35}BF_8N_2S_2]^+$).

((3-Bromophenyl)ethynyl)triisopropylsilane (39):

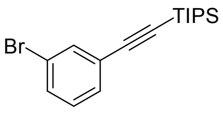

39

To a solution of 1-bromo-3-iodobenzene (4.53 g, 35.5 mmol) in degassed Et_3N (50 mL) was added CuI (0.17 g, 0.88 mmol, 0.025 equiv.), $PdCl_2(PPh_3)_2$ (1.25 g, 1.78 mmol, 0.05 equiv.) and TIPSA (8.76 mL, 39.05 mmol, 1.1 equiv.). Subsequently the mixture was heated at 40 °C for 17 h. The reaction was monitored by TLC, and upon completion the brown mixture was then dissolved in PE and passed through a celite plug. The solvent was then evaporated. Final residue was purified through a silica gel column using PE as eluent. Removal of solvent from the main fraction yielded a colorless oil. Yield 11.84 g, 99%. **^{1}H-NMR (300 MHz, CD_2Cl_2):** δ (ppm) = 7.61 (dd, $^3J_{H,H}$ = 2.6 Hz, $^4J_{H,H}$ = 0.9 Hz, 1 H, CH_{ar}), 7.50 – 7.35 (m, 2 H, CH_{ar}), 7.19 (t, $^3J_{H,H}$ = 7.9 Hz, 1 H, CH_{ar}), 1.12(s, 21 H). **^{13}C NMR (75 MHz, CD_2Cl_2)** δ = 134.97, 131.87, 130.90, 130.17, 125.84, 122.28, 105.57, 92.82, 18.76, 11.64. **HRMS (ESI$^+$):** *m/z* = 337.947 (calcd. 338.089 for $[C_{17}H_{25}BrSi]^+$).

((3-Iodophenyl)ethynyl)triisopropylsilane (40):

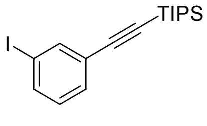

40

To a solution of **39** (2.43 g, 35.5 mmol) in 100 mL anhydrous THF under Ar at -78 ºC was added *n*-BuLi (8.64 mmol, 1.2 equiv.) and left stirring at that temperature for 1 h. Then I_2 (2.19 g, 8.64 mmol, 1.2 equiv.) was added and left stirring for 17 h slowly reaching room temperature. TLC analysis showed completion of the reaction. The mixture was then diluted with Et_2O and washed with a sat. solution of $Na_2S_2O_3$, brine and H_2O. The organic layer was dried over $MgSO_4$ and evaporated. Final residue was purified through a silica gel column using PE as eluent. Removal of solvent from the main fraction yielded a colorless oil. Yield 1.9 g, 69%. **^{1}H-NMR (300 MHz, CD_2Cl_2):** δ (ppm) = 7.82 (t, $^3J_{H,H}$ = 1.6 Hz, 1 H, CH_{ar}), 7.66 (ddd, $^3J_{H,H}$ = 8.0 Hz, $^4J_{H,H}$ = 1.7 Hz, $^4J_{H,H}$ = 1.1 Hz, 1 H, CH_{ar}), 7.44 (ddd, $^3J_{H,H}$ = 8.0 Hz, $^4J_{H,H}$ = 1.7 Hz, $^4J_{H,H}$ = 1.1 Hz, 1 H, CH_{ar}), 7.05 (t, $^3J_{H,H}$ = 7.9 Hz, 1 H, CH_{ar}), 1.11 (s, 21 H). **^{13}C-NMR (75 MHz, CD_2Cl_2)** δ = 140.84, 137.79, 131.45, 130.19, 125.88, 105.45, 18.77, 11.64. **HRMS (ESI$^+$):** *m/z* = 384.045 (calcd. 384.077 for $[C_{17}H_{25}ISi]^+$).

((3-(4-Bromo-5-methylthiophen-2-yl)phenyl)ethynyl)triisopropylsilane (41):

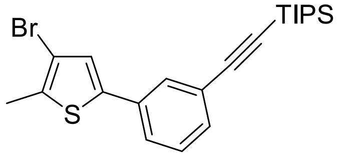

41

To a solution of **29** (3.0 g, 11.7 mmol, 1.0 equiv.) in 100 mL anhydrous THF under Ar at -78 °C was added *n*-BuLi (5.85 mL, 12.87 mmol, 1.1 equiv.) and left stirring at that temperature for 1 h. Then $B(OBu)_3$ (3.47 mL, 12.87 mmol, 1.1 equiv.) was added and left stirring overnight slowly reaching room temperature. Afterwards a 2 M Na_2CO_3 (19.31 mL, 38.61 mmol, 3.3 equiv.) solution was added and the resulting solution was deoxygenated by letting bubble Ar for 15 min. To the deoxygenated solution, **40** (4.49 g, 11.7 mmol, 1.0 equiv.) and the $Pd(PPh_3)_4$ (1.08 g, 0.94 mmol, 0.08 equiv.) catalyst were added. Finally the solution was refluxed for 17 h at 80 °C. TLC analysis showed completion of the reaction. It was then proceeded to dilute the solution with Et_2O, and wash once with brine (100 mL). The organic layer was dried over $MgSO_4$ and concentrated under reduced pressure. It was then purified by column chromatography over silica gel (PE) yielding 4.20g (83%) of **41** as a colorless oil. **^{1}H-NMR (300 MHz, CD_2Cl_2):** δ (ppm) = 7.62 (t, $^4J_{H,H}$ = 1.74 Hz, 1 H, CH_{ar}), 7.51 – 7.45 (m, 1 H, CH_{ar}), 7.42 – 7.28 (m, 2 H, CH_{ar}), 7.17 (s, 1 H, CH_{ar}), 2.42 (s, 3 H, CH_3), 1.15 (s, 21 H).**^{13}C-NMR (75 MHz, CD_2Cl_2):** δ (ppm) = 143.31, 134.84, 133.95, 131.57, 129.34, 128.83, 126.39, 125.71, 125.59, 124.63, 110.23, 91.77, 18.83, 15.05, 11.71. **HRMS (ESI$^+$):** *m/z* = 432.159 (calcd. 434.090 for $[C_{22}H_{29}BrSSi]^+$).

((3-(4-(3,3,4,4,5,5-Hexafluoro-2-(2-methylbenzo[b]thiophen-3-yl)cyclopent-1-en-1-yl)-5-methylthiophen-2-yl)phenyl)ethynyl)triisopropylsilane (42o):

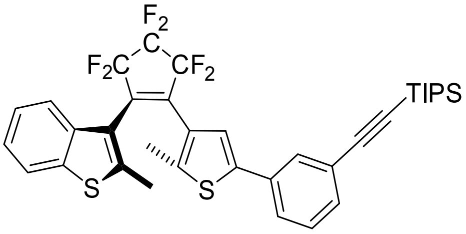

42o

To a solution of **41** (1.69 g, 3.9 mmol, 1.0 equiv.) in 100 mL anhydrous THF under Ar at -78 °C was added *n*-BuLi (1.83 mL, 4.10 mmol, 1.05 equiv.) and left stirring at that temperature for 1 h. Then **34** (1.53 g, 4.49 mmol, 1.15 equiv.) was added and left stirring for 2 h slowly reaching room temperature. TLC analysis showed completion of the reaction. The mixture was then diluted with Et_2O and washed with brine and H_2O. The organic layer was dried over $MgsO_4$ and evaporated. Final residue was purified through a silica gel column (PE : DCM, 8:1). Removal of solvent from the main fraction yielded 1.96 g (74%) of **42o** as a colorless oil. **^{1}H-NMR (300 MHz, CD_2Cl_2):** δ (ppm) = 7.82 – 7.73 (m, 1 H, CH_{ar}), 7.58 – 7.50 (m, 2 H, CH_{ar}), 7.43 – 7.26 (m, 5 H, CH_{ar}), 7.21 (s, 1 H, CH_{ar}), 2.33 (s, 3 H, CH_3), 1.99 (s, 3 H, CH_3), 1.15 (s, 21 H). **^{19}F-NMR (282 MHz, CD_2Cl_2):** δ (ppm) = -109.34 (m, 2 F, CF_2), -110.32 (q, J = 280.21 Hz, 2 F, CF_2), -132.47 (q, J = 262.71 Hz, 2 F, CF_2). **^{13}C-NMR (75 MHz, CD_2Cl_2):** δ (ppm) = 143.36, 142.80, 141.23, 138.73, 138.51, 133.75, 133.10, 131.72, 129.32, 129.00, 125.92, 125.51, 125.32, 124.94, 124.61, 123.44, 122.51, 122.35, 120.42, 110.41, 106.66, 91.85, 18.83, 15.14, 15.00, 11.71. **HRMS (ESI$^+$):** *m/z* = 674.159 (calcd. 674.190 for $[C_{36}H_{36}F_6S_2Si]^+$).

((3-(4-(3,3,4,4,5,5-Hexafluoro-2-(2-methylbenzo[b]thiophen-3-yl)cyclopent-1-en-1-yl)-5-methylthiophen-2-yl)phenyl)ethynyl)triisopropylsilane (42c):

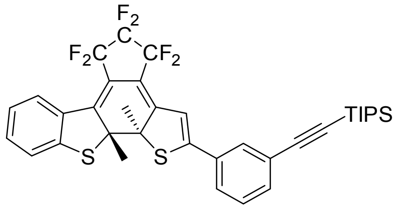

42c

42o was dissolved in an NMR tube in CD_2Cl_2 and irradiated with a 313 nm UV-lamp for 20 min. **^{1}H-NMR (300 MHz, CD_2Cl_2):** δ (ppm) = 7.83 – 7.78 (m, 1 H, *CH$_{ar}$*), 7.69 (s, 1 H, *CH$_{ar}$*), 7.64 – 7.50 (m, 1 H, *CH$_{ar}$*), 7.48 – 7.11 (m, 5 H, *CH$_{ar}$*), 6.78 (m, 1 H, *CH$_{ar}$*), 2.10 (s, 6 H, *CH$_3$*), 1.26 – 1.08 (m, 21 H). **^{19}F-NMR (282 MHz, CD_2Cl_2):** δ (ppm) = -103.71 (d, *J* = 256.7 Hz, 1 F, *CF$_2$*), -103.85 (d, *J* = 256.7 Hz, 1 F, *CF$_2$*), -120.40 (d, *J* = 264.2 Hz, 1 F, *CF$_2$*), -122.64 (d, *J* = 261.1 Hz, 1 F, *CF$_2$*), -128.14 (d, *J*=252.7 Hz, 1 F, *CF$_2$*), -138.16 (d, *J* = 252.0 Hz, 1 F, *CF$_2$*).

((3-((4-(4-Bromo-5-methylthiophen-2-yl)phenyl)ethynyl)phenyl)ethynyl)triisopropylsilane (43):

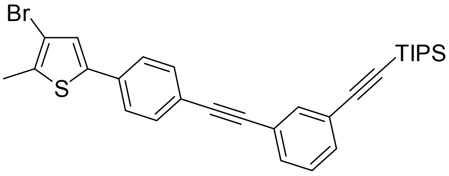

43

To a solution of **31** (1.30 g, 3.0 mmol, 1.0 equiv.) in dry THF (30 mL), TBAF (4.2 mL, 4.2 mmol, 1.4 equiv.) was added. The resulting solution was stirred for 15 min at room temperature. TLC analysis showed completion of the reaction. The mixture was then diluted with Et_2O and washed with sat. NH_4Cl solution and H_2O. The organic layer was then dried over $MgSO_4$ and concentrated under reduced pressure. The residue was then dissolved in Et_3N (50 mL) and degassed. Afterwards CuI (0.01 g, 0.08 mmol, 0.025 equiv.), $PdCl_2(PPh_3)_2$ (0.11 g, 0.15 mmol, 0.05 eq.) and **40** (1.21 g, 3.15 mmol, 1.05 equiv.) were added. Subsequently, the mixture was heated at 40 °C for 3 h. The reaction was monitored by TLC, and upon completion the brown mixture was then dissolved in PE and passed through a celite plug. The solvent was then evaporated. Final residue was purified through a silica gel column (PE : DCM, 8:1).). Removal of solvent from the main fraction yielded 1.30 g (80%) of **43** as a white solid. **^{1}H-NMR (300 MHz, CD_2Cl_2):** δ (ppm) = 7.65 (td, $^4J_{H,H}$ = 1.6 Hz, $^5J_{H,H}$ = 0.6 Hz, 1 H, *CH$_{ar}$*), 7.53 (s, 4 H, *CH$_{ar}$*), 7.50 (dt, $^3J_{H,H}$ = 7.7 Hz, $^4J_{H,H}$ = 1.2 Hz, 1 H, *CH$_{ar}$*), 7.46 (dt, $^3J_{H,H}$ = 7.8 Hz, $^4J_{H,H}$ = 1.2 Hz, 1 H, *CH$_{ar}$*), 7.32 (td, $^3J_{H,H}$ = 7.7 Hz, $^4J_{H,H}$ = 0.6 Hz, 1 H, *CH$_{ar}$*), 7.19 (s, 1 H, *CH$_{ar}$*), 2.43 (s, 3 H, *CH$_3$*), 1.14 (s, 21 H). **^{13}C-NMR (75 MHz, CD_2Cl_2):** δ (ppm) = 140.63, 135.25, 135.15, 133.79, 132.56, 132.10, 131.72, 128.91, 126.50, 125.43, 124.28, 123.74, 122.53, 110.44, 106.38, 91.96, 89.93, 18.81, 15.10, 11.69. **HRMS (ESI$^+$):** *m/z* = 534.159 (calcd. 534.120 for $[C_{30}H_{33}BrSSi]^+$).

((4-((4-(4-(3,3,4,4,5,5-Hexafluoro-2-(2-methylbenzo[b]thiophen-3-yl)cyclopent-1-en-1-yl)-5-methylthiophen-2-yl)phenyl)ethynyl)phenyl)ethynyl)trimethylsilane (44o):

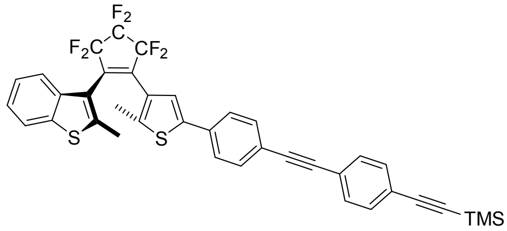

44o

To a solution of **35** (0.47 g, 0.7 mmol, 1.0 equiv.) in dry THF (30 mL), TBAF (0.84 mL, 0.84 mmol, 1.2 equiv.) was added. The resulting solution was stirred for 15 min at room temperature. TLC analysis showed completion of the reaction. The mixture was then diluted with Et_2O and washed with sat. NH_4Cl solution and H_2O. The organic layer was then dried over $MgSO_4$ and concentrated under reduced pressure. The residue was then dissolved in Et_3N (50 mL) and degassed. Afterwards CuI (0.04 g, 0.02 mmol, 0.03 equiv.), $PdCl_2(PPh_3)_2$ (0.06 g, 0.05 mmol, 0.05 equiv.) and ((4-iodophenyl)ethynyl)trimethylsilane (0.23 g, 0.77 mmol, 1.1 equiv.) were added. The reaction was monitored by TLC, and upon completion the brown mixture was then dissolved in PE and passed through a celite plug. The solvent was then evaporated. Final residue was purified through a silica gel column. (PE : DCM, 8:1). Removal of solvent from the main fraction yielded 0.38 g (80%) of **44o** as a yellow solid. **^{1}H-NMR (300 MHz, CD_2Cl_2):** δ (ppm) = 7.81 – 7.74 (m, 1 H, *CH$_{ar}$*), 7.56 (d, $^3J_{H,H}$ = 8.4, 1 H, *CH$_{ar}$*), 7.53 – 7.41 (m, 8 H, *CH$_{ar}$*), 7.40 – 7.29 (m, 2 H, *CH$_{ar}$*), 7.25 (s, 1 H, *CH$_{ar}$*), 2.34 (s, 3 H, *CH$_3$*), 1.97 (s, 3 H, *CH$_3$*), 0.25 (s, 9 H, *CH$_3$*). **^{19}F-NMR (282 MHz, CD_2Cl_2):** δ (ppm) = -109.33 (m, 2 F, *CF$_2$*), -110.37 (q, *J* = 262.94 Hz, 2 F, *CF$_2$*), -132.39 (q, *J* = 247.32 Hz, 2 F, *CF$_2$*). **^{13}C-NMR (75 MHz, CD_2Cl_2):** δ (ppm) = 143.08, 141.42, 138.73, 133.60, 132.51, 132.24, 131.80, 125.72, 125.34, 124.94, 123.54, 123.50, 122.64, 122.52, 122.38, 122.36, 122.31, 110.41, 104.71, 96.84, 91.25, 90.44, 15.04, -0.08. **HRMS (ESI$^+$):** *m/z* = 690.132 (calcd. 690.128 for $[C_{38}H_{28}F_6S_2Si]^+$).

((4-((4-(4-(3,3,4,4,5,5-Hexafluoro-2-(2-methylbenzo[b]thiophen-3-yl)cyclopent-1-en-1-yl)-5-methylthiophen-2-yl)phenyl)ethynyl)phenyl)ethynyl)trimethylsilane (44c):

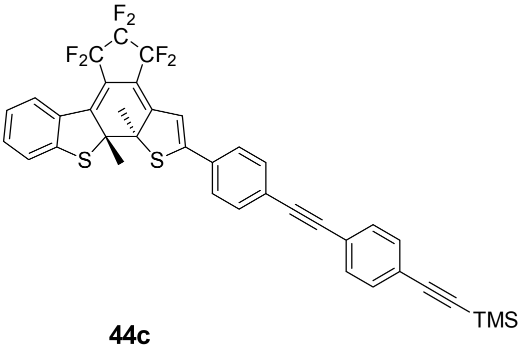

44c

44o was dissolved in an NMR tube in CD_2Cl_2 and irradiated with a 313 nm UV-lamp for 20 min. **^{1}H-NMR (300 MHz, CD_2Cl_2):** δ (ppm) = 7.83 – 7.76 (m, 1 H, *CH$_{ar}$*), 7.65 – 7.56 (m, 4 H, *CH$_{ar}$*), 7.55 – 7.40 (m, 4 H, *CH$_{ar}$*), 7.33 – 7.26 (m, 2 H, *CH$_{ar}$*), 7.20 – 7.11 (m, 1 H, *CH$_{ar}$*), 6.84 – 6.78 (m, 1 H, *CH$_{ar}$*), 2.08 (s, 6 H, *CH$_3$*), 0.25 (s, 9 H, *CH$_3$*). **^{19}F-NMR (282 MHz, CD_2Cl_2):** δ (ppm) = -103.72 (d, *J* = 256.5 Hz, 1 F, *CF$_2$*), -103.98 (d, *J* = 127.0 Hz, 1 F, *CF$_2$*), -120.31 (d, *J* = 260.4 Hz, 1 F, *CF$_2$*), -122.56 (d, *J* = 254.7 Hz, 1 F, *CF$_2$*), -128.14 (d, *J* = 236.4 Hz, 1 F, *CF$_2$*), -138.13 (d, *J* = 259.0 Hz, 1 F, *CF$_2$*).

((3-((4-(4-(3,3,4,4,5,5-Hexafluoro-2-(2-methylbenzo[b]thiophen-3-yl)cyclopent-1-en-1-yl)-5-methylthiophen-2-yl)phenyl)ethynyl)phenyl)ethynyl)triisopropylsilane (45o):

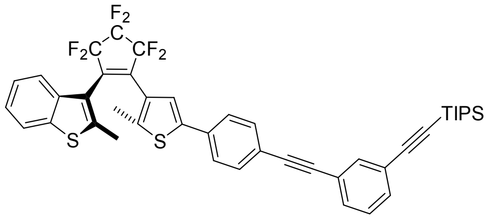

45o

To a solution of **43** (0.77 g, 1.45 mmol, 1.0 equiv.) in 100 mL anhydrous THF under Ar at -78 °C was added *n*-BuLi (0.70 mL, 1.52 mmol, 1.05 equiv.) and left stirring at that temperature for 1 h. Then **34** (0.57 g, 1.67 mmol, 1.15 equiv.) was added and left stirring for

2 h slowly reaching room temperature. TLC analysis showed completion of the reaction. The mixture was then diluted with Et_2O and washed with brine and H_2O. The organic layer was dried over $MgsO_4$ and evaporated. Final residue was purified through a silica gel column (PE : DCM, 8:1). Removal of solvent from the main fraction yielded 0.39 g (35%) of **45o** as a yellow oil. **^{1}H-NMR (300 MHz, CD_2Cl_2):** δ (ppm) = 7.80 – 7.75 (m, 1 H, CH_{ar}), 7.66 – 7.62 (m, 1 H, CH_{ar}), 7.56 (d, $^3J_{H,H}$ = 7.7 Hz, 1 H, CH_{ar}), 7.53 – 7.42 (m, 7 H, CH_{ar}), 7.40 – 7.29 (m, 4 H, CH_{ar}), 7.25 (s, 1 H, CH_{ar}), 2.34 (s, 3 H, CH_3), 1.97 (s, 3 H, CH_3), 1.14 (s, 21 H). **^{19}F-NMR (282 MHz, CD_2Cl_2):** δ (ppm) = -109.33 (m, 2 F, CF_2), -110.31 (q, J = 263.00 Hz, 2 F, CF_2), -132.41 (q, J = 241.30 Hz, 2 F, CF_2). **^{13}C-NMR (75 MHz, CD_2Cl_2):** δ (ppm) = 143.10, 141.02, 138.31, 138.18, 134.83, 133.16, 132.11, 131.71, 131.29, 128.50, 128.02, 127.04, 125.31, 124.93, 124.52, 123.87, 123.28, 123.08, 122.22, 122.11, 121.95, 105.94, 89.53, 89.44, 18.39, 14.73, 14.63, 11.27. **HRMS (ESI$^+$):** m/z = 774.219 (calcd. 774.221 for $[C_{44}H_{40}F_6S_2Si]^+$).

((3-((4-(4-(3,3,4,4,5,5-Hexafluoro-2-(2-methylbenzo[b]thiophen-3-yl)cyclopent-1-en-1-yl)-5-methylthiophen-2-yl)phenyl)ethynyl)phenyl)ethynyl)triisopropylsilane (45c):

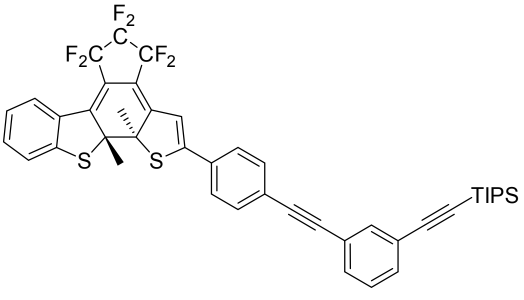

45c

45o was dissolved in an NMR tube in CD_2Cl_2 and irradiated with a 313 nm UV-lamp for 20 min. **^{1}H-NMR (300 MHz, CD_2Cl_2):** δ (ppm) = 7.80 (d, $^3J_{H,H}$ = 8.1 Hz, 1 H, CH_{ar}), 7.69 – 7.55 (m, 5 H, CH_{ar}), 7.55 – 7.41 (m, 2 H, CH_{ar}), 7.39 – 7.25 (m, 3H, CH_{ar}), 7.20 – 7.10 (m, 1 H, CH_{ar}), 6.81 (s, 1 H, CH_{ar}), 2.09 (s, 6 H, CH_{ar}), 1.14 (s, 21 H). **^{19}F-NMR (282 MHz, CD_2Cl_2):** δ (ppm) = -103.72 (d, J = 256.5 Hz, 1 F, CF_2), -103.98 (d, J = 127.0 Hz, 1 F, CF_2), -120.31 (d, J = 260.4 Hz, 1 F, CF_2), -122.56 (d, J = 254.7 Hz, 1 F, CF_2), -128.14 (d, J = 236.4 Hz, 1 F, CF_2), -138.13 (d, J = 259.0 Hz, 1 F, CF_2).

(E)-4-(5-(4'-((2,6-difluorophenyl)diazenyl)-3',5'-difluoro-[1,1'-biphenyl]-3-yl)thiophen-2-yl)-*N,N*-di-p-tolylaniline (46):

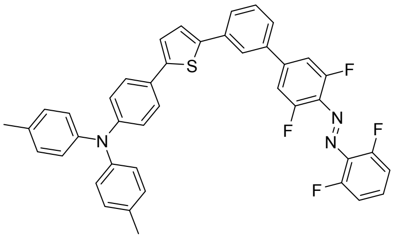

46

To a solution of **47** (0.65 g, 1.27 mmol, 1.1 equiv.) in anhydrous THF under Ar at -78 ºC was added *n*-BuLi (0.58 mL, 1.27 mmol, 1.1 equiv.) and left stirring at that temperature for 1 h. Then B(OiPr)$_3$ (0.29 mL, 1.27 mmol, 1.1 equiv.) was added and left stirring overnight slowly reaching room temperature. Afterwards a 2 M Na$_2$CO$_3$ (2.1 mL, 4.18 mmol, 3.3 equiv.) solution was added and the resulting solution was deoxygenated by letting bubble Ar for 15 min. To the deoxygenated solution, **50** (0.38 g, 1.15 mmol, 1.0 equiv.) and the Pd(PPh$_3$)$_4$ (0.10 g, 0.09 mmol, 0.08 equiv.) catalyst were added. Finally the solution was refluxed for 17 h at 80 °C. TLC analysis showed completion of the reaction. It was then proceeded to dilute the solution with Et$_2$O, and wash once with brine (100 mL). The organic layer was dried over MgSO4 and concentrated under reduced pressure. It was then purified by column chromatography over silica gel (PE : DCM, 4:1).yielding 0.32 g (41%) of **46** as a red solid. **^{1}H-NMR (500 MHz, CD$_2$Cl$_2$):** δ (ppm) = 7.87 (t, $^4J_{H,H}$ = 1.7 Hz, 1 H, CH_{ar}), 7.70 (dt, $^3J_{H,H}$ = 7.2 Hz, $^4J_{H,H}$ = 1.7 Hz, 1 H, CH_{ar}), 7.57 – 7.46 (m, 4 H, CH_{ar}), 7.45 – 7.35 (m, 4 H, CH_{ar}), 7.28 – 7.22 (m, 1 H, CH_{ar}), 7.17 – 7.08 (m, 6 H, CH_{ar}), 7.06 – 6.92 (m, 6 H, CH_{ar}), 2.33 (s, 6 H, CH_3). **^{19}F-NMR (471 MHz, CD$_2$Cl$_2$):** δ (ppm) = -120.82 (d, $^4J_{F,F}$ = 10.52 Hz, 2 F, CF_{ar}), -122.09 (d, $^4J_{F,F}$ = 9.0 Hz, 2 F, CF_{ar}). **^{13}C-NMR (126 MHz, CD$_2$Cl$_2$):** δ (ppm) = 157.25 (dd, J = 46.0 Hz, J = 4.3 Hz), 155.18 (dd, J = 46.0 Hz, J = 5.1 Hz), 148.41, 145.31 (d, J = 4.8 Hz), 144.82, 141.62, 138.89, 138.36, 135.78 (d, J = 13.3 Hz), 133.55, 132.14 (dt, J = 15.1 Hz, J = 10.1 Hz), 130.75 (t, J = 9.6 Hz), 130.35, 130.17, 129.37, 128.56, 127.29, 126.61, 126.46, 126.16, 125.64, 125.31, 125.13, 124.19, 123.32, 122.41, 113.08 (dd, J = 20.2 Hz, J = 3.6 Hz), 111.50 (dd, J = 21.5 Hz, J = 3.3 Hz), 20.95. **HRMS (ESI$^+$):** *m/z* = 683.073 (calcd. 683.202 for [C$_{42}$H$_{29}$F$_4$N$_3$S]$^+$).

4-(5-(3-Bromophenyl)thiophen-2-yl)-*N,N*-di-p-tolylaniline (47):

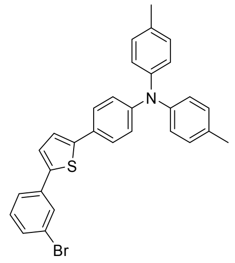

47

To a solution of **52** (1.07 g, 3.0 mmol, 1.0 equiv.) in 25 mL anhydrous THF under Ar at -78 ºC was added *n*-BuLi (31.64 mL, 6 mmol, 1.2 equiv.) and left stirring at that temperature for 1h. Then $SnCl(Bu)_3$ (0.98 mL, 3.6 mmol, 1.2 equiv.) was added and left stirring 1 h at room temperature. Afterwards the solvent was evaporated. The resulting oil was dissolved in 25 mL anhydrous toluene under Ar and 3-bromoiodobenzene (0.85 g, 3.0 mmol, 1.0 equiv.) and the $Pd(PPh_3)_4$ (0.28 g, 0.16 mmol, 0.08 equiv.) catalyst were added. Finally the solution was heated for 17 h at 105 °C. TLC analysis showed completion of the reaction. It was then proceeded to dilute the solution with Et_2O, and wash once with brine (100 mL). The organic layer was dried over MgSO4 and concentrated under reduced pressure. It was then purified by column chromatography over silica gel (PE : DCM, 8:1).yielding 2.54 g (88%) of a yellow solid. **^{1}H-NMR (300 MHz, CD_2Cl_2):** δ (ppm) = 7.76 (t, $^4J_{H,H}$ = 1.8 Hz, 1 H, *CH$_{ar}$*), 7.54 (ddd, $^3J_{H,H}$ = 7.8 Hz, $^4J_{H,H}$ = 1.8, $^4J_{H,H}$ = 1.0 Hz, 1 H, *CH$_{ar}$*), 7.47 – 7.41 (m, 2 H, *CH$_{ar}$*), 7.38 (ddd, $^3J_{H,H}$ = 8.0 Hz, $^4J_{H,H}$ = 1.9 Hz, $^4J_{H,H}$ = 1.0 Hz, 1 H, *CH$_{ar}$*), 7.28 (t, $^4J_{H,H}$ = 2.6 Hz, 1 H, *CH$_{ar}$*), 7.25 (t, $^3J_{H,H}$ = 7.9, 1 H, *CH$_{ar}$*), 7.19 (d, $^3J_{H,H}$ = 3.8 Hz, 1 H, *CH$_{ar}$*), 7.12 – 7.06 (m, 4 H, *CH$_{ar}$*), 7.02 – 6.93 (m, 6 H, *CH$_{ar}$*), 2.30 (s, 6 H, *CH$_3$*). **^{13}C-NMR (75 MHz, CD_2Cl_2)** δ (ppm)= 145.24, 145.07, 140.60, 136.81, 133.58, 130.84, 130.38, 130.33, 128.45, 127.14, 126.62, 125.31, 124.37, 123.28, 122.33, 20.92. **HRMS (ESI$^+$):** *m/z* = 510.926 (calcd. 511.080 for $[C_{30}H_{24}NSBr]^+$).

(E)-1-(3,5-difluoro-[1,1'-biphenyl]-4-yl)-2-(2,6-difluorophenyl)diazene (48):

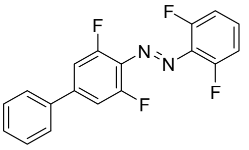

48

To a solution of Phenyl Bromide (0.23 mL, 2.2 mmol, 1.1 equiv.) in 25 mL anhydrous THF under Ar at -78 ºC was added *n*-BuLi (1.05 mL, 2.2 mmol, 1.1 equiv.) and left stirring at that temperature for 1 h. Then $B(OiPr)_3$ (0.51 mL, 2.2 mmol, 1.1 equiv.) was added and left stirring overnight slowly reaching room temperature. Afterwards a 2 M Na_2CO_3 (3.63 mL, 7.26 mmol, 3.3 equiv.) solution was added and the resulting solution was deoxygenated by letting bubble Ar for 15 min. To the deoxygenated solution, **50** (0.66 g, 2.0 mmol, 1.0 equiv.) and the $Pd(PPh_3)_4$ (0.28 g, 0.16 mmol, 0.08 equiv.) catalyst were added. Finally the solution was refluxed for 48 h at 80 °C. TLC analysis showed completion of the reaction. It was then proceeded to dilute the solution with Et_2O, and wash once with brine (100 mL). The organic layer was dried over $MgSO_4$ and concentrated under reduced pressure. It was then purified by column chromatography over silica gel (PE : DCM, 4:1).yielding 0.3 g (91%) of a deep red solid. **^{1}H-NMR (500 MHz, CD_2Cl_2):** δ (ppm) = 7.68 – 7.63 (m, 2 H, CH_{ar}), 7.54 – 7.48 (m, 2 H, CH_{ar}), 7.48 – 7.38 (m, 2 H, CH_{ar}), 7.38 – 7.33 (m, 2 H, CH_{ar}), 7.16 – 7.07 (m, 2 H, CH_{ar}). **^{19}F-NMR (471 MHz, CD_2Cl_2):** δ (ppm) = -121.07 (s, 2 F, CF_{ar}), -122.25 (d, $^4J_{F,F}$ = 10.7 Hz, 2 F, CF_{ar}). **^{13}C-NMR (126 MHz, CD_2Cl_2):** δ (ppm) = 157.43 (d, *J* = 5.7 Hz), 157.04 (d, *J* = 3.7 Hz), 155.36 (d, *J* = 4.8 Hz), 154.97 (d, *J* = 3.6 Hz), 146.22 – 145.13 (m), 138.12 (d, *J* = 2.0 Hz), 132.11 (dt, *J* = 21.4 Hz, *J* = 10.2 Hz), 129.62, 129.57, 127.31, 113.07 (dd, *J* = 20.1 Hz, *J* = 3.7 Hz), 111.36 (dd, *J* = 20.3 Hz, *J* = 3.4 Hz). **HRMS (ESI$^+$):** *m/z* = 331.059 (calcd. 330.078 for $[C_{18}H_{10}F_4N_2]^+$).

2,6-Difluoro-4-bromoaniline (49):

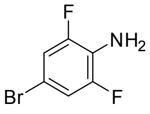

49

To a solution of 2,6-difluoroaniline (12.9 g, 100 mmol) in acetonitrile (200 mL) was added N-bromosuccinimide (17.8 g, 100 mmol) at room temperature. The mixture was stirred overnight, and then diluted with water and PE. The two phases were separated and the organic phase was dried over MgSO4, filtered, and concentrated under reduced pressure. The crude residue was purified by column chromatography (PE : DCM : 4:1) to give **49** as a pale white solid (17.2 g, 99%). **^{1}H-NMR (300 MHz, CDCl$_3$):** δ (ppm) = 7.00 (dd, $^3J_{H,H}$ = 6.1 Hz, $^4J_{H,H}$ = 1.3 Hz, 2 H, CH_{ar}), 3.75 (br s, 2 H, NH_2). **^{19}F-NMR (282 MHz, CDCl$_3$):** δ (ppm) = -130.05 (d, $^4J_{F,F}$ = 6.9 Hz, 2 F, CF_{ar}). **^{13}C-NMR (75 MHz, CDCl$_3$):** δ (ppm) = 153.36, 150.12, 123.50, 114.72, 107.09.

(E)-1-(4-bromo-2,6-difluorophenyl)-2-(2,6-difluorophenyl)diazene (50):

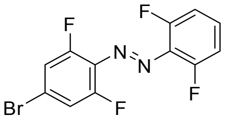

50

Compound **49** (6.89 g, 33.1 mmol, 1.00 equiv) was dissolved in 100 mL of DCM. To this solution, Oxone (40.7 g, 66.2 mmol, 2.00 equiv) dissolved in 400 mL of water was added. The solution was stirred under Ar at room temperature overnight. After separation of the layers, the aqueous layer was extracted with DCM twice. The combined organic layers were washed with 1 N HCl, saturated sodium bicarbonate solution, water, brine, dried over $MgSO_4$ and evaporated to dryness. Afterwards 60 mL of toluene and difluoroaniline (4.27 g, 33.1 mmol, 1.00 equiv.) were added. A mixture of 60 mL of Acetic acid and 10 mL of TFA was prepared and added to the solution. The resulting mixture was stirred at room temperature for 24 h. Afterwards it was evaporated to dryness. Purification by chromatography (DCM : PE,1:4, silica gel) yielded 10.25 g (93%) of a deep red solid. **^{1}H-**

NMR (300 MHz, CDCl$_3$): δ (ppm) = 7.45 - 7.34 (m, 1 H, *CH$_{ar}$*), 7.32 - 7.19 (m, 2 H, *CH$_{ar}$*), 7.06 (t, $^3J_{H,H}$ = 8.7 Hz, 2 H, *CH$_{ar}$*). **^{19}F-NMR (282 MHz, CDCl$_3$):** δ (ppm) = -118.42 (d, *J* = 8.8 Hz, 2 F, *CF$_{ar}$*), -120.09 (dd, *J* = 10.3 Hz, *J* = 5.2 Hz, 2 F, *CF$_{ar}$*). **^{13}C-NMR (75 MHz, CDCl$_3$):** δ (ppm) = 157.43 (dd, *J* = 13.6 Hz, *J* = 4.4 Hz), 153.94 (dd, *J* = 17.0 Hz, *J* = 4.6 Hz), 132.01 (t, *J* = 10.5 Hz), 124.09 (t, *J* = 12.0 Hz), 116.81 (dd, *J* = 23.5 Hz, *J* = 3.8 Hz), 112.83 (dd, *J* = 20.4 Hz, *J* = 3.6 Hz). **HRMS (ESI$^+$):** *m/z* = 332.710 (calcd. 331.957 for [$C_{12}H_5BrF_4N_2$]$^+$).

4-bromo-*N,N*-di-p-tolylaniline (51):

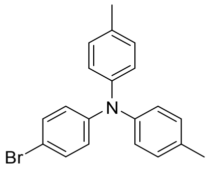

51

To 250 mL of degased anhydrous toluene, 4-bromoaniline (17.2 g, 100.0 mmol, 1.0 equiv.), 4-iodotoluene (45.78 g, 210.0 mmol, 2.1 equiv.), 1,10-phenanthroline (0.65 g, 4.0 mmol, 0.04 equiv.), CuCl (0.36 g, 4.0 mmol, 0.04 equiv.) and KOH flakes (43.89 g, 782.0 mmol, 7.82 equiv.) were added. The reaction mixture was rapidly heated over the course of 30 min to the reflux temperature of ~130 °C and maintained at that temperature overnight. The reaction mixture was then brought to dryness. The product was subjected to further purification by column chromatography over silica gel (PE : DCM, 10:1) yielding 23.5 g (65%) of a white solid. **^{1}H-NMR (300 MHz, CDCl$_3$):** δ (ppm) = 7.27 (d, $^3J_{H,H}$ = 8.9 Hz, 2 H, *CH$_{ar}$*), 7.06 (d, $^3J_{H,H}$ = 8.2 Hz, 4 H, *CH$_{ar}$*), 6.96 (d, $^3J_{H,H}$ = 8.4 Hz, 4 H, *CH$_{ar}$*), 6.88 (d, $^3J_{H,H}$ = 8.9 Hz, 2 H, *CH$_{ar}$*), 2.31 (s, 6 H, *CH$_3$*). **HRMS (ESI$^+$):** *m/z* = 350.915 (calcd. 351.062 for [$C_{20}H_{18}BrN$]$^+$).

4-Methyl-N-(4-(thiophen-2-yl)phenyl)-N-(p-tolyl)aniline (52):

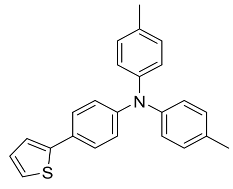

52

To a solution of **51** (11.62 g, 33.0 mmol, 1.0 equiv.) in 150 mL of anhydrous toluene under Ar, 2-(Tributylstannyl)thiophene (108 mL, 33.0 mmol, 1.0 equiv.) and Pd(PPh$_3$)$_4$ (3.05 g, 2.64 mmol, 0.08 equiv.) were added. The solution was heated at 105 °C for 17 h. TLC analysis showed completion of the reaction. The solution was concentrated under reduced pressure. It was then purified by column chromatography over silica gel (PE : DCM, 8:1).yielding 8.48 g (72%) of a yellow fluorescent oil. **^{1}H-NMR (300 MHz, CD_2Cl_2):** δ (ppm) = 7.45 - 7.40 (m, 2 H, CH_{ar}), 7.22 - 7.20 (m, 1 H, CH_{ar}), 7.20 (s, 1 H, CH_{ar}), 7.10 - 7.05 (m, 4 H, CH_{ar}), 7.05 - 7.02 (m, 1 H, CH_{ar}), 6.99 - 6.93 (m, 6 H, CH_{ar}), 2.30 (s, 6 H, CH_3). **^{13}C-NMR (75 MHz, CD_2Cl_2):** δ (ppm) = 148.14, 145.38, 133.36, 130.28, 128.37, 127.80, 126.83, 125.14, 124.11, 122.65, 122.32, 20.90.**HRMS (ESI$^+$):** m/z = 356.122 (calcd. 355.139 for $[C_{24}H_{21}NS]^+$).

Ir(ppy)$_2$-acac-azobenzene dyad (53):

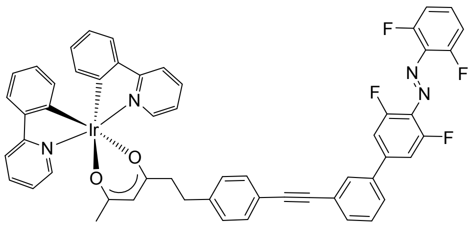

53

[{Ir(μ-Cl)(ppy)$_2$}$_2$] (0.14 g, 0.13 mmol, 1.0 equiv.) and silvertrifluoroacetate (0.06 g, 0.26 mmol, 2 equiv.) were dissolved under nitrogen atmosphere in 40 mL of anhydrous acetone and refluxed for 1 h. After cooling to room temperature, the precipitated AgCl was filtered off. **57** (0.16 g, 1.00 mmol, 2.2 equiv.) and NEt_3 (0.14 mL, 1.0 mmol, 7.7 equiv.) were added and the resulting solution was stirred for 17 h at room temperature whereupon the solvent was evaporated under reduced pressure. The remaining residue was dissolved in 10 mL of DCM and purified by column chromatography on alumina with DCM as the eluant. Subsequently a GPC was performed to eliminate Ir(III) impurities and a further purification by column chromatography on alumina (DCM) was performed. The solvent was reduced to about 3 mL and the compound precipitated by adding PE (20 mL). The precipitate was filtered off, washed twice with 10 mL portions of PE, and dried in vacuum obtaining 0.25 g (92%) of **53** as a red solid. **^{1}H-NMR (500 MHz, CD_2Cl_2):** δ (ppm) = 8.46 (ddd, $^3J_{H,H}$ = 5.8 Hz, $^4J_{H,H}$ = 1.5 Hz, $^5J_{H,H}$ = 0.8 Hz, 1 H, CH_{ar}), 8.30 (ddd, $^3J_{H,H}$ = 5.8 Hz, $^4J_{H,H}$ = 1.5 Hz, $^5J_{H,H}$ = 0.8 Hz, 1 H, CH_{ar}), 7.91 (d, $^3J_{H,H}$ = 7.9 Hz, 1 H, CH_{ar}), 7.89 – 7.86 (m, 1 H, CH_{ar}), 7.86 – 7.79 (m, 2 H, CH_{ar}), 7.80 – 7.74 (m, 1 H, CH_{ar}), 7.66 – 7.61 (m, 2 H, CH_{ar}), 7.58 (ddd, $^3J_{H,H}$ = 7.4 Hz, $^3J_{H,H}$ = 6.0 Hz, $^4J_{H,H}$ = 1.9 Hz, 2 H, CH_{ar}), 7.55 – 7.49 (m, 1 H, CH_{ar}), 7.47 – 7.30 (m, 5 H, CH_{ar}), 7.22 – 7.18 (m, 1 H, CH_{ar}), 7.14 – 7.08 (m, 3 H, CH_{ar}), 6.99 (t, $^3J_{H,H}$ = 6.3 Hz, 2 H, *CH*$_{ar}$), 6.89 – 6.81 (m, 2 H, *CH*$_{ar}$), 6.74 – 6.65 (m, 2 H, *CH*$_{ar}$), 6.25 (td, $^3J_{H,H}$ = 6.9 Hz, $^5J_{H,H}$ = 1.0 Hz, 2 H, *CH*$_{ar}$), 5.26 (s, 1 H, *CH*), 2.77 – 2.63 (m, 2 H, *CH*$_2$), 2.46 – 2.30 (m, 2 H, *CH*$_2$), 1.79 (s, *J*=2.0, 3 H, *CH*$_3$). **^{19}F-NMR (471 MHz, CD_2Cl_2)** δ (ppm) = -120.93 (d, $^4J_{F,F}$ = 10.7 Hz, 2 F, *CF*$_{ar}$), -122.23 (d, $^4J_{F,F}$ = 8.4 Hz, 2 F, *CF*$_{ar}$). **^{13}C-NMR (126 MHz, CD_2Cl_2):** δ (ppm) = 186.48, 185.51, 168.58 (d, *J* = 6.1 Hz), 157.25 (dd, *J* = 47.3 Hz, *J* = 5.0 Hz), 155.18 (dd, *J* = 46.9 Hz, *J* = 4.4 Hz), 148.62 (d, *J* = 8.9 Hz), 147.83 (d, *J* = 5.3 Hz), 145.54 (d, *J* = 2.5 Hz), 144.80, 143.00, 138.50, 137.55 (d, *J* = 5.8 Hz), 133.57 (d, *J* = 4.0 Hz), 132.41, 132.16, 131.85, 130.36, 129.74, 129.16 (d, *J* = 7.4 Hz), 129.02, 127.10, 124.87, 124.23 (d, *J* = 4.2 Hz), 122.18, 121.18, 120.45, 118.93 (d, *J* = 2.3 Hz), 113.10 (dd, *J* = 20.2 Hz, *J* = 3.6 Hz), 111.50 (dd, *J* = 22.6 Hz, *J* = 2.1 Hz), 100.58, 90.75, 88.46, 42.91, 32.85, 28.81. **HRMS (ESI$^+$):** *m/z* = 1065.233 (calcd. 1065.238 for $[C_{54}H_{37}F_4IrN_4O_2Na]^+$).

6-(4-Iodophenyl)hexane-2,4-dione (55):

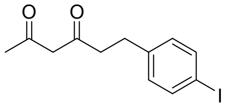

55

In a round-bottom flask with septum, NaH (1.38 g, 10.0 mmol, 2.0 equiv.) was weighed and the apparatus was evacuated and flushed with Ar three times. 100 mL of anhydrous THF and hexamethylphosphamide (0.17 mL, 1.0 mmol, 0.2 equiv.) were added and cooled to 0 °C. Acetyl acetonate (0.51 mL, 5.0 mmol, 1.0 equiv.) was injected while foaming and a white precipitate was formed. The mixture was stirred for 20 min at 0 °C. Subsequently, *n*-BuLi (2.50 mL, 5.5 mmol, 1.1 equiv.) was slowly added and the mixture was stirred for further 20 min. 4-Iodonezyl bromide (1.78 g; 6.0 mmol, 1.2 equiv.) was added slowly and the mixture was allowed to stir 2 h at room temperature. To get rid of spare sodium hydride, 2 N HCl was added slowly until no further gasification could be observed. The reaction mixture was diluted with Et_2O and washed several times with water, dried with $MgSO_4$, filtered and concentrated. Column chromatography (DCM) afforded 1.30g of **55** as a white solid (82% yield). **^{1}H-NMR (300 MHz, $CDCl_3$):** (enol may.) δ (ppm) = 15.41 (s, 1 H, *COH*), 7.60 (d, $^3J_{H,H}$ = 8.3 Hz, 2 H, *CH*$_{ar}$), 6.94 (d, $^3J_{H,H}$ = 8.4, 2 H, *CH*$_{ar}$), 5.45 (s, 1 H, COH*CH*CO), 2.93 – 2.82 (m, 2 H, *CH*$_2$), 2.61 – 2.50 (m, 2 H, *CH*$_2$), 2.04 (s, 3 H, *CH*$_3$). **^{13}C-NMR (75 MHz, $CDCl_3$):** δ (ppm) = 193.08, 190.99, 140.47, 137.66, 130.60, 130.56, 100.22, 91.47, 39.84, 30.98, 24.91. **HRMS (ESI$^+$):** *m/z* = 316.971 (calcd. 315.996 for $[C_{12}H_{13}IO_2]^+$).

(E)-1-(3,5-difluoro-3'-((triisopropylsilyl)ethynyl)-[1,1'-biphenyl]-4-yl)-2-(2,6-difluorophenyl)diazene (56):

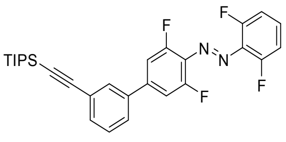

56

To a solution of **39** (5.20 , 15.4 mmol, 1.1 equiv.) in 75 mL anhydrous THF under Ar at -78 ºC was added *n*-BuLi (7.33 mL, 15.4 mmol, 1.1 equiv.) and left stirring at that temperature for 1h. Then $B(OiPr)_3$ (3.55 mL, 15.4 mmol, 1.1 equiv.) was added and left stirring overnight slowly reaching room temperature. Afterwards a 2 M Na_2CO_3 (25.41 mL, 50.82 mmol, 3.3 equiv.) solution was added and the resulting solution was deoxygenated by letting bubble Ar for 15 min. To the deoxygenated solution, **50** (4.66 g, 14.0 mmol, 1.0 equiv.) and the $Pd(PPh_3)_4$ (1.30 g, 1.12 mmol, 0.08 equiv.) catalyst were added. Finally the solution was refluxed for 48 h at 80 °C. TLC analysis showed completion of the reaction. It was then proceeded to dilute the solution with Et_2O, and wash once with brine (100 mL). The organic layer was dried over MgSO4 and concentrated under reduced pressure. It was then purified by column chromatography over silica gel (PE : DCM, 4:1).yielding 6.5 g (91%) of a red solid. **^{1}H-NMR (300 MHz, $CDCl_3$):** δ (ppm) = 7.72 (t, $^4J_{H,H}$ = 1.5 Hz, 1 H, CH_{ar}), 7.58 – 7.53 (m, 2 H, CH_{ar}), 7.47 – 7.24 (m, 4 H, CH_{ar}), 7.13 – 7.02 (m, 2 H, CH_{ar}), 1.17 (s, 21 H). **^{19}F-NMR (282 MHz, $CDCl_3$)** δ (ppm) = -119.13 (d, $^4J_{F,F}$ = 10.9 Hz, 2 F, CF_{ar}), -120.34 – -120.47 (m, 2 F, CF_{ar}). **^{13}C-NMR (75 MHz, $CDCl_3$):** δ (ppm) = 157.82, 157.46, 154.36, 154.00, 144.43, 138.15, 132.78, 132.04, 131.56, 130.65, 130.46, 130.29, 130.00, 129.22, 126.94, 126.77, 124.73, 124.65, 112.91, 112.64, 111.34, 111.05, 106.32, 92.00, 18.81, 11.44. **HRMS (ESI$^+$):** *m/z* = 510.213 (calcd. 510.210 for $[C_{29}H_{30}F_4N_2Si]^+$).

(E)-6-(4-((4'-((2,6-difluorophenyl)diazenyl)-3',5'-difluoro-[1,1'-biphenyl]-3-yl)ethynyl)phenyl)hexane-2,4-dione (57):

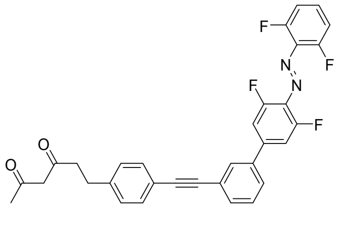

57

To a solution of **56** (1.02 g, 2.0 mmol, 1.0 equiv.) in dry THF (30 mL), TBAF (2.60 mL, 2.60 mmol, 1.3 equiv.) was added. The resulting solution was stirred for 15 min at room temperature. TLC analysis showed completion of the reaction. The mixture was then diluted with Et_2O and washed with sat. NH_4Cl solution and H_2O. The organic layer was then dried over $MgSO_4$ and concentrated under reduced pressure. The residue was then dissolved in Et_3N (50 mL) and degassed. Afterwards CuI (0.02 g, 0.10 mmol, 0.03 equiv.), $PdCl_2(PPh_3)_2$ (0.07 g, 0.10 mmol, 0.05 equiv.) and **55** (0.63 g, 2.0 mmol, 1.0 equiv.) were added. The reaction was monitored by TLC, and upon completion the brown mixture was then dissolved in PE and passed through a celite plug. The solvent was then evaporated. Final residue was purified through a silica gel column. (DCM). Removal of solvent from the main fraction yielded 0.89 g (82%) of **57** as a red solid. **^{1}H-NMR (300 MHz, $CDCl_3$):** (enol may.) δ (ppm) = 7.78 (m, 1 H, *CH$_{ar}$*), 7.64 – 7.54 (m, 3 H, *CH$_{ar}$*), 7.53 – 7.46 (m, 3 H, *CH$_{ar}$*), 7.34 (m, 2 H, *CH$_{ar}$*), 7.20 (d, $^3J_{H,H}$ = 8.2 Hz, 2 H, *CH$_{ar}$*), 7.13 – 7.03 (m, 2 H, *CH$_{ar}$*), 5.47 (s, 1 H, COH*CH*CO), 5.30 (s, 1 H, *COH*), 2.99 – 2.92 (m, 2 H, *CH$_2$*), 2.64 – 2.56 (m, 2 H, *CH$_2$*), 2.04 (s, 3 H, *CH$_3$*). **^{19}F-NMR (282 MHz, $CDCl_3$)** δ (ppm) = -119.19 (d, $^4J_{F,F}$ = 10.7 Hz, 2 F, *CF$_{ar}$*), -120.48 (d, $^4J_{F,F}$ = 10.7 Hz, 2 F, *CF$_{ar}$*). **^{13}C-NMR (75 MHz, $CDCl_3$):** δ (ppm) = 193.10, 191.11, 144.44, 141.59, 138.26, 137.67, 132.22, 131.98, 131.59, 130.56, 130.16, 129.39, 128.61, 126.80, 124.61, 120.87, 112.92, 112.64, 111.36, 111.03, 100.25, 90.44, 88.51, 39.82, 31.49, 24.95, 17.85, 12.41. **HRMS (ESI$^+$):** *m/z* = 543.015 (calcd. 542.162 for $[C_{32}H_{22}F_4N_2O_2]^+$).

5.3 Procedures

All procedures linked to photochemistry were performed using spectrophotometric grade solvents. UV/vis absorption spectroscopy was performed on a Varian Cary 60 UV/vis spectrophotometer equipped with a Peltier thermostated cell holder at 25 ± 0.05 °C if not indicated otherwise. Analytical irradiation was performed employing an Oriel 500 W mercury arc lamp model 68810 in an Oriel universal arc lamp housing model 66055 equipped with an Oriel ¼ m grating monochromator model 77200, an Oriel timed shutter and water filter or on an Oriel 1000 W xenon arc lamp model 66924 using an Oriel timed shutter, water filter, and various cut-off filters. The lamp output beam was wired into the spectrophotometer orthogonal to the beamline of the respective spectrophotometer employing fiber-optics to enable simultaneous irradiation and probing. PSS compositions were determined either by NMR characterization or by ultraperformance liquid chromatography (UPLC) analyses using integration of the UV signal at the wavelengths of the isosbestic points. Irradiation of compounds for NMR analysis were performed in a Rayonet RPR 100 photochemical reactor equipped with 313 nm lamps. Fluorescence spectroscopy was performed on a Cary Eclipse Fluorescence spectrometer.

Fluorescence measurements were executed using a slit width of 2.5 nm for excitation and 5.0 nm for emission. PMT voltage was set to 600 V. Relative quantum efficiencies of fluorescence were obtained by comparing the areas under the corrected emission spectrum of the test sample in various solvent with that of quinine sulfate hydrate (0.546 in 0.1 M H_2SO_4)[227] or oxazine 170 (0.58 in EtOH)[228], respectively. Dilute solutions ($0.01 < A < 0.05$) were used to minimize the reabsorption effects. Fluorescence quantum yields were determined using the following equation[229]:

$$\phi_X = \phi_S \frac{I_X \cdot A_S}{I_S \cdot A_X} \cdot \left(\frac{\eta_X}{\eta_S}\right)^2 \tag{5.3.1}$$

Where ϕ_S stands for the reported quantum yield of the standard, *I* stands for the integrated emission spectra, *A* stands for the absorbance at the excitation wavelength and η stands for the refractive index of the solvent being used. *X* subscript stands for the test sample, and *S* subscript stands for the standard.

Isomerization quantum yields were determined using the initial slope method according to Equation (2.1.9) presented in Chapter 2.1.1 or Equation (5.3.2).[217]

$$\frac{dC_B}{dt} = 1000 \cdot I_0 \cdot \phi_{AB} \cdot \left(1 - 10^{-A'}\right) \tag{5.3.2}$$

where the quantum yield ϕ_{AB} can be extracted as the slope of a pseudo-linear relation. A' is approximated to the Absorbance at the irradiation wavelength of the sample where within 5% conversion $c_B \approx 0$. The concentration of species B at a given time can be directly expressed through

$$C_B^t = \frac{A_t - \varepsilon_B \cdot C_0}{(\varepsilon_A - \varepsilon_B)} \tag{5.3.3}$$

Application of the method is shown on the *trans*→*cis* isomerization of azobenzene in MeOH upon 440 nm irradiation (**Figure 5-1**).

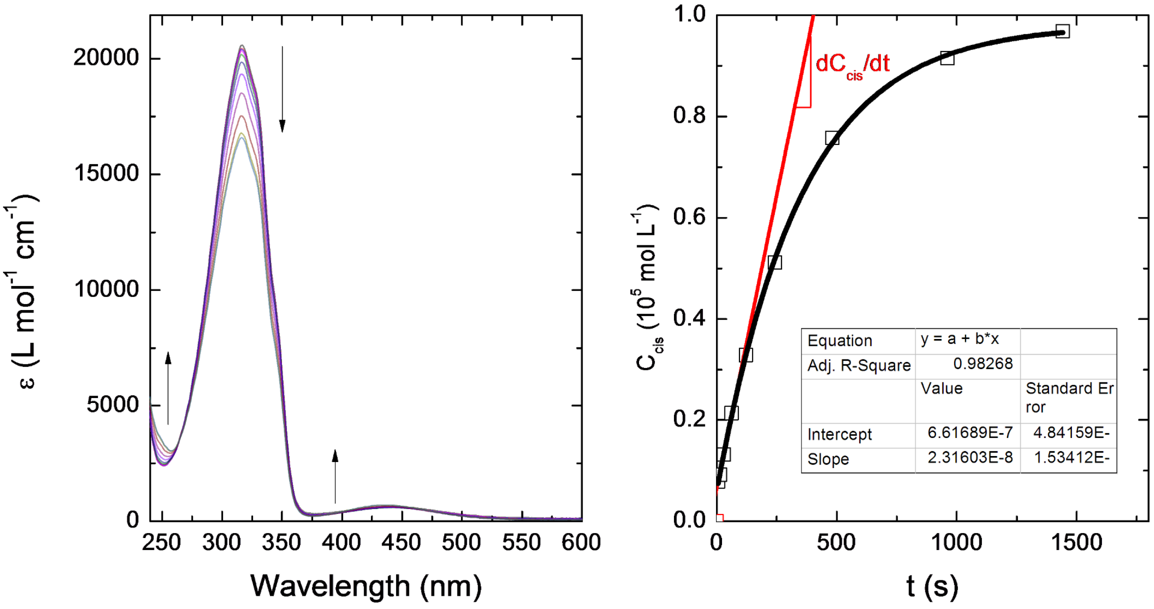

Equation	y = a + b*x	
Adj. R-Square	0.98268	
	Value	Standard Error
Intercept	6.61689E-7	4.84159E-
Slope	2.31603E-8	1.53412E-

Figure 5-1: (left) Absorption spectra of azobenzene in MeOH, irradiation at 440 nm for the given time periods, $C_0 = 4.6 \times 10^{-5}$ mol/ L. (right) Red line is the linear fit until ≈5% conversion, (black squares) concentration of *cis*-azobenzene versus irradiation time. The calculated $\phi_{tc} = 0.24$; the reference $\phi_{tc} = 0.22$.

Due to the intrinsic error in the mathematical approximation (linear fitting of the initial slope) employed and the varying time intervals for cyclization and cycloreversion reactions (longer in the case of cycloreversion), the quantum yields obtained by this method exhibit an estimated relative uncertainty in measurement of 10% of the obtained value for photocyclization and for cycloreversion reactions.[217]

Light intensities required for the determination of the isomerization quantum yields at 310 nm, 330 nm, 380 nm and 440 nm were determined by potassium ferrioxalate actinometry.[230] The "micro-version"[231] consisting of irradiation of 3 mL of a fresh potassium ferrioxalate solution (0.006 M in 0.05 M H_2SO_4) in a cuvette for 2 – 4 min, subsequent addition of 0.5 mL of phenanthroline buffer (0.1 wt % in 0.5 M H_2SO_4/ 1.6 M NaOAc), and absorbance readout at 510 nm was applied. I_0 is obtained from:

$$I_0 = \frac{\Delta A_{510\,nm}}{\Delta t \cdot 1000 \cdot \phi_\lambda \cdot \varepsilon_{510\,nm}} \cdot \frac{3.5\,ml}{3\,ml} \tag{5.3.4}$$

with $\Delta A_{510\,nm}$ the difference in absorbance between sample and reference, $\varepsilon_{510\,nm}$ = 11100 M^{-1} cm^{-1}, and ϕ_λ depending on the literature value for the wavelength to be determined. For the described Hg(Xe) lamp setup light intensities of $I_0 = 4.0 \cdot 10^{-10} - 1.1 \cdot 10^{-9}$ E s^{-1} cm^{-3} have been obtained.

Light intensities at 510 nm and 546 nm were determined using the commercial furyl fulgide Aberchrome 670[232] as reference. Therefore, 3 mL of a *n*-hexanes solution of Aberchrome 670 ($1.0 \cdot 10^{-4}$ M) were irradiated for 4 min at 365 nm (1000 W Xe, interference filter) before irradiation with λ (546 nm or 510 nm) light was performed in 6 steps each consisting of 5% conversion (15 s irradiation time). I_0 is obtained from the depletion of absorbance at 519 nm:

$$I_0 = -\frac{\Delta A_{519\,nm}}{\Delta t \cdot 1000 \cdot \phi_\lambda \cdot \varepsilon_{519\,nm} \cdot (1 - 10^{-A'})} \tag{5.3.5}$$

with *A'* the initial absorbance at the irradiation wavelength, ϕ_λ depending on the literature value for the wavelength to be determined, and $\varepsilon_{519\,nm}$ = 7760 M^{-1} cm^{-1}. The typical standard deviation of the six measurements is 2%.

To perform the kinetic studies of ABs, time evolution of UV-visible absorption spectra of the different compounds in DMSO were recorded at five different temperatures (60, 70, 80, 85, 90 °C) using quartz cuvettes on a Cary 50/ 60 spectrophotometer equipped with a Peltier-thermostated cell holder. For each spectrum, the corresponding amount of *cis*-form was derived from the value of the absorbance at λ_{max} using the following equations:

$$x(t) = \frac{A(t) - A_{cis}}{A_{trans} - A_{cis}} \tag{5.3.6}$$

and

$$y(t) = \frac{A_{trans} - A(t)}{A_{trans} - A_{cis}} \tag{5.3.7}$$

and where *x(t), y(t)* and *A(t)* are the ratio of *trans*-isomer, the ratio of *cis*-isomer, and the absorbance of the mixture at time t, respectively; A_{trans} and A_{cis} are the absorbances of pure *trans-* and *cis*-form, respectively. Plotting % *cis*-isomer *vs.* time gives the rate constants *k* by using the first order kinetic equation

$$[cis] = [cis]_0 e^{-kt} \tag{5.3.8}$$

and the corresponding thermal half-lives with

$$\tau_{1/2} = \frac{\ln 2}{k} \tag{5.3.9}$$

Cyclic voltammetry was performed using a PG310 USB (HEKA Elektronik) potentiostat interfaced to a PC with PotMaster v2x43 (HEKA Elektronik) software for data evaluation. A three-electrode configuration contained in a non-divided cell consisting of a platinum disc (*d* = 1 mm) as working electrode, a platinum plate as counter-electrode, and a saturated calomel electrode (SCE) with an agar-agar-plug in a Luggin capillary with a diaphragm as reference electrode was used. Measurements were carried out in 1·10-3 M solutions in acetonitrile (HPLC-grade, dried over calcium hydride and distilled) containing 0.1 M Bu_4NPF_6 using a scan rate of *dE/dt* = 1 V s-1. The data is given in reference to the ferrocene redox couple (Fc/ Fc^+), which was used as external standard. Cyclic voltammograms of ring-closed isomers of diarylethenes and *cis*-ABs were obtained by irradiation of the electrochemical cell using a standard laboratory UV-lamp equipped with a 313 nm UV-tube (Vilber Lourmat) or an Oriel 1000 W xenon arc lamp model 66924 using an Oriel timed shutter, water filter, and > 500 nm cut-off filter.

Spectroelectrochemistry was performed using a quarz cuvette with 1 mm pathlength in an Avantes AvaSpec-2048x14 spectrometer combined with an AvaLight-DH-S-BAL light source. The cuvette was equipped with a platinum net as working electrode, a platinum wire as counter electrode, and an Ag/ $AgNO_3$ reference electrode connected to an Autolab PGSTAT128N potentiostat from Metrohm GmbH, Germany. An acetonitrile solution of the compound ($c = 5 \cdot 10^{-4}$ M) containing 0.1 M Bu_4NPF_6 was placed in the cuvette and a potential scan was performed using a scan rate of 10 mV/ s while UV/vis-spectra were recorded every 10 mV. As reference the (Fc/ Fc+) redox couple was determined to have an oxidation potential of 0.21 V in this configuration.

6 References

[1] a) I. Yildiz, E. Deniz, F. M. Raymo, *Chem. Soc. Rev.* **2009**, *38*, 1859-1867; b) F. M. Raymo, M. Tomasulo, *Chem. Soc. Rev.* **2005**, *34*, 327-336.

[2] J. J. D. de Jong, L. N. Lucas, R. M. Kellogg, J. H. van Esch, B. L. Feringa, *Science* **2004**, *304*, 278-281.

[3] a) F. Würthner, J. Rebek, *Angew. Chem*. **1995**, *107*, 503-505; b) F. Würthner, J. Rebek, Angew. *Chem. Int. Ed.* **1995**, *34*, 446-448; c) F. Würthner, J. Rebek, *J. Chem. Soc., Perkin Trans. 2* **1995**, 1727-1734; d) D. Sud, T. B. Norsten, N. R. Branda, *Angew. Chem. Int. Ed.* **2005**, *44*, 2019-2021.

[4] a) V. Balzani, M. Gomez-Lopez, J. F. Stoddart, *Acc. Chem. Res.* **1998**, *31*, 405-414; b) M. Sauer, D.Streich, W. Meier, *Adv. Mater.* **2001**, *13*, 1649-1651.

[5] a) A. V. El'tsov, *Organic Photochromes*, Consultants Bureau, New York, **1990**; b) J. C. Crano, R. J.Guglielmetti, Editors, *Organic Photochromic and Thermochromic Compounds, Volume 1: Main Photochromic Families*, **1999**; c) Special-Issue Photochromism, *Chem. Rev.* **2000**, *100(5)*, 1683-1890; d) B. L. Feringa, Editor, *Molecular Switches*, **2001**; e) H. Dürr, H. Bouas-Laurent, *Photochromism: Molecules and Systems*, Elsevier Ltd, Oxford, **2003**.

[6] a) F. Moresco, G. Meyer, K.-H. Rieder, H. Tang, A. Gourdon, C. Joachim, *Phys. Rev. Lett.* **2001**, *86*, 672-675; b) M. J. Comstock, J. Cho, A. Kirakosian, M. F. Crommie, *Phys. Rev. B: Condens.Matter* **2005**, *72*, 153414.

[7] Thomas A. Klar, Stefan W. Hell, *Opt. Lett.* **1999**, *24*, 954-956.

[8] T. Müller, C. Schumann, A. Kraegeloh, *Chem. Phys. Chem.* **2012**, *13*, 1986–2000.

[9] H. Bouas-Laurent, H. Dürr, *Pure Appl. Chem.* **2001**, *73*, 639–665.

[10] M. Irie, *Chem. Rev.* **2000**, *100*, 1685-1716.

[11] C. Dugave, L. Demange, *Chem. Rev.* **2003**, *103*, 2475–2532.

[12] R. Klajn, *Pure Appl. Chem.* **2010**, *82*, 2247–2279.

[13] R. Klajn, J. F. Stoddart, B. A. Grzybowski, *Chem. Soc. Rev.* **2010**, *39*, 2203–2237.

[14] A. Goulet-Hanssens, C. J. Barrett, *J. Polym. Sci. Part Polym. Chem.* **2013**, *51*, 3058-3070.

[15] G. Berkovic, V. Krongauz, V. Weiss, *Chem. Rev.* **2000**, *100*, 1741–1754.

[16] R. Klajn, *Chem. Soc. Rev.* **2013**, *43*, 148–184.

[17] M. Handschuh, M. Seibold, H. Port, H. C. Wolf, *J. Phys. Chem. A* **1997**, 101, 502-506.

[18] J. Kiji, T. Okano, H.Kitamura, Y. Yokoyama, S. Kubota, Y. Kurita, *Bull. Chem. Soc. Jpn.* **1995**, *68*, 616-619.

[19] M. Irie, *Photochem. Photobiol. Sci.* **2010**, *9*, 1535–1542.

[20] a) T. Nakashima, R. Fujii, T. Kawai, Chem. Eur. J. **2011**, *17*, 10951–10957; b) K. Morimitsu, S. Kobatake, M. Irie, *Mol. Cryst. Liqu. Cryst.* **2005**, *431*, 151-154; c) K. Higashiguchi, K. Matsuda, Y. Asano, A. Murakami, S. Nakamura, M. Irie, *Eur. J. Org. Chem.* **2005**, *1*, 91-97.

[21] Y.Jeong, C. Gao, I. Lee, S. Yang, K. Ahn, *Tetrahedron Lett.* **2009**, *50*, 5288–5290.

[22] M. Montalti, A. Credi, L. Prodi, M. T. Gandolfi, *Handbook of Photochemistry*, CRC Press, **2006**.

[23] H. J. Kuhn, S. E. Braslavsky, R. Schmidt, *Pure Appl. Chem.* **2004**, *76*, 2105–2146.

[24] a) G. Gauglitz, *J. Photochem.* **1976**, *5*, 41–47; b) G. Gauglitz, S. Hubig, *J. Photochem.* **1981**, *15*, 255–257; c) G. Gauglitz, S. Hubig, *J. Photochem.* **1985**, *30*, 121–125.

[25] M.Irie, M. Mohri, *J. Org. Chem*. **1988**, *53*, 803-808.

[26] R. M. Kellogg, M. B. Groen, H. Wynberg, *J. Org. Chem.* **1967**, *32*, 3093–3100.

[27] a) M. Irie, O. Miyatake, K. Uchida, T. Eriguchi, *J. Am. Chem. Soc.* **1994**, *116*, 9894–9900; b) Y. Yokoyama, H. Shiraishi, Y. Tani, Y. Yokoyama, Y. Yamaguchi, *J. Am. Chem. Soc.* **2003**, *125*, 7194–7195; c) H. Nakagawa, S. Kawai, T. Nakashima, T. Kawai, *Org. Lett.* **2009**, *11*, 1475–1478.; d)T. Nakashima, Y. Kajiki, S. Fukumoto, M. Taguchi, S. Nagao, S. Hirota, T. Kawai, *J. Am. Chem. Soc.* **2012**, *134*, 19877–19883.

[28] a) M. Irie, K. Uchida, *Bull. Chem. Soc. Jpn.* **1998**, *71*, 985–996; b) T. Yamaguchi, M. Irie, *J. Mater. Chem.* **2006**, *16*, 4690-4694; c) D. Sysoiev, A. Fedoseev, Y. Kim, T. E. Exner, J. Boneberg, T. Huhn, P. Leiderer, E. Scheer, U. Groth, U. E. Steiner, *Chem. – Eur. J.* **2011**, *17*, 6663–6672; d) D. Sysoiev, T. Yushchenko, E. Scheer, U. Groth, U. E. Steiner, T. E. Exner, T. Huhn, *Chem. Commun.* **2012**, *48*, 11355–11357; e) J. Wolf, I. Eberspächer, U. Groth, T. Huhn, *J. Org. Chem.* **2013**, *78*, 8366–8375.

[29] a) P. Ren, R. Wang, S. Pu, G. Liu, C. Fan, *J. Phys. Org. Chem.* **2014**, *27*, 183–190; b) X. Li, S. Pu, H. Li, G. Liu, *Dyes Pigm.* **2014**, *105*, 47–56; c) H. Li, S. Pu, G. Liu, B. Chen, *Dyes Pigm.* **2014**, *101*, 15–24; d) H. Li, G. Liu, S. Pu, B. Chen, *Dyes Pigm.* **2013**, *99*, 812–821; e) S. Pu, R. Wang, G. Liu, W. Liu, S. Cui, P. Yan, *Dyes Pigm.* **2012**, *94*, 195–206.

[30] a) T. Yoshida, K. Arishima, F. Ebisawa, M. Hoshino, K. Sukegawa, A. Ishikawa, T. Kobayashi, M. Hanazawa, Y. Horikawa, *J. Photochem. Photobiol. Chem.* **1996**, *95*, 265-270; b) Z. Sun, H. Li, G. Liu, C. Fan, S. Pu, *Dyes Pigm.* **2014**, *106*, 94–104.

[31] a) K. Uchida, T. Ishikawa, M. Takeshita, M. Irie, *Tetrahedron* **1998**, *54*, 6627–6638; b) T. Nakashima, M. Goto, S. Kawai, T. Kawai, *J. Am. Chem. Soc.* **2008**, *130*, 14570–14575; c) J. Piard, R. Métivier, M. Giraud, A. Léaustic, P. Yu, K. Nakatani, *New J. Chem.* **2009**, *33*, 1420–1426; d) M. Herder, M. Pätzel, L. Grubert, S. Hecht, *Chem. Commun.* **2010**, *47*, 460–462; e) H. Li, S. Pu, G. Liu, W. Liu, *J. Phys. Conf. Ser.* **2011**, *276*, 012132; f) M. Herder, M. Utecht, N. Manicke, L. Grubert, M. Pätzel, P. Saalfrank, S. Hecht, *Chem. Sci.* **2013**, *4*,

1028–1040; g) K. Yuan, J. Boixel, H. L. Bozec, A. Boucekkine, H. Doucet, V. Guerchais, D. Jacquemin, *Chem. Commun.* **2013**, *49*, 7896–7898.

[32] a) S. Pu, P. Yan, G. Liu, W. Miao, W. Liu, *Tetrahedron Lett.* **2011**, *52*, 143–147; b) R. Wang, S. Pu, G. Liu, S. Cui, W. Liu, *Tetrahedron Lett.* **2012**, *53*, 320–324; c) S. Pu, C. Zheng, Q. Sun, G. Liu, C. Fan, *Chem. Commun.* **2013**, *49*, 8036–8038; d) C. Zheng, S. Pu, G. Liu, B. Chen, *Tetrahedron Lett.* **2013**, *54*, 7024–7028.

[33] a) S. Pu, C. Fan, W. Miao, G. Liu, *Tetrahedron* **2008**, *64*, 9464–9470; b) T. Wang, S. Pu, S. Cui, G. Liu, *J. Phys. Conf. Ser.* **2011**, *276*, 012192; c) R. Wang, S. Pu, G. Liu, S. Cui, H. Li, *Tetrahedron Lett.* **2013**, *54*, 5307–5310.

[34] a) S. Hiroto, K. Suzuki, H. Kamiya, H. Shinokubo, *Chem Commun* **2011**, *47*, 7149-7151; b) M. Hanazawa, R. Sumiya, Y. Horikawa, M. Irie, *J. Chem. Soc., Chem. Commun.* **1992**, 206-207.

[35] L. N. Lucas, J. J. D. De Jong, J. H. Van Esch, R. M. Kellogg, B. L. Feringa, *Eur. J. Org. Chem.* **2003**, *1*, 155-166.

[36] T. Yamaguchi, K. Uchida, M. Irie, *J. Am. Chem. Soc.* **1997**, *119*, 6066-6071.

[37] T. Nakashima, K. Atsumi, S. Kawai, T. Nakagawa, Y. Hasegawa, T. Kawai, *Eur. J. Org. Chem.* **2007**, *19*, 3212-3218.

[38] G. Hohlneicher, M. Mueller, M. Demmer, J. Lex, J. H. Penn, L. X. Gan, P. D. Loesel, *J. Am. Chem. Soc.* **1988**, *110*, 4483–4494.

[39] G. Szalóki, J.-L. Pozzo, *Chem. – Eur. J.* **2013**, *19*, 11124–11132.

[40] V. A. Migulin, M. M. Krayushkin, V. A. Barachevsky, O. I. Kobeleva, T. M. Valova, K. A. Lyssenko, *J. Org. Chem.* **2011**, *77*, 332–340.

[41] a) K. Matsuda, M. Irie, *Chem. Lett.* **2006**, *35*, 1204-1209; b) H. Tian, S. Yang, *Chem. Soc. Rev.* **2004**, *33*, 85-97; c) H. Tian, S. Wang, *Chem. Commun.* **2007**, 781-792; d) B. L. Feringa, *J. Org. Chem.* **2007**, *72*, 6635-6652.

[42] R. B. Woodward, R. Hoffmann, *Angew. Chem. Int. Ed.* **1969**, *8*, 781-853.

[43] S. Fukumoto, T. Nakashima, T. Kawai, *Dyes Pigm.* **2012**, *92*, 868-871.

[44] S. Fukumoto, T. Nakashima, T. Kawai, *Angew. Chem. Int. Ed.* **2011**, *50*, 1565-1568.

[45] R. Göstl, B. Kobin, L. Grubert, M. Pätzel, S. Hecht, *Chem. – Eur. J.* **2012**, *18*, 14282-14285.

[46] M. Irie, T. Lifka, K. Uchida, S. Kobatake, Y. Shindo, *Chem. Commun.* **1999**, *0*, 747-750.

[47] P. D. Patel, I. A. Mikhailov, K. D. Belfield, A. E. Masunov, *Int. J. Quantum Chem.* **2009**, *109*, 3711-3722.

[48] G. S. Hartley, *Nature* **1937**, 281.

[49] a) J. Henzl, M. Mehlhorn, H. Gawronski, K.-H. Rieder, K. Morgenstern, *Angew. Chem., Int. Ed.* **2006**, *45*, 603-606; b) X. Tong, M. Pelletier, A. Lasia, Y. Zhao, *Angew. Chem., Int. Ed.* **2008**, *47*, 3596-3599.

[50] R. Turansky, M. Konopka, N. L. Doltsinis, I. Stich, D. Marx, *Phys. Chem. Chem. Phys.* **2010**, *12*, 13922-13932.

[51] H. Rau, E. Lueddecke, *J. Am. Chem. Soc.* **1982**, *104*, 1616-1620.

[52] E. Merino, *Chem. Soc. Rev.* **2011**, *40*, 3835-3853.

[53] B. Priewisch, K. Rück-Braun, *J. Org. Chem.* **2005**, *70*, 2350-2352.

[54] H. Rau, *Photochromism Molecules and Systems, Elsevier* **2003**.

[55] I. Conti, M. Garavelli, G. Orlandi, *J. Am. Chem. Soc.* **2008**, *130*, 5216-5230.

[56] a) G. C. Hampson, J. M. Robertson, *J. Chem. Soc.* **1941**, 409-413; b) A. Mostad, C. Romming, *Acta Chem. Scand.* **1971**, *25*, 3561-3566.

[57] H. M. D. Bandara, S. C. Burdette, *Chem. Soc. Rev.* **2012**, *41*, 1809-1825.

[58] J. L. Magee, W. Shand, H. Eyring, *J. Am. Chem. Soc.* **1941**, *63*, 677-688.

[59] D. Y. Curtin, E. J. Grubbs, C. G. McCarty, *J. Am. Chem. Soc.* **1966**, *88*, 2775-2786.

[60] C. R. Crecca, A. E. Roitberg, *J. Phys. Chem. A* **2006**, *110*, 8188-8203.

[61] T. Fujino, S. Y. Arzhantsev, T. Tahara, *J. Phys. Chem. A* **2001**, *105*, 8123-8129.

[62] a) M. L. Tiago, S. Ismail-Beigi, S. G. Louie, *J. Chem. Phys.* **2005**,*122*, 094311; b) Y. Harabuchi, M. Ishii, A. Nakayama, T. Noro, T. Taketsugu, *J. Chem. Phys.* **2013**, *138*, 064305.

[63] a) E. Wei-Guang Diau, *J. Phys. Chem. A* **2004**, *108*, 950-956; b) T. Pancur, F. Renth, F. Temps, B. Harbaum, A. Kruger, R. Herges, C. Nather, *Phys. Chem. Chem. Phys.* **2005**, *7*, 1985-1989; c) R. Siewertsen, J. B. Schonborn, B. Hartke, F. Renth, F. Temps, *Phys. Chem. Chem. Phys.* **2011**, *13*, 1054-1063; d) M. Bockmann, N. L. Doltsinis, D. Marx, *J. Chem. Phys.* **2012**, *137*, 22A505.

[64] M. Quick, A. L. Dobryakov, M. Gerecke, C. Richter, F. Berndt, I. N. Ioffe, A. A. Granovsky, R. Mahrwald, N. P. Ernsting, S. A. Kovalenko, *J. Phys. Chem. B*, **2014**, *118*, 8756-8771.

[65] C. M. Stuart, R. R. Frontiera, R. A. Mathies, *J. Phys. Chem. A* **2007**, *111*, 12072-12080.

[66] D. G. Whitten, P. D. Wildes, J. G. Pacifici, G. Irick, *J. Am. Chem. Soc.* **1971**, *93*, 2004-2008.

[67] H. Bisle, M. Römer, H. Rau, Ber. der Bunsenges. phys. Chem. **1976**, *80*, 301-305.

[68] N. Nishimura, T. Tanaka, M. Asano, Y. Sueishi, *J. Chem. Soc., Perkin Trans. 2* **1986**, 1839-1845.

[69] G. Lewis, R. Mayfield, Aust. J. Chem. **1966**, *19*, 1445-1454.

[70] a) A. A. Beharry, O. Sadovski, G. A. Woolley, *J. Am. Chem. Soc.* **2011**, *133*, 19684–19687; b) S. Samanta, T. M. McCormick, S. K. Schmidt, D. S. Seferos, G. A. Woolley, *Chem. Commun.* **2013**, *49*, 10314–10316; c) S. Samanta, A. A.

Beharry, O. Sadovski, T. M. McCormick, A. Babalhavaeji, V. Tropepe, G. A. Woolley, *J. Am. Chem. Soc.* **2013**, 135, 9777–9784.

[71] R. Siewertsen, H. Neumann, B. Buchheim-Stehn, R. Herges, C. Nather, F.Renth, F. Temps, *J. Am. Chem. Soc.* **2009**, *131*, 15594–15595.

[72] D. Bléger, J. Schwarz, A. M. Brouwer., S. Hecht, *J. Am. Chem. Soc.* **2012**, *134*, 20597-20600.

[73] E. Laviron, Y. Mugnier, *J. Electroanal. Chem*. **1978**, *93*, 69–73.

[74] P. Hapiot, A. Neudeck, J. Pinson, M. Novi, G. Petrillo, C. Tavani, *J. Electroanal Chem.* **1997**, *422*, 99-114.

[75] X. Tong, M. Pelletier, A. Lasia, Y. Zhao, *Angew. Chem. Int. Ed.* **2008**, *47*, 3596–3599.

[76] T. Enomoto, H. Hagiwara, D. A. Tryk, Z.-F. Liu, K. Hashimoto, A. Fujishima, *J. Phys. Chem. B* **1997**, *101,* 7422-7427.

[77] Y.-C. Liu, K.-T. Cheng, H.-F. Chen, A. Y.-G. Fuh, *O. E.* **2014**, *22*, 4404-4411.

[78] J. R. Lakowicz, *Principles of Fluorescence Spectroscopy*, Springer, **2011**.

[79] B. Valeur, M. Berberán-Santos, *Molecular Fluorescence Principles and Applications*, Wiley-VCH, **2013**.

[80] F. Scandola, V. Balzani, *J. Chem. Ed.* **1983**, *60*, 814-823.

[81] P. Wu, L. Brand, *Anal. Biochem.* **1994**, *218*, 1-13.

[82] K. Cai, V. Schicht, *J. Biol. Chem.* **1996**, *271*, 27311-27320.

[83] E. R. Chapman, K. Alexander, T. Vorherr, E. Carafoli, D. R. Storm, *Biochem.* **1992**, *31*, 12819-12825.

[84] W. T. Mason, *Fluorescent and Luminescent Probes for Biological Activity*, Academic Press, **1993**.

[85] J. R. Silvins, M. J. Zuckermann, *Biochemistry*, **1993**, *24*, 3153-3161.

[86] R. A. Marcus, *Angew. Chem., Int. Ed. Engl.,* **1993**, *32*, 1111–1121.

[87] W. F. Libby, *J. Phys. Chem.* **1952**, *56*, 863-868.

[88] R. A. Marcus, *J. Chem. Phys.* **1956**, *24*, 966-978.

[89] N. J. Turro, V. Ramamurthy, J. C. Scaiano, *Modern Molecular Photochemistry of Organic Molecules*, University Science Books, **2010**.

[90] a) J. Jortner, *J. Chem. Phys.* **1976**, *64*, 4860-4867; b) R. A. Marcus, N. Sutin, *Biochim. Biophys. Acta, Rev. Bioenerg.* **1985**, *811*, 265-322.

[91] (a) H. A. Kramers, *Physica* **1934**, *1*, 182-192; (b) P. W. Anderson, *Phys. Rev.* **1950**, *79*, 350; (c) P. W. Anderson, *Phys. Rev.* **1959**, *115*, 2.

[92] J. Jortner, M. Bixon, T. Langenbacher, M. E. Michel-Beyerle, *Proc. Natl. Acad. Sci. U. S. A.* **1998**, *95*, 12759-12765.

[93] V. Balzani, M. Venturi, A. Credi, *Molecular devices and machines*, Wiley-VCH Weinheim, **2008**.

[94] A. L. Sisson, N. Sakai, N. Banerji, A. Furstenberg, E. Vauthey, S. Matile, *Angew. Chem., Int. Ed.* **2008**, *47*, 3727-3729.

[95] V. May, O. Kühn, *Charge and Energy Transfer Dynamics in Molecular Systems*, WILEY-VCH Verlag Berlin, **2000**.

[96] K. Yoshihara, *Adv. Chem.Phys.* **1999**, *107*, 371-402.

[97] J. Rosenthal, S. J. Lippard, *J. Am. Chem. Soc.* **2010**, *132*, 5536–5537.

[98] I. Moreno, C.-C. Sun, *O. E.* **2008**, *16*, 1808-1819.

[99] M. Göppert-Mayer, *Ann. Phys.* **1931**, *401*, 273-294.

[100] a) W. Kaiser, C. G. B. Garrett, *Phys. Rev. Lett.* **1961**, *7*, 229-231; b) W. L. Peticolas, J. P. Goldsborough, K. E. Rieckhoff, *Phys. Rev. Lett.* **1963**, *10*, 43-45.

[101] E. V. Anslyn, D. A. Dougherty, *Modern Physical Organic Chemistry*, University Science Books, **2006**.

[102] A. Ajani. W. Husinsky, R. Liska, N. Pucher, *J. Opt. Soc. Am. B.* **2010**, *27*, 2290-2297.

[103] G. S. He, L. S. Tan, Q. Zheng*, P. N. Prasad*, *Chem. Rev.* **2008**, *108*, 1245-1330.

[104] B. N. Jagatap, W. J. Meath, *J. Opt. Soc. Am. B* **2002**, *19*, 2673.

[105] M. Drobizhev, Y. Stepanenko, A. Rebane,C. J. Wilson, T. E. O. Screen, H. L. Anderson *J. Am. Chem. Soc.* **2006**, *128*, 12432-12433.

[106] M. Albota, D. Beljonne, J. L. Brédas*, et al.*, *Science* **1998**, *281*, 1653-1656.

[107] K. Susumu, J. A. N. Fisher, J. Zheng, D. N. Beratan, A. G. Yodh, M. J. Therien, *J. Phys. Chem. A*, **2011**, *115*, 5525–5539.

[108] Y. Z. Cui, Q. Fang, G. Xue, G. B. Xu, L. Yin, W. T. Yu, *Chem. Lett.*, **2005**, *34*, 644–645.

[109] J. Zyss, I. Ledoux, *Chem. Rev.* **1994**, *94*, 77-105.

[110] C. W. Spangler, E. H. Elandaloussi, B. Reeves, *Polym. Prepr.* **2000**, *41*, 789.

[111] J. A. Giordmaine, P. M. Rentzepis, S. L. Shapiro*, et al.*, *Appl. Phys. Lett.* **1967**, *11*, 216-218.

[112] C. N. LaFratta, J. T. Fourkas, T. Baldacchini*, et al.*, *Angew. Chem. Int. Ed.* **2007**, *46*, 6238-6258.

[113] .A. Parthenopoulos, P. M. Rentzepis, *Science* **1989**, *245*, 843-845.

[114] H. A. Collins, M. Khurana, E. H. Moriyama, A. Mariampillai, E. Dahlstedt, M. Balaz, M. K. Kuimova, M. Drobizhev, *et al.*, *Nature Photon.* **2008**, *2*, 420-424.

[115] M. Oheim, E. Beaurepaire, E. Chaigneau*, et al.*, *J. Neurosci. Methods* **2001**, *111*, 29-37.

[116] (a) A. Loudet, K. Burgess, *Chem. Rev.* **2007**, *107*, 4891–4932; (b) G. Ulrich, R. Ziessel, A. Harriman, *Angew. Chem., Int. Ed.* **2008**, *47*, 1184–1201.

[117] R. P. Haugland, *The Handbook. A Guide to Fluorescent Probes and Labeling Technologies,Molecular Probes*, Invitrogen, Carlsbad, CA, 10th edn, **2005**.

[118] N. Boens, V. Leen, W. Dehaen, *Chem. Soc. Rev.* **2012**, *41*, 1130–1172.

[119] O. A. Bozdemir, R. Guliyev, O. Buyukcakir, S. Selcuk, S. Kolemen, G. Gulseren, T. Nalbantoglu, H. Boyaci, E. U. Akkaya, *J. Am. Chem. Soc.* **2010**, *132*, 8029-8036.

[120] A. Treibs, F. Kreuzer, *Justus Liebigs Ann. Chem.* **1968**, 718, 208-223.

[121] R. Haugland, *Handbook of Fluorescent Probes and Research Chemicals*, 10th ed. Molecular Probes: Eugene, OR, **2005**.

[122] R. Alford, H. Simpson, J. Duberman, G. Hill, M. Ogawa, C. Regino, H.Kobayashi, P. Choyke, *Molecular Imaging* **2009**, 8, 341-354.

[123] K. Tram, H. Yan, H. A. Jenkins, S. Vassiliev, D. Bruce, *Dyes Pigm.* **2009**, *82*, 392-395.

[124] W. Qin, M. Baruah, W. M. D. Borggraeve, N. Boens, *J. Photochem. Photobiol. A: Chem.* **2006**, *183*, 190-197.

[125] T. V. Goud, A. Tutar, J.-F. Biellmann, *Tetrahedron* **2006**, *62*, 5084-5091.

[126] T. E. Wood, A. Thompson, *Chem. Rev.* **2007**, *107*, 1831-1861.

[127] T. Rohand, W. Qin, N. Boens, W. Dehaen, *Eur. J. Org. Chem.* **2006**, *20*, 4658-4663.

[128] T. Rohand, M. Baruah, W. Qin, N. Boens, W. Dehaen, *Chem. Comm.* **2006**, *3,* 266-268.

[129] T. Ehrenschwender, H. A. Wagenknecht, *J. Org. Chem.* **2011**, *76*, 2301-2304.

[130] S. L. Niu, C. Massif, G. Ulrich, R. Ziessel, P. Y. Renard, A. Romieu, *Org. Biomol. Chem.* **2011**, *9*, 66-69.

[131] M. S. Goncalves, *Chem. Rev.* **2009**, *109*, 190-212.

[132] A. D. McNaught, A. Wilkinson, *IUPAC. Compendium of Chemical Terminology, 2nd ed. (the "Gold Book"),* Blackwell Scientific Publications, Oxford, **1997**.

[133] A. Bhaskar, G. Ramakrishna, Z. Lu, R. Twieg, J. M. Hales, D. J. Hagan, E. V. Stryland, T. Goodson, *J. Am. Chem. Soc.* **2006**, *128*, 11840-11849.

[134] E. Bellmann, S. Shaheen, S. Thayumanavan, S. Barlow, R. Grubbs, S. Marder, B. Kippelen, N. Peyghambarian, *Chem. Mater*. **1998**, *10*, 1668-1676.

[135] J. Lindley, *Tetrahedron* **1984**, *40*, 1433-1456.

[136] J. F. Hartwig, *Angew. Chem., Int. Ed. Engl.* **1998**, *37*, 2046-2067.

[137] H. B. Goodbrand, N.-X. Hu *J. Org. Chem.* **1999,** *64,* 670-674.

[138] E. Ishow, A. Brosseau, G. Clavier, K. Nakatani, P. Tauc, C. Fiorini-Debuisschert, S. Neveu, O. Sandre, A. Leaustic, *Chem. Mater.* **2008**, *20*, 6597–6599.

[139] O. Kwon, S. Barlow, S. A. Odom, L. Beverina, N. J. Thompson, E. Zojer, J. L. Bredas, S. R. Marder, *J. Phys. Chem. A* **2005**, *109*, 9346–9352.

[140] Z. J. Ning, Z. Chen, Q. Zhang, Y. L. Yan, S. X. Qian, Y. Cao, H. Tian, *Adv. Funct. Mater.* **2007**, *17*, 3799–3807.

[141] G. S. He, L. S. Tan, Q. Zheng, P. N. Prasad, *Chem. Rev.* **2008**, *108*, 1245-1330.

[142] A. Facchetti, *Chem. Mater.* **2010**, *23*, 733–758.

[143] M. He, R. J. Twieg, U. Gubler, D. Wright, W. E. Moerner, *Chem. Mater.* **2003**, *15*, 1156-1164.

[144] C. N. LaFratta, J. T. Fourkas, T. Baldacchini, R. A. Farrer, *Angew. Chem., Int. Ed.* **2007**, *46*, 6238–6258.

[145] Y. Wu, W. Zhu, *Chem. Soc. Rev.* **2013**, *42*, 2039–2058.

[146] W. Zhou, S. M. Kuebler, K. L. Braun, T. Yu, J. K. Cammack, C. K. Ober, J. W. Perry, S. R. Marder, *Science* **2002**, *296*, 1106–1109.

[147] H. Yuan, Y. Zhao, F. Wu, *Chem. Mater.* **2012**, *24*, 1371-1377.

[148] M. A. Baldo, D. F. O'Brien, Y. You, A. Shoustikov, S. Sibley, M. E. Thompson, S. R. Forrest, *Nature* **1998**, *395*, 151-154.

[149] S. Lamansky, P. Djurovich, D. Murphy, F. A.-Razzaq, H.-E. Lee, C. Adachi, Paul E. Burrows, S. R. Forrest, M. E. Thompson, *J. Am. Chem. Soc.* **2001,** *123,* 4304-4312.

[150] M. Nonoyama, *Bull. Chem. Soc. Jpn.* **1974**, *47*, 767-768.

[151] G. A. Carlson, P. I. Djurovich, R. Watts, *Inorg. Chem.* **1993**, *32*, 4483-4484.

[152] S. Lamansky, P. Djurovich, D. Murphy, F. A.-Razzaq, R. Kwong, I. Tsyba, M. Bortz, B. Mui, R. Bau, M. E. Thompson, *Inorg. Chem.* **2001,** *40,* 1704-1711.

[153] M. G. Colombo, A. Hauser, H. U. Güdel, *Inorg. Chem.* **1993**, *32*, 3088-3092.

[154] V. Balzani, A. Juris, M. Venturi, S. Campagna, S. Serroni, *Chem. Rev.* **1996**, *96*, 759-834.

[155] C. Lee, J.-H. Yum, H. Choi, S. O. Kang, J. Ko, R. H.- Baker, M. Graetzel, M. K. Nazeeruddin, *Inorg. Chem.* **2008**, *47*, 2267-2273.

[156] A. Kapturkiewicz, J. Nowacki, P. Borowicz, *Electrochim. Acta* **2005**, *50*, 3395-3400.

[157] M. E. Thompson, P. E. Burrows, S. R. Forrest, *Curr. Opin. Solid State Mater. Sci.* **1999**, *4*, 369-372.

[158] Y. Sun, N. C. Giebink, H. Kanno, B. Ma, M. E. Thompson, S. R. Forrest, *Nature* **2006**, *440*, 908-912.

[159] D. G. Moon, R. B. Pode, C. J. Lee, J. I. Han, *Mater. Sci. Eng. B* **2005**, *121*, 232-237.

[160] F. C. Chen, S. C. Chang, G. He, S. Pyo, Y. Yang, M. Kurotaki, J. J. Kido, *Polym. Sci., Part B: Polym. Phys.* **2003**, *41*, 2681-2690.

[161] A. J. Sandee, C. K. Williams, N. R. Evans, J. E. Davies, C. E Boothby,. A. Köhler, R. H. Friend, A. B. Holmes, *J. Am. Chem. Soc.* **2004**, *126*, 7041-7048.

[162] I. Yildiz, E. Deniz, F.M. Raymo, *Chem. Soc. Rev.* **2009**, *38*, 1859-1867.

[163] J. Walz, K. Ulrich, H. Port, H.C. Wolf, J. Wonner, F. Effenberger, *Chem. Phys. Lett.* **1993**, *213*, 321-324.

[164] S. Tsuchiya, *J. Am. Chem. Soc.* **1999**, *121*, 48–53.

[165] S. Shim, T. Joo, S. C. Bae, K. S. Kim, E. Kim, *J. Phys. Chem. A* **2003**, *107*, 8106-8110.

[166] M. Irie, T. Fukaminato, T. Sasaki, N. Tamai, T. Kawai, *Nature* **2002**, *420*, 759-760.

[167] K. Yagi, C. F. Soong, M. Irie, *J. Org. Chem.* **2001**, *66*, 5419-5423.

[168] H. Hayasaka, K. Tamura, K. Akagi, *Macromolecules* **2008**, *41*, 2341-2346.

[169] H. Cho, E. Kim, *Macromolecules* **2002**, *35*, 8684-8687.

[170] R.T.F. Jukes, V. Adamo, F. Hartl, P. Belser, L. De Cola, *Inorg. Chem.* **2004**, *43*, 2779-2792.

[171] N. Soh, K. Yoshida, H. Nakajima, K. Nakano, T. Imato, T. Fukaminato, M. Irie, *Chem. Commun.* **2007**, 5206-5208.

[172] M. Bossi, V. Belov, S. Polyakova, S.W. Hell, *Angew. Chem. Int. Ed.* **2006**, *45*, 7462-7465.

[173] X. Cao, J. Zhou, Y. Zou, M. Zhang, X. Yu, S. Zhang, T. Yi, C. Huang, *Langmuir* **2011**, *27*, 5090-5097.

[174] T. Fukaminato, T. Doi, N. Tamaoki, K. Okuno, Y. Ishibashi, H. Miyasaka, M. Irie, *J. Am. Chem. Soc.* **2011**, *133*, 4984-4990.

[175] M. Irie, T. Eriguchi, T. Takada, K. Uchida, *Tetrahedron* **1997**, *53*, 12263-12271.

[176] T. A. Golovkova, D. V. Kozlov, D. C. Neckers, *J. Org. Chem.* **2005**, *70*, 5545-5549.

[177] M .Beberich, M. Natail, P. Spenst, C. Chiorboli, F. Scandola, F. Würthner, *Chem. Eur. J.* **2012**, *18*, 13651-13664.

[178] M. J. Rust, M. Bates, X. W. Zhuang, *Nat. Methods* **2006**, *3*, 793-796.

[179] K. Uno, H. Niikura, M. Morimoto, Y. Ishibashi, H. Miyasaka, M. Irie, *J. Am. Chem. Soc.* **2011**, *133*, 13558–13564.

[180] S.-C. Pang, H. Hyun, S. Lee, D. Jang, M. J. Lee, S. H. Kang, K.-H. Ahn, *Chem. Commun.* **2012**, *48*, 3745–3747.

[181] D. Bléger, S. Hecht, "Visible Light Activated Molecular Switches" Angew. Chem. Int. Ed. accepted.

[182] R. Murata, T. Yago, M. Wakasa, *Bull. Chem. Soc. Jpn*. **2011**, *84*, 1336−1338.

[183] J. Croissant, M. Maynadier, A. Gallud, H. Peindy N'dongo, J. L. Nyalosaso, G. Derrien, C. Charnay, J.-O. Durand, L. Raehm, F. Serein-Spirau, et al., *Angew. Chem. Int. Ed. Engl.* **2013**, *52*, 13813–13817.

[184] J.-C. Boyer, C.-J. Carling, B. D. Gates, N. R. Branda, *J. Am. Chem. Soc.* **2010**, *132*, 15766–15772.

[185] C.-J. Carling, J.-C. Boyer, N. R. Branda, *J. Am. Chem. Soc.* **2009**, *131*, 10838–10839.

[186] T. Nakashima, Y. Kajiki, S. Fukumoto, M. Taguchi, S. Nagao, S. Hirota, T. Kawai, *J. Am. Chem. Soc.* **2012**, *134*, 19877–19883.

[187] S. Lee, Y. You, K. Ohkubo, S. Fukuzumi, W. Nam, *Chem. Sci.* **2014**, *5*, 1463–1474.

[188] K. Suzuki, T. Ubukata, Y. Yokoyama, *Chem. Commun*. **2012**, *48*, 765–767.

[189] a) J. Folling, V. Belov, R. Kunetsky, R.Medda, A. Schonle, A. Egner, C. Eggeling,M. Bossi, S. W. Hell, *Angew. Chem.* Int. Ed. **2007**, *46*, 6266–6270; b) L. Giordano, T. M. Jovin, M. Irie, E. A. Jares-Erijman, *J. Am. Chem. Soc.* **2002**, *124*, 7481–7489; c) M. Berberich, F. Würthner, *Chem. Sci.* **2012**, *3*, 2771-2777.

[190] a) E. Betzig, G. H. Patterson, R. Sougrat, O. W. Lindwasser, S. Olenych, J. S. Bonifacino, M. W. Davidson, J. Lippincott-Schwartz, H. F. Hess, *Science* **2006**, *313*, 1642-1645; b) S. T. Hess, T. P. K. Girirajan, M. D. Mason, *Biophys. J.* **2006**, *91*, 4258-4272.

[191] J. Moreno, S. Hecht: "Design and Synthesis of Novel Fluorophore-Photochrome Dyads", 13th Conference on Methods and Applications of Fluorescence (MAF'13), Genoa, Italy, 2013

[192] L. Jiao, C. Yu, M. Liu, Y. Wu, K. Cong, T. Meng, Y. Wang, E. Hao, *J. Org. Chem.*, **2010**, *75*, 6035–6038.

[193] a) C. D. Nenitzescu, R.Cantuniari, *Ber. Deutsch. Chem. Ges.* **1933**, *66*, 1097–1100; b) K. Yu. Koltunov, G. K. S. Prakash, G. Rasul, G. A. Olah, *Eur. J. Org. Chem.,* **2006**, 4861-4866.

[194] H. v. Dobeneck, H. Reinhard, H. Deuhel, D. Wolkenstein, *Chem. Ber.* **1969**, *102*, 1357-1362.

[195] I. Stara, I. Stary, A. Kollarovic, F. Teply, D. Saman, P. Fiedler, *Tetrahedron* **1998**, *54*, 11209–11234.

[196] V. Leen, T. Leemans, N. Boens, W.Dehaen, *Eur. J. Org. Chem.* **2011**, *23*, 4386–4396.

[197] G. C. Fu, *Acc. Chem. Res.* **2008**, *41*, 1555-1564.

[198] C. Lambert, G. Nöll, E. Schmälzlin, K. Meerholz, C. Bräuchle, *Chem. Eur. J.* **1998**, *4*, 2129-2135.

[199] H. Utsumi, D. Nagahama, H. Nakano, Y. Shirota, *J. Mater. Chem.* **2002**, *12*, 2612–2619.

[200] M. Irie, T. Fukaminato, K. Matsuda, S. Kobatake, *Chem. Rev.* **2014**, *114*, 12174–12277.

[201] L. Jiao, C. Yu, T. Uppal, M. Liu, Y. Li, Y. Zhou, E. Hao, X. Hu, M. G. H. Vicente, *Org. Biol. Chem.* **2010**, *8*, 2517.

[202] J. Pommerehne, H. Vestweber, W. Guss, R.F. Mahrt, H. Bässler, M. Porsch, J. Daub, *Adv.Mater.* **1995**, *7*, 551-554.

[203] S. Castellanos, A. A. Vieira, B. M. Illescas, V. Sacchetti, C. Schubert, J. Moreno, D. M. Guldi, S. Hecht, N. Martín, *Angew. Chem.* **2013**, *125*, 14235-14240; *Angew. Chem. Int. Ed.* **2013**, *52*, 13985-13990.

[204] R.Berera, R. v. Grondelle, J. T. M. Kennis, *Photosynth. Res*. **2009**, *101*, 105–118.

[205] C. Slavov, H. Hartmann, J. Wachtveitl, *Anal. Chem.* **2015**, *87*, 2328–2336.

[206] a) F. Schweighöfer, L. Dworak, M. Braun, M. Zastrow, J. Wahl, I. Burghardt, K. Rück-Braun, J Wachtveitl, *Sci. Rep.* **2015**, *5*, 9368; b) L. Dworak, M. Zastrow, G. Zeyat, K. Rück-Braun, J. Wachtveitl, *J. Phys.: Condens. Matter* **2012**, *24*, 394007-394014; c) Y. Asano, A. Murakami, T. Kobayashi, A. Goldberg, D. Guillaumont, S. Yabushita, M. Irie, S. Nakamura, *J. Am. Chem. Soc.* **2004,** *126*, 12112-12120.

[207] Y. Ishibashi, T. Umesato, S. Kobatake, M. Irie, H. Miyasaka, *J. Phys. Chem. C* **2012**, *116*, 4862−4869.

[208] T. Sumi, Y. Takagi, A. Yagi, M. Morimoto, M. Irie, *Chem. Commun.* **2014**, *50*, 3928-3930.

[209] S. L., Gilat, S. H. Kawai, J. M. Lehn, *Chem. Eur. J.* **1995**, *1*, 275-284.

[210] D. Vomasta, C. Högner, N. R. Branda, B. König, *Angew. Chem. Int. Ed.* **2008**, *47*, 7644–7647.

[211] O. Babii, S. Afonin, M. Berditsch, S. Reißer, P. K. Mykhailiuk, V. S. Kubyshkin, T. Steinbrecher, A. S. Ulrich, I. V. Komarov, *Angew. Chem. Int. Ed.* **2014**, *53*, 3392–3395.

[212] a) Y. Shoji, A. Yagi, M. Horiuchi, M. Morimoto, M. Irie, *Isr. J. Chem.* **2013**, *53*, 303–311; b) Y. Zou, T. Yi, S. Xiao, F. Li, C. Li, X. Gao, J. Wu, M. Yu, C. Huang, *J. Am. Chem. Soc.* **2008**, *130*, 15750–15751; c) S. Pu, H. Liu, G. Liu, B. Chen, Z. Tong, *Tetrahedron* **2014**, *70*, 852–858; d) X. Yao, T. Li, S. Wang, X. Ma, H. Tian, *Chem. Commun.* **2014**, *50*, 7166–7168.

[213] M. I. Angelova, D. S. Dimitrov, *Faraday Discuss. Chem. Soc.* **1986**, *81*, 303.

[214] K. C. D. Robson, B. D. Koivisto, T. J. Gordon, T. Baumgartner, C. P. Berlinguette, *Inorg. Chem.* **2010**, *49*, 5335–5337.

[215] A. L. Thompson, K. M. Gaab, J. Xu, C. J. Bardeen, T. J. Martínez, *J. Phys. Chem. A* **2004**, *108,* 671-682.

[216] H. Eyring, *Chem. Rev.* **1935**, *17*, 65 –77.

[217] M. Herder, B. M. Schmidt, L. Grubert, M. Pätzel, J. Schwarz, S. Hecht, *J. Am. Chem. Soc.* **2015,** *137*, 2738-2747.

[218] S.Faure, C. Stern, R. Guilard, P. D. Harvey, *J. Am. Chem. Soc.* **2004**, *126*, 1253–1261.

[219] S. Welter, N. Salluce, P. Belser, M. Groeneveld, L. De Cola, *Coord. Chem. Rev.* **2005**, *249*, 1360-1371.

[220] A. Molina-Ontoria, G. Fernández, M. Wielopolski, C. Atienza, L. Sánchez, A. Gouloumis, T.Clark, N. Martín, D. M. Guldi, *J. Am. Chem. Soc.* **2009**, *131*, 12218–12229.

[221] M. Soler, J. K. McCusker, *J. Am. Chem. Soc.* **2008**, *130*, 4708–4724.

[222] W. R. Zipfel, R. M. Williams, W. W. Webb, *Nat. Biotechnol.* **2003**, *21*, 1369.

[223] S. W. Magennis, F. S. Mackay, A. C. Jones, K. M. Tait, P. J. Sadler, *Chem. Mater.* **2005,** *17,* 2059-2062

[224] T. Fujino, S. Y. Arzhantsev, T. Tahara, *J. Phys. Chem. A* **2001**, *105*, 8123–8129.

[225] W. J. Finkenzeller, H. Yersin, *Chem. Phys. Lett.* **2003**, *377*, 299-305.

[226] H. E. Gottlieb, V. Kotlyar, A. Nudelman, *J. Org. Chem.* **1997**, *62*, 7512–7515.

[227] W. H. Melhuish, *J. Phys. Chem.*, **1961**, *65*, 229-235.

[228] a) K. Rurack, M. Spieles, *Anal. Chem.* **2011**, *83*, 1232-1242; b) R. Sens, K. H. Drexhage, *J. Luminesc.* **1981**, *24*, 709-712.

[229] A. T. R. Williams, S. A. Winfield, J. N. Miller, *Analyst* **1983**, *108*, 1067-1071.

[230] C. G. Hatchard, C. A. Parker, *Proc. R. Soc. London, Ser. A* **1956**, *235*, 518-536.

[231] M. Montalti, A. Credi, L. Prodi, M. T. Gandolfi, In *Handbook of Photochemistry, Third Edition*; CRC Press: Boca Raton, **2006**.

[232] A. P. Glaze, H. G. Heller, J. Whittall, *J. Chem. Soc. Perk. Trans. 2* **1992**, 591-594.

7 List of Abbreviations

2PA	Two-photon absorption
3D	Three-dimensional
A	Acceptor
AB	Azobenzene
acac	Acetylacetonate
a-p	anti-parallel
AROP	Anionic ring-opening polymerization
ATRP	Atom transfer radical polymerization
BODIPY	Boron-dipyrromethene
CT	Charge transfer
CV	Cyclic voltammetry
D	Donor
DAE	Diarylethene
DAS	Differential absorption spectrum
dba	Dibenzylideneacetone
DCM	Methylene chloride
DMF	Dimethylformamide
DNA	Deoxyribonucleic acid
DVD	Digital versatile disc
DOPC	Dioleoylphosphatidylcholine
DPPC	Dipalmitoylphosphatidylcholine
ET	Electron transfer
EET	Excited-state energy transfer
equiv.	equivalent
ESA	Excited-state absorption

ESI	Electrospray ionization
EWG	Electron withdrawing group
FRET	Förster radiative energy transfer
Fc	Ferrocene
GUV	Giant uni-lamellar vesicle
GPC	Gel permeation chromatography
GSB	Ground-state bleach
HOMO	Highest occupied molecular orbital
HRMS	High-resolution mass spectrometry
ICT	Intramolecular charge transfer
LC	Ligand centered
LED	Light emitting diode
LMCT	Ligand-to-metal charge transfer
LUMO	Lowest unoccupied molecular orbital
^{i}Pr	*iso*-Propyl
ISC	Intersystem crossing
m	meta-position
MC	Metal-centered
MLCT	Metal-to-ligand charge transfer
MS	Mass spectrometry
n-Bu	*n*-Butyl
NIR	Near-infrared light
NBS	*N*-Bromosuccinimide
o	ortho-position
OLED	Organic light emiting diode
p	parallel
ppy	2-Phenylpyridine ligand
p	para-position

PE	Petroleum ether
PET	Photoinduced electron transfer
PBS	Phosphate buffered saline
PSS	Photostationary state
RNA	Ribonucleic acid
SDS	Sodium dodecylsulfate
SE	Stimulated emission
SEC	Spectroelectrochemistry
S_EAr	Electrophilic aromatic substitution
S_NAr	Nucleophilic aromatic substitution
STM	Scanning tunneling microscope
SVD	Singular value decomposition
TA	Transient absorption
TAA	Triarylamine
TEA	Triethylamine
TBAF	Tetra-*n*-butylammonium fluoride
TEM	Transmission electron microscopy
TIPSA	Triisopropylsylilacetylene
TLC	Thin-layer chromatography
TMSA	Trimethylsylilacetylene
THF	Tetrahydrofurane
Tol	Toluene
UCNP	Upconverting nanoparticle
UPLC	Ultra-high performance liquid chromatography
UV	Ultraviolet light
vis	Visible light